

**ANGULAR SPECTRUM REPRESENTATION OF
ULTRAWIDEBAND ELECTROMAGNETIC PULSE
PROPAGATION IN LOSSY, DISPERSIVE
DIELECTRIC SLAB WAVEGUIDES**

A Dissertation Presented

by

John Arthur Marozas

to

The Faculty of the Graduate College

of

The University of Vermont

In Partial Fulfillment of the Requirements
for the Degree of Doctor of Philosophy
Specializing in Electrical Engineering

March 1998

Abstract

The theory of reflection and refraction phenomena of inhomogeneous plane waves at a planar interface is a crucial step in developing the theory of both pulsed electromagnetic beam field reflection and refraction and dielectric slab waveguides. In the first case, inhomogeneous plane waves form the basic elements of the angular spectrum representation of both the reflected and refracted fields of pulsed electromagnetic beams at a planar interface separating two lossy, dispersive dielectric media. In the second case, dielectric slab waveguides inherently have two planar interfaces at which the electromagnetic energy interacts to form guided modes which are the sum of two inhomogeneous plane waves. Both formulations fully account for the temporally dispersive behavior of the lossy dielectric medium and the vector nature of the electromagnetic fields involved. The double resonance Lorentz model accurately represents dielectric dispersion in the infrared to ultraviolet spectral region. This model adheres to the *Kramers–Kronig* relations and is therefore causal. Inhomogeneous plane waves result as general solutions to *Maxwell's* equations in an infinitely extended dielectric medium with a complex refractive index. Many new results are discovered when these plane waves are utilized to form the generalized theory of reflection and refraction and the generalized *Fresnel* equations. For example, certain spectral regions will not support near total internal reflection which is a necessary condition of guiding of electromagnetic energy. Further, even if an inhomogeneous plane wave is at supercritical angles of incidence, near total internal reflection may be lost when both the incident and transmitted inhomogeneous plane waves become primarily attenuative.

Acknowledgements

I would like to extend my deepest gratitude to my thesis advisor, Dr. Kurt E. Oughstun. This dissertation represents my greatest achievement and would not have been possible without his guidance and perseverance. He was able to refocus my efforts and was there to wade through page after page while offering comments that assisted me in producing this dissertation. I would then like to thank the rest of my committee members (Dr. Kenneth I. Golden, Dr. J. Michael Wilson, chairperson, and Dr. Jun Yu) for taking the extra time and effort to assist me through my defense. Next, I would like to acknowledge the sources which funded this dissertation: the Patricia Harris Fellowship, the American Indian Science and Engineering Fellowship and the United States Air Force Office of Scientific Research under Grant F49620-94-1-0430.

I would like to dearly thank my wife Diana the most. She supported me through the worst of times. She had a way, like no other, to inspire me to never give up. She was my muse and my greatest comfort. Next in line are my two boys: Ian, a six year-old sparkle-boy and Brendan, a four year-old spitz-bub, whose constant demands never let me forget the important things in life; my family and the wonderful times that we have spent together from hiking in the Rocky Mountains to holding hands as we walk to the play ground. I would like to thank my mother and my sister Dianne for the confidence they gave me. They took the time to listen to me complain on the phone and, in return, offered advice and encouragement based on their own bewildering experiences in a doctoral program. Next, I would especially like to thank my friend Takla Gardey who took time off from her world travels to be my editor-in-residence. Her tireless efforts, in sifting through every page of my dissertation multiple times, will never be forgotten. Lastly, I would like to thank the rest of my family and friends who were there to spend fun times with me as I struggled to complete my dissertation. I will fondly remember our family reunions and the late nights brewing beer.

As an after thought, like always, I would like to thank Maquah whom I never seem to think of when things go well. Maquah doesn't appear to mind. She whispers into my ear whenever I'm willing to listen.

Table of Contents

| | |
|---|-----------|
| Acknowledgements | ii |
| List of Tables | vii |
| List of Figures | ix |
| | |
| CHAPTER I | |
| INTRODUCTION | 1 |
| 1.1 Motivations and Applications | 3 |
| 1.2 Previous Research | 8 |
| 1.3 Description of Methods and Results | 15 |
| | |
| CHAPTER II | |
| Fundamental Theory and Mathematical Preliminaries | 19 |
| 2.1 <i>Fourier</i> and <i>Laplace</i> Transform Analysis | 21 |
| 2.1.1 The Temporal <i>Fourier–Laplace</i> Transform | 21 |
| 2.1.2 The Two Dimensional Spatial <i>Fourier</i> Transform | 27 |
| 2.1.3 The One Dimensional Spatial <i>Laplace</i> Transform with Respect to the <i>z</i> -Dimension | 29 |
| 2.2 <i>Maxwell’s</i> Field Equations in a Lossy, Dispersive Dielectric | 31 |
| 2.2.1 Space–Time Domain Form of the Field Equations | 31 |
| 2.2.2 Space–Time Domain Form of the Source Free Field Equations in Dielectric Media | 33 |
| 2.2.3 Temporal Frequency Domain Form of the Field Equations | 35 |
| 2.2.4 Poynting’s Theorem and the Conservation of Energy | 35 |
| 2.2.5 Spatio–Temporal Frequency Domain Form of the Planar Boundary Value Problem for the Source–Free <i>Maxwell’s</i> Equations | 38 |
| 2.3 Theoretical Description of Dielectric Dispersion; The Double Resonance Lorentz Model | 42 |
| 2.3.1 The Lorentz Model | 43 |
| 2.3.2 The Double Resonance Lorentz Model for Glass | 46 |
| 2.4 Properties of Complex Vectors | 50 |
| 2.5 Inhomogeneous Plane Wave Solution of <i>Maxwell’s</i> Equations in an Infinitely Extended Dielectric with Complex Permittivity | 55 |
| 2.5.1 The Transversality Conditions | 61 |

Table of Contents

| | | |
|------------|--|-----------|
| 2.5.2 | Direction Cosine Form of the Inhomogeneous Plane Wave | 63 |
| 2.5.3 | The Poynting Vector and the Time Averaged Power Density of an Inhomogeneous Plane Wave | 65 |
| 2.5.4 | The Energy Transport Velocity for a Plane Wave in an Infinitely Extended Double Resonance Lorentz Model Dielectric | 67 |
| 2.6 | Polarization Properties for Propagating Electromagnetic Inhomogeneous Plane Waves | 70 |
| 2.6.1 | The Polarization Ellipse for the Complex Field Vectors | 71 |
| 2.6.2 | The Linearly Polarized Inhomogeneous Plane Wave Field: TE and TM Cases | 73 |
| 2.6.3 | The Homogeneous Plane Wave Field | 77 |

CHAPTER III

| | | |
|------------|--|------------|
| | Reflection and Transmission of a Pulsed Inhomogeneous Plane Wave Electromagnetic Field at a Planar Interface Separating Two Lossy Dielectrics | 79 |
| 3.1 | Inhomogeneous Plane Wave Reflection and Refraction from a Planar Interface Separating Two Lossy Dielectrics | 82 |
| 3.1.1 | Tangential Boundary Conditions | 99 |
| 3.1.2 | The Generalized Laws of Reflection and Refraction | 103 |
| 3.1.3 | The Generalized Fresnel Equations | 116 |
| 3.1.4 | Special cases of the Generalized Laws of Reflection and Refraction and the Generalized Fresnel Equations | 124 |
| 3.2 | The Reflected and Refracted Inhomogeneous Plane Wave Fields Expressed Within Their Respective Local Coordinate Systems | 131 |
| 3.3 | Pulsed Electromagnetic Inhomogeneous Plane Waves Incident Upon a Planar Interface Separating Two Lossy, Dispersive Dielectric Half-Spaces | 140 |

CHAPTER IV

| | | |
|------------|--|------------|
| | Reflection of Linearly Polarized TM Plane Waves Incident Upon a Planar Interface Separating Two Lossy, Dispersive Dielectrics | 143 |
| 4.1 | Double Resonance Lorentz Models of the Two Lossy, Dispersive Dielectric Media | 145 |

Table of Contents

| | |
|--|------------|
| 4.2 The Transmitted Complex Wavevector | 146 |
| 4.2.1 The Asymptotic Behavior of the Normal Component and the Angle of the Transmitted Complex Wavevector | 149 |
| 4.2.2 The Transmitted Normal Complex Wavenumber, Critical Angles and the Critical Transverse Wavenumbers | 152 |
| 4.3 Results of the Generalized Fresnel Reflection Coefficient for Incident Linearly Polarized TM Plane Waves | 166 |
| 4.3.1 Results of the Generalized Fresnel Reflection Coefficient for an Incident Linearly Polarized TM Homogeneous Plane Wave Where Both Media are Lossless | 167 |
| 4.3.2 Results of the Generalized Fresnel Reflection Coefficient for an Incident Linearly Polarized TM Homogeneous Plane Wave | 170 |
| 4.3.3 Results of the Generalized Fresnel Reflection Coefficient for an Incident Linearly Polarized TM Inhomogeneous Plane Wave | 174 |
| CHAPTER V | |
| Reflection and Transmission of a Pulsed Electromagnetic Beam Field at a Planar Interface Separating Two Lossy Dielectrics | 185 |
| 5.1 Angular Spectrum Representation of Pulsed Electromagnetic Beam Fields When the Field is Known at a Planar Boundary Surface | 187 |
| 5.2 Reflection and Refraction of a Pulsed Electromagnetic Beam Field at a Planar Interface Separating Two Lossy Dielectrics | 200 |
| CHAPTER VI | |
| Modal Analysis of Asymmetric Dielectric Slab Waveguides | 209 |
| 6.1 Electromagnetic Field Equations in “Two-Dimensional” Dielectric Regions | 211 |
| 6.2 Guided Modes of the Asymmetric Dielectric Slab Waveguide ... | 215 |
| 6.2.1 Guided TE Modes in an Asymmetric Dielectric Slab Waveguide | 216 |
| 6.2.2 Physical Connection for the Guided TE Modes in an Asymmetric Dielectric Slab Waveguide | 222 |
| References | 229 |

List of Tables

| | | |
|-------------|---|-----|
| Table 2.3.1 | Numerically determined double resonance Lorentz parameters for a fluoride (CLAP) glass found by applying the complex Levenberg–Marquardt nonlinear least–squares fit algorithm. | 48 |
| Table 4.1.1 | Double resonance Lorentz model parameters of the two media separated by an interface where the only difference lies in the choice of the parameter ϵ_{j1} | 147 |
| Table 4.1.2 | Double resonance Lorentz model parameters of the two media separated by an interface where the behavior of the real part of the complex refractive index switches from the normal optically dense to rare transition to optically rare to dense transition within the anomalous dispersion regions. | 148 |
| Table 4.2.1 | The values of the propagation factor and the attenuation factor for various frequencies. This example utilizes the double resonance Lorentz model parameters taken from Table 4.1.1. | 156 |
| Table 4.2.2 | The values of the propagation factor and the attenuation factor for various frequencies. This example utilizes the double resonance Lorentz model parameters taken from Table 4.1.2. | 156 |
| Table 4.2.3 | The critical angles for an interface for various frequencies. This example utilizes the double resonance Lorentz model parameters taken from Table 4.1.1. | 160 |
| Table 4.2.4 | The critical angles for an interface for various frequencies. This example utilizes the double resonance Lorentz model parameters taken from Table 4.1.2. | 160 |
| Table 4.2.5 | The critical values of the transverse wavenumber. The angle of the incident local coordinate system $\Theta_i = 20^\circ$. This example utilizes the double resonance Lorentz model with parameters taken from Table 4.1.1. | 164 |
| Table 4.2.6 | The critical values of the transverse wavenumber. The angle of the incident local coordinate system $\Theta_i = 50^\circ$. This example utilizes the double resonance Lorentz model with parameters taken from Table 4.1.1. | 164 |
| Table 4.2.7 | The critical values of the transverse wavenumber. The angle of the incident local coordinate system $\Theta_i = 50^\circ$. This example utilizes the double resonance Lorentz model with parameters taken from Table 4.1.2. | 165 |
| Table 4.3.1 | The angles of the incident propagation vector that correspond to the critical values of the transverse wavenumber. The angle of the incident local coordinate system $\Theta_i = 20^\circ$. This example utilizes the double resonance Lorentz model with parameters taken from Table 4.1.1. | 182 |
| Table 4.3.2 | The angles of the incident propagation vector that correspond to the critical values of the transverse wavenumber. The angle of the incident local coordinate system $\Theta_i = 50^\circ$. This example utilizes the double resonance Lorentz model with parameters taken from Table 4.1.1. | 183 |
| Table 4.3.3 | The angles of the incident propagation vector that correspond to the critical values of the transverse wavenumber. The angle of the incident local coordinate system $\Theta_i = 50^\circ$. This example utilizes the double resonance Lorentz model with parameters taken from Table 4.1.2. | 183 |
| Table 4.3.4 | The critical values of the transverse wavenumber for the frequency 173.79THz. The angle of the incident local coordinate system varies as indicated. This example utilizes the double resonance Lorentz model with parameters taken from Table 4.1.1. | 184 |
| Table 4.3.5 | The critical values of the transverse wavenumber for the frequency 302.01THz. The angle of the incident local coordinate system varies as indicated. This example utilizes the double resonance Lorentz model with parameters taken from Table 4.1.1. | 184 |

List of Figures

| | | |
|--------------|--|----|
| Figure 2.2.1 | Schematic diagram of an unknown isolated current source imbedded within the dielectric medium somewhere within the range $z < Z $. The current source is the sole source of the electromagnetic energy propagating in the region $z > Z $. However, the electromagnetic field behavior is only prescribed on the planar boundary $z = z_0$ which serves as a boundary condition and acts as a pseudo-source for <i>Maxwell's</i> equations in the source-free half space $z > z_0$ | 39 |
| Figure 2.3.1 | Index of refraction data for a fluoride (CLAP) glass plotted along with the complex <i>Levenberg–Marquardt</i> nonlinear least-squares fit of the double resonance Lorentz model with the numerically determined Lorentz model parameters $\epsilon_1 = 1.9938$, $\omega_0 = 1.7412 \times 10^{14} \text{Hz}$, $b_0 = 1.2155 \times 10^{14} \text{Hz}$, $\delta_0 = 4.9555 \times 10^{13} \text{Hz}$, $\omega_2 = 9.1448 \times 10^{15} \text{Hz}$, $b_2 = 6.7198 \times 10^{15} \text{Hz}$, $\delta_2 = 1.4341 \times 10^{15} \text{Hz}$ | 49 |
| Figure 2.3.2 | Error of the <i>Levenberg–Marquardt</i> nonlinear least-squares fit of the double resonance Lorentz model parameters to the index of refraction data for a fluoride (CLAP) glass with the found Lorentz model parameters $\epsilon_1 = 1.9938$, $\omega_0 = 1.7412 \times 10^{14} \text{Hz}$, $b_0 = 1.2155 \times 10^{14} \text{Hz}$, $\delta_0 = 4.9555 \times 10^{13} \text{Hz}$, $\omega_2 = 9.1448 \times 10^{15} \text{Hz}$, $b_2 = 6.7198 \times 10^{15} \text{Hz}$, $\delta_2 = 1.4341 \times 10^{15} \text{Hz}$ | 51 |
| Figure 2.4.1 | If \mathbf{c}_1 is expressible in polar form, then the vector \mathbf{a}_1 is orthogonal to both vectors \mathbf{b}_2 and \mathbf{a}_2 | 54 |
| Figure 2.5.1 | The first sheet of the Riemann surface and its range. The sheet divides into two distinct regions depending on the sign of the real-valued frequency ω as indicated by the differently shaded areas. | 60 |
| Figure 2.5.2 | An example of an inhomogeneous plane wave phase front propagating in the direction specified by the propagation vector. The attenuation vector is directed along the positive w -axis. The quantities δ , ζ and ξ represent the direction cosines for the propagation vector. | 62 |
| Figure 2.5.3 | Frequency dependence of the normalized magnitude of the energy transport velocity of a monochromatic plane wave for a double resonance Lorentz model of a fluoride glass (CLAP) with Lorentz model parameters taken from Table 2.3.1. | 69 |
| Figure 3.1.1 | Planar interface separating two lossy, dispersive half-spaces with complex refractive n_1 for the medium of incidence and n_2 for the medium of transmittance. | 83 |
| Figure 3.1.2 | The longitudinal component of the complex wavevector originates at the complex point $\bar{k}_1(\omega)$ for some real-valued frequency ω when $k_T=0$ and follows the indicated curve as the transverse spatial frequency k_T increases. A family of such curves is generated as the frequency ω changes. The sign of $\Re(\bar{k}_1(\omega))$ directly corresponds to the sign of the frequency ω . The imaginary part of $\gamma_i(\omega)$ is always positive. As the curve crosses the dashed line $\text{re}^{-\frac{1}{2}\pi/4}$, + for $\omega > 0$ and – for $\omega < 0$, $\gamma_i(\omega)$ becomes predominantly imaginary. As $k_T \rightarrow \infty$, $\gamma_i(\omega)$ asymptotically approaches the positive imaginary axis. | 86 |
| Figure 3.1.3 | The incident inhomogeneous plane wave field and complex wavevector are specified in relation to the incident local coordinate system. The w -axis is oriented at an angle Θ_i with respect to the interface normal. The origin of the incident local coordinate system is situated a distance w_0 away from the interface along the w -axis. The origin for the x, y, z coordinate system of the interface is defined at the point where the w -axis intersects the interface. The out of plane vector tangential to the interface is taken to be coincident with the out of plane incident local vector. | 90 |

List of Figures

| | | |
|---------------|---|-----|
| Figure 3.1.4 | The propagation and attenuation vectors in the interface coordinate system given in spherical coordinates. Notice that the attenuation vector only requires an elevation angle. | 94 |
| Figure 3.1.5 | The incident, reflected and transmitted fields and complex wavevectors are defined in their respective incident, reflected and transmitted local coordinate systems. The w' -axis and the w'' -axis make the angles $\pi - \theta_r$ and θ_t , respectively with respect to the interface normal. | 97 |
| Figure 3.1.6 | Geometry for the derivation of the tangential boundary conditions for an arbitrarily shaped boundary separating two dielectric media. A rectangle is situated between the two media and its surface area is shrunk to zero while holding its perimeter at a non-zero length. | 100 |
| Figure 3.1.7 | Geometry for the derivation of the normal boundary condition for an arbitrarily shaped boundary separating two dielectric media. | 102 |
| Figure 3.1.8 | Diagram of the β -plane of incidence, which contains the incident, reflected, and transmitted propagation vectors and also the interface normal vector. The transmitted propagation vector is not shown in order to reduce clutter. | 107 |
| Figure 3.1.9 | Diagram of the α -plane of incidence, which contains the incident, reflected, and transmitted attenuation vectors and also the interface normal vector. | 108 |
| Figure 3.1.10 | Geometry of the inhomogeneous plane wave reflection and refraction at a planar interface separating two lossy, dispersive dielectric half-spaces when the α -plane of incidence is coplanar with the β -plane of incidence. | 125 |
| Figure 4.1.1 | The complex refractive index for both the medium of incidence (solid lines) and the medium of transmittance (dashed lines) using the double resonance Lorentz model with parameters taken from Table 4.1.1. | 147 |
| Figure 4.1.2 | The complex refractive index for both the medium of incidence (solid lines) and the medium of transmittance (dashed lines) using the double resonance Lorentz model with parameters taken from Table 4.1.2. | 148 |
| Figure 4.2.1 | Plot of the transmitted normal complex wavenumber squared as a function of the angle of the incident local coordinate system for the fixed frequencies a) 174 THz and b) 933 THz for a homogeneous plane wave incident upon the interface separating two lossy, dispersive media. | 157 |
| Figure 4.2.2 | Plot of the transmitted normal complex wavenumber as a function of the angle of the incident local coordinate system for the fixed frequencies a) 174 THz and b) 933 THz for a homogeneous plane wave incident upon the interface separating two lossy, dispersive media. | 158 |
| Figure 4.3.1 | Plots of the a) real part and b) magnitude of the isotropic generalized <i>Fresnel</i> reflection coefficient for the TM mode as a function of the angle of the incident local coordinate system. Homogeneous plane waves are incident upon the interface separating two lossy, dispersive media. This example represents lossless media where the values of the dielectric permittivity are taken from Table 4.1.1. | 169 |
| Figure 4.3.2 | a) Three and b) two dimensional plots of the real part of the isotropic generalized <i>Fresnel</i> reflection coefficient for the TM mode as a function of the angle of the incident local coordinate system and frequency ω as indicated. Homogeneous plane waves are incident upon the interface separating two lossy, dispersive media. This example utilizes the double resonance Lorentz model with parameters taken from Table 4.1.1. | 171 |

List of Figures

| | | |
|--------------|---|-----|
| Figure 4.3.3 | a) Three and b) two dimensional plots of magnitude of the isotropic generalized <i>Fresnel</i> reflection coefficient for the TM mode as a function of the angle of the incident local coordinate system and frequency ω as indicated. Homogeneous plane waves are incident upon the interface separating two lossy, dispersive media. This example utilizes the double resonance Lorentz model with parameters taken from Table 4.1.1. | 172 |
| Figure 4.3.4 | a) Three and b) two dimensional plots of the real part of the isotropic generalized <i>Fresnel</i> reflection coefficient for the TM mode as a function of the angle of the incident local coordinate system and frequency ω as indicated. Homogeneous plane waves are incident upon the interface separating two lossy, dispersive media. This example utilizes the double resonance Lorentz model with parameters taken from Table 4.1.2. | 173 |
| Figure 4.3.5 | a) Three and b) two dimensional plots of the real part of the isotropic generalized <i>Fresnel</i> reflection coefficient for the TM mode as a function of k_u and frequency ω as indicated. Inhomogeneous plane waves are incident upon the interface separating two lossy, dispersive media. The angle of the incident local coordinate system is fixed at $\Theta_i = 50^\circ$. This example utilizes the double resonance Lorentz model with parameters taken from Table 4.1.1. | 178 |
| Figure 4.3.6 | a) Three and b) two dimensional plots of magnitude of the isotropic generalized <i>Fresnel</i> reflection coefficient for the TM mode as a function of k_u and frequency ω as indicated. Inhomogeneous plane waves are incident upon the interface separating two lossy, dispersive media. The angle of the incident local coordinate system is fixed at $\Theta_i = 50^\circ$. This example utilizes the double resonance Lorentz model with parameters taken from Table 4.1.1. | 179 |
| Figure 4.3.7 | a) Three and b) two dimensional plots of the real part of the isotropic generalized <i>Fresnel</i> reflection coefficient for the TM mode as a function of k_u and frequency ω as indicated. Inhomogeneous plane waves are incident upon the interface separating two lossy, dispersive media. The angle of the incident local coordinate system is fixed at $\Theta_i = 20^\circ$. This example utilizes the double resonance Lorentz model with parameters taken from Table 4.1.1. | 180 |
| Figure 4.3.8 | Plots of the real part of the isotropic generalized <i>Fresnel</i> reflection coefficient for the TM mode as a function of k_u and frequency ω as indicated for the angle of the incident local coordinate system fixed at a) $\Theta_i = 10^\circ$ and a) $\Theta_i = 0^\circ$. Inhomogeneous plane waves are incident upon the interface separating two lossy, dispersive media. This example utilizes the double resonance Lorentz model with parameters taken from Table 4.1.1. | 181 |
| Figure 5.1.1 | Schematic diagram of an unknown isolated current source imbedded within the dielectric region $w < W $. The current source is solely responsible for the electromagnetic energy propagating in the region $w > W $. The electromagnetic field is known on the planar boundary $w = W_0$ which then serves as a pseudo-source term for the <i>Maxwell's</i> equations in the source-free half space $w > W_0$ | 188 |
| Figure 5.1.2 | The contour of integration in the complex k_w -plane. The shaded region indicates the Region of Convergence. | 193 |
| Figure 5.1.3 | Construction of the closed path of integration in the complex k_w -plane. | 196 |
| Figure 5.1.4 | The first sheet of the Riemann surface and the range of the longitudinal wavenumber γ given that the imaginary part of the frequency $a = 0$. The sheet divides into two distinct regions depending on the sign of the real-valued angular frequency ω' as indicated by the differently shaded areas. | 200 |

List of Figures

| | | |
|--------------|---|-----|
| Figure 5.2.1 | Planar interface separating two lossy, dispersive half spaces with complex refractive indexes n_1 for the incident medium and n_2 for the transmission medium. | 202 |
| Figure 5.2.2 | The incident, reflected and transmitted fields and complex wavevectors are defined on their respective incident, reflected and transmitted local coordinate systems. The w -axis, w' -axis and the w'' -axis are defined to make angles Θ_i , $\pi - \Theta_r$ and Θ_t , respectively with respect to the interface normal. | 205 |
| Figure 6.1.1 | Diagram of a finite section of a dielectric slab waveguide, depicting three separate and distinct dielectric regions: the substrate, core and cladding dielectric materials. The substrate and cladding are both semi-infinite slabs that are abutted to the core region. The core region is infinite in two directions (in y and z) but of a finite thickness (in x). In general, all three regions are composed of different dielectric materials and as a consequence have different dielectric constants at a given frequency. | 212 |
| Figure 6.2.1 | Two dimensional cross section of the dielectric slab waveguide, indicating the directions of the propagation vectors at a xy -plane in all three dielectric regions: the core, cladding and substrate. | 218 |
| Figure 6.2.2 | The region of cutoff is depicted as the shaded area. | 222 |
| Figure 6.2.3 | Two dimensional cross section of the dielectric slab waveguide, indicating the modal solution for either the planar phase front or the planar amplitude front. | 225 |

CHAPTER I
INTRODUCTION

1.1 Motivations and Applications

The study of pulsed electromagnetic beam wave propagation is fundamental to many applications of electromagnetic theory such as dielectric slab waveguides. A complete understanding of this phenomena permits accurate prediction of the shape and arrival time of a given pulse after it has travelled a certain distance through an optical transmission system. This includes an understanding of the dispersion characteristics of these optical transmission systems and the manner in which electromagnetic fields interact with a boundary surface.

The media through which an electromagnetic field propagates has certain dynamical properties that strongly influence the behavior of propagation. For optical systems, the most common type is dielectric media such as glass because of its low transmission loss at optical frequencies and the fact that near lossless guidance is easily attained at supercritical angles of incidence. The common physical properties of all dielectric media, other than vacuum, are loss and dispersion, whose frequency behavior is coupled through the *Kramers–Kronig* relations[1]. The physical processes involved in dispersion are well understood[2] (e.g. the infrared polarization mechanism and the ultraviolet electronic absorption mechanism), and the complicated manner in which they effect pulsed electromagnetic plane wave propagation in an infinitely extended medium has been extensively investigated using asymptotic techniques[3]. This mathematically rigorous research has provided a complete, accurate description of the transient phenomena associated with such fields and has provided a correct description of the signal velocity for ultrashort/ultrawideband electromagnetic pulses in a linear, homogenous, isotropic and temporally dispersive medium.

Most data communication systems utilize electromagnetic radiation in some specific frequency band to relay information from a transmitter to a receiver through a specified transmission system. High performance data communications depend on the quality, the data transmission rate of the transmitted signal and the fidelity of the transmitted signal. A transmission system achieves high fidelity by being tolerant of electromagnetic interference(EMI), radiative and internal losses, the external environment, system imperfections,

invasive monitoring (for security purposes), and distortion that is caused by dispersion after the signal has traveled some distance through the transmission system. A high data rate depends on the pulse's width, rise time, repetition rate, and the frequency bandwidth of the transmitting source. Optical laser systems offer an abundance of these four attributes. It is for this reason that the current trend in the communications industry is to establish a high performance communications network that utilizes the optical portion of the electromagnetic spectrum. Unfortunately, as the pulse width decreases and more importantly as the pulse rise time becomes shorter, the effects of dielectric loss and dispersion increase and dominate the entire dynamical field evolution in the ultrawideband/ultrashort pulse limit.

The most fundamental technological issue is that of determining the optimum transmission system for high performance optical communications. Utilization of the atmosphere as the transmission system would be desirable from an economical standpoint since many kilometers of cabling would not be necessary; however, Rayleigh scattering, diffraction, and the diurnal interference from the sun render the atmosphere inhospitable to high performance optical data communications. Consequently, a method of cabling or guiding must be used to properly employ optical data transmission for high speed communications. Optical waveguides conveniently provide this capability.

Optical waveguiding structures are capable of containing and guiding optical radiation in a well-controlled and predictable manner, thereby satisfying most of the restrictions imposed by fidelity. Optical waveguides are typically constructed from two types of dielectric media. The media with the greater refractive index forms the core of the waveguide while the cladding has a smaller refractive index which forms the surrounding outer layer. Optical containment can be achieved by the phenomenon of total internal reflection at the core/cladding interface. Because the guided fields are virtually inaccessible external to the core of the guiding structure, optical containment of radiation naturally alleviates radiative losses, invasive monitoring, EMI, and other external environmental effects. Internal losses have been overcome with the introduction of low-loss glass that is used in the manufacture of opti-

cal fibers. Additionally, the materials used are chemically tolerant to most solvents, so that dielectric optical waveguides may be used in chemically hostile areas, and are mechanically tolerant to smooth bending. Each of these assets was once a problem that needed to be overcome in order that dielectric optical communication systems would become a viable technology.

The modern history of dielectric optical waveguides began with the coining of the terms *fiber optics* by N. S. Kapany in 1956[4] and *integrated optics* by S. E. Miller in 1969[5]. Developments in fiber optics have been nearly continuous since its inception, with the world's first optical link being installed by the General Telephone Company on April 22, 1977[6]. Research in integrated optics, however, has been somewhat sporadic. This research has been spurred by developments in fibers and slowed by funding only to be stimulated again through extensive international exchanges[7]. Recently the use of both classes of dielectric waveguides has proliferated to such a degree that they are commonplace in everyday life, as exemplified by fiber optic telephone cables and the optoelectronic integrated circuits within commercially available compact disc (CD) players. Optical waveguides not only play a major role in the household, but also in the technology of relaying massive amounts of data between remote computers connected together by high-speed optical fiber networks, as well as in Opto-Electronic Integrated Circuits (OEIC) which are used as switching networks, repeaters for fibers and analog computers.

Improvements in the performance level of optical waveguides constitute a major portion of the current international research effort. Performance issues may be categorized under three main categories: material properties, signal characterization, and information bandwidth. Improvements in material purity may result in lower loss and lower dispersion. Improvements in the signal properties are characterized by less distortion and an increased control of shape in both space and time. Both are a consequence of the material properties and the electronics which initially produce the pulse and later condition the pulse. Improvements

in the information bandwidth result in an increased data rate and is a consequence of improved signal production and decreased material dispersion.

There is a trend to increase the information bandwidth of existing data networks in order to cope with an increased load that results from concurrently sending computer data, audio data and video data. If the information bandwidth is increased, then there must be an increase in data rate which, in turn, necessitates the production of shorter data pulses. As the data pulse width diminishes, the pulses eventually become both ultrashort (where the temporal width of the pulse approaches the period of the carrier) and ultrawideband (where the resultant bandwidth of an ultrashort pulse spreads over a large portion of the electromagnetic spectrum). Useful pulse widths in the foreseeable future for data communication systems are still far from the ultrashort/ultrawideband pulses that are considered here. Currently, the rate at which a state of the art network operates is limited by multiplex switching and repeater electronics[8]. However, it is inevitable that further research will provide a means to overcome these limitations. There are also other applications that do require such ultrashort/ultrawideband pulses, e.g. in femtosecond spectroscopy[9] and stroboscopic measurements of fast-flowing processes like chemical reactions.

The theory of idealized waveguiding structures that are comprised of ideal, lossless dielectrics is well understood and can be found in a variety of textbooks such as those authored by Marcuse[10] and Sodha and Ghatak[11]. However, dielectric waveguides that are comprised of realistic media, which are both lossy and dispersive, have yet to be considered in full detail. Consequently, an accurate description of both loss and dispersion of the complex refractive index must be included.

Many authors apply simplifying assumptions in an effort to make dispersive waveguide theory admissible to rather simple analytical solutions. However, all of these approaches become invalid as they approach the ultrawideband limit. These assumptions typically rely on both the low loss of the medium and on the small bandwidth of a slowly modulated signal.

The latter assumption is known as the quasimonochromatic approximation. This quasimonochromatic approximation enables one to use a truncated Taylor series expansion to model the material dispersion in the region of normal dispersion of the dielectric while the low loss approximation enables one to neglect the coupling of loss and dispersion. However, when the pulse envelope becomes extremely short, its bandwidth extends beyond the range of validity of the truncated Taylor series expansion and into the region of anomalous dispersion of the dielectric. This can result in an incorrect description of the pulse velocity as well as yielding noncausal results (i.e. an output preceding the input). Since, the bandwidth of ultrashort pulsed signals can extend over regions of anomalous dispersion where the material loss is no longer negligible, the coupled frequency dispersion of the material loss and dispersion can no longer be neglected to any acceptable degree of approximation. A rigorous theory of pulse propagation in optical waveguides that includes the coupled effects of loss and dispersion is currently nonexistent.

The ultimate goal of this general area of research is to obtain a rigorous description of ultrashort pulse propagation in dielectric waveguides. This entails understanding the dispersion characteristics of dielectric waveguides. Dielectric waveguide dispersion can be classified into three distinct groupings: intramodal, intermodal and material. Modal dispersion is inherent to guiding structures in general, whether or not material dispersion exists. In order for a wave to propagate in a repeating, self-sustaining pattern, certain eigenmode equations must be satisfied. Only a discrete set of solutions of these eigenvalue equations is allowed, each of which represents a guided mode. Each guided mode has its own distinct velocity which varies with frequency, thereby producing what is known as intramodal dispersion. The velocity also varies from mode to mode, and this produces what is known as intermodal dispersion. A rigorous incorporation of material dispersion into dielectric waveguide theory poses a rather formidable problem, since this entails coupling material dispersion with both types of modal dispersion. For example, adding loss implies a complex propagation vector and this causes an ambiguity of mode cutoff because there is no longer a

trenchant distinction between propagating and radiating modes. Both mode types will lose energy to both the cladding and the core media and thereby have the same general functional form.

1.2 Previous Research

Published research in the areas of dispersive pulse propagation and dielectric waveguides is widely varied and extensive. The present account only discusses the major works and attempts to categorize them into a minimum number of logical groups. The earliest attempt at the problem of dispersive wave propagation was made by Sir William Hamilton in which the concept of group velocity seems to have been first introduced[23]. Subsequently, Lord Rayleigh presented the distinction between the group and phase velocities that are associated with plane wave propagation[24][25].

Dispersive wave propagation analysis requires a model that represents the dispersive behavior of the medium. A classical atomistic model, known as the Lorentz model, was developed for this purpose over the years (as early as 1869 by *Maxwell* as footnoted by Paul Drude[26]) and culminated in Lorentz's work[27]–[30]. This model described a dielectric as an ensemble of independent charged particles each harmonically bound to a nucleus at a fixed site in the material which are driven by the local electric field. A simple, consistent development of the Lorentz theory is found in the introductory text by Wooten[31]. The importance of this classical model lies in the fact that it is causal and provides an adequate description of anomalous dispersion in lossy dielectrics from the infrared through the visible regions of the electromagnetic spectrum[20]–[22].

The earliest attempt to obtain an asymptotic description of dispersive signal propagation in a single resonance Lorentz model medium with a step-modulated scalar wave was made by Sommerfeld[32] and Brillouin[33][34]; a brief review of Brillouin's results appears in §7.11 of Jackson[1]. Their work demonstrated that the signal did not propagate with the group velocity in the region of anomalous dispersion, thereby demonstrating that the true

signal velocity was not given by the group velocity in general. Their asymptotic analysis clearly showed that the signal always arrived with a velocity less than or equal to the speed of light, c . Additionally the first description of the transient fields known as precursors was made. However, only a rough, qualitative description of the field evolution of these precursors was obtained. A close examination by Brillouin[33][34] of the complex phase function that was associated with the complex frequency behavior of a single resonance frequency Lorentz model of the refractive index was found to yield two sets of saddle points: a pair of distant saddle points that evolved in the high frequency domain above the medium absorption band and a pair of near saddle points that evolved in the low frequency domain near the origin and below the absorption band. The associated exact integral representation of the propagated field was then evaluated asymptotically for large propagation distances by the method of steepest descent through these saddle points. However, the unnecessary constraint imposed upon the deformed contour of integration by the method of steepest descent resulted in an erroneous description of the frequency dependence of the signal arrival at the associated signal velocity, which was partially corrected later on by Baerwald in 1930[35].

Oughstun et al. extended the accuracy of the asymptotic description of this problem by employing modern asymptotic techniques in an effort to provide a correct description of the signal velocity and also to provide an accurate description of the complete field evolution. The basic approach relies upon Olver's theorem which relaxes the condition on the deformed contour of integration through the saddle points[36]. Olver's theorem uses an Olver-type path[36] through the saddle points, instead of the steepest descents path, in order to obtain an asymptotic approximation of the propagation integral. By a careful application of this technique to the case of a simple resonance Lorentz model medium, an accurate description of the entire field evolution was obtained. This included a correct, quantitative description of the entire precursor evolution and signal arrival, the signal and energy velocities, and the resultant signal distortion from closed form analytic expressions[3].

Other mathematical techniques have also been proposed to solve this problem. One popular approach is to use a Taylor series approximation of the complex phase function[1][10][37][38][39]. The Taylor series approximation converts the Helmholtz wave equation into a high-order Schrödinger type equation, which has been well studied and solved in quantum mechanics by a technique in which the wave packet is described in terms of the moments of its complex envelope function[39]. A second technique, which also applies a Taylor series expansion of the complex phase function, utilizes a recursive method to solve a system of coupled first order differential equations[38][39]. Both of these methods are valid only in the quasimonochromatic (or slowly varying envelope) approximation if only the first few terms in the Taylor series expansion are retained, as is typically the case, and consequently yield noncausal results for ultrawideband signals[40]. Two other important analytic methods utilize ray techniques[41][42][43] as an alternate asymptotic approach to a solution. One ray technique, known as the direct-ray method[41], obtains the approximate solution of a class of partial differential equations with prescribed boundary or initial conditions. This is accomplished by assuming that the solution may be represented by an asymptotic series of a specific form which is then substituted into the partial differential equation that describes the wave propagation system. As a result, families of rays are introduced along which the functional terms of the assumed series satisfy ordinary differential equations which can then be solved by standard approaches. An alternate approach is provided by the space-time ray theory[42] which relies upon “the plotting of rays and dispersion surfaces along with the initial or boundary values of the field to demonstrate the propagation phenomena and develop the asymptotic representation”[12]. Both of these ray techniques are applicable only in certain situations. They are heuristic in origin, complicate the problem, and obscure any physical insight regarding the solution of the problem.

Finally, in addition to a straightforward application of the Fast Fourier Transform algorithm, purely numerical solutions have been developed with specific application to dispersive pulse propagation studies. These include the Hosono Inverse *Laplace* Transform algo-

rithm and the Finite Difference Time Domain[FDTD] technique. The latter approach provides a direct integration of *Maxwell's* equations[47] but suffers from numerically introduced dispersion due to the finite stepping procedure in time that it relies upon. The Hosono algorithm[44] provides a numerical integration of the associated propagation integral when expressed in the form of an inverse *Laplace* transform. The Hosono algorithm provides accurate results for ultrashort signals provided that it is carefully implemented. The application of this algorithm to ultrashort pulse propagation in a linear dispersive medium has been found to provide very accurate results which can then be used to confirm the asymptotic description[45][46]. Unfortunately there is currently no known error bound for either numerical approach. In any case, a purely numerical solution primarily serves as a verification for analytic results since they cannot offer any physical insight.

Dielectric waveguide structures of various geometries and refractive index profiles comprise the second category of previous research and have been thoroughly examined and presented in the open literature. Both integrated optics and fibers have been the central focus since they have the most practical application. Some of the earliest papers discussing the guided mode solution and applications of integrated optics were authored by Herwig Kogelnik[5] and P. K. Tien[48], both at Bell Telephone Laboratories. The paper by Kogelnik presents an extensive overview on the previous literature covering the history and the mathematical development of integrated optics. Many textbooks cover the same material and include the discussion of the solution to fibers[10][11]. The solution methods are widely varied, differing not only in approach but in accuracy and simplicity. Exact solutions have only been obtained for the simplest geometries of the slab waveguide[10] and the cylindrical fiber with infinite cladding[49]. The modal solution to other waveguide geometries and refractive index profiles may be obtained by using either well-known approximate analytical techniques or numerical techniques. The approximate analytical techniques used to solve the complicated geometrical problems with a continuous refractive index profile are typically based on either perturbation methods or variational methods[11]. These two techniques are useful

when a rigorous solution is not possible. In the perturbational approach, a reference waveguide solution, which must be known *a priori*, is used as a basis set. A small perturbation is then added to this known reference solution and the corresponding solution is found from an expectation value of the perturbation alone. This approach is limited since the number of rigorous solutions that are currently known is limited. An alternate approach which avoids this limitation is provided by the variational method. This method assumes a trial function that depends on certain parameters; the appropriate solution is then obtained by minimizing an energy relationship with respect to those parameters. The variational method overcomes the requirement of having any *a priori* knowledge of a reference solution, but the error is predetermined by the choice of trial function and its parameters. A Steepest Descent Approximation Theory (SDAT), which uses a quantum mechanical or Schrödinger-like equation to represent the Helmholtz wave equation[50], can be applied to both the perturbation and variation methods in order to make them amenable to a numerical calculation. The advantage of this approach is that the choice of either the reference solution or trial function is not limited to known functions, but can be a purely numerical choice which can then be optimized using the SDAT method. Both the approximate analytical and numerical techniques are restricted to a continuous variation of refractive index profile and are not applicable to a stepped index profile since the derivative of such a profile is infinite at the core/cladding interface.

The third important category of previous research is connected with the phenomena of the reflection and refraction of electromagnetic waves as described by the *Fresnel* equations. The most general physical situation for which these equations are known exactly is that of a planar interface when the incident medium is a vacuum and the transmitting medium is a lossy dielectric with a complex refractive index[2]. A well-developed paper that discussed the improved treatment of the *Fresnel* equations for the planar vacuum/lossy dielectric interface was recently published by M. A. B. Whitaker [51]. It is of considerable importance to this research to obtain a generalization of these equations to the situation in which both the

incident and transmitted media are both lossy dielectrics because the planar dielectric interface is fundamental to the slab waveguide problem.

Gitterman and Gitterman presented a thorough explanation of the transient refraction process when the medium in which the incident field propagates is a vacuum and the medium in which the transmitted field propagates is described by a single resonance Lorentz model dielectric[52]. They presented their results for a spatially bounded monochromatic signal. Their results depicted a similar precursor field and signal evolution as that obtained for a freely propagating wave with the additional angular spreading of the precursors upon oblique incidence. The steady-state portion of the field (i.e. the main signal) is refracted and reflected just as it would be for a non-modulated monochromatic signal. The angular spreading of the precursors upon refraction occurs because the refractive index varies as the frequency structure of each precursor changes. The first or Sommerfeld precursor's angle of refraction begins at the incident angle because the precursor's instantaneous frequency of oscillation begins at infinity where the dielectric permittivity equals that of vacuum. As the instantaneous angular frequency of the Sommerfeld precursor field chirps downward from its initial infinite frequency, the refractive index decreases, below that of vacuum, and the Sommerfeld precursor's angle of refraction sweeps away from the angle of incidence as it grows more oblique. The angle of refraction for the second or Brillouin precursor field begins at a value appropriate for a static field because the instantaneous angular frequency of oscillation of this precursor field begins at zero as the field amplitude builds up to its peak value. As the Brillouin precursor amplitude decreases from its peak value and begins to oscillate with an instantaneous frequency that chirps upward from zero, the Brillouin precursor's angle of refraction sweeps away from its static value towards the perpendicular and approaches the angle of refraction of the main signal at the input carrier frequency ω_c when ω_c is less than the medium resonance frequency. The reflected transient field was also considered by Gitterman and Gitterman, but only for the special case of a plasma model (a high frequency limiting case of the Lorentz model). The most significant difference between the

reflected and refracted fields was the delay time associated with the transient reflection. This delay time may be understood from a physical point of view as being due to the inertial reaction delay of the electrons and ions to the incident field in the sense that a reflected field cannot exist until there is an interaction of the incident field energy with the transmission medium.

Each of the phenomena discussed above are present in the problem of dispersive pulse propagation in dielectric waveguides that are constructed from lossy, dispersive media. As previously mentioned, dispersion in waveguides is manifested three ways: intermodal, intramodal and material. Intermodal and intramodal dispersion are inherent to dielectric waveguides. The two are a function of the geometry and refractive index profile. Material dispersion is a quality of all dielectrics and can only be controlled by processing techniques (e.g. by controlling the material purity during fabrication), varying composition and through appropriate material choices. Material dispersion has a dominant effect on intramodal dispersion and some effects can be minimized by a careful adjustment of the refractive index profile[53]. All three dispersion sources must be accounted for in a careful analysis of pulse propagation in dielectric waveguides.

An exact integral representation of the electromagnetic field vectors may be obtained for dispersive pulse propagation in a given waveguide that is comprised from two different dispersive dielectric materials. However, the analytic evaluation of the required integrations is intractable even if one assumes the simplest case of a single resonance Lorentz model dielectric and a slab waveguide configuration. Consequently, some approximations must be made. Many authors[10][11][54] have chosen to apply the same aforementioned numerical and heuristic analytic approaches solve this problem. However, these solutions do not include the coupled effects of frequency dependant loss and dispersion in the refractive index, and so they cannot predict the precursor field evolution which is of critical importance for ultrawideband/ultrashort pulses. Other authors[53][55][56] have included a nonlinear effect by adding a nonlinear term to the Schrödinger equation in the slowly varying envelope

approximation. This nonlinearity is a result of a high power density associated with the optical pulse. The increased power density is caused by pulse compression, which is needed to generate ultrashort pulses. Zhao and Bourkoff note that the third and fourth-order Taylor series approximations will not be adequate when pulse widths grow shorter than the present capabilities of current ultrashort pulsed laser systems[57].

1.3 Description of Methods and Results

A precise formulation of linear, causally dispersive dielectric slab waveguide theory is developed in this dissertation. This formulation fully accounts for the temporally dispersive behavior of the lossy waveguide medium and the vector nature of the electromagnetic fields. New and exact solutions of the reformulated waveguide eigenvalue equation are derived. The understanding gained here is important from a practical point of view because of the recent development of near femtosecond laser pulses[58] which may find use in optical fiber communication systems and optoelectronic devices and systems.

The double resonance Lorentz model accurately represents dielectric dispersion in the infrared to ultraviolet spectral region. Numerical computations are presented in this dissertation which utilize data taken from a commercially available glass to determine the appropriate parameter values for the double resonance Lorentz model. These glass data should be representative of the complex dielectric permittivity (i.e. the dispersion and absorption characteristics of the medium) of typical glass materials that are currently used in fiber and integrated optics systems.

Inhomogeneous plane waves result as general solutions to *Maxwell's* equations in an infinitely extended dielectric medium with a complex refractive index. Inhomogeneous plane waves have a complex wavevector whose real-part is the propagation vector and imaginary-part is the attenuation vector. The propagation vector describes the direction of propagation of the planar phase front and the attenuation vector describes the direction of propagation of the planar amplitude front. In general these vectors are not collinear.

Inhomogeneous plane waves are used to develop the generalized theory of reflection and refraction and the generalized *Fresnel* equations. Many new results are discovered which are not found in the lossless case. For example, total internal reflection is never achievable due to the loss terms. However, near total internal reflection is achievable in regions of low loss and supercritical angles of incidence. Another possibility is that no critical angle occurs even though the medium of incidence is optically denser than the medium of transmittance. This can happen when the loss of the medium of incidence is much greater than that of the medium of transmittance. It is also possible that the real-parts of the complex refractive indices switch from a normal optically dense to rare transition to the inverted optically rare to dense transition when going from the medium of incidence to the medium of transmittance within and about the regions of anomalous dispersion. These situations imply that certain spectral regions will never support near total internal reflection which is a necessary condition of guiding of electromagnetic energy. Lastly, even if an inhomogeneous plane wave is at supercritical angles of incidence, near total internal reflection may be lost when both the incident and transmitted inhomogeneous plane waves become primarily attenuative.

The theory of reflection and refraction of pulsed electromagnetic beam fields at a planar interface separating two lossy, dispersive dielectric media is also developed. Exact integral relationships are derived for both the reflected and transmitted fields within local coordinate systems. The basic elements of a pulsed electromagnetic beam field are inhomogeneous plane waves. These basic elements are summed by integrals that form the angular spectrum representation. Each of the inhomogeneous plane waves of this decomposition can be considered separately based on the an assumed linearity of the dielectric media.

The theory of reflection and refraction phenomena of pulsed electromagnetic beam fields at a planar interface is a crucial step in the development of the electromagnetic theory of dielectric slab waveguides. Dielectric slab waveguides inherently have two planar interfaces at which electromagnetic energy interacts forming guided modes. These guided modes are the sum of two inhomogeneous plane waves that solve certain eigenmode equations.

These modes are shown to be equivalent to an inhomogeneous plane wave that is repeatedly reflected from both planar interfaces such that every other reflection is identical.

The solution to the dielectric slab waveguide is an important canonical problem because it lays the groundwork for more complex problems of pulsed wave propagation in optical fiber optic systems and integrated optics. The dielectric slab waveguide contains all of the fundamental interrelations between the spatial and temporal properties of the field so that its solution will provide the physical intuition that is required to understand the behavior in more complex problems.

CHAPTER II

Fundamental Theory and Mathematical Preliminaries

In this chapter some mathematical preliminaries that are required to develop the fundamental theory of pulsed electromagnetic inhomogeneous plane wave propagation and pulsed electromagnetic beam field propagation are presented. The media considered here are homogeneous, isotropic, locally linear, temporally dispersive dielectrics. Media that possess electric conductivity will not be considered. The analysis here focuses on the source-free form of *Maxwell's* equations and the general inhomogeneous plane wave solutions in such simple, temporally dispersive media. In addition, since the general field solution is an inhomogeneous plane wave with both a complex wavevector and a complex vector amplitude, the properties of complex vectors are presented in this chapter. These properties delineate the distinction between the direction of phase front propagation and the direction of amplitude front propagation and permit the mathematical description and interpretation of the various polarization properties.

2.1 *Fourier and Laplace Transform Analysis*

An important method for solving the differential space-time form of *Maxwell's* equations is provided by either the *Fourier* or *Laplace* transform which take advantage of the linear aspect of both *Maxwell's* equations and the material response. Through the appropriate application of either transform technique, the first order linear differential *Maxwell's* equations become simple algebraic equations. These transformed equations may then be solved within the associated frequency domain. The appropriate inverse transform operations are then applied to the derived frequency domain solutions in order to obtain the space-time domain form of the solution.

2.1.1 The Temporal *Fourier–Laplace* Transform

The temporal *Fourier–Laplace* transform pair may be defined by the pair of equations[60]

$$\mathcal{A}(\mathbf{r}, \omega) \equiv \mathcal{L}\{\mathcal{A}(\mathbf{r}, t)\} = \int_{-\infty}^{\infty} \mathcal{A}(\mathbf{r}, t) e^{+i\omega t} dt, \quad (2.1.1a)$$

$$\mathcal{A}(\mathbf{r}, t) \equiv \mathcal{L}^{-1}\{A(\mathbf{r}, \omega)\} = \frac{1}{2\pi} \int_{C_\omega} A(\mathbf{r}, \omega) e^{-i\omega t} d\omega , \quad (2.1.1b)$$

provided that $\mathcal{A}(\mathbf{r}, t) \in \mathcal{L}^1$ and that the inverse temporal *Fourier–Laplace* transform given by Eq. (2.1.1b) is represented by the *Poisson* summation

$$\mathcal{A}(\mathbf{r}, t) \equiv \mathcal{L}^{-1}\{A(\mathbf{r}, \omega)\} = \lim_{\varepsilon \rightarrow 0} \left\{ \frac{1}{2\pi} \int_{C_\omega} e^{-\varepsilon|\omega|} A(\mathbf{r}, \omega) e^{-i\omega t} d\omega \right\} ,$$

when the transform is of the *Fourier* type. Here, ω is the temporal frequency variable and $A(\mathbf{r}, \omega)$ is known either as the temporal *Fourier–Laplace* transform or as the temporal frequency spectrum of $\mathcal{A}(\mathbf{r}, t)$. The function $\mathcal{A}(\mathbf{r}, t)$ is assumed to be analytic along the path of integration except at any finite jump discontinuities. As suggested by its name, the *Fourier–Laplace* transform behaves as a hybrid form of both the *Fourier* and *Laplace* transforms.

If the function $\mathcal{A}(\mathbf{r}, t) \in \mathcal{L}^1$ and the temporal behavior at any fixed position \mathbf{r} possesses neither an explicit beginning nor ending while remaining absolutely integrable, so that

$$\int_{-\infty}^{\infty} |\mathcal{A}(\mathbf{r}, t)| dt < M < \infty , \quad (2.1.2)$$

where M is a finite upper bound then $A(\mathbf{r}, \omega)$ exists and represents its *Fourier* transform[60]. These conditions also provide a sufficient condition[60] for the existence and uniqueness of the inverse *Fourier* transform in that $\mathcal{F}^{-1}\{\mathcal{F}\{\mathcal{A}(\mathbf{r}, t)\}\}$ equals $\mathcal{A}(\mathbf{r}, t)$ at any time t where $\mathcal{A}(\mathbf{r}, t)$ is continuous, or else it equals $\frac{1}{2}[\mathcal{A}(\mathbf{r}, t^-) + \mathcal{A}(\mathbf{r}, t^+)]$ wherever $\mathcal{A}(\mathbf{r}, t)$ has a finite jump discontinuity. A more physically realistic sufficiency condition states that the *Fourier* transform exists whenever the function $\mathcal{A}(\mathbf{r}, t)$ represents a physically realizable quantity[60]. For the *Fourier* transform, the contour of integration C_ω denotes the straight line path along the real axis in the complex ω -plane.

The *Laplace* transform applies to the function $\mathcal{A}(\mathbf{r}, t)$ if it vanishes for $t < 0$. In this case, it is unnecessary to state initial conditions for the function $\mathcal{A}(\mathbf{r}, t)$ at $t = 0^+$ because the function is explicitly defined for all time.¹ The *Laplace* transform of $\mathcal{A}(\mathbf{r}, t)$ with respect to the time t is defined here as

$$\mathcal{L}\{\mathcal{A}(\mathbf{r}, t)\} = \int_0^{\infty} \mathcal{A}(\mathbf{r}, t) e^{+i\omega t} dt, \quad (2.1.3)$$

which is simply a *Fourier* transform with complex ω that is taken over only the positive time interval². Let $\mathcal{A}'(\mathbf{r}, t)$ be another function of both position and time such that

$$\mathcal{A}(\mathbf{r}, t) = \mathcal{A}'(\mathbf{r}, t); \quad t > 0, \quad (2.1.4)$$

but which may not vanish for $t \leq 0$. The *Laplace* transform Eq. (2.1.3) may then be written as

$$\mathcal{L}\{\mathcal{A}(\mathbf{r}, t)\} = \int_{-\infty}^{\infty} u(t) \mathcal{A}'(\mathbf{r}, t) e^{+i\omega t} dt, \quad (2.1.5)$$

where $u(t) = 0$ for $t < 0$ and $u(t) = 1$ for $t > 0$ is the *Heaviside unit-step function*. It is then seen that, for real ω , the *Laplace* transform of $\mathcal{A}(\mathbf{r}, t)$ is equal to the *Fourier* transform of $u(t) \mathcal{A}'(\mathbf{r}, t)$, viz.

$$\mathcal{L}\{\mathcal{A}(\mathbf{r}, t)\} = \mathcal{F}_{\omega}\{u(t) \mathcal{A}'(\mathbf{r}, t)\}; \quad \text{for real } \omega, \quad (2.1.6)$$

where the subscript ω indicates that it is the *Fourier* transform variable. The inverse *Fourier* transform of Eq. (2.1.6) then yields

$$u(t) \mathcal{A}'(\mathbf{r}, t) = \mathcal{F}_{\omega}^{-1}\{\mathcal{L}\{\mathcal{A}(\mathbf{r}, t)\}\} \quad (2.1.7)$$

for real ω .

1. If the function was unknown prior to the turn-on time, then it would be necessary to include the temporal initial conditions. This distinction becomes important when the *Fourier-Laplace* transform operates on a temporal derivative.

2. See Oughstun and Sherman [59] pp. 53–56 for the source of this development.

For complex $\omega = \omega' + i\omega''$, where $\omega' = \Re\{\omega\}$ and $\omega'' = \Im\{\omega\}$, the *Laplace* transform given in Eq. (2.1.5) becomes

$$\begin{aligned}\mathcal{L}\{\mathcal{A}(\mathbf{r}, t)\} &= \int_{-\infty}^{\infty} [u(t)\mathcal{A}'(\mathbf{r}, t)e^{-\omega''t}]e^{+i\omega't}dt \\ &= \mathcal{F}_{\omega'}\{u(t)\mathcal{A}'(\mathbf{r}, t)e^{-\omega''t}\}.\end{aligned}\quad (2.1.8)$$

The inverse Fourier transform of Eq. (2.1.8) then yields

$$\begin{aligned}u(t)\mathcal{A}'(\mathbf{r}, t)e^{-\omega''t} &= \mathcal{F}_{\omega'}^{-1}\{\mathcal{L}\{\mathcal{A}(\mathbf{r}, t)\}\} \\ &= \frac{1}{2\pi} \int_{-\infty}^{\infty} \mathcal{L}\{\mathcal{A}(\mathbf{r}, t)\}e^{-i\omega't}d\omega',\end{aligned}\quad (2.1.9)$$

which may be rewritten as

$$\begin{aligned}u(t)\mathcal{A}'(\mathbf{r}, t) &= \frac{1}{2\pi} \int_{-\infty}^{\infty} \mathcal{L}\{\mathcal{A}(\mathbf{r}, t)\}e^{-i(\omega' + i\omega'')t}d\omega' \\ &= \frac{1}{2\pi} \int_{-\infty + i\omega''}^{\infty + i\omega''} \mathcal{L}\{\mathcal{A}(\mathbf{r}, t)\}e^{-i\omega t}d\omega \\ &= \frac{1}{2\pi} \int_{C_{\omega}} \mathcal{L}\{\mathcal{A}(\mathbf{r}, t)\}e^{-i\omega t}d\omega.\end{aligned}\quad (2.1.10)$$

Here C_{ω} is the straight line contour $\omega = \omega' + i\omega''$ with ω'' fixed and ω' ranging from $-\infty$ to $+\infty$. Since $\mathcal{A}(\mathbf{r}, t) = u(t)\mathcal{A}'(\mathbf{r}, t)$, Eqs. (2.1.1a,b) then define the *Laplace* transform pair relationship where $\mathcal{A}(\mathbf{r}, \omega)$ is the complex temporal frequency spectrum of $\mathcal{A}(\mathbf{r}, t)$ with $\omega = \omega' + i\omega''$. Notice that $\omega'' = \Im\{\omega\}$ plays a passive role in the *Laplace* transform operation since it remains constant in both the forward and inverse transformations. Nevertheless, its presence can be important because the factor $e^{-\omega''t}$ appearing in the integrand of the transformation Eq. (2.1.1a) may serve as a convergence factor when $\omega'' > 0$. In particular,

$$A(\mathbf{r}, \omega) = \int_0^{\infty} \mathcal{A}(\mathbf{r}, t) e^{-\omega'' t} e^{i\omega' t} dt, \quad (2.1.11)$$

is just the *Fourier* transform $\mathcal{F}_{\omega} \{ \mathcal{A}(\mathbf{r}, t) e^{-\omega'' t} \}$. The *Fourier* transform of $\mathcal{A}(\mathbf{r}, t)$ alone is

$$A(\mathbf{r}, \omega) = \int_0^{\infty} \mathcal{A}(\mathbf{r}, t) e^{+i\omega' t} dt, \quad (2.1.12)$$

which exists provided that $\mathcal{A}(\mathbf{r}, t)$ is absolutely integrable, viz. that the condition given in Eq. (2.1.2) is met. If $\mathcal{A}(\mathbf{r}, t)$ does not vanish properly at infinity then the absolute integration of $\mathcal{A}(\mathbf{r}, t)$ diverges and the existence of the *Fourier* transform $\mathcal{F}_{\omega} \{ \mathcal{A}(\mathbf{r}, t) \}$ is not guaranteed. However, if there exists a real number γ such that

$$\int_0^{\infty} |\mathcal{A}(\mathbf{r}, t) e^{-\gamma t}| dt < M < \infty, \quad (2.1.13)$$

where M is a finite, constant upper bound, then $\mathcal{A}(\mathbf{r}, t)$ is transformable for all $\omega'' \geq \gamma$ and its temporal frequency spectrum is given by the *Laplace* transform given in Eq. (2.1.1a); note that some authors refer to this as the one-sided *Laplace* transform[60]. The lower bound γ_a of all of the values of γ which satisfy the inequality in Eq. (2.1.13) is called the *abscissa of absolute convergence* for the function $\mathcal{A}(\mathbf{r}, t)$. The *region of convergence* is defined as any complex $\omega = \omega' + i\omega''$ satisfying $\omega'' \geq \gamma$. The complex frequency spectrum $A(\mathbf{r}, \omega)$ is analytic within the region of convergence. The contour C_{ω} is also known as the *Bromwich contour* which guarantees that the inverse *Laplace* transform given in Eq. (2.1.1b) uniquely determines $\mathcal{A}(\mathbf{r}, t)$ so long as C_{ω} denotes the straight line path given by $\omega = \omega' + ia$, with a being a real constant that resides within the region of convergence and where $\omega' \equiv \text{Re}(\omega)$ ranges from negative to positive infinity[62].

The temporal partial derivative and convolution integral are two important operations that the *Fourier–Laplace* transform operation itself will encounter when applied to the

source-free form of *Maxwell's* equations. The former situation is best illustrated by defining the function $\mathcal{A}(\mathbf{r}, t)$ as the temporal partial derivative of another function $\mathcal{U}(\mathbf{r}, t)$, so that

$$\mathcal{A}(\mathbf{r}, t) \equiv \frac{\partial}{\partial t} \mathcal{U}(\mathbf{r}, t) \quad . \quad (2.1.14)$$

The forward *Fourier-Laplace* transform given in Eq. (2.1.1a) operates on the function $\mathcal{A}(\mathbf{r}, t)$ as

$$A(\mathbf{r}, \omega) = \mathcal{L}\{\mathcal{A}(\mathbf{r}, t)\} = \int_{-\infty}^{\infty} \frac{\partial}{\partial t} \mathcal{U}(\mathbf{r}, t) e^{+i\omega t} dt \quad , \quad (2.1.15)$$

and integration by parts then yields

$$A(\mathbf{r}, \omega) = \mathcal{U}(\mathbf{r}, t) e^{+i\omega t} \Big|_{-\infty}^{\infty} - i\omega \int_{-\infty}^{\infty} \mathcal{U}(\mathbf{r}, t) e^{+i\omega t} dt \quad . \quad (2.1.16)$$

The integral in Eq. (2.1.16) is just the forward *Fourier-Laplace* transform $U(\mathbf{r}, \omega)$ of the function $\mathcal{U}(\mathbf{r}, t)$. The reality condition[60], which stipulates that a given signal must have finite energy, implies that at both the upper and lower limits of integration the signal must vanish when ω resides in the region of convergence, so that $\lim_{t \rightarrow -\infty} \left\{ \mathcal{U}(\mathbf{r}, t) e^{+i\omega t} \right\} = 0$ and $\lim_{t \rightarrow \infty} \left\{ \mathcal{U}(\mathbf{r}, t) e^{+i\omega t} \right\} = 0$. The *Fourier-Laplace* transform of a temporal partial derivative is then given by

$$A(\mathbf{r}, \omega) = \mathcal{L}\left\{ \frac{\partial}{\partial t} \mathcal{U}(\mathbf{r}, t) \right\} = -i\omega U(\mathbf{r}, \omega) \quad . \quad (2.1.17)$$

For the second special case of a convolution integral, consider the function $\mathcal{A}(\mathbf{r}, t)$ that is given by the convolution of $\mathcal{U}(\mathbf{r}, t)$ with $\hat{v}(t)$ as

$$\mathcal{A}(\mathbf{r}, t) \equiv \int_{-\infty}^{\infty} \hat{v}(t - \tau) \mathcal{U}(\mathbf{r}, \tau) d\tau \quad . \quad (2.1.18)$$

The forward *Fourier-Laplace* transform (2.1.1a) operates on the function $\mathcal{A}(\mathbf{r}, t)$ as

$$\begin{aligned}
A(\mathbf{r}, \omega) &= \int_{-\infty}^{\infty} \left\{ \int_{-\infty}^{\infty} \hat{v}(t - \tau) \mathcal{U}(\mathbf{r}, \tau) d\tau \right\} e^{+i\omega t} dt \\
&= \int_{-\infty}^{\infty} d\tau \mathcal{U}(\mathbf{r}, \tau) \left\{ \int_{-\infty}^{\infty} \hat{v}(t - \tau) e^{+i\omega t} dt \right\} .
\end{aligned}$$

The change of variable $\xi \equiv t - \tau$ then gives

$$A(\mathbf{r}, \omega) = \int_{-\infty}^{\infty} d\tau \mathcal{U}(\mathbf{r}, \tau) e^{+i\omega\tau} \left\{ \int_{-\infty}^{\infty} \hat{v}(\xi) e^{+i\omega\xi} d\xi \right\} . \quad (2.1.19)$$

The inner integral of Eq. (2.1.19) may be identified as the forward *Fourier–Laplace* transform $\tilde{v}(\omega)$ of $\hat{v}(t)$, so that

$$A(\mathbf{r}, \omega) = \tilde{v}(\omega) \int_{-\infty}^{\infty} \mathcal{U}(\mathbf{r}, \tau) e^{+i\omega\tau} d\tau . \quad (2.1.20)$$

Similarly, the integral appearing in Eq. (2.1.20) may be identified as the forward *Fourier–Laplace* transform $U(\mathbf{r}, \omega)$ of $\mathcal{U}(\mathbf{r}, \tau)$. The *Fourier–Laplace* transform of a convolution integral can then be expressed as

$$A(\mathbf{r}, \omega) = \mathcal{FL} \left\{ \int_{-\infty}^{\infty} v(t - \tau) \mathcal{U}(\mathbf{r}, \tau) d\tau \right\} = \tilde{v}(\omega) U(\mathbf{r}, \omega) , \quad (2.1.21)$$

so that the temporal *Fourier–Laplace* transform of the convolution integral is given by the product of the temporal spectra of the individual functions.

2.1.2 The Two Dimensional Spatial *Fourier* Transform

A two dimensional spatial *Fourier* transform pair may be defined by the pair of equations[60]

$$A(\mathbf{k}_T, z, \omega) \equiv \mathcal{F}_{2D}\{\mathcal{A}(\mathbf{r}, \omega)\} = \int_{-\infty}^{\infty} \int_{-\infty}^{\infty} \mathcal{A}(\mathbf{r}, \omega) e^{-i\mathbf{k}_T \cdot \mathbf{r}} dx dy , \quad (2.1.22a)$$

$$\mathcal{A}(\mathbf{r}, \omega) \equiv \mathcal{F}_{2D}^{-1}\{A(\mathbf{k}_T, z, \omega)\} = \frac{1}{(2\pi)^2} \int_{-\infty}^{\infty} \int_{-\infty}^{\infty} A(\mathbf{k}_T, z, \omega) e^{+i\mathbf{k}_T \cdot \mathbf{r}_T} dk_x dk_y, \quad (2.1.22b)$$

provided that $\mathcal{A}(\mathbf{r}, \omega) \in \mathcal{L}^1$ and that the two dimensional inverse spatial *Fourier* transform given by Eq. (2.1.22b) is represented by the *Poisson* summation

$$\mathcal{A}(\mathbf{r}, \omega) \equiv \mathcal{F}_{2D}^{-1}\{A(\mathbf{k}_T, z, \omega)\} = \lim_{\varepsilon \rightarrow 0} \left\{ \frac{1}{(2\pi)^2} \int_{-\infty}^{\infty} \int_{-\infty}^{\infty} e^{-\varepsilon r_T} A(\mathbf{k}_T, z, \omega) e^{+i\mathbf{k}_T \cdot \mathbf{r}_T} dk_x dk_y \right\}.$$

Here,

$$\mathbf{r}_T \equiv x\hat{x} + y\hat{y}, \quad (2.1.23)$$

is the transverse position vector, and

$$\mathbf{k}_T \equiv k_x\hat{x} + k_y\hat{y}, \quad (2.1.24)$$

is the transverse spatial frequency wavevector. The field $A(\mathbf{k}_T, z, \omega)$ is known as the two dimensional spatial *Fourier* transform or as the two dimensional spatial frequency spectrum of $\mathcal{A}(\mathbf{r}, \omega)$. If the function $\mathcal{A}(\mathbf{r}, \omega) \in \mathcal{L}^1$, for any value ω , so that

$$\int_{-\infty}^{\infty} |\mathcal{A}(\mathbf{r}, \omega)| dx dy < M < \infty,$$

where M is a finite upper bound then $A(\mathbf{k}_T, z, \omega)$ exists and represents its two dimensional spatial *Fourier* transform[60]. The two dimensional inverse spatial *Fourier* transform, written as $\mathcal{F}_{2D}^{-1}\{\mathcal{F}_{2D}[\mathcal{A}(\mathbf{r}, \omega)]\}$, equals $\mathcal{A}(\mathbf{r}, \omega)$ at any position \mathbf{r} where $\mathcal{A}(\mathbf{r}, \omega)$ is continuous.

The curl operation is operated on by the two dimensional spatial *Fourier* transform with the resultant equivalence

$$\mathcal{F}_{2D}\{\nabla \times \} \leftrightarrow \left[i\mathbf{k}_T, \frac{\partial}{\partial z} \hat{z} \right] \times \equiv \left(ik_x, ik_y, \frac{\partial}{\partial z} \right) \times \quad (2.1.25a)$$

while the divergence operation is operated on by the two dimensional spatial *Fourier* trans-

form with the resultant equivalence

$$\mathcal{F}_{2D}\{\nabla \cdot \} \leftrightarrow \left[i\mathbf{k}_T, \frac{\partial}{\partial z} \hat{z} \right] \cdot \equiv \left(ik_x, ik_y, \frac{\partial}{\partial z} \right) \cdot \quad (2.1.25b)$$

2.1.3 The One Dimensional Spatial *Laplace* Transform with Respect to the z -Dimension

A one-sided spatial *Laplace* transform pair in the z -variable may be defined by the pair of equations[60]

$$A(\mathbf{k}, \omega) \equiv \mathcal{L}\{\mathcal{A}(\mathbf{k}_T, z, \omega)\} = \int_{z_0}^{\infty} \mathcal{A}(\mathbf{k}_T, z, \omega) e^{-ik_z z} dz, \quad (2.1.26a)$$

$$\mathcal{A}(\mathbf{k}_T, z, \omega) \equiv \mathcal{L}^{-1}\{A(\mathbf{k}, \omega)\} = \frac{1}{2\pi} \int_C A(\mathbf{k}, \omega) e^{+ik_z z} dk_z, \quad (2.1.26b)$$

where

$$\mathbf{k} \equiv k_x \hat{x} + k_y \hat{y} + k_z \hat{z} \quad (2.1.27)$$

is the three-dimensional spatial frequency wavevector. The quantity $A(\mathbf{k}, \omega)$ is known as the one-sided spatial *Laplace* transform of $\mathcal{A}(\mathbf{k}_T, z, \omega)$. The following two conditions provide for the existence and uniqueness of the one-sided spatial *Laplace* transform: if, for any frequency ω and any transverse position \mathbf{r}_T , $\mathcal{A}(\mathbf{k}_T, z, \omega)$ is absolutely integrable

$$\int_{z_0}^{\infty} |\mathcal{A}(\mathbf{k}_T, z, \omega) e^{az}| dz < M < \infty, \quad (2.1.28)$$

where M is a finite uniform upper bound and where a is some real constant number and if $\mathcal{A}(\mathbf{k}_T, z, \omega)$ only possesses finite discontinuities, then $A(\mathbf{k}, \omega)$ exists and represents its *Laplace* transform. If a increases, assuming that the condition given in Eq. (2.1.28) remains valid, the resultant integral increases. As a continues to increase, eventually a limit is reached due to the inability of the term e^{az} to keep the integral bounded. This upper limit called γ_b is then related to the behavior of $\mathcal{A}(\mathbf{k}_T, z, \omega)$ for $z > z_0$. As long as $a < \gamma_b$

(known as the region of convergence[62]) then the integral in Eq. (2.1.28) converges. In terms of the one–sided spatial *Laplace* transform given in Eq. (2.1.26a), the real constant a represents the value taken by $\Im\{k_z\}$ which must reside within the region of convergence $\Im\{k_z\} < \gamma_b$ so that the integral appearing in Eq. (2.1.26a) converges. The quantity γ_b is sometimes referred to as the upper abscissa of convergence[62]. In this case, the lower abscissa of convergence is given by $\gamma_a = -\infty$ because the lower limit of integration in Eq. (2.1.26a) is finite. The integration contour C must be a *Bromwich contour* so that the inverse one–sided *Laplace* transform given in Eq. (2.1.26b) uniquely determines $\mathcal{A}(\mathbf{k}_T, z, \omega)$ [62]. The *Bromwich contour* denotes the straight line path given by $k_z = -\infty + ia$ to $k_z = \infty + ia$ with a being a real constant that resides within the region of convergence $-\infty < a < \gamma_b$. The definition of the integration contour C as the *Bromwich contour* implies that $\mathcal{L}^{-1}\{\mathcal{L}\{\mathcal{A}(\mathbf{k}_T, z, \omega)\}\}$ equals $\mathcal{A}(\mathbf{k}_T, z, \omega)$ wherever $\mathcal{A}(\mathbf{k}_T, z, \omega)$ is continuous, or else it equals $\frac{1}{2}[\mathcal{A}(\mathbf{k}_T, z^+, \omega) + \mathcal{A}(\mathbf{k}_T, z^-, \omega)]$ wherever $\mathcal{A}(\mathbf{k}_T, z, \omega)$ has a finite jump discontinuity.

The one–sided spatial *Laplace* transform of the spatial derivative with respect to z is best illustrated by defining the function $\mathcal{A}(\mathbf{k}_T, z, \omega)$ as a spatial partial derivative of another function $\mathcal{U}(\mathbf{k}_T, z, \omega)$ as

$$\mathcal{A}(\mathbf{k}_T, z, \omega) \equiv \frac{\partial}{\partial z} \mathcal{U}(\mathbf{k}_T, z, \omega) . \quad (2.1.29)$$

The forward one–sided spatial *Laplace* transform (2.1.26a) operates on the function $\mathcal{A}(\mathbf{k}_T, z, \omega)$ as

$$\mathcal{A}(\mathbf{k}, \omega) = \mathcal{L}\{\mathcal{U}(\mathbf{k}_T, z, \omega)\} = \int_{z_0}^{\infty} \frac{\partial}{\partial z} \mathcal{U}(\mathbf{k}_T, z, \omega) e^{-ik_z z} dz , \quad (2.1.30)$$

and integration by parts then yields

$$A(\mathbf{k}, \omega) = \mathcal{U}(\mathbf{k}_T, z, \omega) e^{-ik_z z} \Big|_{z_0}^{\infty} + ik_z \int_{z_0}^{\infty} \mathcal{U}(\mathbf{k}_T, z, \omega) e^{-ik_z z} dz . \quad (2.1.31)$$

The integral appearing in Eq. (2.1.31) is the forward one-sided spatial *Laplace* transform $U(\mathbf{k}, \omega)$ of the function $\mathcal{U}(\mathbf{k}_T, z, \omega)$. The condition given in Eq. (2.1.28) stipulates that $\lim_{z \rightarrow \infty} \{\mathcal{U}(\mathbf{k}_T, z, \omega) e^{-ik_z z}\} = 0$. The forward one-sided spatial *Laplace* transform of a partial spatial derivative can then be written as

$$A(\mathbf{k}, \omega) = \mathcal{L} \left\{ \frac{\partial}{\partial z} \mathcal{U}(\mathbf{k}_T, z, \omega) \right\} = ik_z U(\mathbf{k}, \omega) - \mathcal{U}(\mathbf{k}_T, z_0, \omega) e^{-ik_z z_0} . \quad (2.1.32)$$

2.2 *Maxwell's* Field Equations in a Lossy, Dispersive Dielectric

The formulation of the problem has its origin in the macroscopic *Maxwell's* equations together with the proper constitutive (or material) relations that are appropriate for a linear, homogeneous, isotropic, locally linear, temporally dispersive dielectric. Throughout this thesis both Gaussian and MKS units are employed through use of a double bracket notation in each effected equation. If the quantity * appearing in the double brackets $\|\ast\|$ is included in the particular equation, then that equation is in Gaussian (or cgs) units where $\epsilon_0 = 1$ and $\mu_0 = 1$, whereas if that quantity is replaced by unity then that equation is in MKS units. Equations with no double bracketed quantities are valid in either system of units. The equivalency

$$\left\| \frac{1}{c} \right\| \sqrt{\mu_0 \epsilon_0} = \frac{1}{c} , \quad (2.2.1)$$

is found to be a useful relationship between the Gaussian and MKS unit systems.

2.2.1 Space-Time Domain Form of the Field Equations

Maxwell's equations for the macroscopic electromagnetic field vectors in a linear, causal, spatially and temporally homogeneous, isotropic, spatially locally linear and temporally dispersive medium are given by[1]

$$\nabla \times \mathfrak{E}(\mathbf{r}, t) = -\left\|\frac{1}{c}\right\| \frac{\partial}{\partial t} \mathfrak{B}(\mathbf{r}, t) , \quad (2.2.2a)$$

$$\nabla \times \mathfrak{H}(\mathbf{r}, t) = \left\|\frac{4\pi}{c}\right\| \mathfrak{J}(\mathbf{r}, t) + \left\|\frac{1}{c}\right\| \frac{\partial}{\partial t} \mathfrak{D}(\mathbf{r}, t) , \quad (2.2.2b)$$

$$\nabla \cdot \mathfrak{D}(\mathbf{r}, t) = \left\|4\pi\right\| \varrho(\mathbf{r}, t) , \quad (2.2.2c)$$

$$\nabla \cdot \mathfrak{B}(\mathbf{r}, t) = 0 . \quad (2.2.2d)$$

Here, $\mathfrak{E}(\mathbf{r}, t)$ and $\mathfrak{H}(\mathbf{r}, t)$ denote the electric and magnetic field intensity vectors, respectively, $\mathfrak{D}(\mathbf{r}, t)$ represents the electric displacement vector and $\mathfrak{B}(\mathbf{r}, t)$ represents the magnetic induction vector. The remaining two quantities, $\mathfrak{J}(\mathbf{r}, t)$ and $\varrho(\mathbf{r}, t)$, represent the total macroscopic conduction current density vector and the scalar charge density. For a complete description of the electromagnetic field within a ponderable medium, three types of macroscopic response functions of the medium must be defined: the dielectric response, the magnetic response and the conductivity response. Together these three medium response functions form the set of constitutive relations. They are defined for ponderable media that possesses the attributes of being linear, causal, spatially and temporally homogeneous, isotropic, spatially locally linear and temporally dispersive[21] as

$$\mathfrak{D}(\mathbf{r}, t) = \int_{-\infty}^t \hat{\varepsilon}(t-\tau) \mathfrak{E}(\mathbf{r}, \tau) d\tau , \quad (2.2.3a)$$

$$\mathfrak{B}(\mathbf{r}, t) = \int_{-\infty}^t \hat{\mu}(t-\tau) \mathfrak{H}(\mathbf{r}, \tau) d\tau , \quad (2.2.3b)$$

$$\mathfrak{J}(\mathbf{r}, t) = \mathfrak{J}_0(\mathbf{r}, t) + \int_{-\infty}^t \hat{\sigma}(t-\tau) \mathfrak{E}(\mathbf{r}, \tau) d\tau . \quad (2.2.3c)$$

Here, $\hat{\varepsilon}(t)$ represents the dielectric permittivity response function, $\hat{\mu}(t)$ represents the magnetic permeability response function and $\hat{\sigma}(t)$ represents the conductivity response function of the material, and $\mathfrak{J}_0(\mathbf{r}, t)$ denotes the current density solely due to the exciting current source. The three functions $\hat{\varepsilon}(t)$, $\hat{\mu}(t)$ and $\hat{\sigma}(t)$ contain all the information about the manner

in which the medium responds to the applied electromagnetic field vectors $\mathfrak{E}(\mathbf{r}, t)$ and $\mathfrak{H}(\mathbf{r}, t)$. In addition, the requirement of causality[1] requires that each response $\hat{\epsilon}(t)$, $\hat{\mu}(t)$ and $\hat{\sigma}(t)$ function must be identically zero for all time $t < 0$, as indicated by the upper limit of integration in the constitutive relations given in Eqs. (2.2.3a–c).

2.2.2 Space–Time Domain Form of the Source Free Field Equations in Dielectric Media

This research deals with electromagnetic wave propagation within general optical materials (such as glass), which implies that the materials of interest are nonmagnetic. Nonmagnetic materials possess a magnetic permeability response function that is nonhysteretic, so that

$$\hat{\mu}(t) = \mu\delta(t) \quad , \quad (2.2.4)$$

where μ is the constant scalar magnetic permeability. With this substitution, the constitutive relation given in Eq. (2.2.3b) becomes

$$\mathfrak{B}(\mathbf{r}, t) = \mu \int_{-\infty}^t \delta(t-\tau)\mathfrak{H}(\mathbf{r}, \tau)d\tau = \mu\mathfrak{H}(\mathbf{r}, t) \quad . \quad (2.2.5)$$

The dielectric materials examined in this research are considered ideal dielectrics in the sense that they possess no conductive loss mechanisms. Conductivity is generally a low frequency phenomenon and consequently has negligible influence on optical signals as considered within the context of this current work. The conductivity response function for an ideal dielectric is then given by

$$\hat{\sigma}(t) = 0 \quad . \quad (2.2.6)$$

The vector $\mathfrak{J}(\mathbf{r}, t)$ appearing in Eq. (2.2.2b) denotes the total macroscopic current density due to both conduction currents and an externally supplied current source $\mathfrak{J}_0(\mathbf{r}, t)$. In any source free, nonconducting medium the constitutive relation given in Eq. (2.2.3c) becomes

$$\mathfrak{J}(\mathbf{r}, t) = \mathbf{0} \quad . \quad (2.2.7)$$

This relation is always satisfied in a passive waveguide, and so is valid throughout this research. The equation of continuity (which follows from the divergence of Eq. (2.2.2b) and the time derivative of Eq. (2.2.2c))

$$\nabla \cdot \mathfrak{J} + \frac{\partial \varrho}{\partial t} = 0 \quad , \quad (2.2.8)$$

then yields the simple differential equation $\frac{\partial \varrho}{\partial t} = 0$, so that if ϱ is zero at any time in the infinite past, then

$$\varrho(\mathbf{r}, t) = 0 \quad (2.2.9)$$

for all time.

The source-free form of *Maxwell's* equations for optical dielectric media are then given by

$$\nabla \times \mathfrak{E}(\mathbf{r}, t) = -\left\| \frac{1}{c} \right\| \frac{\partial}{\partial t} \mathfrak{B}(\mathbf{r}, t) \quad , \quad (2.2.10a)$$

$$\nabla \times \mathfrak{H}(\mathbf{r}, t) = \left\| \frac{1}{c} \right\| \frac{\partial}{\partial t} \mathfrak{D}(\mathbf{r}, t) \quad , \quad (2.2.10b)$$

$$\nabla \cdot \mathfrak{D}(\mathbf{r}, t) = 0 \quad , \quad (2.2.10c)$$

$$\nabla \cdot \mathfrak{B}(\mathbf{r}, t) = 0 \quad , \quad (2.2.10d)$$

with the constitutive relations

$$\mathfrak{D}(\mathbf{r}, t) = \int_{-\infty}^t \hat{\varepsilon}(t - \tau) \mathfrak{E}(\mathbf{r}, \tau) d\tau \quad , \quad (2.2.11a)$$

$$\mathfrak{B}(\mathbf{r}, t) = \mu \mathfrak{H}(\mathbf{r}, t) \quad , \quad (2.2.11b)$$

which are appropriate for any dielectric that is nonmagnetic, nonconducting, source-free, linear, causal, spatially and temporally homogeneous, isotropic, spatially locally linear and temporally dispersive, which will be hereafter referred to as a simple dispersive dielectric. Here $\hat{\varepsilon}(t - \tau)$ denotes the real-valued dielectric permittivity response function of the general dispersive medium. By causality, $\hat{\varepsilon}(t - \tau) = 0$ for $t < \tau$, as exhibited in the upper limit

of integration in the constitutive relation given in Eq. (2.2.11a)³. It should be noted that the field vectors $\mathfrak{D}(\mathbf{r}, t)$ and $\mathfrak{B}(\mathbf{r}, t)$ are solenoidal as a direct consequence of the divergence relations given in Eqs. (2.2.10 c,d).

2.2.3 Temporal Frequency Domain Form of the Field Equations

With the results of §2.1.1 appropriately generalized to apply to vector fields, the *Fourier-Laplace* transform of the source-free form of *Maxwell's* equations given in Eqs. (2.2.10a–d) yields the set of temporal frequency domain relations

$$\nabla \times \mathbf{E}(\mathbf{r}, \omega) = \left\| \frac{1}{c} \right\| i\omega \mathbf{B}(\mathbf{r}, \omega) , \quad (2.2.12a)$$

$$\nabla \times \mathbf{H}(\mathbf{r}, \omega) = -\left\| \frac{1}{c} \right\| i\omega \mathbf{D}(\mathbf{r}, \omega) , \quad (2.2.12b)$$

$$\nabla \cdot \mathbf{D}(\mathbf{r}, \omega) = 0 , \quad (2.2.12c)$$

$$\nabla \cdot \mathbf{B}(\mathbf{r}, \omega) = 0 , \quad (2.2.12d)$$

and the constitutive relations given in Eqs. (2.2.11a,b) take the form

$$\mathbf{D}(\mathbf{r}, \omega) = \tilde{\epsilon}(\omega) \mathbf{E}(\mathbf{r}, \omega) , \quad (2.2.13a)$$

$$\mathbf{B}(\mathbf{r}, \omega) = \mu \mathbf{H}(\mathbf{r}, \omega) . \quad (2.2.13b)$$

Here

$$\tilde{\epsilon}(\omega) \equiv \mathcal{L}\{\hat{\epsilon}(t)\} = \epsilon_r(\omega) + i\epsilon_i(\omega) \quad (2.2.14)$$

is the complex valued dielectric permittivity and the real-valued functions $\epsilon_r(\omega)$ and $\epsilon_i(\omega)$ represent the real and imaginary parts, respectively.

Since the dielectric permittivity response function $\hat{\epsilon}(t)$ is real-valued, by definition, its *Fourier-Laplace* transform $\tilde{\epsilon}(\omega)$ is subject to the restriction

$$\tilde{\epsilon}(\omega) = \tilde{\epsilon}^*(-\omega^*) , \quad (2.2.15)$$

so that $\tilde{\epsilon}(\omega)$ is Hermitian. This then implies that $\epsilon_r(\omega)$ is an even function and $\epsilon_i(\omega)$ is an odd function when the angular frequency ω is real-valued.

3. See Oughstun and Sherman [59] §2.1.

2.2.4 Poynting's Theorem and the Conservation of Energy

Energy flow and conservation of energy play an important part in the interpretation of electromagnetic field propagation. These interpretations can be obtained from direct manipulation of the temporal frequency domain form of *Maxwell's* equations. The general formulation of this problem begins by taking the scalar product of $\mathbf{E}(\mathbf{r}, \omega)$ with the complex conjugate of Eq. (2.2.12b), yielding

$$\mathbf{E}(\mathbf{r}, \omega) \cdot \nabla \times \mathbf{H}^*(\mathbf{r}, \omega) = \left\| \frac{1}{c} \right\| i\omega \mathbf{E}(\mathbf{r}, \omega) \cdot \mathbf{D}^*(\mathbf{r}, \omega) .$$

Similarly, taking the scalar product of $\mathbf{H}^*(\mathbf{r}, \omega)$ with Eq. (2.2.12a) yields

$$\mathbf{H}^*(\mathbf{r}, \omega) \cdot \nabla \times \mathbf{E}(\mathbf{r}, \omega) = \left\| \frac{1}{c} \right\| i\omega \mathbf{H}^*(\mathbf{r}, \omega) \cdot \mathbf{B}(\mathbf{r}, \omega) .$$

The difference between the two relations then yields the *differential form of Poynting's theorem*

$$\nabla \cdot [\mathbf{E}(\mathbf{r}, \omega) \times \mathbf{H}^*(\mathbf{r}, \omega)] = \left\| \frac{1}{c} \right\| i\omega [\mathbf{H}^*(\mathbf{r}, \omega) \cdot \mathbf{B}(\mathbf{r}, \omega) - \mathbf{E}(\mathbf{r}, \omega) \cdot \mathbf{D}^*(\mathbf{r}, \omega)] .$$

The *complex Poynting vector* $\mathbf{S}(\mathbf{r}, \omega)$ of the electromagnetic field is defined as

$$\mathbf{S}(\mathbf{r}, \omega) \equiv \frac{1}{2} \left\| \frac{c}{4\pi} \right\| [\mathbf{E}(\mathbf{r}, \omega) \times \mathbf{H}^*(\mathbf{r}, \omega)] , \quad (2.2.16)$$

which has the dimensional units of power per unit area. With this definition, the *differential form of Poynting's theorem* may then be written as

$$\nabla \cdot \mathbf{S}(\mathbf{r}, \omega) = 2i\omega [u_m(\mathbf{r}, \omega) - u_e(\mathbf{r}, \omega)] , \quad (2.2.17)$$

where the scalar quantities $u_e(\mathbf{r}, \omega)$ and $u_m(\mathbf{r}, \omega)$ are known as the *harmonic energy densities*[59] of the electric and magnetic fields (with dimensional units of energy per unit volume), defined by the relations

$$u_e(\mathbf{r}, \omega) \equiv \frac{1}{4} \left\| \frac{1}{4\pi} \right\| [\mathbf{E}(\mathbf{r}, \omega) \cdot \mathbf{D}^*(\mathbf{r}, \omega)] , \quad (2.2.18)$$

$$u_m(\mathbf{r}, \omega) \equiv \frac{1}{4} \left\| \frac{1}{4\pi} \right\| [\mathbf{H}^*(\mathbf{r}, \omega) \cdot \mathbf{B}(\mathbf{r}, \omega)] . \quad (2.2.19)$$

Integration of Eq. (2.2.17) over an arbitrary volume V bounded by a closed surface S and application of the divergence theorem yields the *integral form of Poynting's theorem*

$$\oint_S \oint \mathbf{S}(\mathbf{r}, \omega) \cdot \hat{\mathbf{n}} \, da = 2i\omega \int_V \int \int [u_m(\mathbf{r}, \omega) - u_e(\mathbf{r}, \omega)] \, d^3\mathbf{r} \, , \quad (2.2.20)$$

where $\hat{\mathbf{n}}$ is the outward unit normal vector to the closed surface S . The integral form of *Poynting's theorem* given in Eq. (2.2.20) is a rigorous consequence of *Maxwell's equations* and is therefore a self-consistent relationship within the framework of classical electrodynamics[59].

The physical interpretations of the quantities appearing in Eq. (2.2.20) depend to a certain degree on hypothesis[59]. The classical interpretation of the conservation of energy comes from the real part of the *integral form of Poynting's theorem*, viz.

$$-\oint_S \oint \Re\{\mathbf{S}(\mathbf{r}, \omega) \cdot \hat{\mathbf{n}}\} \, da = -2\omega \int_V \int \int \Im\{u_e(\mathbf{r}, \omega) - u_m(\mathbf{r}, \omega)\} \, d^3\mathbf{r} \, .(2.2.21)$$

As a consequence of this interpretation, the surface integral on the left-hand side of Eq. (2.2.21) is interpreted as the time time-averaged electromagnetic power flow into the region V across the boundary surface S , while the volume integral on the right-hand side of Eq. (2.2.21) is interpreted as the time-averaged rate of energy dissipated by the electromagnetic field the region V [59].

All media considered in this research are attenuative, which implies that the time-averaged power flow into any given region V across the boundary surface S must be positive for any non-zero field[59]. This then means that

$$-\omega \int_V \int \int \Im\{u_e(\mathbf{r}, \omega) - u_m(\mathbf{r}, \omega)\} \, d^3\mathbf{r} > 0 \, , \quad (2.2.22)$$

for all real, non-zero frequencies $\omega > 0$. The harmonic electric energy density $u_e(\mathbf{r}, \omega)$ together with the constitutive relation given in Eq. (2.2.13a) yields

$$u_e(\mathbf{r}, \omega) = \frac{1}{4} \left\| \frac{1}{4\pi} \right\| \left[\tilde{\epsilon}^*(\omega) \mathbf{E}(\mathbf{r}, \omega) \cdot \mathbf{E}^*(\mathbf{r}, \omega) \right] \, ,$$

so that the imaginary part gives

$$\Im\{u_e(\mathbf{r}, \omega)\} = -\frac{1}{4} \left\| \frac{1}{4\pi} \right\| \left[\varepsilon_i(\omega) |\mathbf{E}(\mathbf{r}, \omega)|^2 \right] .$$

Similarly, the harmonic magnetic energy density $u_m(\mathbf{r}, \omega)$ together with the constitutive relation given in Eq. (2.2.13b) yields

$$u_m(\mathbf{r}, \omega) = \frac{1}{4} \left\| \frac{1}{4\pi} \right\| \left[\mu |\mathbf{H}(\mathbf{r}, \omega)|^2 \right] ,$$

and since the magnetic permeability μ is pure real the imaginary part gives

$$\Im\{u_m(\mathbf{r}, \omega)\} = 0 .$$

Since the inequality appearing in Eq. (2.2.22) is valid over an arbitrary region and the magnitude of the electric field vector is positive, it then follows that

$$\omega \varepsilon_i(\omega) > 0 ,$$

for all real, non-zero frequencies $\omega > 0$. This condition then requires $\varepsilon_i(\omega)$ to be positive when the angular frequency ω is real-valued and positive, so that

$$\varepsilon_i(\omega) > 0 , \quad \forall \omega > 0 . \quad (2.2.23a)$$

In addition, since that $\varepsilon_i(\omega)$ is an odd function of the real-valued frequency ω [cf. §2.2.3], then

$$\varepsilon_i(\omega) < 0 , \quad \forall \omega < 0 . \quad (2.2.23b)$$

By continuity, it then follows that

$$\varepsilon_i(0) = 0 . \quad (2.2.23c)$$

2.2.5 Spatio-Temporal Frequency Domain Form of the Planar Boundary Value Problem for the Source-Free *Maxwell's* Equations

An electromagnetic field that propagates within a source free region of space originates from some isolated current source such as an antenna or a laser. If the behavior of an isolated current source $\mathfrak{J}_0(\mathbf{r}, t)$ is known, then the electromagnetic radiation produced can be expressed explicitly in terms of the source. However, the detailed structure of the current source is often not known and only the electromagnetic field structure (e.g. the mode pattern of a laser source) is known at a planar boundary some distance away from the true source.

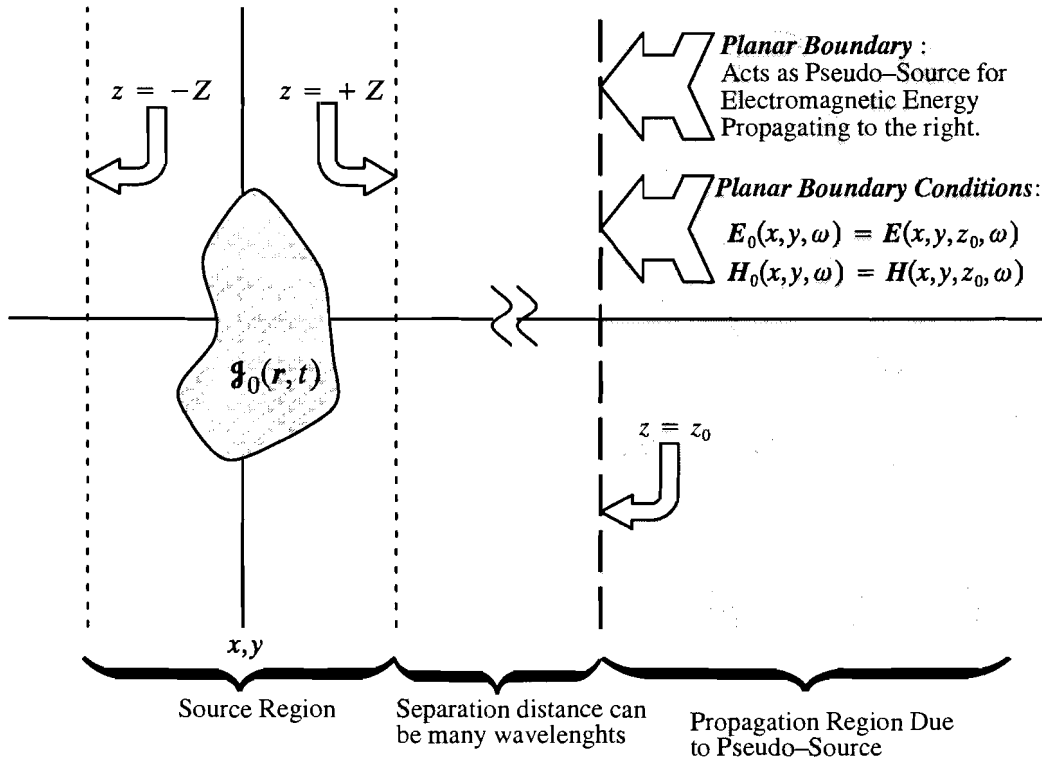


Figure 2.2.1 Schematic diagram of an unknown isolated current source imbedded within the dielectric medium somewhere within the range $z < |Z|$. The current source is the sole source of the electromagnetic energy propagating in the region $z > |Z|$. However, the electromagnetic field behavior is only prescribed on the planar boundary $z = z_0$ which serves as a boundary condition and acts as a pseudo-source for *Maxwell's equations* in the source-free half space $z > z_0$.

In this situation, one has a planar boundary value problem for *Maxwell's equations* that is valid in the region beyond the known planar boundary, as indicated schematically in Figure 2.2.1. The known planar boundary values act as a pseudo-source term that drives the electromagnetic fields which propagate to the right of that boundary.

Application of the two-dimensional spatial *Fourier* transform of the curl and divergence operators given in Eqs. (2.1.25a,b) to the temporal frequency domain form of the source-free form of *Maxwell equations* given in Eqs. (2.2.12a-d) yields the set of mixed space and spatio-temporal frequency relations

$$\left[ik_T \frac{\partial}{\partial z} \hat{z} \right] \times \mathbf{E}(\mathbf{k}_T, z, \omega) = \left\| \frac{1}{c} \right\| i\omega \mathbf{B}(\mathbf{k}_T, z, \omega), \quad (2.2.24a)$$

$$\left[ik_T \frac{\partial}{\partial z} \hat{z} \right] \times \mathbf{H}(\mathbf{k}_T, z, \omega) = -\left\| \frac{1}{c} \right\| i\omega \mathbf{D}(\mathbf{k}_T, z, \omega), \quad (2.2.24b)$$

$$\left[\mathbf{i}\mathbf{k}_T, \frac{\partial}{\partial z} \hat{\mathbf{z}} \right] \cdot \mathbf{D}(\mathbf{k}_T, z, \omega) = 0, \quad (2.2.24c)$$

$$\left[\mathbf{i}\mathbf{k}_T, \frac{\partial}{\partial z} \hat{\mathbf{z}} \right] \cdot \mathbf{B}(\mathbf{k}_T, z, \omega) = 0, \quad (2.2.24d)$$

and the constitutive relations given in Eqs. (2.2.13a,b) take the form

$$\mathbf{D}(\mathbf{k}_T, z, \omega) = \tilde{\epsilon}(\omega) \mathbf{E}(\mathbf{k}_T, z, \omega), \quad (2.2.25a)$$

$$\mathbf{B}(\mathbf{k}_T, z, \omega) = \mu \mathbf{H}(\mathbf{k}_T, z, \omega). \quad (2.2.25b)$$

The forward one-sided spatial *Laplace* transform, as defined in Eq. (2.1.26b), of *Faraday's Law* given in Eq. (2.2.24a) yields

$$\begin{aligned} \mathcal{L} \left\{ \left[\mathbf{i}\mathbf{k}_T, \frac{\partial}{\partial z} \hat{\mathbf{z}} \right] \times \mathbf{E}(\mathbf{k}_T, z, \omega) \right\} &= \int_{z_0}^{\infty} \left[\mathbf{i}\mathbf{k}_T, \frac{\partial}{\partial z} \hat{\mathbf{z}} \right] \times \mathbf{E}(\mathbf{k}_T, z, \omega) e^{-ikz} dz \\ &= \int_{z_0}^{\infty} \left\{ \left[ik_y E_z(\mathbf{k}_T, z, \omega) - \frac{\partial E_y(\mathbf{k}_T, z, \omega)}{\partial z} \right] \hat{\mathbf{x}} \right. \\ &\quad - \left[ik_x E_z(\mathbf{k}_T, z, \omega) - \frac{\partial E_x(\mathbf{k}_T, z, \omega)}{\partial z} \right] \hat{\mathbf{y}} \\ &\quad \left. + \left[ik_x E_y(\mathbf{k}_T, z, \omega) - ik_y E_x(\mathbf{k}_T, z, \omega) \right] \hat{\mathbf{z}} \right\} e^{-ikz} dz. \quad (2.2.26) \end{aligned}$$

Application of the transform of a partial spatial derivative given in Eq. (2.1.32) to Eq. (2.2.26) then yields

$$\begin{aligned} \mathcal{L} \left\{ \left[\mathbf{i}\mathbf{k}_T, \frac{\partial}{\partial z} \hat{\mathbf{z}} \right] \times \mathbf{E}(\mathbf{k}_T, z, \omega) \right\} &= [ik_y E_z(\mathbf{k}, \omega) - ik_z E_y(\mathbf{k}, \omega)] \hat{\mathbf{x}} + E_{y_0}(\mathbf{k}_T, \omega) e^{-ikz_0} \hat{\mathbf{x}} \\ &\quad - [ik_x E_z(\mathbf{k}, \omega) - ik_z E_x(\mathbf{k}, \omega)] \hat{\mathbf{y}} - E_{x_0}(\mathbf{k}_T, \omega) e^{-ikz_0} \hat{\mathbf{y}} \\ &\quad + [ik_x E_y(\mathbf{k}, \omega) - ik_y E_x(\mathbf{k}, \omega)] \hat{\mathbf{z}} \\ &= \mathbf{i}\mathbf{k} \times \mathbf{E}(\mathbf{k}, \omega) - \hat{\mathbf{z}} \times \mathbf{E}_0(\mathbf{k}_T, \omega) e^{-ikz_0}, \quad (2.2.27) \end{aligned}$$

where,

$$E_{x_0}(\mathbf{k}_T, \omega) \equiv E_x(\mathbf{k}_T, z_0, \omega) , \quad (2.2.28a)$$

$$E_{y_0}(\mathbf{k}_T, \omega) \equiv E_y(\mathbf{k}_T, z_0, \omega) , \quad (2.2.28b)$$

$$E_{z_0}(\mathbf{k}_T, \omega) \equiv E_z(\mathbf{k}_T, z_0, \omega) , \quad (2.2.28c)$$

and

$$\mathbf{E}_0(\mathbf{k}_T, \omega) \equiv E_{x_0}(\mathbf{k}_T, \omega)\hat{x} + E_{y_0}(\mathbf{k}_T, \omega)\hat{y} + E_{z_0}(\mathbf{k}_T, \omega)\hat{z} = \mathbf{E}(\mathbf{k}_T, z_0, \omega) . \quad (2.2.29)$$

Similarly, from *Ampère's Law* given in Eq. (2.2.24b) one obtains

$$\mathcal{L}\left\{\left[\mathbf{ik}_T, \frac{\partial}{\partial z}\hat{z}\right] \times \mathbf{H}(\mathbf{k}_T, z, \omega)\right\} = \mathbf{ik} \times \mathbf{H}(\mathbf{k}, \omega) - \hat{z} \times \mathbf{H}_0(\mathbf{k}_T, \omega)e^{-\mathbf{ik}z_0} , \quad (2.2.30)$$

where,

$$H_{x_0}(\mathbf{k}_T, \omega) \equiv H_x(\mathbf{k}_T, z_0, \omega) , \quad (2.2.31a)$$

$$H_{y_0}(\mathbf{k}_T, \omega) \equiv H_y(\mathbf{k}_T, z_0, \omega) , \quad (2.2.31b)$$

$$H_{z_0}(\mathbf{k}_T, \omega) \equiv H_z(\mathbf{k}_T, z_0, \omega) , \quad (2.2.31c)$$

and

$$\mathbf{H}_0(\mathbf{k}_T, \omega) \equiv H_{x_0}(\mathbf{k}_T, \omega)\hat{x} + H_{y_0}(\mathbf{k}_T, \omega)\hat{y} + H_{z_0}(\mathbf{k}_T, \omega)\hat{z} = \mathbf{H}(\mathbf{k}_T, z_0, \omega) . \quad (2.2.32)$$

The forward one-sided spatial *Laplace* transform of *Gauss' Law* (2.2.24c) yields

$$\begin{aligned} \mathcal{L}\left\{\left[\mathbf{ik}_T, \frac{\partial}{\partial z}\hat{z}\right] \cdot \mathbf{D}(\mathbf{k}_T, z, \omega)\right\} &= \int_{z_0}^{\infty} \left[\mathbf{ik}_T, \frac{\partial}{\partial z}\hat{z}\right] \cdot \mathbf{D}(\mathbf{k}_T, z, \omega)e^{-\mathbf{ik}z} dz \\ &= \mathbf{ik} \cdot \mathbf{D}(\mathbf{k}, \omega) - D_{z_0}(\mathbf{k}_T, \omega)e^{-\mathbf{ik}z_0} , \end{aligned} \quad (2.2.33)$$

where,

$$D_{z_0}(\mathbf{k}_T, \omega) \equiv D_z(\mathbf{k}_T, z_0, \omega) . \quad (2.2.34)$$

Similarly, from Eq. (2.2.24d) one obtains

$$\mathcal{L}\left\{\left[\mathbf{ik}_T, \frac{\partial}{\partial z}\hat{z}\right] \cdot \mathbf{B}(\mathbf{k}_T, z, \omega)\right\} = \mathbf{ik} \cdot \mathbf{B}(\mathbf{k}, \omega) - B_{z_0}(\mathbf{k}_T, \omega)e^{-\mathbf{ik}z_0} , \quad (2.2.35)$$

where,

$$B_{z_0}(\mathbf{k}_T, \omega) \equiv B_z(\mathbf{k}_T, z_0, \omega) . \quad (2.2.36)$$

These expressions then yield the spatio–temporal frequency domain form of the source–free form of *Maxwell's* equations when the field is specified on the plane $z = z_0$, viz.

$$i\mathbf{k} \times \mathbf{E}(\mathbf{k}, \omega) - \hat{z} \times \mathbf{E}_0(\mathbf{k}_T, \omega)e^{-ikz_0} = \left\| \frac{1}{c} \right\| i\omega \mathbf{B}(\mathbf{k}, \omega) , \quad (2.2.37a)$$

$$i\mathbf{k} \times \mathbf{H}(\mathbf{k}, \omega) - \hat{z} \times \mathbf{H}_0(\mathbf{k}_T, \omega)e^{-ikz_0} = -\left\| \frac{1}{c} \right\| i\omega \mathbf{D}(\mathbf{k}, \omega) , \quad (2.2.37b)$$

$$i\mathbf{k} \cdot \mathbf{D}(\mathbf{k}, \omega) - D_z(\mathbf{k}_T, z_0, \omega)e^{-ikz_0} = 0 , \quad (2.2.37c)$$

$$i\mathbf{k} \cdot \mathbf{B}(\mathbf{k}, \omega) - B_z(\mathbf{k}_T, z_0, \omega)e^{-ikz_0} = 0 , \quad (2.2.37d)$$

and the constitutive relations given in Eqs. (2.2.25a,b) take the form

$$\mathbf{D}(\mathbf{k}, \omega) = \tilde{\epsilon}(\omega)\mathbf{E}(\mathbf{k}, \omega) , \quad (2.2.38a)$$

$$\mathbf{B}(\mathbf{k}, \omega) = \mu\mathbf{H}(\mathbf{k}, \omega) . \quad (2.2.38b)$$

2.3 Theoretical Description of Dielectric Dispersion; The Double Resonance Lorentz Model

In the previous section, a linear relationship between the applied electric field and the induced electric flux density is implied by the constitutive relation $\mathbf{D}(\mathbf{r}, \omega) = \tilde{\epsilon}(\omega)\mathbf{E}(\mathbf{r}, \omega)$. A complete solution to the macroscopic *Maxwell's* equations requires this auxiliary equation which specifies the manner that the host medium responds to an applied external electric field. The *Maxwell's* equations are then complete with an appropriate specification of the proportionality factor represented by the complex permittivity $\tilde{\epsilon}(\omega)$. The proper description of $\tilde{\epsilon}(\omega)$ must model the observed dispersive behavior of the given dielectric medium. The choice of dielectric media for this research is restricted to media where there exists neither free charge nor conduction mechanisms. Finally, the linear constitutive relation $\mathbf{D}(\mathbf{r}, \omega) = \tilde{\epsilon}(\omega)\mathbf{E}(\mathbf{r}, \omega)$ assumes that the field strengths involved are always sufficiently small in order to make any nonlinear effects negligible. This in turn implies that the principle of superposition applies throughout the analysis.

The Lorentz model describes the frequency dispersion of the complex permittivity, and hence of the complex refractive index $\tilde{n}(\omega) \equiv \sqrt{\frac{\mu\tilde{\epsilon}_r(\omega)}{\mu_0\epsilon_0}}$, over the entire temporal frequency domain considered in this research, where it is also assumed that $\mu = \mu_0$. The Lorentz model was chosen for its ability to accurately model the observed dispersive behavior of glass (the most commonly used dielectric material in dielectric waveguides) and other types of dielectrics within the infrared, visible and ultraviolet portions of the electromagnetic spectrum. The model was also chosen for its inherent simplicity. Further, the Lorentz model satisfies the *Kramers–Kronig* relations[1] so that it is causal. The Lorentz model is classical and therefore is inherently heuristic; quantum mechanical theory is required in order to accurately explain the true origin of the dispersion mechanisms. For example, the location of the resonance frequencies and the strength of the spectral lines cannot be derived by classical methods[63] but can, in principle, be obtained quantum mechanically.

The type of electromagnetic field of interest to this research has its spectrum in the extended optical regime from the far infrared (IR) to the hard ultraviolet (UV). For this reason, the dielectric dispersion of glass will be modeled only in this spectral region. Optical glass typically possesses two absorption bands or resonances in this extended optical regime; one resonance is in the IR range due to induced motion of ions and the other resonance is in the UV due to electronic transitions of the constituent atoms. Consequently, a double resonance Lorentz model sufficiently and accurately describes the complex refractive index's frequency dispersion.

2.3.1 The Lorentz Model

Under the assumptions of a negligible magnetic field and an oscillation amplitude small enough that the electric field may be evaluated at the electron's average position the dynamical equation of motion of a harmonically bound electron driven by an external electromagnetic source becomes[1]

$$m\left(\ddot{\mathbf{r}} + 2\delta\dot{\mathbf{r}} + \omega_j''^2 \mathbf{r}\right) = -e\mathbf{E}_{\omega loc}(\mathbf{r}, t) \quad (2.3.1)$$

where m is the electron's mass, δ is a phenomenological damping constant, ω_j'' is the undamped angular frequency of oscillation related to the harmonic restoring force and where $\mathbf{E}_{\omega loc}(\mathbf{r}, t)$ is the local complex time-harmonic electric field oscillating at the angular frequency ω . If the *Mosotti field*[63] $\mathbf{E}_{\omega loc}(\mathbf{r}, t) \equiv \mathbf{E}_\omega(\mathbf{r}, t) + \frac{\|4\pi\|\mathbf{P}_\omega(\mathbf{r}, t)}{3\epsilon_0}$ is substituted for

the local electric field, Eq. (2.3.1) becomes

$$m\left(\ddot{\mathbf{r}} + 2\delta\dot{\mathbf{r}} + \omega_j^2 \mathbf{r}\right) = -e\mathbf{E}_\omega(\mathbf{r}, t) , \quad (2.3.2)$$

where the effect of the term $\frac{\|4\pi\|\mathbf{P}_\omega(\mathbf{r}, t)}{3\epsilon_0}$ has been subsumed into the resonance frequency

$$\omega_j^2 \equiv \omega_j''^2 - \frac{\|4\pi\|Ne^2}{3m\epsilon_0} , \quad (2.3.3)$$

since $\mathbf{P}_\omega(\mathbf{r}, t) = -Ner$ where N represents the number density of electrons. The factor $\frac{\|4\pi\|Ne^2}{3m\epsilon_0}$ in Eq. (2.3.3) represents a small correction factor to the resonance frequency ω_j'' for transparent or non-optically dense materials such as glass. For this reason, some authors elect to neglect this factor. However, the form of the final equation for the dielectric constant appears unaltered whether or not the correction factor $\frac{\|4\pi\|Ne^2}{3m\epsilon_0}$ is included. The difference between ω_j'' and ω_j becomes a moot point since the resonance frequency either ω_j'' or ω_j can only be determined in the classical theory via a numerical fit to experimental data. Inclusion of this correction factor merely serves to illustrate the microscopic details of the problem.

With the complex time-harmonic field oscillating at the angular frequency ω as $e^{-i\omega t}$, the elementary dipole moment due to this harmonically bound electron becomes[63]

$$\mathbf{p}_\omega(\mathbf{r}, t) = -e\mathbf{r}_\omega(\mathbf{r}, t) = \frac{e^2}{m} \frac{\mathbf{E}_\omega(\mathbf{r}, t)}{\omega_j^2 - \omega^2 - 2i\omega\delta_j} . \quad (2.3.4)$$

The definition of the macroscopic polarization vector $\mathbf{P}_\omega(\mathbf{r}, t) \equiv \epsilon_0 \tilde{\chi}_e(\omega) \mathbf{E}_\omega(\mathbf{r}, t)$, where $\tilde{\chi}_e(\omega)$ is the complex electric susceptibility, together with the assumption of a uniform distribution N of elementary dipoles $\mathbf{P}_\omega(\mathbf{r}, t) = N \mathbf{p}_\omega(\mathbf{r}, t)$ combines with Eq. (2.3.4) to yield

$$\tilde{\chi}_e(\omega) \mathbf{E}_\omega(\mathbf{r}, t) = \frac{N \mathbf{p}_\omega(\mathbf{r}, t)}{\epsilon_0} = \frac{N e^2}{\epsilon_0 m} \frac{1}{\omega_j^2 - \omega^2 - 2i\omega\delta_j} \mathbf{E}_\omega(\mathbf{r}, t) ,$$

so that the complex electric susceptibility is given by

$$\tilde{\chi}_e(\omega) \equiv \frac{N e^2}{\epsilon_0 m} \frac{1}{\omega_j^2 - \omega^2 - 2i\omega\delta_j} . \quad (2.3.5)$$

In general, there are many different species of electronic oscillators; one for each electron in each atomic and/or molecular component of the dielectric substance. For each type of oscillator, let N_j represent the number density with binding frequency ω_j and phenomenological damping constant δ_j . The definition of the relative complex dielectric constant $\frac{\tilde{\epsilon}(\omega)}{\epsilon_0} = 1 + \|\mathbb{4}\pi\| \tilde{\chi}_e(\omega)$ together with the Eq. (2.3.5) for the complex electric susceptibility $\tilde{\chi}_e(\omega)$ then yields[63]

$$\frac{\tilde{\epsilon}(\omega)}{\epsilon_0} = 1 - \frac{\|\mathbb{4}\pi\| e^2}{\epsilon_0 m} \sum_{j=0,2,\dots} \frac{N_j}{\omega^2 - \omega_j^2 + 2i\omega\delta_j} . \quad (2.3.6)$$

An oscillating ionic system can also be modeled with this equation by reinterpreting N_j as the density of the oscillating ionic system, q_j as the charge of a single species of the oscillating ionic system and m_j as the reduced mass of the ionic system.

The complex refractive index is obtained from Eq. (2.3.6) as

$$\tilde{n}(\omega) \equiv \sqrt{\frac{\tilde{\epsilon}(\omega)}{\epsilon_0}} = \sqrt{1 - \sum_{j=0,2,\dots} \frac{b_j^2}{\omega^2 - \omega_j^2 + 2i\delta_j\omega}} , \quad (2.3.7)$$

where

$$b_j^2 \equiv \frac{\|\mathbb{4}\pi\| N_j q_j^2}{\epsilon_0 m_j} , \quad (2.3.8)$$

where b_j is the plasma frequency. The j 'th Lorentz oscillator is then completely described by specifying the three parameters ω_j , b_j and δ_j . The real part of Eq. (2.3.7) yields the real refractive index of the medium and the imaginary part is related to the extinction coefficient. The Lorentz model given in Eq. (2.3.7) provides an accurate representation of the electronic and atomic contributions to the complex refractive index[63].

The resonance frequencies ω_j and the phenomenological damping constants δ_j are specified as positive real constants, so that the poles of Eq. (2.3.7), given by

$$\omega_{poles} = -i\delta_j \pm \left(\omega_j^2 - \delta_j^2 \right)^{1/2}, \quad (2.3.9)$$

reside in the lower half of the complex ω -plane. This means that the Lorentz model is analytic in the upper half of the complex ω -plane so that an inverse *Fourier* transform of $\tilde{\epsilon}(\omega)$ yields a causal dielectric permittivity response function $\hat{\epsilon}(t)$, i.e. $\hat{\epsilon}(t) = 0$ for all negative time $t < 0$.

2.3.2 The Double Resonance Lorentz Model for Glass

The bandwidth of the signals considered in this research resides within the extended optical regime from the far infrared to the hard ultraviolet. In general, glass possesses two absorption bands or resonances in this extended optical regime: one resonance in the far infrared range due to induced motion of ions, and one resonance in the hard ultraviolet due to electronic transitions of the constituent atoms. The frequency dispersion due to these two resonance structures is modeled here using a double resonance Lorentz model.

A simple modification of Eq. (2.3.7) yields the double resonance Lorentz model for the complex refractive index, viz.

$$\tilde{n}(\omega) \equiv \sqrt{\frac{\tilde{\epsilon}(\omega)}{\epsilon_0}} = \sqrt{\epsilon_\infty - \sum_{j=0,2} \frac{b_j^2}{\omega^2 - \omega_j^2 + 2i\delta_j\omega}}, \quad (2.3.10)$$

where

$$b_j^2 \equiv \frac{4\pi N_j q_j^2}{\epsilon_0 m_j} . \quad (2.3.11)$$

The parameter $\epsilon_\infty \equiv \lim_{\omega \gg \omega_2} \frac{\tilde{\epsilon}(\omega)}{\epsilon_0}$ represents a correction factor of the Lorentz model for other resonances that exist. If the other resonances are sufficiently far away from the IR and UV resonances then their contributions to the refractive index appear constant within the modeled spectrum as assumed in Eq. (2.3.10).

It should be noted here, that there exists some discrepancies with only using two resonances. If a model completely and physically describes a medium's refractive index then certain sum rules must be satisfied[2]. Sum rules are derived using the *Kramers–Kronig* relations which follow from little more than the assumption of causality (whose basis is the analyticity of $\tilde{n}(\omega)$ in the upper half ω plane)[1]. The sum rules dictate certain properties that a proper dispersion relationship must possess. Although the double resonance Lorentz model is causal (i.e. it's analytic in the upper half ω plane), it fails to satisfy the zero frequency sum rule, the f–sum rule and the average over the real part of the refractive index. This suggests that there exist additional pieces required to completely specify the refractive index over the entire electromagnetic spectrum. By examining real glass data over the entire spectral domain, the low frequency plateau and the infinite frequency asymptote (the refractive index must asymptotically approach 1) are not described by the double resonance Lorentz model given in Eq. (2.3.10). The complete description of dielectric dispersion can be written by separating the double resonance Lorentz model piece from the low and high frequency behavior, viz.

$$\frac{\tilde{\epsilon}(\omega)}{\epsilon_0} = \sum_{\omega_j < \omega_0} \frac{\tilde{\epsilon}(\omega)}{\epsilon_0} - \sum_{\omega_0, \omega_2} \frac{b_j^2}{\omega^2 - \omega_j^2 + 2i\delta_j\omega} + \sum_{\omega_j > \omega_2} \frac{\tilde{\epsilon}(\omega)}{\epsilon_0} . \quad (2.3.12)$$

Debye's relaxation and any Lorentz lines that may exist below ω_0 describes the low frequency behavior, and Lorentz lines above ω_2 describes the high frequency behavior. The spectral content of the real pulses considered in this research do not significantly spread past the ex-

tended optical regime. So, the addition frequency behavior of the complex refractive index which is not modeled only slightly modifies the precursor behavior.

Values for the two resonance frequencies ω_0 and ω_2 are selected to lie in their respective spectral regions: the far infrared and hard ultraviolet. Then reasonable values are chosen to represent the phenomenological damping constants, plasma frequencies and ϵ_∞ . Alternatively, the double resonance Lorentz model is numerically fit to experimentally measured refractive index data. The end result of the fit defines numerical values of the Lorentz parameters (ω_j , b_j and δ_j for each resonances and ϵ_∞) that accurately resemble observed physical data. The *Levenberg–Marquardt* Method “has become the standard of nonlinear least–squares routines”[67]. For this reason, it has been chosen as the numerical data modeling method for this research. The *Levenberg–Marquardt* method and the C routines given in ref. [67] were written for real data and functions. This necessitated a careful reformulation of the method and consequently a revision of the C routines to account for complex data and functions. The *Levenberg–Marquardt* method uses the merit function χ^2 as a maximum likelihood estimator defined as

$$\chi^2(\mathbf{a}) \equiv \sum_{i=1}^N \left| \frac{\tilde{n}_i - \tilde{n}(\omega_i, \mathbf{a})}{\sigma_i} \right|^2 \quad (2.3.13)$$

where $\tilde{n}(\omega_i, \mathbf{a})$ represents the double resonance Lorentz model given in Eq. (2.3.10) as a function of the Lorentz parameters

$$\mathbf{a} \equiv \{\omega_0, b_0, \delta_0, \omega_2, b_2, \delta_2, \tilde{\epsilon}_\infty\} .$$

Here, \tilde{n}_i represents the experimentally measured refractive index data, ω_i represents the frequency where the experimental data was measured and σ_i represents the experimental data’s standard deviation. Basically, the *Levenberg–Marquardt* method executes as an iterative procedure which improves a trial solution by a steepest descent method when the merit function’s value χ^2 deems that the trial solution lay far away from convergence. The procedure smoothly converts to an inverse Hessian method as χ^2 decreases. The Hessian method

| Double Resonance Lorentz Model Parameters | | | | |
|--|-------------------------|------------------------------------|-------------------------------|------------------------------------|
| ϵ_{∞} | Resonance Number j | ω_j ($10^{14}rad/sec$) | b_j ($10^{14}rad/sec$) | δ_j ($10^{13}rad/sec$) |
| 1.9938 | 0 | 1.7412 | 1.2155 | 4.9555 |
| | 2 | 91.448 | 67.198 | 143.41 |

Table 2.3.1 Numerically determined double resonance Lorentz parameters for a fluoride (CLAP) glass found by applying the complex *Levenberg–Marquardt* nonlinear least-squares fit algorithm.

approximates Eq. (2.3.13) as a quadratic and then minimizes the equation to find an accurate trial solution as convergence is approached. The iteration procedure stops when χ^2 effectively stops decreasing.

As an example, the double resonance Lorentz model given in Eq. (2.3.10) was numerically fit to the fluoride glass $CdF_2 - LiF - AlF_3 - PbF_2$ (which is referred to as a CLAP glass)[64] using the *Levenberg–Marquardt* method. The calculated double resonance Lorentz parameters are presented in Table 2.3.1. The resultant optimized Lorentz model is illustrated in Figure 2.3.1 and the corresponding error of the numerical fit is presented in Figure 2.3.2. The standard deviations were assigned the value of unity due to their unavailability and the numerical fitting routine minimized the merit function as $\chi^2 = 7.4017 \times 10^{-7}$ from 29 data points. A maximum likelihood estimate of the variance is $\sigma^2 \approx \frac{\chi^2}{N}$, where N is the number of data points, which yields a value of $\sigma^2 \approx 2.4672 \times 10^{-8}$ for the variance. In this particular example, experimental data was not available for the absorption spectra. The fitting program automatically compensates for this deficiency by minimizing the phenomenological damping constants δ_j . The impetus of this procedure is the assumption that a optical glass manufacture attempts to create a high quality product by minimizing loss, therefore minimizing the loss represented in the Lorentz

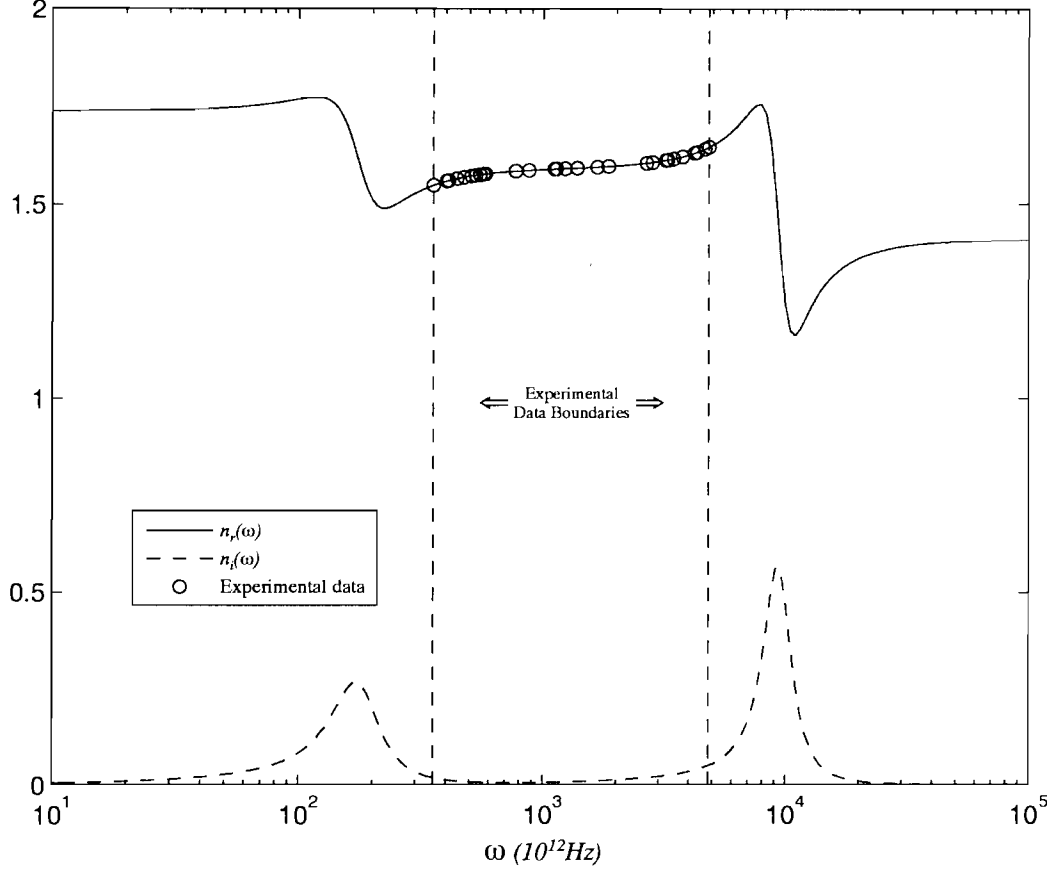


Figure 2.3.1 Index of refraction data for a fluoride (CLAP) glass plotted along with the complex *Levenberg–Marquardt* nonlinear least-squares fit of the double resonance Lorentz model with the numerically determined Lorentz model parameters $\epsilon_{\infty} = 1.9938$, $\omega_0 = 1.7412 \times 10^{14} \text{Hz}$, $b_0 = 1.2155 \times 10^{14} \text{Hz}$, $\delta_0 = 4.9555 \times 10^{13} \text{Hz}$, $\omega_2 = 9.1448 \times 10^{15} \text{Hz}$, $b_2 = 6.7198 \times 10^{15} \text{Hz}$, $\delta_2 = 1.4341 \times 10^{15} \text{Hz}$.

model simulates manufacturing goals. Of course, if absorption spectra data were available, then the fitting program would incorporate that data in the algorithm. The minimum loss, where loss is defined as $\Im\left\{\tilde{n}(\omega)\frac{\omega}{c}\right\}$, that occurs within the spectral range of the plotted data is 155.46 m^{-1} at $\omega = 1.0 \times 10^{13} \text{Hz}$ and the minimum loss that occurs within the spectral range of the data is $1.2002 \times 10^4 \text{ m}^{-1}$ at $\omega = 7.1340 \times 10^{14} \text{Hz}$. In contrast, the maximum loss that occurs within the spectral range of the plotted data is $1.7867 \times 10^7 \text{ m}^{-1}$ at $\omega = 9.4044 \times 10^{15} \text{Hz}$ and the maximum loss that occurs within the spectral range of the data is $7.7676 \times 10^5 \text{ m}^{-1}$ at $\omega = 4.7863 \times 10^{15} \text{Hz}$.

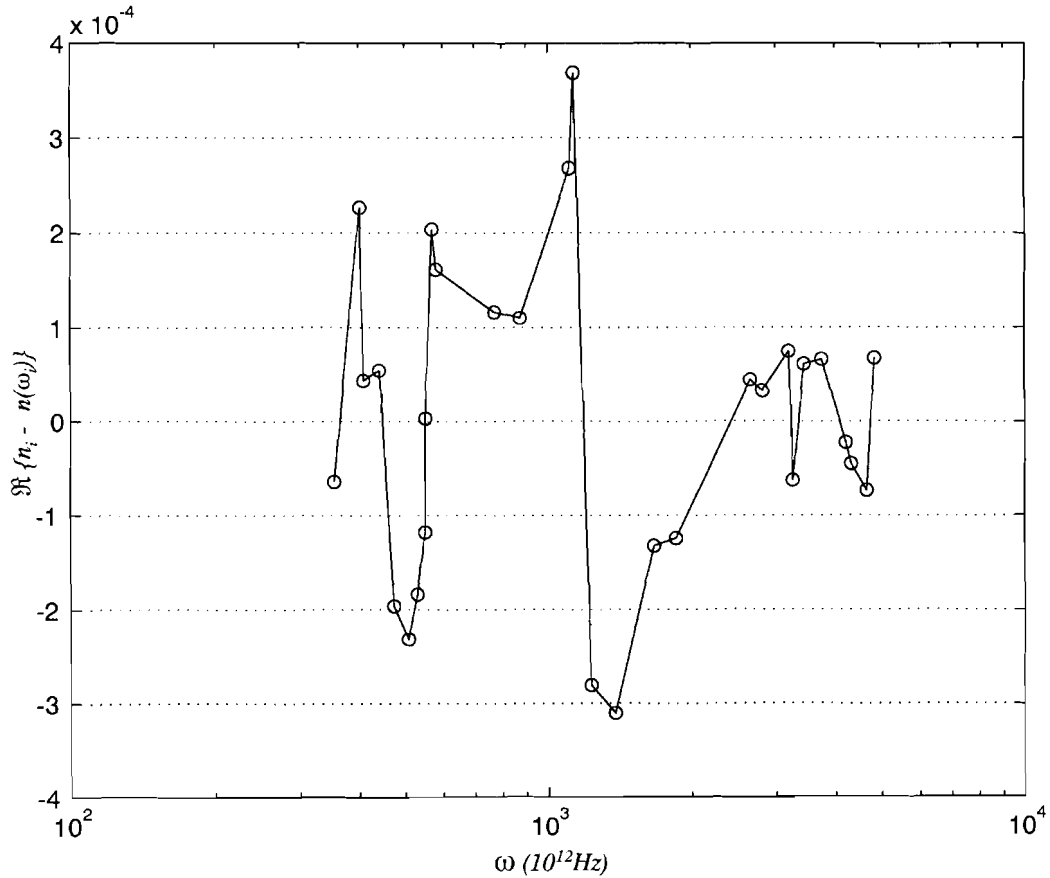


Figure 2.3.2 Error of the *Levenberg–Marquardt* nonlinear least-squares fit of the double resonance Lorentz model parameters to the index of refraction data for a fluoride (CLAP) glass with the found Lorentz model parameters $\epsilon_{\infty} = 1.9938$, $\omega_0 = 1.7412 \times 10^{14} \text{Hz}$, $b_0 = 1.2155 \times 10^{14} \text{Hz}$, $\delta_0 = 4.9555 \times 10^{13} \text{Hz}$, $\omega_2 = 9.1448 \times 10^{15} \text{Hz}$, $b_2 = 6.7198 \times 10^{15} \text{Hz}$, $\delta_2 = 1.4341 \times 10^{15} \text{Hz}$.

2.4 Properties of Complex Vectors

Certain properties of complex vectors must be addressed in order to evaluate certain properties of complex wavevectors and the particular properties of an electromagnetic field's polarization state. Any complex vector \mathbf{c} can be written in terms of two real vectors as

$$\mathbf{c} = \mathbf{p} + i\mathbf{q},$$

where $\mathbf{p} \equiv \Re\{\mathbf{c}\}$ and $\mathbf{q} \equiv \Im\{\mathbf{c}\}$. The plane that contains both \mathbf{p} and \mathbf{q} defines the *characteristic plane* of the complex vector \mathbf{c} . If the real vectors \mathbf{p} and \mathbf{q} satisfy $\mathbf{p} \times \mathbf{q} \neq \mathbf{0}$, then the complex vector \mathbf{c} can be written in terms of two orthogonal real vectors \mathbf{a} and \mathbf{b} , viz.

$$\mathbf{c} = \mathbf{p} + i\mathbf{q} = (\mathbf{a} + i\mathbf{b})e^{i\phi} . \quad (2.4.1)$$

Exploiting the orthogonality of \mathbf{a} and \mathbf{b} allows the the real-valued phase quantity ϕ to be written as

$$\tan 2\phi = \frac{2\mathbf{p} \cdot \mathbf{q}}{\mathbf{p} \cdot \mathbf{p} - \mathbf{q} \cdot \mathbf{q}} . \quad (2.4.2)$$

The magnitudes of the vectors \mathbf{a} and \mathbf{b} are readily obtained from the previous two equations as [59]

$$|\mathbf{a}|^2 = a^2 = \frac{1}{2} \left\{ p^2 + q^2 + \left[(p^2 - q^2)^2 + 4(\mathbf{p} \cdot \mathbf{q})^2 \right]^{1/2} \right\} , \quad (2.4.3a)$$

$$|\mathbf{b}|^2 = b^2 = \frac{1}{2} \left\{ p^2 + q^2 - \left[(p^2 - q^2)^2 + 4(\mathbf{p} \cdot \mathbf{q})^2 \right]^{1/2} \right\} . \quad (2.4.3b)$$

If $\mathbf{p} \times \mathbf{q} = \mathbf{0}$ then the complex vector takes on the polar form

$$\mathbf{c} = \mathbf{p} + i\mathbf{q} = \varrho e^{i\theta} \mathbf{a} , \quad (2.4.4)$$

where ϱ and θ are real valued scalars and where the characteristic plane of \mathbf{c} is now undetermined.

Given two complex vectors \mathbf{c}_1 and \mathbf{c}_2 , a vanishing inner product leads to some interesting consequences not found in the pure real counterpart⁴. Let the two complex vectors be written as $\mathbf{c}_1 = \mathbf{p}_1 + i\mathbf{q}_1$ and $\mathbf{c}_2 = \mathbf{p}_2 + i\mathbf{q}_2$, whose inner product yields

$$\mathbf{c}_1 \cdot \mathbf{c}_2 = \mathbf{p}_1 \cdot \mathbf{p}_2 - \mathbf{q}_1 \cdot \mathbf{q}_2 + i(\mathbf{p}_1 \cdot \mathbf{q}_2 + \mathbf{p}_2 \cdot \mathbf{q}_1) .$$

When $\mathbf{c}_1 \cdot \mathbf{c}_2 = 0$ the the real and imaginary parts separately equal zero, which produces the following two conditions

$$\mathbf{p}_1 \cdot \mathbf{p}_2 = \mathbf{q}_1 \cdot \mathbf{q}_2 , \quad \mathbf{p}_1 \cdot \mathbf{q}_2 = -\mathbf{p}_2 \cdot \mathbf{q}_1 . \quad (2.4.5)$$

The subsequent analysis naturally divides into two classes: when the real vector component pairs $\mathbf{p}_1, \mathbf{q}_1$ and $\mathbf{p}_2, \mathbf{q}_2$ are not parallel and when at least one pair is parallel.

4. See Caviglia and Morro [69] §1.2 for a additional information on this development.

For the first class, the real vector component pairs satisfy $\mathbf{p}_1 \times \mathbf{q}_1 \neq \mathbf{0}$ and $\mathbf{p}_2 \times \mathbf{q}_2 \neq \mathbf{0}$ which permit \mathbf{c}_1 and \mathbf{c}_2 to be expressed in the form of Eq. (2.4.1)

$$\mathbf{c}_1 = \mathbf{p}_1 + i\mathbf{q}_1 = (\mathbf{a}_1 + i\mathbf{b}_1)e^{i\phi_1}, \quad \mathbf{a}_1 \cdot \mathbf{b}_1 = 0, \quad (2.4.6a)$$

$$\mathbf{c}_2 = \mathbf{p}_2 + i\mathbf{q}_2 = (\mathbf{a}_2 + i\mathbf{b}_2)e^{i\phi_2}, \quad \mathbf{a}_2 \cdot \mathbf{b}_2 = 0. \quad (2.4.6b)$$

Consequently, the conditions given in Eq. (2.4.5) become

$$\mathbf{a}_1 \cdot \mathbf{a}_2 = \mathbf{b}_1 \cdot \mathbf{b}_2, \quad \mathbf{a}_1 \cdot \mathbf{b}_2 = -\mathbf{a}_2 \cdot \mathbf{b}_1. \quad (2.4.7)$$

First, consider the case when the characteristic planes of \mathbf{c}_1 and \mathbf{c}_2 are coplanar, i.e. the plane that contains $\mathbf{a}_1, \mathbf{b}_1$ also contains $\mathbf{a}_2, \mathbf{b}_2$, then \mathbf{c}_2 can be written as a linear combination of $\mathbf{a}_1, \mathbf{b}_1$ given as

$$\mathbf{c}_2 = [\mu\mathbf{a}_1 + \lambda\mathbf{b}_1 + i(\nu\mathbf{a}_1 + \eta\mathbf{b}_1)]e^{i\phi_2}, \quad \mu, \lambda, \nu, \eta \in \mathbb{R}.$$

Under the condition of a vanishing inner product, $\mathbf{c}_1 \cdot \mathbf{c}_2 = 0$, the vector \mathbf{c}_2 becomes

$$\mathbf{c}_2 = \left[\frac{\mathbf{a}_1 \cdot \mathbf{a}_1}{\mathbf{b}_1 \cdot \mathbf{b}_1} \mathbf{a}_1 + i\mathbf{b}_1 \right] (\eta - i\lambda) e^{i\phi_2}.$$

Next, consider the vectors $\mathbf{p}_1 \times \mathbf{q}_1$ and $\mathbf{p}_2 \times \mathbf{q}_2$ which are perpendicular to the characteristic planes of \mathbf{c}_1 and \mathbf{c}_2 , respectively. Their inner product produces⁵

$$(\mathbf{p}_1 \times \mathbf{q}_1) \cdot (\mathbf{p}_2 \times \mathbf{q}_2) = (\mathbf{p}_1 \cdot \mathbf{p}_2)(\mathbf{q}_1 \cdot \mathbf{q}_2) - (\mathbf{p}_1 \cdot \mathbf{q}_2)(\mathbf{p}_2 \cdot \mathbf{q}_1).$$

Under the condition of a vanishing inner product, $\mathbf{c}_1 \cdot \mathbf{c}_2 = 0$, the inner product of the orthogonal vectors yields the following strictly positive inequality

$$(\mathbf{p}_1 \times \mathbf{q}_1) \cdot (\mathbf{p}_2 \times \mathbf{q}_2) = (\mathbf{p}_1 \cdot \mathbf{p}_2)^2 + (\mathbf{p}_2 \cdot \mathbf{q}_1)^2 > 0. \quad (2.4.8)$$

The inequality given in Eq. (2.4.8) establishes that the characteristic planes are never orthogonal and that the vectors $\mathbf{p}_1 \times \mathbf{q}_1$ and $\mathbf{p}_2 \times \mathbf{q}_2$ are either parallel or at an acute angle due to conditions given in Eq. (2.4.7) together with the fact that the real vector component pairs are not parallel.

5. See Phillips [61] p. 18 (27).

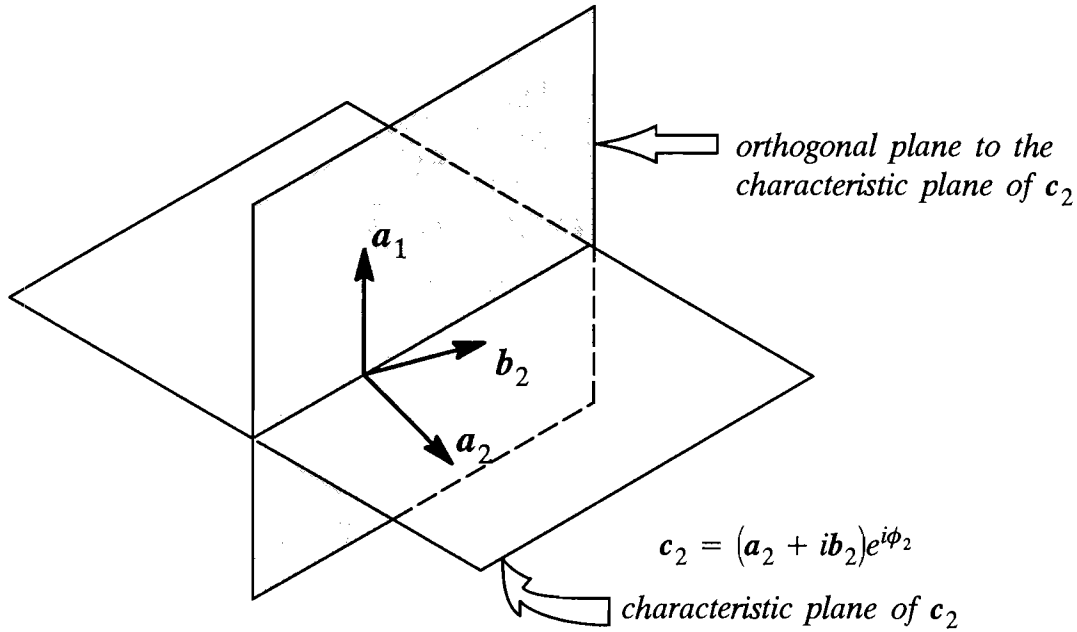


Figure 2.4.1 If c_j is expressible in polar form, then the vector a_j is orthogonal to both vectors b_2 and a_2 .

For the second class, consider the case when at least one of the real vector component pairs is parallel which permits at least one of the two complex vectors to be expressed in polar form of Eq. (2.4.4). For example, let c_1 satisfy $p_1 \times q_1 = \mathbf{0}$, so that

$$c_1 = p_1 + iq_1 = \rho_1 e^{i\theta_1} a_1 ,$$

where the characteristic plane of c_1 is now undetermined and, without loss of generality, let c_2 be given as in Eq. (2.4.6b). Consequently, the conditions given in Eq. (2.4.5) become

$$a_1 \cdot a_2 = 0 \quad , \quad a_1 \cdot b_2 = 0 . \quad (2.4.9)$$

Therefore, by the conditions given in Eq. (2.4.9), *if at least one complex vector is expressible in polar form then that vector is orthogonal to both of the orthogonal real vector components of the other complex vector*, as depicted in Figure 2.4.1.

These cases demonstrate that great care must be taken when interpreting the geometric consequences of a vanishing inner product of a pair of complex vectors. Complex vector space analysis labels two vectors c_1 and c_2 as ‘orthogonal’, in a general sense, under the

condition $\mathbf{c}_1 \cdot \mathbf{c}_2 = 0^6$. However, without any other supplementary information, the label ‘orthogonal’ leads to an apparently ambiguous geometrical meaning.

2.5 Inhomogeneous Plane Wave Solution of *Maxwell’s* Equations in an Infinitely Extended Dielectric with Complex Permittivity

The purpose of the present section is to determine the general inhomogeneous plane wave solution of *Maxwell’s* equations within source free regions of space. This general solution will be utilized later to develop the generalized reflection and refraction laws and the generalized *Fresnel* equations.

Upon taking the curl of the the first two space–frequency *Maxwell’s* equations Eqs. (2.2.12 a,b) and using the corresponding constitutive relations given in Eqs. (2.2.13a,b) one obtains the pair of relations

$$\nabla \times \nabla \times \mathbf{E}(\mathbf{r}, \omega) = \nabla(\nabla \cdot \mathbf{E}(\mathbf{r}, \omega)) - \nabla^2 \mathbf{E}(\mathbf{r}, \omega) = \left\| \frac{1}{c} \right\| i\omega\mu \nabla \times \mathbf{H}(\mathbf{r}, \omega) , \quad (2.5.1a)$$

$$\nabla \times \nabla \times \mathbf{H}(\mathbf{r}, \omega) = \nabla(\nabla \cdot \mathbf{H}(\mathbf{r}, \omega)) - \nabla^2 \mathbf{H}(\mathbf{r}, \omega) = -\left\| \frac{1}{c} \right\| i\omega\tilde{\epsilon}(\omega) \nabla \times \mathbf{E}(\mathbf{r}, \omega). \quad (2.5.1b)$$

Since, the field vectors $\mathbf{D}(\mathbf{r}, \omega)$ and $\mathbf{B}(\mathbf{r}, \omega)$ are solenoidal, their divergences vanish in Eqs. (2.5.1a,b). Cross–substituting Eq. (2.2.12b) into Eq. (2.5.1a) and Eq. (2.2.12a) into Eq. (2.5.1b) yields the homogeneous vector wave equations known as the homogeneous vector *Helmholtz* equations

$$\left\{ \nabla^2 + \tilde{k}^2(\omega) \right\} \mathbf{E}(\mathbf{r}, \omega) = \mathbf{0} , \quad (2.5.2a)$$

$$\left\{ \nabla^2 + \tilde{k}^2(\omega) \right\} \mathbf{H}(\mathbf{r}, \omega) = \mathbf{0} . \quad (2.5.2b)$$

Here

$$\tilde{k}^2(\omega) \equiv \tilde{n}^2(\omega)k_0^2 \quad (2.5.3)$$

where $\tilde{k}(\omega)$ is the *complex wavenumber* of the electromagnetic disturbance with angular fre-

6. cf. Cater [72] §5–1. Cater defines the inner product as $\mathbf{c}_1 \cdot \mathbf{c}_2 = \mathbf{p}_1 \cdot \mathbf{p}_2 + \mathbf{q}_1 \cdot \mathbf{q}_2 + i(\mathbf{p}_1 \cdot \mathbf{q}_2 - \mathbf{q}_1 \cdot \mathbf{p}_2)$ so that the vector space is be unitarian. That is, the vector space has a metric defined such that $\mathbf{c}_l \cdot \mathbf{c}_l$ is strictly positive. However, similar geometric consequences occur as a result of this metric.

quency ω that is propagating in the medium with *complex refractive index*

$$\tilde{n}(\omega) \equiv \sqrt{\frac{\mu\tilde{\epsilon}(\omega)}{\mu_0\epsilon_0}} , \quad (2.5.4)$$

where $k_0 \equiv \frac{\omega}{c}$ is the vacuum wavenumber and $c \equiv \frac{\|c\|}{\sqrt{\mu_0\epsilon_0}}$ is the vacuum speed of light.

Let the complex wavenumber be defined as

$$\tilde{k}(\omega) \equiv \beta(\omega) + i\alpha(\omega) , \quad (2.5.5)$$

where $\beta(\omega) \equiv \Re\{\tilde{k}(\omega)\}$ is the *propagation factor* and $\alpha(\omega) \equiv \Im\{\tilde{k}(\omega)\}$ is the *attenuation factor*. Substitution of Eq. (2.5.5) into Eq. (2.5.3) yields

$$\beta^2(\omega) - \alpha^2(\omega) + 2i\beta(\omega)\alpha(\omega) = \frac{\mu\tilde{\epsilon}(\omega)}{\mu_0\epsilon_0} k_0^2 ,$$

which, upon equating the real and imaginary parts, yields the pair of equations

$$\beta^2(\omega) - \alpha^2(\omega) = \left\| \frac{1}{c^2} \right\| \omega^2 \mu \epsilon_r(\omega) , \quad (2.5.6a)$$

$$2\beta(\omega)\alpha(\omega) = \left\| \frac{1}{c^2} \right\| \omega^2 \mu \epsilon_i(\omega) , \quad (2.5.6b)$$

where $\epsilon_r(\omega) = \Re\{\tilde{\epsilon}(\omega)\}$ and $\epsilon_i(\omega) = \Im\{\tilde{\epsilon}(\omega)\}$. It is possible that Eq. (2.5.6a) is negative for an arbitrary dielectric within the absorptive spectral regions, however, for optical glass Eq. (2.5.6a) is positive in the extended optical regime since it is assumed to have a low attenuation factor $\alpha(\omega)$. The conditions given in Eqs. (2.2.23a,b) demand that Eq. (2.5.6b) behaves as an odd function of ω , such that

$$2\beta(\omega)\alpha(\omega) \begin{cases} > 0 & , \forall \omega > 0 \\ < 0 & , \forall \omega < 0 \end{cases} . \quad (2.5.7)$$

Upon solving Eq. (2.5.6b) for $\beta(\omega)$ and substituting the result into Eq. (2.5.6a), one obtains the fourth order equation

$$\alpha^4(\omega) + \left\| \frac{1}{c^2} \right\| \omega^2 \mu \epsilon_r(\omega) \alpha^2(\omega) - \left\| \frac{1}{c^4} \right\| \omega^4 \mu^2 \epsilon_i^2(\omega) = 0 ,$$

with the solution

$$\beta(\omega) = \left\| \frac{1}{c} \right\| \omega \left[\frac{1}{2} \mu \right]^{\frac{1}{2}} \left\{ \left[\varepsilon_r^2(\omega) + \varepsilon_i^2(\omega) \right]^{\frac{1}{2}} + \varepsilon_r(\omega) \right\}^{\frac{1}{2}}, \quad (2.5.8a)$$

$$\alpha(\omega) = \left\| \frac{1}{c} \right\| |\omega| \left[\frac{1}{2} \mu \right]^{\frac{1}{2}} \left\{ \left[\varepsilon_r^2(\omega) + \varepsilon_i^2(\omega) \right]^{\frac{1}{2}} - \varepsilon_r(\omega) \right\}^{\frac{1}{2}}, \quad (2.5.8b)$$

where $\varepsilon_r(\omega)$ is allowed to be negative with no alteration to the above two equations⁷. The quantity $|\omega|$ in Eq. (2.5.8b) effectively selects the branch cut for Eqs. (2.5.4) and (2.5.5) which lies along the positive real axis. This branch cut causes the propagation factor and the real part of the refractive index to be odd functions of frequency ω , viz.

$$\beta(\omega), \Re\{\tilde{n}(\omega)\} \begin{cases} > 0 & , \forall \omega > 0 \\ < 0 & , \forall \omega < 0 \end{cases}, \quad (2.5.9a)$$

and the attenuation factor and the imaginary part of the refractive index to be an even functions of frequency ω , viz.

$$\alpha(\omega), \Im\{\tilde{n}(\omega)\} > 0, \quad \forall \omega, \quad (2.5.9b)$$

since, physically, for a lossy medium $\alpha(\omega)$ must always be positive because it represents loss.

A general solution to the homogeneous vector *Helmholtz* equations given in Eqs. (2.5.2a,b) in an infinitely extended lossy medium is given by the inhomogeneous plane waves

$$\mathbf{E}(\mathbf{r}, \omega) = \mathbf{E}_+(\omega) e^{i\tilde{\mathbf{k}}^+(\omega) \cdot \mathbf{r}} + \mathbf{E}_-(\omega) e^{i\tilde{\mathbf{k}}^-(\omega) \cdot \mathbf{r}}, \quad (2.5.10a)$$

$$\mathbf{H}(\mathbf{r}, \omega) = \mathbf{H}_+(\omega) e^{i\tilde{\mathbf{k}}^+(\omega) \cdot \mathbf{r}} + \mathbf{H}_-(\omega) e^{i\tilde{\mathbf{k}}^-(\omega) \cdot \mathbf{r}}. \quad (2.5.10b)$$

Let the position vector

$$\mathbf{r} \equiv u\hat{u} + v\hat{v} + w\hat{w}, \quad (2.5.11)$$

be defined in an arbitrarily oriented rectangular coordinate system (u, v, w) with corresponding unit vectors $(\hat{u}, \hat{v}, \hat{w})$. Here the *complex wavevector* $\tilde{\mathbf{k}}^{\pm}(\omega)$ describes the planar

7. cf. Oughstun and Sherman [59] §2.3 pp. 39–40.

phase and amplitude front propagation of the electromagnetic inhomogeneous plane wave disturbance. The complex wavevector must satisfy

$$\tilde{\mathbf{k}}^{\pm}(\omega) \cdot \tilde{\mathbf{k}}^{\pm}(\omega) \equiv \tilde{k}^2(\omega) . \quad (2.5.12)$$

The real and imaginary parts of the complex wavevector $\tilde{\mathbf{k}}^{\pm}(\omega)$ have precise physical interpretations. Let the complex wavevector be defined in terms of two real vector quantities as

$$\tilde{\mathbf{k}}^{\pm}(\omega) \equiv \boldsymbol{\beta}^{\pm}(\omega) + i\boldsymbol{\alpha}^{\pm}(\omega) . \quad (2.5.13)$$

Here the *propagation vector* $\boldsymbol{\beta}^{\pm}(\omega) \equiv \Re\left\{\tilde{\mathbf{k}}^{\pm}(\omega)\right\}$ specifies the direction of propagation

of the planar phase front for $\omega > 0$ while the *attenuation vector* $\boldsymbol{\alpha}^{\pm}(\omega) \equiv \Im\left\{\tilde{\mathbf{k}}^{\pm}(\omega)\right\}$

specifies the direction of propagation of the planar amplitude front for any ω . When $\omega < 0$ the phase factor in Eqs. (2.5.10a,b), $\boldsymbol{\beta}^{\pm}(\omega) \cdot \mathbf{r} - \omega t$, establishes that the surfaces of constant phase propagate in the direction $-\boldsymbol{\beta}^{\pm}(\omega)$ for $\omega < 0$. The propagation vector $\boldsymbol{\beta}^{\pm}(\omega)$ is normal to the surfaces of constant phase such that

$$\boldsymbol{\beta}^{\pm}(\omega) \cdot \mathbf{r} = \text{constant} ,$$

while the attenuation vector $\boldsymbol{\alpha}^{\pm}(\omega)$ is normal to the surfaces of constant amplitude such that

$$\boldsymbol{\alpha}^{\pm}(\omega) \cdot \mathbf{r} = \text{constant} ,$$

where \mathbf{r} is the position vector as defined in Eq. (2.5.11). Substitution of Eq. (2.5.13) into Eq. (2.5.12) yields

$$|\boldsymbol{\beta}^{\pm}(\omega)|^2 - |\boldsymbol{\alpha}^{\pm}(\omega)|^2 + 2i\boldsymbol{\beta}^{\pm}(\omega) \cdot \boldsymbol{\alpha}^{\pm}(\omega) = \tilde{k}^2(\omega) . \quad (2.5.14)$$

The imaginary part of Eq. (2.5.14) must then obey the condition given in Eq. (2.5.7), viz.

$$2\boldsymbol{\beta}^{\pm}(\omega) \cdot \boldsymbol{\alpha}^{\pm}(\omega) \begin{cases} > 0 & , \forall \omega > 0 \\ < 0 & , \forall \omega < 0 \end{cases} . \quad (2.5.15)$$

Therefore, the angle between $\boldsymbol{\beta}^{\pm}(\omega)$ and $\boldsymbol{\alpha}^{\pm}(\omega)$ is less than $\frac{\pi}{2}$ for $\omega > 0$. Although an

inhomogeneous plane wave decays at its maximum rate in the direction of $\boldsymbol{\alpha}^\pm(\omega)$, the condition given in Eq. (2.5.15) demands that the amplitude also decays in the direction of $\boldsymbol{\beta}^\pm(\omega)$ for $\omega > 0$ ⁸. Define a position vector in the direction of $\boldsymbol{\beta}^\pm(\omega)$, viz. $\mathbf{r}_\beta = \frac{\boldsymbol{\beta}^\pm(\omega)}{|\boldsymbol{\beta}^\pm(\omega)|} r_\beta$.

Therefore, the amplitude portion of Eqs. (2.5.10a,b) becomes

$$e^{-\boldsymbol{\alpha}^\pm(\omega) \cdot \mathbf{r}_\beta} = e^{-\boldsymbol{\alpha}^\pm(\omega) \cdot \frac{\boldsymbol{\beta}^\pm(\omega)}{|\boldsymbol{\beta}^\pm(\omega)|} r_\beta} \quad (2.5.16)$$

so that the amplitude decays in the direction of $\boldsymbol{\beta}^\pm(\omega)$ as r_β increases for $\omega > 0$. However, the condition given in Eq. (2.5.15) for $\omega < 0$ together with the fact that the direction of phase front propagation is $-\boldsymbol{\beta}^\pm(\omega)$ for $\omega < 0$ demands that the amplitude decays in the direction of $-\boldsymbol{\beta}^\pm(\omega)$ as r_β increases by virtue of Eq. (2.5.16).

In the most general sense, for some complex frequency ω , all but one of the various complex components of $\tilde{\mathbf{k}}^\pm(\omega)$ may be chosen arbitrarily whereas the relationship given in Eq. (2.5.12) constrains and wholly determines the remaining complex component⁹. For example, let the complex wavevector be defined in the same (u, v, w) rectangular coordinate system as the position vector, viz.

$$\tilde{\mathbf{k}}^\pm(\omega) \equiv k_u \hat{\mathbf{u}} + k_v \hat{\mathbf{v}} \pm \gamma(\omega) \hat{\mathbf{w}}, \quad (2.5.17)$$

where k_u and k_v are known as the *transverse wavenumbers* which are the arbitrarily chosen components of $\tilde{\mathbf{k}}^\pm(\omega)$. The transverse wavenumbers are defined to be real-valued. Consequently, the remaining quantity $\gamma(\omega)$, which is known as the *longitudinal wavenumber*, is complex-valued since it is defined through the complex relationship given in Eq. (2.5.12). Substitution of Eq. (2.5.17) into Eq. (2.5.12) defines the longitudinal wavenumber as the principal branch of the expression

8. See Caviglia and Morro [69] §1.3 p. 10.

9. See Stratton [68] p. 363.

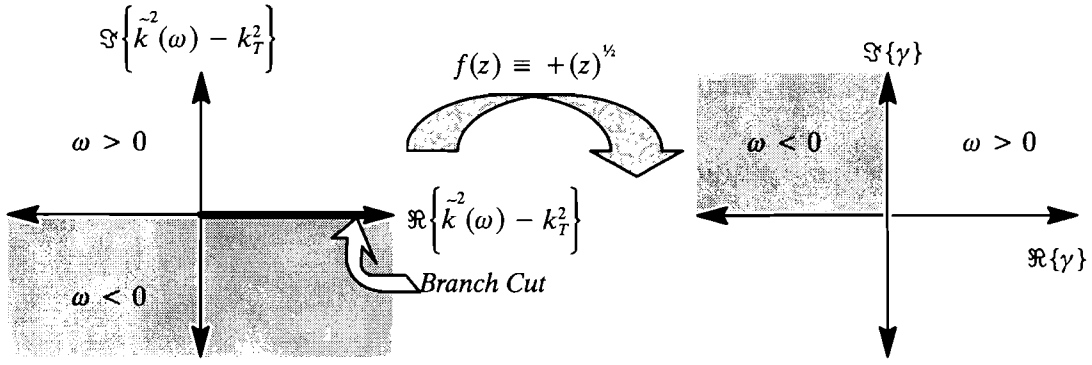


Figure 2.5.1 The first sheet of the *Riemann surface* and its range. The sheet divides into two distinct regions depending on the sign of the real-valued frequency ω as indicated by the differently shaded areas.

$$\gamma(\omega) \equiv \left(\tilde{k}^2(\omega) - k_T^2 \right)^{1/2} = \sqrt{\Gamma} e^{i\frac{\theta}{2}} \quad ; \quad 0 \leq \frac{\theta}{2} < \pi \quad (2.5.18)$$

where $k_T^2 \equiv k_u^2 + k_v^2$.

Examining the nature of the square $\gamma^2(\omega)$ of the complex longitudinal wavenumber reveals that the first sheet of the *Riemann surface* separates into two distinct regions depending of the sign of the real-valued frequency ω . The quantity k_T^2 , which is pure real by definition, together with Eq. (2.5.6b) and the condition given in Eq. (2.5.7) yields

$$\tilde{k}^2(\omega) - k_T^2 = \left\| \frac{1}{c^2} \right\| \omega^2 \mu \begin{cases} \varepsilon_i(\omega) > 0 & , \forall \omega > 0 \\ \varepsilon_i(\omega) < 0 & , \forall \omega < 0 \end{cases} \quad (2.5.19)$$

The first sheet of the *Riemann surface* then divides into two distinct regions, viz.

$$\tilde{k}^2(\omega) - k_T^2 = \Gamma e^{i\theta} \quad ; \quad \begin{cases} 0 \leq \theta < \pi & , \forall \omega > 0 \\ \pi \leq \theta < 2\pi & , \forall \omega < 0 \end{cases}$$

Consequently, the range of first sheet of the *Riemann surface* divides accordingly into

$$\gamma = \sqrt{\Gamma} e^{i\frac{\theta}{2}} \quad ; \quad \begin{cases} 0 \leq \frac{\theta}{2} < \frac{\pi}{2} & , \forall \omega > 0 \\ \frac{\pi}{2} \leq \frac{\theta}{2} < \pi & , \forall \omega < 0 \end{cases} \quad (2.5.20)$$

The first sheet of the *Riemann surface* and its range are both illustrated in Figure 2.5.1.

Based on the results of Eq. (2.5.20), when $\omega > 0$ then $\Re\{\gamma(\omega)\} > 0$ which in turn establishes that the surfaces of constant phase propagate along the positive \hat{w} direction. Similarly, when $\omega < 0$ then $\Re\{\gamma(\omega)\} < 0$ which still establishes that the surfaces of constant phase propagate along the positive \hat{w} direction because the direction of phase front propagation is $-\boldsymbol{\beta}^+(\omega)$ for $\omega < 0$. Consequently, $\tilde{\mathbf{k}}^+$ can be appropriately labeled the forward complex wavevector for any frequency ω .

Therefore, the vector field pair $\{\mathbf{E}_+(\omega)e^{i\tilde{\mathbf{k}}^+(\omega)\cdot\mathbf{r}}, \mathbf{H}_+(\omega)e^{i\tilde{\mathbf{k}}^+(\omega)\cdot\mathbf{r}}\}$ represents an inhomogeneous plane wave disturbance propagating into the positive half-space $w > 0$ in a direction specified by the complex wavevector $\tilde{\mathbf{k}}^+(\omega)$. Analogously, the other vector field pair $\{\mathbf{E}_-(\omega)e^{i\tilde{\mathbf{k}}^-(\omega)\cdot\mathbf{r}}, \mathbf{H}_-(\omega)e^{i\tilde{\mathbf{k}}^-(\omega)\cdot\mathbf{r}}\}$ represents an inhomogeneous plane wave propagating into the negative half-space $w < 0$ in a direction specified by $\tilde{\mathbf{k}}^-(\omega)$. Let the complex wavevector be given again by Eq. (2.5.17) so that the propagation vector may be written as

$$\boldsymbol{\beta}^\pm(\omega) \equiv k_u \hat{u} + k_v \hat{v} \pm \Re\{\gamma(\omega)\} \hat{w} \quad (2.5.21a)$$

and the attenuation vector may be written as

$$\boldsymbol{\alpha}^\pm(\omega) \equiv \pm \Im\{\gamma(\omega)\} \hat{w} . \quad (2.5.21b)$$

An example of these propagation and attenuation vectors is presented in Figure 2.5.2. As illustrated, the propagation and attenuation vectors do not necessarily point in the same direction. When $\boldsymbol{\beta}^\pm(\omega)$ and $\boldsymbol{\alpha}^\pm(\omega)$ are not collinear, the general wave solution is referred to as an inhomogeneous plane wave, otherwise the general wave solution is a homogeneous plane wave.

2.5.1 The Transversality Conditions

Either inhomogeneous plane wave solution of Eq. (2.5.10) may be represented by the vector field pair

$$\mathbf{E}(\mathbf{r}, \omega) = \mathbf{E}(\omega)e^{+i\tilde{\mathbf{k}}^\pm(\omega)\cdot\mathbf{r}} , \quad (2.5.22a)$$

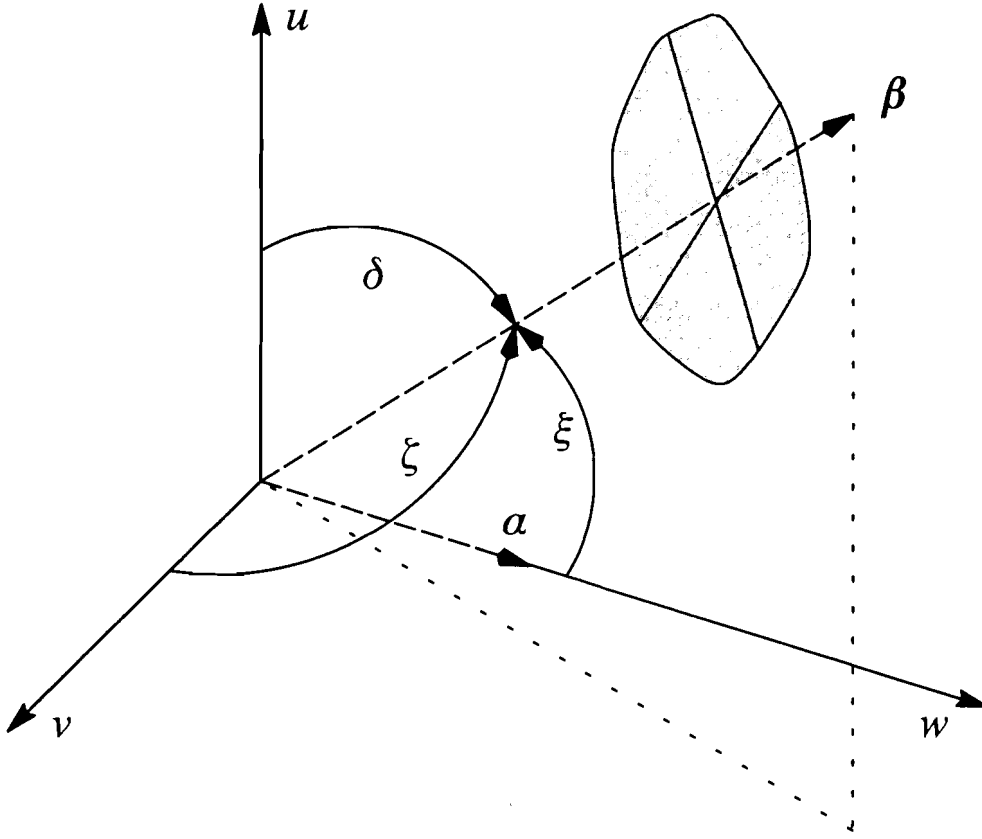


Figure 2.5.2 An example of an inhomogeneous plane wave phase front propagating in the direction specified by the propagation vector. The attenuation vector is directed along the positive w -axis. The quantities δ , ζ and ξ represent the direction cosines for the propagation vector.

$$\mathbf{H}(\mathbf{r}, \omega) = \mathbf{H}(\omega) e^{+i\tilde{\mathbf{k}}^{\pm}(\omega) \cdot \mathbf{r}} \quad (2.5.22b)$$

If Eq. (2.5.22b) is substituted into Eq. (2.2.12b) using Eq. (2.2.13a), then the electric field intensity can be written in terms of the complex wavevector and the magnetic field intensity as

$$\mathbf{E}(\mathbf{r}, \omega) = -\frac{\|c\|}{\tilde{\epsilon}(\omega)\omega} \tilde{\mathbf{k}}^{\pm}(\omega) \times \mathbf{H}(\mathbf{r}, \omega) \quad (2.5.23)$$

while substitution of Eq. (2.5.22a) into Eq. (2.2.12a) using Eq. (2.2.13b) allows the magnetic field intensity to be expressed in terms of the complex wavevector and the electric field intensity as

$$\mathbf{H}(\mathbf{r}, \omega) = \frac{\|c\|}{\mu\omega} \tilde{\mathbf{k}}^{\pm}(\omega) \times \mathbf{E}(\mathbf{r}, \omega) \quad (2.5.24)$$

Finally, the dot product of $\tilde{\mathbf{k}}^{\pm}(\omega)$ with Eqs. (2.5.23) and (2.5.24) yields

$$\tilde{\mathbf{k}}^{\pm}(\omega) \cdot \mathbf{E}(\mathbf{r}, \omega) = 0, \quad (2.5.25a)$$

$$\tilde{\mathbf{k}}^{\pm}(\omega) \cdot \mathbf{H}(\mathbf{r}, \omega) = 0, \quad (2.5.25b)$$

and the dot product of $\mathbf{H}(\mathbf{r}, \omega)$ with Eq. (2.5.23) yields

$$\mathbf{H}(\mathbf{r}, \omega) \cdot \mathbf{E}(\mathbf{r}, \omega) = 0. \quad (2.5.25c)$$

Eqs. (2.5.25a–c) together with relations Eqs. (2.5.23) and (2.5.24) are known as the transversality conditions.

2.5.2 Direction Cosine Form of the Inhomogeneous Plane Wave

Consider the inhomogeneous plane wave spectral components of the electromagnetic field vectors in the positive half space as given in Eqs. (2.5.22a,b), each with the complex wavevector

$$\tilde{\mathbf{k}}^+(\omega) \equiv k_u \hat{\mathbf{u}} + k_v \hat{\mathbf{v}} + \gamma(\omega) \hat{\mathbf{w}} \quad (2.5.26)$$

which has the complex direction cosine representation[59]

$$\tilde{\mathbf{k}}^+(\omega) \equiv \tilde{k}(\omega) [p \hat{\mathbf{u}} + q \hat{\mathbf{v}} + m \hat{\mathbf{w}}] \quad (2.5.27)$$

with the complex wavenumber

$$\tilde{k}(\omega) \equiv \beta(\omega) + i\alpha(\omega) = \tilde{n}(\omega)k_0 \quad (2.5.28)$$

where $p \equiv k_u/\tilde{k}(\omega)$, $q \equiv k_v/\tilde{k}(\omega)$, and $m \equiv \gamma(\omega)/\tilde{k}(\omega)$. The quantities $\beta(\omega)$ and $\alpha(\omega)$ are not to be confused with the magnitudes of the propagation and attenuation vectors. Since both k_u and k_v are chosen to be real valued, then $p = p' + ip''$ and $q = q' + iq''$ must both be complex valued with

$$p'' = -\frac{\alpha(\omega)}{\beta(\omega)}p', \quad (2.5.29a)$$

$$q'' = -\frac{\alpha(\omega)}{\beta(\omega)}q'. \quad (2.5.30b)$$

The complex direction cosine $m = m' + im''$ is then given by the principle branch of the expression

$$\begin{aligned} m &\equiv \sqrt{1 - p'^2 - q'^2} \\ &= \sqrt{1 - \left[1 - \frac{\alpha^2(\omega)}{\beta^2(\omega)}\right] [p'^2 + q'^2] + 2i \frac{\alpha(\omega)}{\beta(\omega)} [p'^2 + q'^2]} . \end{aligned} \quad (2.5.31)$$

With these results, the spatial phase term appearing in the exponential factor of the inhomogeneous plane wave disturbance given in Eq. (2.5.22) is seen to be given by

$$\begin{aligned} \tilde{\mathbf{k}}^+(\omega) \cdot \mathbf{r} &\equiv k_u u + k_v v + \gamma(\omega) w \\ &= \beta(\omega) \left[1 + \frac{\alpha^2(\omega)}{\beta^2(\omega)}\right] [p' u + q' v] + [\beta(\omega) m' - \alpha(\omega) m''] w + i [\alpha(\omega) m' + \beta(\omega) m''] w . \end{aligned} \quad (2.5.32)$$

This then represents the spatial part of the inhomogeneous plane wave disturbance of angular frequency ω whose surfaces of constant amplitude $w = \text{constant}$ are, in general, different from the surfaces of constant phase

$$\left[1 + \frac{\alpha^2(\omega)}{\beta^2(\omega)}\right] [p' u + q' v] + \left[m' - \frac{\alpha(\omega)}{\beta(\omega)} m''\right] w = \text{constant} . \quad (2.5.33)$$

The attenuation vector for the inhomogeneous plane wave disturbance is directed along the \hat{w} as before, while the propagation vector's direction is specified by the real-valued vector

$$\mathbf{s} \equiv \left[1 + \frac{\alpha^2(\omega)}{\beta^2(\omega)}\right] [p' \hat{u} + q' \hat{v}] + \left[m' - \frac{\alpha(\omega)}{\beta(\omega)} m''\right] \hat{w} \quad (2.5.34)$$

with magnitude

$$s \equiv \sqrt{\left[1 + \frac{\alpha^2(\omega)}{\beta^2(\omega)}\right]^2 [p'^2 + q'^2] + \left[m' - \frac{\alpha(\omega)}{\beta(\omega)} m''\right]^2} . \quad (2.5.35)$$

This direction is then completely specified by the set of real-valued direction cosines

$$\{\xi, \psi, \zeta\} = \left\{ \frac{1}{s} \left[1 + \frac{\alpha^2(\omega)}{\beta^2(\omega)} \right] p', \frac{1}{s} \left[1 + \frac{\alpha^2(\omega)}{\beta^2(\omega)} \right] q', \frac{1}{s} \left[m' - \frac{\alpha(\omega)}{\beta(\omega)} m'' \right] \right\}, \quad (2.5.36)$$

as illustrated in Figure 2.5.2.

2.5.3 The Poynting Vector and the Time Averaged Power Density of an Inhomogeneous Plane Wave

The phase fronts and amplitude fronts of an inhomogeneous plane wave propagate in different directions. The question concerning the manner in which power flows for such a wave naturally arises. The *complex Poynting vector* for an arbitrary electromagnetic field was defined in Eq. (2.2.16). Utilizing the transversality condition given in Eq. (2.5.24) for an inhomogeneous plane wave, the *complex Poynting vector* becomes

$$\mathbf{S}(\mathbf{r}, \omega) \equiv \frac{1}{2} \left\| \frac{c^2}{4\pi} \right\| \frac{1}{\mu\omega} \mathbf{E}(\mathbf{r}, \omega) \times \left[\tilde{\mathbf{k}}^{\pm*}(\omega) \times \mathbf{E}^*(\mathbf{r}, \omega) \right],$$

where the application of the vector identity $\mathbf{A} \times (\mathbf{B} \times \mathbf{C}) = \mathbf{B}(\mathbf{A} \cdot \mathbf{C}) - \mathbf{C}(\mathbf{A} \cdot \mathbf{B})$ yields

$$\mathbf{S}(\mathbf{r}, \omega) \equiv \frac{1}{2} \left\| \frac{c^2}{4\pi} \right\| \frac{1}{\mu\omega} \left\{ \tilde{\mathbf{k}}^{\pm*}(\omega) |\mathbf{E}(\mathbf{r}, \omega)|^2 - \mathbf{E}^*(\mathbf{r}, \omega) \left[\tilde{\mathbf{k}}^{\pm*}(\omega) \cdot \mathbf{E}(\mathbf{r}, \omega) \right] \right\}. \quad (2.5.37)$$

Let the complex wavevector be defined in terms of Eqs. (2.5.21a,b) so that

$$\mathbf{E}(\mathbf{r}, \omega) = \left[E_u(\omega) \hat{u} + E_v(\omega) \hat{v} + E_w(\omega) \hat{w} \right] e^{+i\tilde{\mathbf{k}}^{\pm}(\omega) \cdot \mathbf{r}}, \quad (2.5.38)$$

and

$$\tilde{\mathbf{k}}^{\pm*}(\omega) \cdot \mathbf{E}(\mathbf{r}, \omega) = \left[E_u(\omega) k_u + E_v(\omega) k_v \pm E_w(\omega) \gamma^*(\omega) \right] e^{+i\tilde{\mathbf{k}}^{\pm}(\omega) \cdot \mathbf{r}}.$$

Substitution of Eq. (2.5.38) into the transversality condition given in Eq. (2.5.25a) yields

$$\tilde{\mathbf{k}}^{\pm}(\omega) \cdot \mathbf{E}(\mathbf{r}, \omega) = \left[E_u(\omega) k_u + E_v(\omega) k_v \pm E_w(\omega) \gamma(\omega) \right] e^{+i\tilde{\mathbf{k}}^{\pm}(\omega) \cdot \mathbf{r}} = 0,$$

which, when solved for the transverse components, becomes

$$E_u(\omega) k_u + E_v(\omega) k_v = \mp E_w(\omega) \gamma(\omega).$$

The appropriate substitution yields

$$\begin{aligned}\tilde{\mathbf{k}}^{\pm*}(\omega) \cdot \mathbf{E}(\mathbf{r}, \omega) &= [\mp \gamma(\omega) \pm \gamma^*(\omega)] E_w(\omega) e^{+i\tilde{\mathbf{k}}^{\pm}(\omega) \cdot \mathbf{r}} \\ &= \mp 2i\Im\{\gamma(\omega)\} E_w(\omega) e^{+i\tilde{\mathbf{k}}^{\pm}(\omega) \cdot \mathbf{r}}.\end{aligned}\quad (2.5.39)$$

The *complex Poynting vector* can now be written, using Eq. (2.5.39), as

$$\mathbf{S}(\mathbf{r}, \omega) \equiv \frac{1}{2} \left\| \frac{c^2}{4\pi} \right\| \frac{1}{\mu\omega} \left\{ \tilde{\mathbf{k}}^{\pm*}(\omega) |\mathbf{E}(\mathbf{r}, \omega)|^2 \pm \mathbf{E}^*(\mathbf{r}, \omega) 2i\Im\{\gamma(\omega)\} E_w(\omega) e^{+i\tilde{\mathbf{k}}^{\pm}(\omega) \cdot \mathbf{r}} \right\}.$$

A similar expression for the *complex Poynting vector* can be derived in terms of the magnetic field, viz.

$$\mathbf{S}(\mathbf{r}, \omega) \equiv \frac{1}{2} \left\| \frac{c^2}{4\pi} \right\| \frac{1}{\bar{\epsilon}(\omega)\omega} \left\{ \tilde{\mathbf{k}}^{\pm}(\omega) |\mathbf{H}(\mathbf{r}, \omega)|^2 \mp \mathbf{H}(\mathbf{r}, \omega) 2i\Im\{\gamma(\omega)\} H_w^*(\omega) e^{+i\tilde{\mathbf{k}}^{\pm}(\omega) \cdot \mathbf{r}} \right\}.$$

As reasoned with Eq. (2.2.21), the real part of the *complex Poynting vector* represents the time-averaged power density, so that

$$\begin{aligned}\Re\{\mathbf{S}(\mathbf{r}, \omega)\} &= \frac{1}{2} \left\| \frac{c^2}{4\pi} \right\| \frac{1}{\mu\omega} \left[\boldsymbol{\beta}^{\pm}(\omega) |\mathbf{E}(\mathbf{r}, \omega)|^2 \right. \\ &\quad \left. \mp 2\Im\{\gamma(\omega)\} \Im\left\{ \mathbf{E}^*(\mathbf{r}, \omega) E_w(\omega) e^{+i\tilde{\mathbf{k}}^{\pm}(\omega) \cdot \mathbf{r}} \right\} \right].\end{aligned}\quad (2.5.40)$$

represents the time-averaged power density of an inhomogeneous plane wave of frequency ω . The terms within the imaginary operator of the second term of Eq. (2.5.40), using the complex conjugate of Eq. (2.5.38), yield

$$\mathbf{E}^*(\mathbf{r}, \omega) E_w(\omega) e^{+i\tilde{\mathbf{k}}^{\pm}(\omega) \cdot \mathbf{r}} = \left\{ \mathbf{E}_T^*(\omega) E_w(\omega) + |E_w(\omega)|^2 \hat{\mathbf{w}} \right\} e^{+i \left[\tilde{\mathbf{k}}^{\pm}(\omega) - \tilde{\mathbf{k}}^{\pm*}(\omega) \right] \cdot \mathbf{r}}, \quad (2.5.41)$$

where

$$\mathbf{E}_T^*(\omega) \equiv E_u^*(\omega) \hat{\mathbf{u}} + E_v^*(\omega) \hat{\mathbf{v}}. \quad (2.5.42)$$

The exponent in Eq. (2.5.41) reduces to

$$+ i \left[\tilde{\mathbf{k}}^{\pm}(\omega) - \tilde{\mathbf{k}}^{\pm*}(\omega) \right] \cdot \mathbf{r} = \mp 2\Im\{\gamma(\omega)\} w, \quad (2.5.43)$$

where \mathbf{r} is defined in Eq. (2.5.11). Substitution of Eq. (2.5.41) into Eq. (2.5.40) together with

Eq. (2.5.43) yields

$$\Re\{\mathbf{S}(\mathbf{r}, \omega)\} = \frac{1}{2} \left\| \frac{c^2}{4\pi} \right\| \frac{1}{\mu\omega} \left[\boldsymbol{\beta}^\pm(\omega) |\mathbf{E}(\mathbf{r}, \omega)|^2 \mp 2\Im\{\gamma(\omega)\} \Im\{\mathbf{E}_T^*(\omega) \mathbf{E}_w(\omega)\} e^{\mp 2\Im\{\gamma(\omega)\}w} \right], \quad (2.5.44)$$

because the \hat{w} component of Eq. (2.5.41) is pure real. This means that the second term present in Eq. (2.5.44) only contributes to the time averaged power in the transverse directions \hat{u} and \hat{v} .

The second term present in Eq. (2.5.44) generalizes typical representations¹⁰ for time-harmonic plane wave *Poynting vectors*. This additional term results from the unique nature of inhomogeneous plane waves, namely the fact that the propagation and attenuation vectors are not collinear. This term will direct power in directions not dictated by the propagation vector. However, if the electric field is transverse to the uw plane then $\mathbf{E}_w(\omega) = 0$ or if the wave is homogeneous (i.e. $k_u, k_v = 0$) then $\tilde{\mathbf{k}}^\pm(\omega) = \tilde{k}^\pm \hat{w}$. Both cases imply that $\mathbf{E}_w(\omega) = 0$, due to the transversality condition given in Eq. (2.5.25a), so that Eq. (2.5.40) reduces to the typical form of

$$\Re\{\mathbf{S}(\mathbf{r}, \omega)\} = \frac{1}{2} \left\| \frac{c^2}{4\pi} \right\| \frac{1}{\mu\omega} \left[\boldsymbol{\beta}^\pm(\omega) |\mathbf{E}(\mathbf{r}, \omega)|^2 \right],$$

where all the power is directed by the propagation vector.

2.5.4 The Energy Transport Velocity for a Plane Wave in an Infinitely Extended Double Resonance Lorentz Model Dielectric

The derivation of the velocity of energy transport begins with the differential form of *Poynting's theorem*, which may be written as[30]

$$\nabla \cdot \mathbf{S} = \left\| \frac{1}{4\pi} \right\| \left\{ \mathbf{H} \cdot \frac{\partial \mathbf{H}}{\partial t} + \mathbf{E} \cdot \frac{\partial \mathbf{E}}{\partial t} + 4\pi \mathbf{E} \cdot \frac{\partial \mathbf{P}}{\partial t} \right\}. \quad (2.5.45)$$

Upon taking a volume integral of this expression over some arbitrary region, the *Poynting vector* \mathbf{S} (Watts/m² in MKS units) can be interpreted as the amount of electromagnetic power

10. See Oughstun and Sherman [59] p. 43 §2.3.

per unit surface area that is either leaving or entering the region, and the three scalar quantities appearing on the right hand side may be interpreted as the time rate of change of the magnetic field energy density, the electric field energy density and the energy density stored in the medium.

The energy transport velocity of a monochromatic plane wave field is defined as the rate of electromagnetic energy flow in the medium and is given by the ratio of the time–average *Poynting vector* to the total time–average electromagnetic energy density of the coupled field–medium system[19], so that

$$\mathbf{v}_E = \frac{\langle \mathbf{S} \rangle}{W_{total}} . \quad (2.5.46)$$

For a monochromatic homogeneous plane wave field in a nonconducting, dispersive dispersive dielectric with $\mu = \mu_0$, the time average of the magnitude of the *Poynting vector* is found to be[19][34][68][70][59],

$$\langle |\mathbf{S}| \rangle = \left\| \frac{c^2}{4\pi} \right\| \frac{1}{2\mu_0 c} n_r(\omega) |\mathbf{E}|^2 , \quad (2.5.47)$$

where c is the vacuum speed of light.

The quantity W_{total} is given by the sum of the time–average energy density of both the electric and magnetic energy densities and the amount of time–average energy density stored in the medium, so that

$$W_{total} \equiv W_{field} + W_{osc} . \quad (2.5.48)$$

The time–average energy density of the electromagnetic field is then found to be given by[59]

$$W_{field} = \left\| \frac{1}{4\pi} \right\| \frac{\epsilon_0}{4} (n_r^2(\omega) + n_i^2(\omega) + 1) |\mathbf{E}|^2 , \quad (2.5.49)$$

where n_r is the real part and n_i is the imaginary part of the complex index of refraction \tilde{n} . The stored time–average energy density of the double resonance Lorentz model dielectric medium is also found as[59],

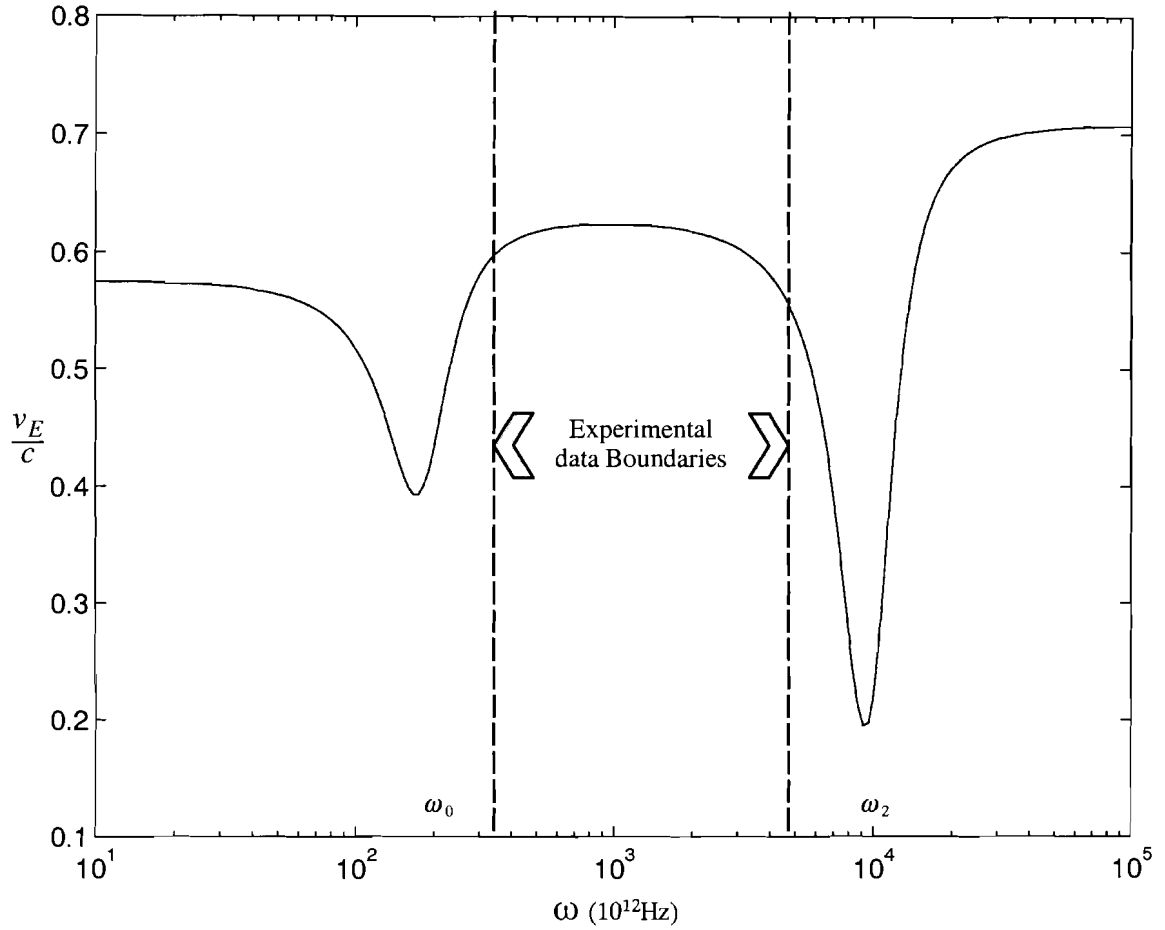


Figure 2.5.3 Frequency dependence of the normalized magnitude of the energy transport velocity of a monochromatic plane wave for a double resonance Lorentz model of a fluoride glass (CLAP) with Lorentz model parameters taken from Table 2.3.1.

$$W_{osc} = \left\| \frac{1}{4\pi} \right\| \frac{\epsilon_0}{4} |\mathbf{E}|^2 \sum_{j=0,2} \frac{b_j^2 (\omega^2 + \omega_j^2)}{(\omega^2 - \omega_j^2)^2 + 4\delta_j^2 \omega^2} . \quad (2.5.50)$$

The total time-average electromagnetic energy density stored in both the field and the double resonance Lorentz model dielectric medium is then given by[59]

$$W_{total} = \left\| \frac{1}{4\pi} \right\| \frac{\epsilon_0}{2} |\mathbf{E}|^2 \left[n_r^2(\omega) + \sum_{j=0,2} \frac{b_j^2 \omega^2}{(\omega^2 - \omega_j^2)^2 + 4\delta_j^2 \omega^2} \right] . \quad (2.5.51)$$

The final expression for the magnitude of the energy transport velocity of a monochromatic plane wave field in a double resonance Lorentz model is then given by[59]

$$v_E = \frac{\langle S \rangle}{W_{total}} = \frac{c}{n_r(\omega) + \frac{1}{n_r(\omega)} \sum_{j=0,2} \frac{b_j^2 \omega^2}{(\omega^2 - \omega_j^2)^2 + 4\delta_j^2 \omega^2}} . \quad (2.5.52)$$

This result is a generalization of the well known expression for a single resonance Lorentz medium given by Loudon[70] and Eq. (2.5.52) reduces to that expression in the limit of that special case. The frequency dispersion of the energy transport velocity of a monochromatic plane wave in the double resonance Lorentz model for the CLAP fluoride glass: $CdF_2 - LiF - AlF_3 - PbF_2$ that was considered in § 2.3.2, is depicted in Figure 2.5.3.

2.6 Polarization Properties for Propagating Electromagnetic Inhomogeneous Plane Waves

One of the principle characteristics that describes an electromagnetic field is its polarization state. Generally speaking, the polarization state for either the electric or magnetic field vectors can be linear, elliptical or circular. In addition, the electric and magnetic field vectors can have different polarization states. Elliptical and circular polarization states possess, as an additional characteristic, a left or right handed sense that describes the particular direction in which the field vector rotates. Further, for a particular space–time point, circular polarization is a linear combination of properly phased and orthogonally oriented linear polarized fields and elliptical polarization is a linear combination of properly phased and oriented circular polarized fields. The polarization state refers to the behavior of the field at a particular space–time point and, in general, varies from point to point for arbitrary pulsed beam fields¹¹.

On the other hand, inhomogeneous plane waves expressed as [cf. §2.5]

$$\mathbf{A}(\mathbf{r}, \omega) = \mathbf{A}(\omega) e^{+i\mathbf{k}^{\pm}(\omega) \cdot \mathbf{r}}$$

are uniformly polarized. The vector $\mathbf{A}(\mathbf{r}, \omega)$ represents either the electric or magnetic field

11. For a complete description of these and other polarization phenomena see Oughstun and Sherman [59] §4.2.

and, in general, $\mathbf{A}(\omega)$ and $\tilde{\mathbf{k}}^{\pm}(\omega)$ are complex vectors which are functions of frequency. The vector nature of $\mathbf{A}(\omega)$ determines the polarization state: either linear, elliptical or circular. Uniform polarization refers to a characteristic independence of $\mathbf{A}(\omega)$, and accordingly the polarization state, with respect to space and time. The independence with respect to time can be understood by considering the field vector $\mathbf{A}(\mathbf{r}, \omega)$ of an inhomogeneous plane wave to be a particular monochromatic spectral component for a real-valued angular frequency ω , which when transformed yields

$$\mathcal{A}(\mathbf{r}, t) = A(\omega)e^{+i\tilde{\mathbf{k}}^{\pm}(\omega)\cdot\mathbf{r}-i\omega t} ,$$

where it is evident that $\mathbf{A}(\omega)$ is neither a function of position nor of time.

2.6.1 The Polarization Ellipse for the Complex Field Vectors

Let the complex spectral amplitude vector $\mathbf{A}(\omega)$ of an inhomogeneous plane wave be expressed in terms of two real vectors as in the §2.4, viz.

$$\mathbf{A}(\omega) = \mathbf{p}(\omega) + i\mathbf{q}(\omega) = [\mathbf{a}(\omega) + i\mathbf{b}(\omega)]e^{i\phi(\omega)} .$$

Assuming that $\mathbf{p} \times \mathbf{q} \neq 0$ and that $\mathbf{a} \cdot \mathbf{b} = 0$, then Eqs. (2.4.3a,b) define the magnitudes $|\mathbf{a}(\omega)|$ and $|\mathbf{b}(\omega)|$ of the orthogonal vectors and Eq. (2.4.2) defines the real-valued phase quantity ϕ . Consider a particular monochromatic spectral component for a real-valued frequency ω , the transform of the field vector of an inhomogeneous plane wave yields

$$\mathcal{A}(\mathbf{r}, t) = [\mathbf{a}(\omega) + i\mathbf{b}(\omega)]e^{+i\tilde{\mathbf{k}}^{\pm}(\omega)\cdot\mathbf{r}-i\omega t+i\phi(\omega)} .$$

where the complex wavevector $\tilde{\mathbf{k}}^{\pm}(\omega) \equiv \boldsymbol{\beta}^{\pm}(\omega) + i\boldsymbol{\alpha}^{\pm}(\omega)$ is also expressed in terms of two real vectors. At a particular space point $\mathbf{r} = \mathbf{r}_0$, the real and imaginary parts of the field vector $\mathcal{A}(\mathbf{r}_0, t)$ are given by¹²

$$\Re\{\mathcal{A}(\mathbf{r}_0, t)\} = [\cos(\xi)\mathbf{a}(\omega) - \sin(\xi)\mathbf{b}(\omega)]e^{-\boldsymbol{\alpha}^{\pm}\cdot\mathbf{r}_0} , \quad (2.6.1a)$$

12. cf. Oughstun and Sherman [59] §4.2.1.

$$\Im\{\mathcal{A}(\mathbf{r}_0, t)\} = \left[\cos\left(\xi + \frac{\pi}{2}\right)\mathbf{a}(\omega) - \sin\left(\xi + \frac{\pi}{2}\right)\mathbf{b}(\omega) \right] e^{-\mathbf{a}^\pm \cdot \mathbf{r}_0}, \quad (2.6.1b)$$

where $\xi \equiv \boldsymbol{\beta}^\pm(\omega) \cdot \mathbf{r}_0 - \omega t + \phi(\omega)$. As time increases, the tips of vectors $\Re\{\mathcal{A}(\mathbf{r}_0, t)\}$ and $\Im\{\mathcal{A}(\mathbf{r}_0, t)\}$ both describe the same ellipse while jointly $\frac{\pi}{2}$ out of phase. The semi-axes lengths of the ellipse are $|\mathbf{a}(\omega)|e^{-\mathbf{a}^\pm \cdot \mathbf{r}_0}$ and $|\mathbf{b}(\omega)|e^{-\mathbf{a}^\pm \cdot \mathbf{r}_0}$. The field vector is said to be *elliptically polarized*.

If the vectors $\mathbf{p}(\omega)$ and $\mathbf{q}(\omega)$ are orthogonal and of equal amplitude such that

$$\mathbf{p}(\omega) \cdot \mathbf{q}(\omega) = p^2 - q^2 = 0,$$

then the vectors $\mathbf{a}(\omega)$ and $\mathbf{b}(\omega)$ are indeterminate and consequently the real-valued phase quantity ϕ is also indeterminate. As an example, let the vector $\mathbf{p}(\omega)$ lie in the $\hat{\mathbf{u}}$ direction and let $\mathbf{q}(\omega)$ lie in the $\hat{\mathbf{v}}$ direction so that the field vector can be written

$$\mathcal{A}(\mathbf{r}, t) = |\mathbf{p}(\omega)| \left[\hat{\mathbf{u}} + i\hat{\mathbf{v}} \right] e^{+i\bar{\mathbf{k}}^\pm(\omega) \cdot \mathbf{r} - i\omega t + i\phi(\omega)}.$$

At a particular space point $\mathbf{r} = \mathbf{r}_0$, the real and imaginary parts of the field vector $\mathcal{A}(\mathbf{r}_0, t)$ are given by

$$\Re\{\mathcal{A}(\mathbf{r}_0, t)\} = |\mathbf{p}(\omega)| \left[\cos \xi \hat{\mathbf{u}} - \sin \xi \hat{\mathbf{v}} \right] e^{-\mathbf{a}^\pm \cdot \mathbf{r}_0}, \quad (2.6.2a)$$

$$\Im\{\mathcal{A}(\mathbf{r}_0, t)\} = |\mathbf{p}(\omega)| \left[\cos\left(\xi + \frac{\pi}{2}\right)\hat{\mathbf{u}} - \sin\left(\xi + \frac{\pi}{2}\right)\hat{\mathbf{v}} \right] e^{-\mathbf{a}^\pm \cdot \mathbf{r}_0}, \quad (2.6.1b)$$

where $\xi \equiv \boldsymbol{\beta}^\pm(\omega) \cdot \mathbf{r}_0 - \omega t + \phi(\omega)$. Now, as time increases, the tips of vectors $\Re\{\mathcal{A}(\mathbf{r}_0, t)\}$ and $\Im\{\mathcal{A}(\mathbf{r}_0, t)\}$ both describe the same circle while jointly $\frac{\pi}{2}$ out of phase. The field vector is said to be *circularly polarized*. From this example, it is readily understood that circular polarization is a linear superposition of properly phased and orthogonally oriented linearly polarized fields.

Depending on $\mathbf{a}(\omega)$ and $\mathbf{b}(\omega)$'s orientation with respect to each other and the perspective of an observer, the ellipse described by Eqs. (2.6.1a,b) may rotate in either a counterclock-

wise or clockwise sense. According to traditional terminology, if the scalar triple product $\mathbf{a}(\omega) \times \mathbf{b}(\omega) \cdot \boldsymbol{\beta}^{\pm}(\omega) > 0$ then the polarization sense is *left-handed*; the field vector describes an ellipse in the counterclockwise direction to an observer looking in the direction opposite to the direction of propagation[59]. Correspondingly, if the scalar triple product $\mathbf{a}(\omega) \times \mathbf{b}(\omega) \cdot \boldsymbol{\beta}^{\pm}(\omega) < 0$ then the polarization sense is *right-handed*; the field vector describes an ellipse in the clockwise direction.

Based on the information presented in §2.4, the characteristic planes of the complex wavevector $\tilde{\mathbf{k}}^{\pm}(\omega)$ and the complex spectral amplitude vector $\mathbf{A}(\omega)$ can be coplanar while the transversality condition $\tilde{\mathbf{k}}^{\pm}(\omega) \cdot \mathbf{A}(\omega) = 0$ remains satisfied, e.g. the magnetic field is elliptical and coplanar with $\tilde{\mathbf{k}}^{\pm}(\omega)$ for a TE field. This causes the scalar triple product to vanish, viz. $\mathbf{a}(\omega) \times \mathbf{b}(\omega) \cdot \boldsymbol{\beta}^{\pm}(\omega) = 0$. In other words, although the field $\mathbf{A}(\omega)$ is elliptically polarized, it appears to be linearly polarized when observed in the direction opposite to the direction of propagation. Therefore, some other means must be established in order to assign the polarization sense to this anomalous case if it is desirable to know the direction of rotation of the field. Using the normal to the characteristic plane of the complex wavevector $\boldsymbol{\alpha}^{\pm}(\omega) \times \boldsymbol{\beta}^{\pm}(\omega)$ instead of the propagation vector provides satisfactory results. For the anomalous case when the characteristic planes of $\tilde{\mathbf{k}}^{\pm}(\omega)$ and $\mathbf{A}(\omega)$ are coplanar, if $\mathbf{a}(\omega) \times \mathbf{b}(\omega) \cdot [\boldsymbol{\alpha}^{\pm}(\omega) \times \boldsymbol{\beta}^{\pm}(\omega)] > 0$ then the polarization sense is considered to be *left-handed* and if $\mathbf{a}(\omega) \times \mathbf{b}(\omega) \cdot [\boldsymbol{\alpha}^{\pm}(\omega) \times \boldsymbol{\beta}^{\pm}(\omega)] < 0$ then the polarization sense is considered to be *right-handed*.

2.6.2 The Linearly Polarized Inhomogeneous Plane Wave Field: TE and TM Cases

If $\mathbf{p} \times \mathbf{q} = \mathbf{0}$ the spectral amplitude vector $\mathbf{A}(\omega)$ of the inhomogeneous plane wave may be expressed in polar form as [cf. §2.4]

$$\mathbf{A}(\omega) = \mathbf{p}(\omega) + i\mathbf{q}(\omega) = \varrho(\omega)\mathbf{a}(\omega)e^{i\theta(\omega)},$$

where ϱ and θ are real valued scalars. The field vector is now considered to be linearly polarized. However, the other field vector is elliptically polarized in general as shown in the following development. While the field vector is linearly polarized any vanishing inner products

$$\mathbf{A}(\omega) \cdot \mathbf{c}_2 = 0$$

force the complex vector \mathbf{c}_2 to lie in the plane orthogonal to the real vector \mathbf{a} as mandated by conditions given in Eq. (2.4.9). This form of the field is of particular importance because other polarization states are linear combinations of properly phased and oriented linear polarized fields: circular polarization is a linear combination of properly phased and orthogonally oriented linearly polarized fields and elliptical polarization is a linear combination of properly phased and oriented circular polarized fields.

Given a particular reference plane, for example the uw -plane, let a linear polarized inhomogeneous plane wave field be oriented such that it is transverse to this reference plane. The transverse linearly polarized inhomogeneous plane wave field can then be written as

$$\mathbf{A}(\mathbf{r}, \omega) = \mathbf{A}(\omega)e^{+i\bar{\mathbf{k}}^\pm(\omega) \cdot \mathbf{r}}, \quad \mathbf{A}(\omega) = \varrho(\omega)\hat{\mathbf{v}}e^{i\theta(\omega)},$$

where the complex wavevector is defined as in Eqs. (2.5.21a,b), and attenuation is assumed to only exist along the $\hat{\mathbf{w}}$ -direction. Since $\mathbf{A}(\mathbf{r}, \omega)$ represents an inhomogeneous plane wave then $\boldsymbol{\beta}(\omega) \times \boldsymbol{\alpha}(\omega) \neq \mathbf{0}$. Conditions given in Eq. (2.4.9) force the complex wavevector to lie in the uw reference plane i.e. $k_v = 0$. If $\mathbf{A}(\mathbf{r}, \omega)$ represents the electric field then the field is called TE or Transverse Electric and is sometimes referred to as s-polarization (where 's' stands for *senkrecht* which means perpendicular in German). If $\mathbf{A}(\mathbf{r}, \omega)$ represents the magnetic field then the field is called TM or Transverse Magnetic and is sometimes referred to as p-polarization (where 'p' stands for parallel). Conversely, if it is known, *a priori*, that $k_v \neq 0$ then conditions given in Eq. (2.4.9) determine that the field $\mathbf{A}(\mathbf{r}, \omega)$ cannot be transverse to the reference plane.

Let the electric field be TE, viz.

$$\mathbf{E}(\mathbf{r}, \omega) = \mathbf{E}(\omega) e^{+i\tilde{\mathbf{k}}^{\pm}(\omega) \cdot \mathbf{r}}, \quad \mathbf{E}(\omega) = \varrho_e(\omega) \hat{\mathbf{v}} e^{i\theta_e(\omega)}.$$

The transversality condition given in Eq. (2.5.25a) gives

$$\varrho_e(\omega) \left[\tilde{\mathbf{k}}^{\pm}(\omega) \cdot \hat{\mathbf{v}} \right] e^{+i\tilde{\mathbf{k}}^{\pm}(\omega) \cdot \mathbf{r} + i\theta_e(\omega)} = 0.$$

Conditions given in Eq. (2.4.9) force the complex wavevector to lie in the uw reference plane i.e. $k_v = 0$. Additionally, the transversality condition given in Eq. (2.5.25c) gives

$$\varrho_e(\omega) [\mathbf{H}(\mathbf{r}, \omega) \cdot \hat{\mathbf{v}}] e^{+i\tilde{\mathbf{k}}^{\pm}(\omega) \cdot \mathbf{r} + i\theta_e(\omega)} = 0.$$

Again, by conditions given in Eq. (2.4.9), the magnetic field vector also must lie in the uw reference plane, i.e. $H_v(\mathbf{r}, \omega) = 0$. This causes the characteristic planes of $\mathbf{H}(\mathbf{r}, \omega)$ and the complex wavevector $\tilde{\mathbf{k}}^{\pm}(\omega)$ to be coplanar. Further, the transversality condition given in Eq. (2.5.24) defines the magnetic field as

$$\mathbf{H}(\mathbf{r}, \omega) = \frac{\|c\|}{\mu\omega} \varrho_e(\omega) \left[\tilde{\mathbf{k}}^{\pm}(\omega) \times \hat{\mathbf{v}} \right] e^{+i\tilde{\mathbf{k}}^{\pm}(\omega) \cdot \mathbf{r} + i\theta_e(\omega)}.$$

The vector $\tilde{\mathbf{k}}^{\pm}(\omega) \times \hat{\mathbf{v}}$ is complex and $\boldsymbol{\beta}(\omega) \times \boldsymbol{\alpha}(\omega) \neq \mathbf{0}$. Consequently, the magnetic field vector is elliptically polarized. The spectral amplitude vector can then be written as

$$\mathbf{H}(\omega) = [\mathbf{p}_m(\omega) + i\mathbf{q}_m(\omega)] e^{+i\theta_e(\omega)} = [\mathbf{a}_m(\omega) + i\mathbf{b}_m(\omega)] e^{+i\theta_m(\omega) + i\theta_e(\omega)},$$

where $\mathbf{p}_m(\omega) = \frac{\|c\|}{\mu\omega} \varrho_e(\omega) [\boldsymbol{\beta}(\omega) \times \hat{\mathbf{v}}]$, $\mathbf{q}_m(\omega) = \frac{\|c\|}{\mu\omega} \varrho_e(\omega) [\boldsymbol{\alpha}(\omega) \times \hat{\mathbf{v}}]$, $\mathbf{p}_m \times \mathbf{q}_m \neq \mathbf{0}$ and $\mathbf{a}_m \cdot \mathbf{b}_m = 0$. Because the characteristic planes of $\tilde{\mathbf{k}}^{\pm}(\omega)$ and $\mathbf{H}(\mathbf{r}, \omega)$ are coplanar the polarization sense is determined by

$$\mathbf{a}_m(\omega) \times \mathbf{b}_m(\omega) \cdot [\boldsymbol{\alpha}^{\pm}(\omega) \times \boldsymbol{\beta}^{\pm}(\omega)] \begin{cases} > 0; & \text{left-handed} \\ < 0; & \text{right-handed} \end{cases}, \quad (2.6.3)$$

where $\mathbf{a}_m(\omega)$ and $\mathbf{b}_m(\omega)$ are the orthogonal components of the magnetic field.

The complementary TM case yields analogous results. Let the magnetic field be TM, viz.

$$\mathbf{H}(\mathbf{r}, \omega) = \mathbf{H}(\omega) e^{+i\tilde{\mathbf{k}}^{\pm}(\omega) \cdot \mathbf{r}}, \quad \mathbf{H}(\omega) = \varrho_m(\omega) \hat{\mathbf{v}} e^{i\theta_m(\omega)}.$$

The transversality condition given in Eq. (2.5.25b) gives

$$\varrho_m(\omega) \left[\tilde{\mathbf{k}}^{\pm}(\omega) \cdot \hat{\mathbf{v}} \right] e^{+i\tilde{\mathbf{k}}^{\pm}(\omega) \cdot \mathbf{r} + i\theta_m(\omega)} = 0.$$

Conditions given in Eq. (2.4.9) force the complex wavevector to lie in the $u-w$ reference plane i.e. $k_v = 0$. The transversality condition given in Eq. (2.5.25c) gives

$$\varrho_m(\omega) \left[\mathbf{E}(\mathbf{r}, \omega) \cdot \hat{\mathbf{v}} \right] e^{+i\tilde{\mathbf{k}}^{\pm}(\omega) \cdot \mathbf{r} + i\theta_m(\omega)} = 0.$$

Again, by conditions given in Eq. (2.4.9), the electric field vector also must lie in the $u-w$ reference plane, i.e. $E_v(\mathbf{r}, \omega) = 0$. This causes the characteristic planes of $\mathbf{E}(\mathbf{r}, \omega)$ and the complex wavevector $\tilde{\mathbf{k}}^{\pm}(\omega)$ to be coplanar. Further, the transversality condition given in Eq. (2.5.23) defines the electric field as

$$\mathbf{E}(\mathbf{r}, \omega) = -\frac{\|c\|}{\tilde{\epsilon}(\omega)\omega} \varrho_m(\omega) \left[\tilde{\mathbf{k}}^{\pm}(\omega) \times \hat{\mathbf{v}} \right] e^{+i\tilde{\mathbf{k}}^{\pm}(\omega) \cdot \mathbf{r} + i\theta_m(\omega)}.$$

The vector $\tilde{\mathbf{k}}^{\pm}(\omega) \times \hat{\mathbf{v}}$ is complex and $\boldsymbol{\beta}(\omega) \times i\boldsymbol{\alpha}(\omega) \neq \mathbf{0}$, consequently the electric field vector is elliptically polarized. The spectral amplitude vector can then be written as

$$\mathbf{E}(\omega) = [\mathbf{p}_e(\omega) + i\mathbf{q}_e(\omega)] e^{+i\theta_m(\omega)} = [\mathbf{a}_e(\omega) + i\mathbf{b}_e(\omega)] e^{+i\theta_e(\omega) + i\theta_m(\omega)},$$

where $\mathbf{p}_e(\omega) = \frac{\|c\|}{\mu\omega} \varrho_m(\omega) [\boldsymbol{\beta}(\omega) \times \hat{\mathbf{v}}]$, $\mathbf{q}_e(\omega) = \frac{\|c\|}{\mu\omega} \varrho_m(\omega) [\boldsymbol{\alpha}(\omega) \times \hat{\mathbf{v}}]$, $\mathbf{p}_e \times \mathbf{q}_e \neq \mathbf{0}$ and $\mathbf{a}_e \cdot \mathbf{b}_e = 0$. Because the characteristic planes of $\tilde{\mathbf{k}}^{\pm}(\omega)$ and $\mathbf{E}(\mathbf{r}, \omega)$ are coplanar the polarization sense is determined by

$$\mathbf{a}_e(\omega) \times \mathbf{b}_e(\omega) \cdot [\boldsymbol{\alpha}^{\pm}(\omega) \times \boldsymbol{\beta}^{\pm}(\omega)] \begin{cases} > 0; & \text{left-handed} \\ < 0; & \text{right-handed} \end{cases}, \quad (2.6.4)$$

where $\mathbf{a}_e(\omega)$ and $\mathbf{b}_e(\omega)$ are the orthogonal components of the electric field.

In summary, *if a given field vector is a linearly polarized inhomogeneous plane wave then the complex wavevector lies in the plane orthogonal to this field vector and the other field vector is elliptically polarized and coplanar with the complex wavevector.* The other field vector cannot be linearly polarized if the complex wavevector corresponds to an inhomogeneous plane wave.

2.6.3 The Homogeneous Plane Wave Field

If the field vector is a homogeneous plane wave then the complex wavevector can be written in polar form as [cf. §2.4]

$$\tilde{\mathbf{k}}^{\pm}(\omega) = \tilde{k}^{\pm}(\omega)\hat{\mathbf{s}}, \quad (2.6.5)$$

where $\hat{\mathbf{s}}$ is a real unit vector that directs both the phase fronts and amplitude fronts and $\tilde{k}^{\pm}(\omega)$ is the complex wavenumber. When the complex wavevector corresponds to a homogeneous plane wave any vanishing inner products

$$\tilde{\mathbf{k}}^{\pm}(\omega) \cdot \mathbf{c}_2 = 0$$

force the complex vector \mathbf{c}_2 to lie in the plane orthogonal to the real unit vector $\hat{\mathbf{s}}$ as mandated by conditions given in Eq. (2.4.9). Therefore, the transversality conditions given in Eqs. (2.5.25a,b) determine that the electric and magnetic field vectors are coplanar within the plane orthogonal to the real unit vector $\hat{\mathbf{s}}$.

If one of the field vectors is linearly polarized then the transversality condition given in Eq. (2.5.25c), by conditions given in Eq. (2.4.9), forces the other field vector to be linearly polarized as well since both vectors must lie in the plane orthogonal to $\hat{\mathbf{s}}$. On the other hand, if one of the field vectors is elliptically polarized then the transversality condition given in Eq. (2.5.25c), by conditions given in Eq. (2.4.8), determines that the other field vector must be elliptically polarized as well.

CHAPTER III

Reflection and Transmission
of a
Pulsed Inhomogeneous Plane Wave
Electromagnetic Field
at a
Planar Interface Separating
Two Lossy Dielectrics

The physical phenomenon of plane wave reflection and refraction from a planar interface is a fundamental problem in electromagnetic wave theory with particular importance to the mode formation in a dielectric slab waveguide[10]. The exact modal solution set for the ideal dielectric slab waveguide, as derived from *Maxwell's* equations for lossless dielectric media, reveals that two superimposed homogeneous plane waves comprise each mode. One plane wave is incident on the upper core/cladding interface and is superimposed upon the other plane wave that is incident on the lower core/substrate interface. These two plane wave components are interrelated in that each is the other's reflection from its associated interface and each interferes constructively with the other to form the modal solution. This constructive interference then results in a discrete set of modes.

A similar description is sought for the nonideal dielectric slab waveguide, i.e. when the core and surrounding regions are comprised of lossy, dispersive dielectric media. This description will then provide insight into the modal solutions of the nonideal dielectric slab waveguide as it does in the ideal case. The dielectric permittivities are considered to be complex and the general solutions to *Maxwell's* equations are inhomogeneous plane waves [cf. §2.5]. The analysis of inhomogeneous plane waves that are incident upon a planar interface separating two lossy, dispersive dielectric media then becomes a necessary step in the evaluation of the dielectric slab waveguide and is then the impetus for this chapter.

This chapter contains a complete derivation of the generalized laws of reflection and refraction, as well as the generalized *Fresnel* equations. The exact analysis of this problem when loss is included in the dielectric permittivity of both the medium of incidence and transmittance is developed here for the first time. A simplified version of this problem which accounts for loss only in the medium of transmittance has been given by Whitaker[51] in 1979. In addition, these results are extended to describe a pulsed electromagnetic inhomogeneous plane wave incident upon the interface through an application of an inverse *Fourier Laplace* transform.

3.1 Inhomogeneous Plane Wave Reflection and Refraction from a Planar Interface Separating Two Lossy Dielectrics

A propagating electromagnetic field is both reflected and refracted as it encounters any spatial discontinuities of the refractive index. A discontinuity alters the local homogeneity of the medium and the electromagnetic field reacts by producing reflected and refracted fields. This discontinuity is treated as a boundary or interface between two homogeneous media with different refractive indices. The medium that contains the incident propagating electromagnetic field is called the medium of incidence. After the incident field reacts to the boundary the medium of incidence also contains the reflected field. The second medium is called the medium of transmittance and it contains the transmitted field.

This section will treat the simple case where the boundary is a planar interface separating two half-spaces of dielectric media. Both dielectrics are considered to be lossy and temporally dispersive. The incident electromagnetic field is chosen to be an inhomogeneous plane wave as discussed in §2.5. The laws that govern this situation are called the generalized laws of reflection and refraction and the generalized *Fresnel* equations.

The dielectric medium of incidence and medium of transmittance are described by the frequency dependent complex refractive indices

$$\tilde{n}_1(\omega) \equiv \sqrt{\frac{\mu\tilde{\epsilon}_1(\omega)}{\mu_0\epsilon_0}}, \quad (3.1.1)$$

and

$$\tilde{n}_2(\omega) \equiv \sqrt{\frac{\mu\tilde{\epsilon}_2(\omega)}{\mu_0\epsilon_0}}, \quad (3.1.2)$$

respectively. The interface coordinate system is the standard rectangular x, y, z coordinate system with corresponding unit vectors $(\hat{x}, \hat{y}, \hat{z}) = (\hat{\tau}, \hat{\nu}, \hat{n})$ chosen to delineate the tangential and normal components of the field vectors with respect to the interface. The xy -plane (or the $z = 0$ plane) defines the separation between the two media and therefore represents the planar interface. The xz -plane defines the *reference plane* containing the incident attenua-

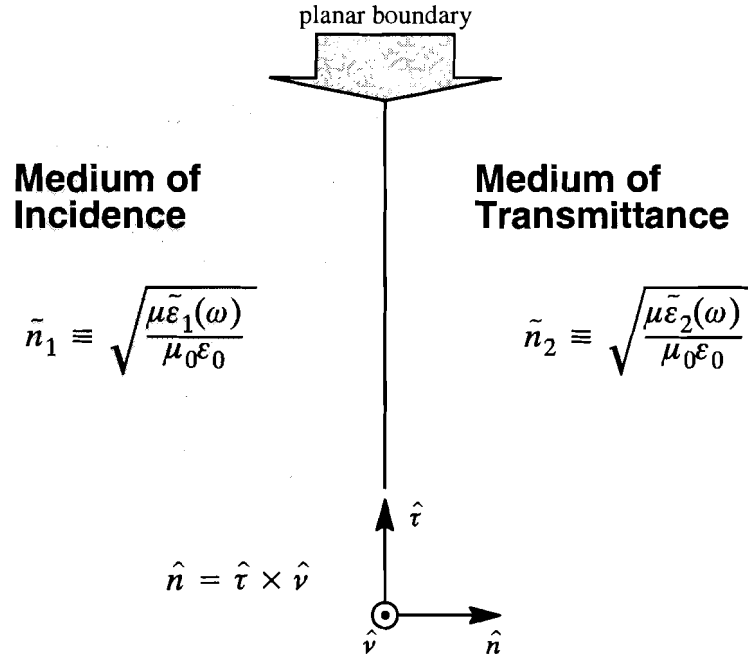


Figure 3.1.1 Planar interface separating two lossy, dispersive half-spaces with complex refractive n_1 for the medium of incidence and n_2 for the medium of transmittance.

tion vector and the normal vector to the interface. With this choice, the in-plane tangential component is in the $\hat{\tau}$ direction, the out of plane tangential component is in the $\hat{\nu}$ direction, and the normal component is in the \hat{n} direction for any given field vector with respect to the interface coordinate system, as illustrated in Figure 3.1.1.

The orientation of the incident inhomogeneous plane wave is defined by the incident local rectangular u, v, w coordinate system with corresponding unit vectors $(\hat{u}, \hat{v}, \hat{w})$. The position vector \mathbf{r}_i is given by

$$\mathbf{r}_i \equiv u\hat{u} + v\hat{v} + w\hat{w} . \quad (3.1.3)$$

In this problem the incident electromagnetic field vectors defined in the incident local coordinate system are given by [cf. §2.5]

$$\mathbf{E}_i(\mathbf{r}_i, \omega) = \mathbf{E}_i(\omega)e^{+i\tilde{\mathbf{k}}_i(\omega) \cdot \mathbf{r}_i} , \quad (3.1.4a)$$

$$\mathbf{H}_i(\mathbf{r}_i, \omega) = \mathbf{H}_i(\omega)e^{+i\tilde{\mathbf{k}}_i(\omega) \cdot \mathbf{r}_i} , \quad (3.1.4b)$$

which satisfy the homogeneous vector *Helmholtz* equations given in Eqs. (2.5.2a,b) and are

defined only in the medium of incidence (i.e. for $z \leq 0$). Therefore, the *incident complex wavevector* $\tilde{\mathbf{k}}_i(\omega)$ satisfies the relation [cf. Eq. (2.5.12)]

$$\tilde{\mathbf{k}}_i(\omega) \cdot \tilde{\mathbf{k}}_i(\omega) \equiv \tilde{k}_1^2(\omega) , \quad (3.1.5)$$

where

$$\tilde{k}_1(\omega) \equiv \tilde{n}_1(\omega)k_0 , \quad (3.1.6)$$

and $\tilde{n}_1(\omega)$ is given by Eq. (3.1.1). Here $k_0 \equiv \frac{\omega}{c}$ is the vacuum wavenumber. In general, the frequency $\omega \equiv \omega' + ia$ is complex, where ω' and a are both real-valued. However, for the present it is assumed that $a = 0$ so that the angular frequency ω is real-valued.

Let the incident complex wavevector be defined within the incident local coordinate system as [cf. Eq. (2.5.17)]

$$\tilde{\mathbf{k}}_i(\omega) \equiv k_u \hat{u} + k_v \hat{v} + \gamma_i(\omega) \hat{w} , \quad (3.1.7)$$

where the transverse wavenumbers k_u and k_v are real-valued and the *longitudinal component* $\gamma_i(\omega)$ is given by the principal branch of the expression [cf. §2.5]

$$\gamma_i(\omega) = \left(\tilde{k}_1^2(\omega) - k_T^2 \right)^{1/2} = \sqrt{\Gamma} e^{i\frac{\theta}{2}} \quad ; \quad 0 \leq \frac{\theta}{2} < \pi . \quad (3.1.8a)$$

This describes a function of both the angular frequency ω and the real-valued transverse spatial frequency $k_T^2 \equiv k_u^2 + k_v^2$, where Γ is a positive real-valued quantity. The angular range of the phase of $\gamma_i(\omega)$ dictates that $\Im\{\gamma_i(\omega)\} > 0$, which implies that the imaginary part of the complex wavevector is directed in the positive \hat{w} direction. Further, as was shown in §2.5 [cf. Eq (2.5.20)]

$$\gamma_i = \sqrt{\Gamma} e^{i\frac{\theta}{2}} \quad ; \quad \begin{cases} 0 \leq \frac{\theta}{2} < \frac{\pi}{2} & , \forall \omega > 0 \\ \frac{\pi}{2} \leq \frac{\theta}{2} < \pi & , \forall \omega < 0 \end{cases} , \quad (3.1.8b)$$

for a real-valued angular frequency ω . The surfaces of constant phase propagate along the

positive \hat{w} direction as a consequence of Eq. (3.1.8b), regardless of the sign of the frequency ω .

The incident complex wavevector may be defined in terms of two real vector quantities as $\tilde{\mathbf{k}}_i(\omega) \equiv \boldsymbol{\beta}_i(\omega) + i\boldsymbol{\alpha}_i(\omega)$. The *incident propagation vector* $\boldsymbol{\beta}_i(\omega) \equiv \Re\{\tilde{\mathbf{k}}_i(\omega)\}$ specifies the direction of propagation of the planar phase front while the *incident attenuation vector* $\boldsymbol{\alpha}_i(\omega) \equiv \Im\{\tilde{\mathbf{k}}_i(\omega)\}$ specifies the direction of propagation of the planar amplitude front. From Eq. (3.1.7), the incident propagation vector is given by

$$\boldsymbol{\beta}_i(\omega) \equiv k_u \hat{u} + k_v \hat{v} + \Re\{\gamma_i(\omega)\} \hat{w} , \quad (3.1.9)$$

and the incident attenuation vector is given by

$$\boldsymbol{\alpha}_i(\omega) \equiv + \Im\{\gamma_i(\omega)\} \hat{w} . \quad (3.1.10)$$

The complex components of the incident complex wavevector in the incident local coordinate system are represented in matrix form as

$$\tilde{\mathbf{k}}_i(\omega) \equiv \begin{bmatrix} k_u \\ k_v \\ \gamma_i(\omega) \end{bmatrix} . \quad (3.1.11)$$

In this problem, the given real-valued transverse wavenumbers k_u and k_v cover the range

$$-\infty < k_u < \infty , \quad (3.1.12a)$$

$$-\infty < k_v < \infty . \quad (3.1.12b)$$

For a realistic dispersive dielectric, the refractive index $\tilde{n}_1(\omega)$ remains bounded as the real-valued frequency covers the range $-\infty < \omega < \infty$. For every frequency ω , the longitudinal component $\gamma_i(\omega)$ of the complex wavevector, as defined by Eq. (3.1.8a), originates at the complex point $\tilde{\mathbf{k}}_1(\omega)$ when $k_T = 0$. As the transverse wavenumbers k_u and k_v vary within their range, the transverse spatial frequency covers the range $0 \leq k_T < \infty$ and the longitudinal component $\gamma_i(\omega)$ of the complex wavevector traces the trajectory depicted in

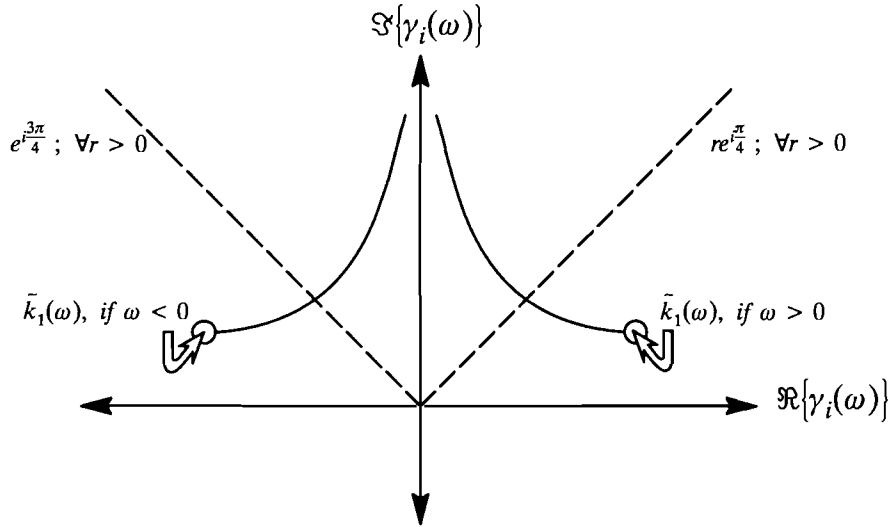


Figure 3.1.2 The longitudinal component of the complex wavevector originates at the complex point $\tilde{k}_1(\omega)$ for some real-valued frequency ω when $k_T=0$ and follows the indicated curve as the transverse spatial frequency k_T increases. A family of such curves is generated as the frequency ω changes. The sign of $\Re\{\tilde{k}_1(\omega)\}$ directly corresponds to the sign of the frequency ω . The imaginary part of $\gamma_i(\omega)$ is always positive. As the curve crosses the dashed line $re^{\pm i\pi/4}$, + for $\omega > 0$ and - for $\omega < 0$, $\gamma_i(\omega)$ becomes predominantly imaginary. As $k_T \rightarrow \infty$, $\gamma_i(\omega)$ asymptotically approaches the positive imaginary axis.

Figure 3.1.2. The longitudinal component $\gamma_i(\omega)$ of the complex wavevector asymptotically approaches the imaginary axis in the limit as $k_T \gg |\tilde{k}_1(\omega)|$, which can be understood by first

expressing $\gamma_i(\omega) = ik_T \left[1 - \frac{\tilde{k}_1(\omega)}{k_T} \right]^{\frac{1}{2}}$ as a binomial series¹³

$$\gamma_i(\omega) = ik_T \left\{ \sum_{k=0}^{n-1} \binom{1/2}{k} \left[-\frac{\tilde{k}_1(\omega)}{k_T} \right]^k - O \left[\left[\frac{\tilde{k}_1(\omega)}{k_T} \right]^n \right] \right\}, \quad n \in \mathbb{N}, \quad (3.1.13)$$

so that its asymptotic behavior¹⁴ is given by

$$\gamma_i(\omega) \sim ik_T, \quad (3.1.14)$$

as $k_T \rightarrow \infty$.

13. See Abramowitz and Stegun [73] p. 14, where the results are generalized to complex variables.

14. See Bleistein and Handelsman [74] §1.3 cf. Eq. (1.3.16).

For a low loss medium, $\Im\{\tilde{k}_1(\omega)\}$ is small compared to $\Re\{\tilde{k}_1(\omega)\}$ for frequencies removed from any resonances. In that case, the longitudinal component $\gamma_i(\omega)$ of the complex wavevector represents a strongly propagative component of the inhomogeneous plane wave for small $k_T \sim 0$ and frequencies removed from any resonances. However, as Eq. (3.1.14) clearly demonstrates, $\gamma_i(\omega)$ becomes predominantly an attenuative factor for large $k_T \gg |\tilde{k}_1(\omega)|$. The transition from a propagative to an attenuative factor occurs when the trajectory of $\gamma_i(\omega)$ crosses the line $re^{\pm i\frac{\pi}{4}}$ indicated in Figure 3.1.2. The line $re^{\pm i\frac{\pi}{4}}$ is equivalent to the square root of all positive imaginary numbers.

For a fixed real-valued angular frequency ω , the straight line generated by $\tilde{k}_1^2(\omega) - k_T^2$, as a function of real-valued k_T , crosses the imaginary axis and consequently $\gamma_i(\omega)$ crosses the line $re^{\pm i\frac{\pi}{4}}$ when

$$\Re\left\{\tilde{k}_1^2(\omega)\right\} = k_T^2. \quad (3.1.15)$$

The *critical transverse wavenumber for the longitudinal component* $\gamma_i(\omega)$ of the complex wavevector which satisfies this condition is given by

$$k_{T_{c\gamma}} = \pm \frac{\omega}{c} \sqrt{\frac{\mu\epsilon_1(\omega)}{\mu_0\epsilon_0}}, \quad (3.1.16)$$

where $\epsilon_1(\omega) = \Re\{\tilde{\epsilon}_1(\omega)\}$. The following results then apply

$$\begin{aligned} \Re\{\gamma_i^2(\omega)\} &< 0 & ; & k_T > |k_{T_{c\gamma}}| \\ \Re\{\gamma_i^2(\omega)\} &= 0 & ; & k_T = |k_{T_{c\gamma}}| \\ \Re\{\gamma_i^2(\omega)\} &> 0 & ; & k_T < |k_{T_{c\gamma}}| \end{aligned} \quad (3.1.17)$$

Let the complex number c be defined as $c^2 = r^2 e^{i2\theta}$, where the square root yields $c = re^{i\theta}$. The branch cut is then defined along the negative real axis and r is a positive real

number. If $\Re\{c^2\} < 0$, then the angle 2θ lies either in the range $\frac{\pi}{2} < 2\theta < \pi$ or the range $-\pi < 2\theta < -\frac{\pi}{2}$. Then $\Re\{c\} < \Im\{c\}$ since the complex number c can be written as $c = r(\cos \theta + i \sin \theta)$ and $\cos \theta < |\sin \theta|$ for this range of the angle θ . Conversely, if $\Re\{c^2\} > 0$, then the angle 2θ lies in the range $-\frac{\pi}{2} < 2\theta < \frac{\pi}{2}$. Then $\Re\{c\} > \Im\{c\}$ since $\cos \theta > |\sin \theta|$ for this range of the angle θ . These results are summarized by the inequalities

$$\begin{aligned} \Re\{c\} &< |\Im\{c\}| && ; \Re\{c^2\} < 0 \\ \Re\{c\} &= |\Im\{c\}| && ; \Re\{c^2\} = 0 \\ \Re\{c\} &> |\Im\{c\}| && ; \Re\{c^2\} > 0 \end{aligned} \quad (3.1.18)$$

Application of the results given in Eq. (3.1.18) to the inequalities given in Eq. (3.1.17) yields the inequalities

$$\begin{aligned} \Re\{\gamma_i(\omega)\} &< |\Im\{\gamma_i(\omega)\}| && ; k_T > |k_{T_{c_T}}| \\ \Re\{\gamma_i(\omega)\} &= |\Im\{\gamma_i(\omega)\}| && ; k_T = |k_{T_{c_T}}| \\ \Re\{\gamma_i(\omega)\} &> |\Im\{\gamma_i(\omega)\}| && ; k_T < |k_{T_{c_T}}| \end{aligned} \quad (3.1.19)$$

When $k_T < |k_{T_{c_T}}|$ then the term $\gamma_i(\omega)$ is labeled *propagative* and when $k_T > |k_{T_{c_T}}|$ then the term $\gamma_i(\omega)$ is labeled *attenuative*.

The complete range of the longitudinal component $\gamma_i(\omega)$ of the complex wavevector is then given by the inequalities

$$0 < |\Re\{\gamma_i(\omega)\}| \leq |\Re\{\bar{k}_1(\omega)\}|, \quad (3.1.20a)$$

$$0 \leq \Im\{\bar{k}_1(\omega)\} \leq \Im\{\gamma_i(\omega)\} < \max\{k_T\}, \quad (3.1.20b)$$

where the absolute values appearing in Eq. (3.1.20a) are required because the sign of the real parts correspond to the sign of the angular frequency ω and the operator $\max\{\}$ denotes the

maximum value of the set contained within the braces. Based on the range covered in Eq. (3.1.12), the quantity $\max\{k_T\}$ is obviously equal to ∞ . However, the quantity $\max\{k_T\}$ is used in Eq. (3.1.20b) instead of ∞ to emphasize the manner in which $\gamma_i(\omega)$, as a function of k_u and k_v , asymptotically approaches the imaginary axis, as given by the expansion appearing in Eq. (3.1.14). Further, in some applications, the complete range of Eq. (3.1.12) may not be covered and as long as $\max\{k_T\} \gg |\tilde{k}_1(\omega)|$, then Eq. (3.1.20b) will appropriately limit the range of $\Im\{\gamma_i(\omega)\}$.

In this problem the incident local unit vector \hat{w} is directed towards the interface and is oriented at an angle Θ_i with respect to the interface normal \hat{n} . Where the angle Θ_i is confined to the quadrant

$$0 \leq \Theta_i < \frac{\pi}{2} . \quad (3.1.21)$$

The origin of the incident local coordinate system is situated the distance w_0 away from the interface along the w -coordinate axis, as illustrated in Figure 3.1.3. Up until this point in the development, the incident transverse unit vectors \hat{u} , \hat{v} have not been fixed in any particular orientation. The transverse unit vector \hat{v} is chosen to coincide with the out of plane tangential unit vector \hat{v} of the interface coordinate system. The origin of the interface x, y, z coordinate system is defined as the point where the w -axis of the incident local coordinate system intersects the interface, as depicted in Figure 3.1.3.

Any vector in the incident local coordinate system $(\hat{u}, \hat{v}, \hat{w})$ transforms into the interface coordinate system $(\hat{t}, \hat{v}, \hat{n})$ through use of the projection operation

$$V_{interface} = \vec{\mathbf{R}}_{ot_i} \cdot V_{local} , \quad (3.1.22)$$

where the incident transformation matrix $\vec{\mathbf{R}}_{ot_i}$ is a function of the angle Θ_i and is given by

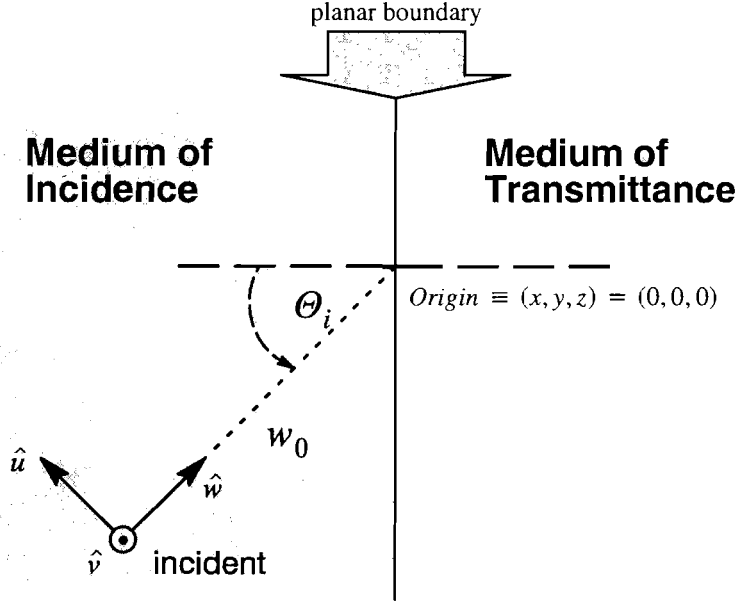


Figure 3.1.3 The incident inhomogeneous plane wave field and complex wavevector are specified in relation to the incident local coordinate system. The w -axis is oriented at an angle Θ_i with respect to the interface normal. The origin of the incident local coordinate system is situated a distance w_0 away from the interface along the w -axis. The origin for the x, y, z coordinate system of the interface is defined at the point where the w -axis intersects the interface. The out of plane vector tangential to the interface is taken to be coincident with the out of plane incident local vector.

$$\vec{\mathbf{R}}_{ot_i} \equiv \begin{bmatrix} \cos \Theta_i & 0 & \sin \Theta_i \\ 0 & 1 & 0 \\ -\sin \Theta_i & 0 & \cos \Theta_i \end{bmatrix}. \quad (3.1.23)$$

The incident transformation matrix $\vec{\mathbf{R}}_{ot_i}$ is orthonormal so that its inverse is equal to its transpose, viz.

$$\vec{\mathbf{R}}_{ot_i}^{-1} = \vec{\mathbf{R}}_{ot_i}^T. \quad (3.1.24)$$

The given propagation vector $\boldsymbol{\beta}_i(\omega)$ that is defined with respect to the incident local coordinate system [cf. Eq. (3.1.9)] transforms into the interface coordinate system as

$$\boldsymbol{\beta}_i(\omega) = \begin{bmatrix} \beta_{i_r}(\omega) \\ \beta_{i_v} \\ \beta_{i_n}(\omega) \end{bmatrix} = \vec{\mathbf{R}}_{ot_i} \cdot \begin{bmatrix} k_u \\ k_v \\ \Re\{\gamma_i(\omega)\} \end{bmatrix} = \begin{bmatrix} k_u \cos \Theta_i + \Re\{\gamma_i(\omega)\} \sin \Theta_i \\ k_v \\ -k_u \sin \Theta_i + \Re\{\gamma_i(\omega)\} \cos \Theta_i \end{bmatrix}. \quad (3.1.25)$$

In this case, notice that the term β_{i_v} is not a function of frequency ω . The range of the inde-

pendent variables k_u , k_v and Θ_i and the function $\gamma_i(\omega)$, which are given in Eqs. (3.1.12), (3.1.21) and (3.1.20a,b) define the ranges of the propagation vector components within the interface coordinate system as

$$\min\{k_u\} \cos \Theta_i \leq \beta_{i_r}(\omega) < \max\{k_u\} \cos \Theta_i , \quad (3.1.26a)$$

$$- \min\{k_v\} < \beta_{i_v} < \max\{k_v\} , \quad (3.1.26b)$$

$$- \max\{k_u\} \sin \Theta_i \leq \beta_{i_n}(\omega) < \Re\{\gamma_i(\omega)\} \cos \Theta_i - \min\{k_u\} \sin \Theta_i , \quad (3.1.26c)$$

where the quantity $\Re\{\gamma_i(\omega)\}$ was included in the upper limit of Eq. (3.1.26c) in order to include the special case when the angle $\Theta_i = 0$. The operator $\min\{\}$ represents the minimum value of the quantity contained within the braces. In some applications, the complete range given in Eq. (3.1.12) may not be covered and as long as $\max\{k_u\} \geq |\tilde{k}_1(\omega)|$, $\max\{k_v\} \geq |\tilde{k}_1(\omega)|$, $-\min\{k_u\} \geq |\tilde{k}_1(\omega)|$ and $-\min\{k_v\} \geq |\tilde{k}_1(\omega)|$, then Eqs. (3.1.26a–c) appropriately limit the ranges of $\beta_{i_r}(\omega)$, β_{i_v} and $\beta_{i_n}(\omega)$, respectively.

Similarly, the given attenuation vector $\alpha_i(\omega)$ defined with respect to the incident local coordinate system [cf. Eq. (3.1.10)] transforms into the interface coordinate system as

$$\alpha_i(\omega) = \begin{bmatrix} \alpha_{i_r}(\omega) \\ \alpha_{i_v} \\ \alpha_{i_n}(\omega) \end{bmatrix} = \vec{R}_{ot_i} \cdot \begin{bmatrix} 0 \\ 0 \\ \Im\{\gamma_i(\omega)\} \end{bmatrix} = \begin{bmatrix} \Im\{\gamma_i(\omega)\} \sin \Theta_i \\ 0 \\ \Im\{\gamma_i(\omega)\} \cos \Theta_i \end{bmatrix} . \quad (3.1.27)$$

Here, the term $\alpha_{i_v} = 0$. The range of the independent variables k_u , k_v and Θ_i and the function $\gamma_i(\omega)$, which are given in Eqs. (3.1.12), (3.1.21) and (3.1.20a,b), respectively, define the ranges of the attenuation vector components within the interface coordinate system as

$$0 \leq \Im\{\tilde{k}_1(\omega)\} \sin \Theta_i < \alpha_{i_r}(\omega) < \max\{k_T\} \sin \Theta_i , \quad (3.1.28a)$$

$$0 \leq \Im\{\tilde{k}_1(\omega)\} \leq \frac{\alpha_{i_n}(\omega)}{\cos \Theta_i} < \max\{k_T\} . \quad (3.1.28b)$$

In some applications, the complete range given in Eq. (3.1.12) may not be covered, but as

long as $\max\{k_T\} \gg |\tilde{k}_1(\omega)|$, then Eqs. (3.1.28a,b) appropriately limit the ranges of $\alpha_{i_t}(\omega)$ and $\alpha_{i_n}(\omega)$, respectively.

The complex components of the incident complex wavevector in the interface coordinate system are summarized in matrix form as

$$\tilde{\mathbf{k}}_i(\omega) = \begin{bmatrix} \tilde{k}_{i_t}(\omega) \\ \beta_{i_v} \\ \tilde{k}_{i_n}(\omega) \end{bmatrix} = \begin{bmatrix} \beta_{i_t}(\omega) + i\alpha_{i_t}(\omega) \\ \beta_{i_v} \\ \beta_{i_n}(\omega) + i\alpha_{i_n}(\omega) \end{bmatrix}, \quad (3.1.29)$$

where the \hat{v} component is pure real and independent of the frequency ω .

Similarly, the incident electromagnetic field vectors $\mathbf{E}_i(\omega)$ and $\mathbf{H}_i(\omega)$ defined with respect to the local coordinate system [cf. Eq. (3.1.4)] transform into the interface coordinate system as

$$\begin{bmatrix} E_{i_t}(\omega) \\ E_{i_v}(\omega) \\ E_{i_n}(\omega) \end{bmatrix} = \tilde{\mathbf{R}}_{ot_i} \cdot \begin{bmatrix} E_{i_u}(\omega) \\ E_{i_v}(\omega) \\ E_{i_w}(\omega) \end{bmatrix} = \begin{bmatrix} E_{i_u}(\omega) \cos \Theta_i + E_{i_w}(\omega) \sin \Theta_i \\ E_{i_v}(\omega) \\ -E_{i_u}(\omega) \sin \Theta_i + E_{i_w}(\omega) \cos \Theta_i \end{bmatrix}, \quad (3.1.30)$$

$$\begin{bmatrix} H_{i_t}(\omega) \\ H_{i_v}(\omega) \\ H_{i_n}(\omega) \end{bmatrix} = \tilde{\mathbf{R}}_{ot_i} \cdot \begin{bmatrix} H_{i_u}(\omega) \\ H_{i_v}(\omega) \\ H_{i_w}(\omega) \end{bmatrix} = \begin{bmatrix} H_{i_u}(\omega) \cos \Theta_i + H_{i_w}(\omega) \sin \Theta_i \\ E_{i_v}(\omega) \\ -H_{i_u}(\omega) \sin \Theta_i + H_{i_w}(\omega) \cos \Theta_i \end{bmatrix}. \quad (3.1.31)$$

While in the interface coordinate system, the incident propagation and attenuation vectors are conveniently expressed in terms of their magnitude, elevation angle and azimuthal angle, as illustrated in Figure 3.1.4. The incident propagation vector $\boldsymbol{\beta}_i(\omega)$, as defined in Eq. (3.1.9), requires three degrees of freedom to be completely described within the interface coordinate system, viz.

$$\boldsymbol{\beta}_i(\omega) \equiv \beta_i \left[\cos \phi_i^\beta \sin \theta_i^\beta \hat{\tau} + \sin \phi_i^\beta \sin \theta_i^\beta \hat{v} + \cos \theta_i^\beta \hat{n} \right]. \quad (3.1.32)$$

The magnitude of the incident propagation vector is defined as

$$\beta_i \equiv \sqrt{\beta_{i_r}^2 + \beta_{i_v}^2 + \beta_{i_n}^2} , \quad (3.1.33)$$

where β_{i_r} , β_{i_v} and β_{i_n} are defined in terms of the independent variables k_u , k_v and Θ_i in the matrix given in Eq. (3.1.25). Substituting the matrix components given in Eq. (3.1.25) into Eq. (3.1.33) yields,

$$\beta_i = \sqrt{k_u^2 + k_v^2 + [\Re\{\gamma_i(\omega)\}]^2} , \quad (3.1.34)$$

whose range is

$$\Re\{\tilde{k}_1(\omega)\} < \beta_i \leq \max\{k_T\} . \quad (3.1.35)$$

The azimuthal angle is defined as

$$\phi_i^\beta \equiv \text{Tan}^{-1} \left\{ \frac{\beta_{i_v}}{\beta_{i_r}} \right\} , \quad (3.1.36)$$

where the multi-branched inverse tangent function is sensitive to the signs of both arguments¹⁵ β_{i_r} and β_{i_v} which vary as given in Eqs. (3.1.26a,b) so that the range of ϕ_i^β becomes

$$0 \leq \phi_i^\beta < 2\pi , \quad (3.1.37)$$

in order to cover the allowed azimuthal range of $\beta_i(\omega)$. The elevation angle is defined in terms of spherical coordinates as

$$\theta_i^\beta \equiv \cos^{-1} \left\{ \frac{\beta_{i_n}}{\beta_i} \right\} , \quad (3.1.38)$$

where only the principle branch of \cos^{-1} is required¹⁶. The quantity $\beta_i > 0$, by definition, and the quantity β_{i_n} both vary over the range specified in Eq. (3.1.26c), so that the range of θ_i^β is restricted to the domain

15. See Abramowitz and Stegun [73] p. 80. The multi-branched $\text{Tan}^{-1} = \tan^{-1} + k\pi$ where k is an arbitrary integer. The complete range of the principle branch is $0 \leq \tan^{-1}x \leq \pi/2$ for $0 \leq x < \infty$ and $-\pi/2 \leq \tan^{-1}x < 0$ for $-\infty < x < 0$.

16. See Abramowitz and Stegun [73] p. 80. The complete range of the principle branch is $0 \leq \cos^{-1}x \leq \pi/2$ for $0 \leq x \leq 1$ and $\pi/2 < \cos^{-1}x \leq \pi$ for $-1 \leq x < 0$.

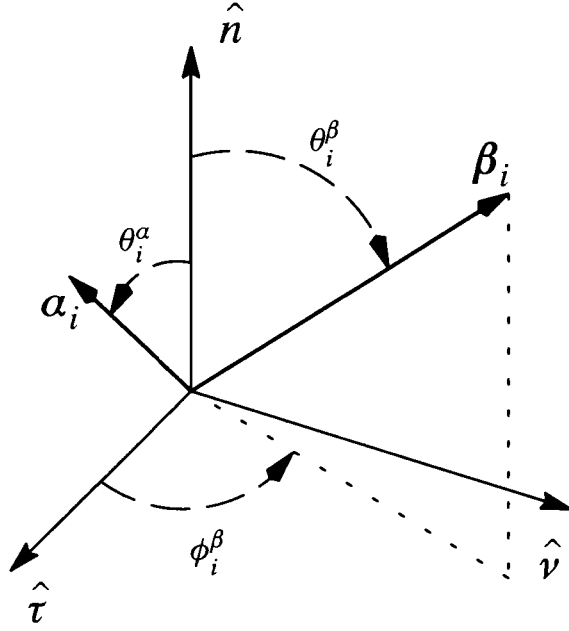


Figure 3.1.4 The propagation and attenuation vectors in the interface coordinate system given in spherical coordinates. Notice that the attenuation vector only requires an elevation angle.

$$0 \leq \theta_i^\beta \leq \frac{\pi}{2} + \Theta_i \max\{\cos \phi_i^\beta\}. \quad (3.1.39)$$

The quantity $\cos \phi_i^\beta$ is required in Eq. (3.1.39) because $\beta_i(\omega)$ only covers the upper hemisphere while in the u, v, w coordinate system. It is possible that the complete range of ϕ_i^β that is given in Eq. (3.1.37) is not needed for certain situations. This then implies that the full range given in Eq. (3.1.39) may not be covered because $\max\{\cos \phi_i^\beta\}$ can be less than unity. For example, if the propagation vectors are known *a priori* to lie in one plane with $\phi_i^\beta = \pi$ and the angle of the incident local coordinate system is $\Theta_i = \frac{\pi}{4}$ then $\max\{\cos \phi_i^\beta\} = \frac{\pi}{4}$.

The range of θ_i^β , given in Eq. (3.1.39), represents the complete span of forward propagating inhomogeneous plane waves that can emanate from the planar boundary u, v of the incident local coordinate system defined in §2.5. If $\theta_i^\beta > \frac{\pi}{2}$, then as shown by Eq. (2.5.44), the time-averaged power that is in the direction specified by $\beta_i(\omega)$ will not be incident on the interface. Positive values of the transverse wavenumber k_u that are large enough to cause

$\theta_i^\beta > \frac{\pi}{2}$ will be excluded from this analysis, so that the range of θ_i^β will be limited to

$$0 \leq \theta_i^\beta \leq \frac{\pi}{2} , \quad (3.1.40)$$

bearing in mind that the range given in Eq. (3.1.39) still applies if the term $\cos \phi_i^\beta$ causes the maximum value of θ_i^β to be less than $\frac{\pi}{2}$. Consequently, the range of k_u will be limited to the range

$$-\infty < k_u \leq k_{u_{max}} , \quad (3.1.41)$$

where $k_{u_{max}}$ is defined as the positive-valued transverse wavenumber for which $\theta_i^\beta = \frac{\pi}{2}$ for a particular value of frequency ω and azimuthal angle ϕ_i^β .

The incident attenuation vector $\mathbf{a}_i(\omega)$, defined in Eq. (3.1.10), is restricted to lie along the \hat{w} -axis and requires only two degrees of freedom to be completely described within the interface coordinate system, where

$$\mathbf{a}_i(\omega) \equiv \alpha_i [\sin \theta_i^\alpha \hat{\tau} + \cos \theta_i^\alpha \hat{n}] . \quad (3.1.42)$$

The magnitude of the incident attenuation vector is defined as

$$\alpha_i \equiv \sqrt{\alpha_{i_r}^2 + \alpha_{i_n}^2} , \quad (3.1.43)$$

where α_{i_r} and α_{i_n} are defined in terms of the independent variables k_u , k_v and Θ_i in the matrix given in Eq. (3.1.27). Substitution of the matrix components given in Eq. (3.1.27) into Eq. (3.1.43) yields,

$$\alpha_i = \sqrt{[\mathfrak{S}\{\gamma_i(\omega)\} \sin \Theta_i]^2 + [\mathfrak{S}\{\gamma_i(\omega)\} \cos \Theta_i]^2} = \mathfrak{S}\{\gamma_i(\omega)\} , \quad (3.1.44)$$

so that the range is the same as given in Eq. (3.1.20b), viz.

$$\mathfrak{S}\{\tilde{k}_1(\omega)\} \leq \alpha_i < \max\{k_T\} . \quad (3.1.45)$$

The elevation angle is defined as

$$\theta_i^\alpha \equiv \tan^{-1} \left\{ \frac{\alpha_{i_r}}{\alpha_{i_n}} \right\}, \quad (3.1.46)$$

where only the principle branch of the arctangent is required since the quantity α_{i_r} is always positive. Substitution of the matrix components given in Eq. (3.1.27) into Eq. (3.1.46) yields

$$\theta_i^\alpha \equiv \tan^{-1} \left\{ \frac{\Im\{\gamma_i(\omega)\} \sin \Theta_i}{\Re\{\gamma_i(\omega)\} \cos \Theta_i} \right\} = \Theta_i, \quad (3.1.47)$$

so that the range of $\theta_i^\alpha = \Theta_i$ is the same as that given in Eq. (3.1.21), viz.

$$0 \leq \theta_i^\alpha < \frac{\pi}{2}. \quad (3.1.48)$$

The resultant reflected and refracted fields are defined in their respective local coordinate systems in an analogous manner to that for the incident field. The reflected field is defined in the *reflected local rectangular u', v', w' coordinate system* with corresponding unit vectors $(\hat{u}', \hat{v}', \hat{w}')$. The unit vector \hat{w}' is directed away from the interface into the medium of incidence at the angle $\pi - \Theta_r$ with respect to the interface normal \hat{n} and intersects the interface at the interface origin O . The origin of the reflected local coordinate system is situated the distance w'_0 away from the interface along the w' -coordinate axis and lies in the medium of incidence. The refracted field is defined in the *transmitted local rectangular u'', v'', w'' coordinate system* with corresponding unit vectors $(\hat{u}'', \hat{v}'', \hat{w}'')$. The unit vector \hat{w}'' is directed away from the interface into the medium of transmittance at the angle Θ_t with respect to the interface normal \hat{n} and intersects the interface at the interface origin O . The origin of the transmitted local coordinate system is situated the distance w''_0 away from the interface along the w'' -coordinate axis and lies in the transmitted medium. The out of plane local unit vectors \hat{v}' and \hat{v}'' are both oriented parallel to the unit vector \hat{v} . The entire geometry is depicted in Figure 3.1.5.

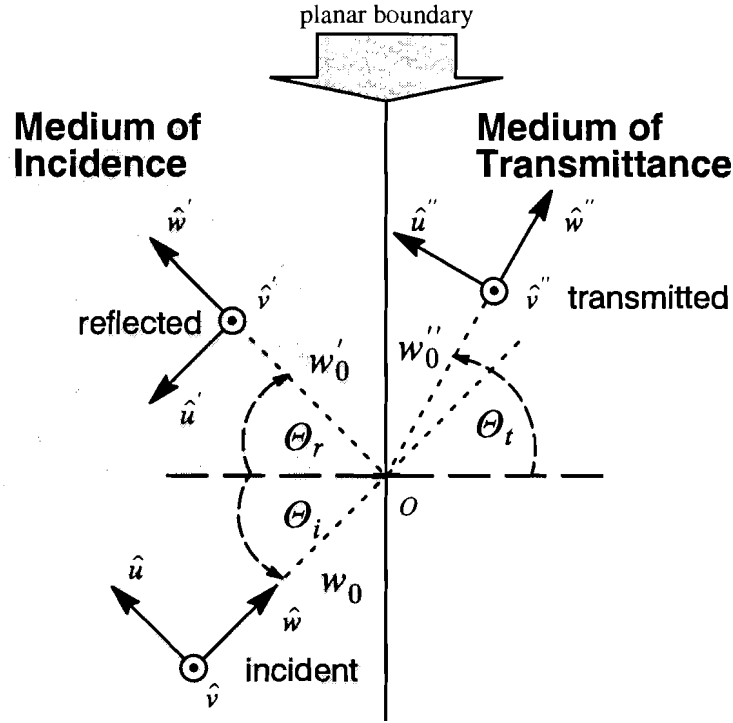


Figure 3.1.5 The incident, reflected and transmitted fields and complex wavevectors are defined in their respective incident, reflected and transmitted local coordinate systems. The w' -axis and the w'' -axis make the angles $\pi - \Theta_r$ and Θ_t , respectively with respect to the interface normal.

The reflected field vectors in the medium of incidence ($z \leq 0$) are expressed as [cf. §2.5]

$$\mathbf{E}_r(\mathbf{r}_r, \omega) = \mathbf{E}_r(\omega) e^{+i\tilde{\mathbf{k}}_r(\omega) \cdot \mathbf{r}_r}, \quad (3.1.49a)$$

$$\mathbf{H}_r(\mathbf{r}_r, \omega) = \mathbf{H}_r(\omega) e^{+i\tilde{\mathbf{k}}_r(\omega) \cdot \mathbf{r}_r}, \quad (3.1.49b)$$

and the transmitted field vectors in the medium of transmittance ($z \geq 0$) are expressed as [cf. §2.5]

$$\mathbf{E}_t(\mathbf{r}_t, \omega) = \mathbf{E}_t(\omega) e^{+i\tilde{\mathbf{k}}_t(\omega) \cdot \mathbf{r}_t}, \quad (3.1.50a)$$

$$\mathbf{H}_t(\mathbf{r}_t, \omega) = \mathbf{H}_t(\omega) e^{+i\tilde{\mathbf{k}}_t(\omega) \cdot \mathbf{r}_t}. \quad (3.1.50b)$$

Here \mathbf{r}_r and \mathbf{r}_t denote the position vectors in each respective local coordinate system and are given by

$$\mathbf{r}_r \equiv u' \hat{u}' + v' \hat{v}' + w' \hat{w}', \quad (3.1.51)$$

and

$$\mathbf{r}_t \equiv u'' \hat{\mathbf{u}}'' + v'' \hat{\mathbf{v}}'' + w'' \hat{\mathbf{w}}'' . \quad (3.1.52)$$

The inhomogeneous plane wave fields given in Eqs. (3.1.49) and (3.1.50) independently satisfy the homogeneous vector *Helmholtz* equations given in Eqs. (2.5.2a,b) and are defined only in their respective half-spaces. Therefore, the complex wavevectors $\tilde{\mathbf{k}}_r(\omega)$ and $\tilde{\mathbf{k}}_t(\omega)$ for the reflected and transmitted waves are each governed by the respective relation [cf. Eq. (2.5.12)]

$$\tilde{\mathbf{k}}_r(\omega) \cdot \tilde{\mathbf{k}}_r(\omega) \equiv \tilde{k}_1^2(\omega) , \quad \tilde{\mathbf{k}}_t(\omega) \cdot \tilde{\mathbf{k}}_t(\omega) \equiv \tilde{k}_2^2(\omega) , \quad (3.1.53)$$

where $\tilde{k}_1(\omega) = \tilde{n}_1(\omega)k_0$ and

$$\tilde{k}_2(\omega) \equiv \tilde{n}_2(\omega)k_0 \quad (3.1.54)$$

where $\tilde{n}_2(\omega)$ is given by Eq. (3.1.2).

Any vector in the reflected or transmitted local coordinate system transforms into the interface coordinate system through use of one of the transformations

$$\mathbf{V}_{interface} = \vec{\vec{\mathbf{R}}}_{ot_r} \cdot \mathbf{V}_{local} , \quad \mathbf{V}_{interface} = \vec{\vec{\mathbf{R}}}_{ot_t} \cdot \mathbf{V}_{local} , \quad (3.1.55)$$

where the transformation matrices are functions of the angles Θ_r and Θ_t , respectively, and are given by

$$\vec{\vec{\mathbf{R}}}_{ot_r} \equiv \begin{bmatrix} -\cos \Theta_r & 0 & \sin \Theta_r \\ 0 & 1 & 0 \\ -\sin \Theta_r & 0 & -\cos \Theta_r \end{bmatrix} , \quad (3.1.56)$$

$$\vec{\vec{\mathbf{R}}}_{ot_t} \equiv \begin{bmatrix} \cos \Theta_t & 0 & \sin \Theta_t \\ 0 & 1 & 0 \\ -\sin \Theta_t & 0 & \cos \Theta_t \end{bmatrix} , \quad (3.1.57)$$

respectively. The transformation matrices $\vec{\vec{\mathbf{R}}}_{ot_r}$ and $\vec{\vec{\mathbf{R}}}_{ot_t}$ are orthonormal, so that their inverses are equal to their transposes, viz.

$$\vec{\vec{\mathbf{R}}}_{ot_r}^{-1} = \vec{\vec{\mathbf{R}}}_{ot_r}^T , \quad \vec{\vec{\mathbf{R}}}_{ot_t}^{-1} = \vec{\vec{\mathbf{R}}}_{ot_t}^T . \quad (3.1.58)$$

Therefore, any vector in the interface coordinate system transforms into either the reflected or transmission local coordinate system through use of one of the transformations

$$\mathbf{V}_{local} = \vec{\mathbf{R}}_{otr}^T \cdot \mathbf{V}_{interface} , \quad \mathbf{V}_{local} = \vec{\mathbf{R}}_{otl}^T \cdot \mathbf{V}_{interface} . \quad (3.1.59)$$

3.1.1 Tangential Boundary Conditions

The tangential boundary conditions are obtained from the curl relations of *Maxwell* equations given in Eqs. (2.2.12a,b) by first taking the surface integral over an open region \mathfrak{R} bounded by a contour \mathfrak{C} that traverses the interface Σ , as shown in Figure 3.1.6, so that

$$\int_{\mathfrak{R}} \int [\nabla \times \mathbf{E}(\mathbf{r}, \omega)] \cdot \hat{\mathbf{n}}' da = \left\| \frac{1}{c} \right\| \int_{\mathfrak{R}} \int i\omega \mathbf{B}(\mathbf{r}, \omega) \cdot \hat{\mathbf{n}} da , \quad (3.1.60a)$$

$$\int_{\mathfrak{R}} \int [\nabla \times \mathbf{H}(\mathbf{r}, \omega)] \cdot \hat{\mathbf{n}}' da = -\left\| \frac{1}{c} \right\| \int_{\mathfrak{R}} \int i\omega \mathbf{D}(\mathbf{r}, \omega) \cdot \hat{\mathbf{n}} da , \quad (3.1.60b)$$

where $\hat{\mathbf{n}}$ is the unit outward normal to the open surface \mathfrak{R} . The surface \mathfrak{R} is a rectangle where the long sides are on opposite sides of the interface Σ . The positive normal is the unit vector $\hat{\mathbf{v}}$ which is tangent to the interface Σ , as depicted by Figure 3.1.6. The positive normal to the interface Σ is $\hat{\mathbf{n}}$, which makes a right handed coordinate system with the definition of the second interface tangent unit vector $\hat{\boldsymbol{\tau}} = \hat{\mathbf{v}} \times \hat{\mathbf{n}}$. Application of *Stokes' Theorem* to Eqs. (3.1.60a,b) then results in

$$\oint_{\mathfrak{C}} \mathbf{E}(\mathbf{r}, \omega) \cdot d\mathbf{l} = \left\| \frac{1}{c} \right\| \int_{\mathfrak{R}} \int i\omega \mathbf{B}(\mathbf{r}, \omega) \cdot \hat{\mathbf{v}} da , \quad (3.1.61a)$$

$$\oint_{\mathfrak{C}} \mathbf{H}(\mathbf{r}, \omega) \cdot d\mathbf{l} = -\left\| \frac{1}{c} \right\| \int_{\mathfrak{R}} \int i\omega \mathbf{D}(\mathbf{r}, \omega) \cdot \hat{\mathbf{v}} da , \quad (3.1.61b)$$

where the differential vector length $d\mathbf{l}$ lies along the contour \mathfrak{C} and is directed in the right-handed sense. The surface integrals appearing in Eqs. (3.1.61) vanish and $d\mathbf{l}$ becomes parallel to the interface tangent $\hat{\boldsymbol{\tau}}$ in the limit as the contour \mathfrak{C} shrinks to the interface Σ . The

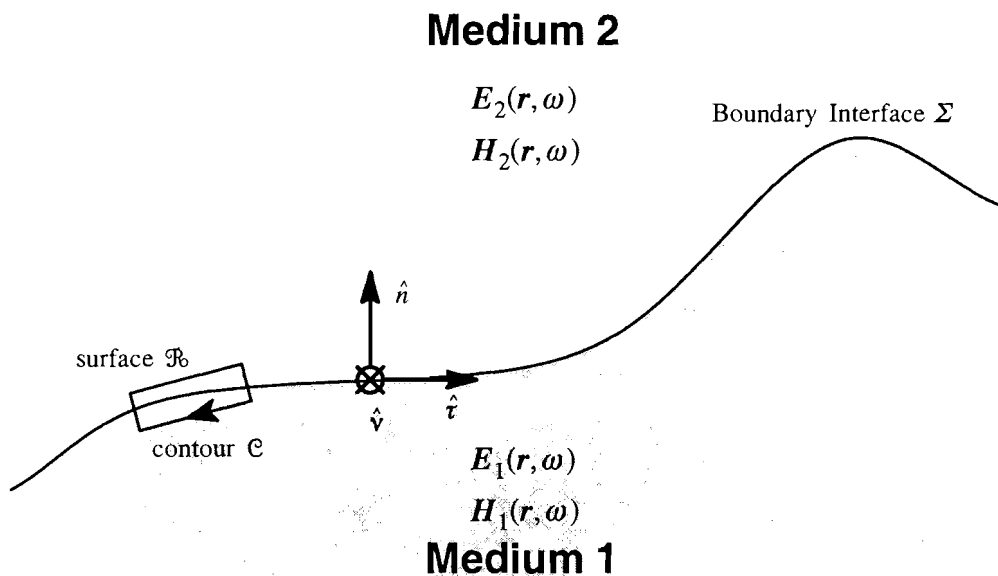


Figure 3.1.6 Geometry for the derivation of the tangential boundary conditions for an arbitrarily shaped boundary separating two dielectric media. A rectangle is situated between the two media and its surface area is shrunk to zero while holding its perimeter at a non-zero length.

contour integrals become

$$\lim_{\mathfrak{R} \rightarrow 0} \left\langle \oint_{\mathcal{C}} \mathbf{E}(\mathbf{r}, \omega) \cdot d\mathbf{l} \right\rangle = \hat{\mathbf{v}} \times \hat{\mathbf{n}} \cdot [\mathbf{E}_2(\mathbf{r}_p, \omega) - \mathbf{E}_1(\mathbf{r}_p, \omega)] \Delta l ,$$

$$\lim_{\mathfrak{R} \rightarrow 0} \left\langle \oint_{\mathcal{C}} \mathbf{H}(\mathbf{r}, \omega) \cdot d\mathbf{l} \right\rangle = \hat{\mathbf{v}} \times \hat{\mathbf{n}} \cdot [\mathbf{H}_2(\mathbf{r}_p, \omega) - \mathbf{H}_1(\mathbf{r}_p, \omega)] \Delta l ,$$

in that limit. Upon combining the above results, applying the vector identity $\mathbf{a} \cdot \mathbf{b} \times \mathbf{c} = \mathbf{b} \cdot \mathbf{c} \times \mathbf{a}$ and dividing out the quantity Δl , the tangential boundary conditions become

$$\hat{\mathbf{n}} \times [\mathbf{E}_2(\mathbf{r}_p, \omega) - \mathbf{E}_1(\mathbf{r}_p, \omega)] \cdot \hat{\mathbf{v}} = \mathbf{0} ,$$

$$\hat{\mathbf{n}} \times [\mathbf{H}_2(\mathbf{r}_p, \omega) - \mathbf{H}_1(\mathbf{r}_p, \omega)] \cdot \hat{\mathbf{v}} = \mathbf{0} .$$

The orientation of the rectangular surface \mathfrak{R} and its normal $\hat{\mathbf{v}}$ are entirely arbitrary¹⁷ relative to the direction of the electromagnetic field vectors, so that

$$\hat{\mathbf{n}} \times [\mathbf{E}_2(\mathbf{r}_p, \omega) - \mathbf{E}_1(\mathbf{r}_p, \omega)] = \mathbf{0} , \quad (3.1.62a)$$

$$\hat{\mathbf{n}} \times [\mathbf{H}_2(\mathbf{r}_p, \omega) - \mathbf{H}_1(\mathbf{r}_p, \omega)] = \mathbf{0} . \quad (3.1.62b)$$

The tangential boundary conditions given in Eqs. (3.1.62a,b) represent the continuity of the tangential components of the electric and magnetic field intensity vectors across the interface Σ , where \mathbf{r}_p describes any given point in the interface.

The normal boundary conditions are obtained by taking volume integrals of the divergence relations of *Maxwell* equations given in Eqs. (2.2.12c,d), with the results

$$\iiint_{\mathcal{V}} \{\nabla \cdot \mathbf{D}(\mathbf{r}, \omega)\} dv = 0 , \quad (3.1.63a)$$

$$\iiint_{\mathcal{V}} \{\nabla \cdot \mathbf{B}(\mathbf{r}, \omega)\} dv = 0 . \quad (3.1.63b)$$

In this case, the region \mathcal{V} is represented by a small cylinder situated half in medium 1 and half in medium 2 and whose generators are perpendicular to the interface. The region \mathcal{V} is situated such that the normal to the boundary surface $\hat{\mathbf{n}}$ is perpendicular to both end caps of the cylinder, as depicted in Figure 3.1.7. Application of the *divergence theorem* to Eqs. (3.1.63a,b) then yields

$$\oint_{\mathcal{J}} \mathbf{D}(\mathbf{r}, \omega) \cdot \hat{\mathbf{n}}'' da = 0 , \quad (3.1.64a)$$

$$\oint_{\mathcal{J}} \mathbf{B}(\mathbf{r}, \omega) \cdot \hat{\mathbf{n}}'' dv = 0 , \quad (3.1.64b)$$

where $\hat{\mathbf{n}}''$ is the unit outward normal to the bounding surface \mathcal{J} of the region \mathcal{V} . Now let the

17. See Stratton [68] §1.13.

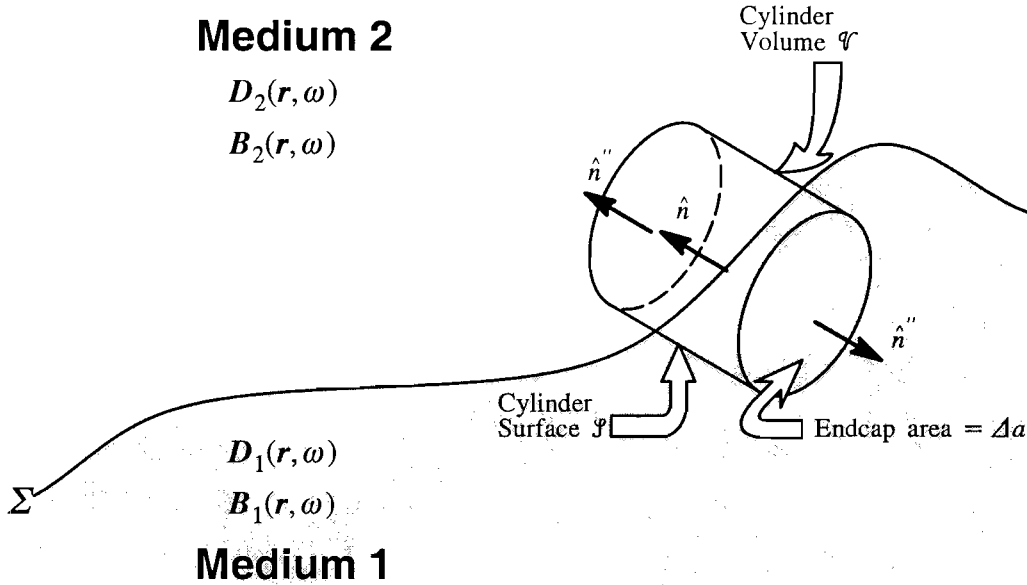


Figure 3.1.7 Geometry for the derivation of the normal boundary condition for an arbitrarily shaped boundary separating two dielectric media.

volume \mathcal{V} shrink to zero in such a way that the length of the cylinder goes to zero faster than the radius of both end caps. The surface integrals appearing in Eqs. (3.1.64a,b) become

$$\lim_{\mathcal{V} \rightarrow 0} \left\{ \oint_{\mathcal{S}} \oint D(\mathbf{r}, \omega) \cdot \mathbf{n}'' da \right\} = [D_2(\mathbf{r}_p, \omega) - D_1(\mathbf{r}_p, \omega)] \cdot \hat{n} \Delta a ,$$

$$\lim_{\mathcal{V} \rightarrow 0} \left\{ \oint_{\mathcal{S}} \oint \mathbf{B}(\mathbf{r}, \omega) \cdot \mathbf{n}'' dv \right\} = [B_2(\mathbf{r}_p, \omega) - B_1(\mathbf{r}_p, \omega)] \cdot \hat{n} \Delta a ,$$

in that limit. Upon combining the above results and dividing out the quantity Δa , the normal boundary conditions become

$$[D_2(\mathbf{r}_p, \omega) - D_1(\mathbf{r}_p, \omega)] \cdot \hat{n} = 0 , \quad (3.1.65a)$$

$$[B_2(\mathbf{r}_p, \omega) - B_1(\mathbf{r}_p, \omega)] \cdot \hat{n} = 0 . \quad (3.1.65b)$$

Eqs. (3.1.65a,b) represent the continuity of the normal components of the electric displacements.

ment vector and the magnetic induction vector across the interface at the point described by the position vector \mathbf{r}_p .

The above boundary conditions apply to the total fields in both medium 1 and medium

2. The total field in medium 1 is given by the sum of the incident and reflected fields as

$$\mathbf{E}_{total_1}(\mathbf{r}, \omega) = \mathbf{E}_i(\mathbf{r}, \omega) + \mathbf{E}_r(\mathbf{r}, \omega) , \quad (3.1.66a)$$

$$\mathbf{H}_{total_1}(\mathbf{r}, \omega) = \mathbf{H}_i(\mathbf{r}, \omega) + \mathbf{H}_r(\mathbf{r}, \omega) , \quad (3.1.66b)$$

while the total field for medium 2 is just the transmitted field

$$\mathbf{E}_{total_2}(\mathbf{r}, \omega) = \mathbf{E}_t(\mathbf{r}, \omega) , \quad (3.1.67a)$$

$$\mathbf{H}_{total_2}(\mathbf{r}, \omega) = \mathbf{H}_t(\mathbf{r}, \omega) . \quad (3.1.67b)$$

Substitution of these total field quantities into the boundary conditions given in Eqs. (3.1.62a,b) and (3.1.65a,b) results in the system of equations

$$\hat{\mathbf{n}} \times \left[\mathbf{E}_{total_2}(\mathbf{r}_p, \omega) - \mathbf{E}_{total_1}(\mathbf{r}_p, \omega) \right] = \mathbf{0} , \quad (3.1.68a)$$

$$\hat{\mathbf{n}} \times \left[\mathbf{H}_{total_2}(\mathbf{r}_p, \omega) - \mathbf{H}_{total_1}(\mathbf{r}_p, \omega) \right] = \mathbf{0} , \quad (3.1.68b)$$

$$\hat{\mathbf{n}} \cdot \left[\tilde{\epsilon}_2(\omega) \mathbf{E}_{total_2}(\mathbf{r}_p, \omega) - \tilde{\epsilon}_1(\omega) \mathbf{E}_{total_1}(\mathbf{r}_p, \omega) \right] = 0 , \quad (3.1.68c)$$

$$\hat{\mathbf{n}} \cdot \left[\mu \mathbf{H}_{total_2}(\mathbf{r}_p, \omega) - \mu \mathbf{H}_{total_1}(\mathbf{r}_p, \omega) \right] = 0 , \quad (3.1.68d)$$

where \mathbf{r}_p is the position vector that describes any point along the boundary interface Σ separating medium 1 from medium 2.

3.1.2 The Generalized Laws of Reflection and Refraction

The generalized laws of reflection and refraction relate the incident, reflected and transmitted complex wavevectors within the interface coordinate system. They specify each rectangular component of the reflected and transmitted complex wavevectors in terms of the known rectangular components of the incident complex wavevector. Further, if the complex wavevectors are written in terms of their magnitude, elevation angle and azimuthal angle, then the generalized laws specify the associated angular relationships between them.

In this problem, the incident electromagnetic field vectors and the incident complex wavevector are known. The incident electromagnetic field vectors $\mathbf{E}_i(\omega)$ and $\mathbf{H}_i(\omega)$ are expressed in the interface coordinate system as

$$\mathbf{E}_i(\omega) \equiv E_{i_t} \hat{\mathbf{t}} + E_{i_v} \hat{\mathbf{v}} + E_{i_n} \hat{\mathbf{n}}, \quad \mathbf{H}_i(\omega) \equiv H_{i_t} \hat{\mathbf{t}} + H_{i_v} \hat{\mathbf{v}} + H_{i_n} \hat{\mathbf{n}}, \quad (3.1.69)$$

where their components are defined by the matrices given in Eqs. (3.1.30) and (3.1.31), respectively. The incident complex wavevector $\tilde{\mathbf{k}}_i(\omega) = \boldsymbol{\beta}_i(\omega) + i\boldsymbol{\alpha}_i(\omega)$ is expressed in terms of the propagation and attenuation vectors in the interface coordinate system as

$$\boldsymbol{\beta}_i(\omega) \equiv \beta_{i_t} \hat{\mathbf{t}} + \beta_{i_v} \hat{\mathbf{v}} + \beta_{i_n} \hat{\mathbf{n}}, \quad \boldsymbol{\alpha}_i(\omega) \equiv \alpha_{i_t} \hat{\mathbf{t}} + \alpha_{i_n} \hat{\mathbf{n}}, \quad (3.1.70)$$

where their components are defined by the matrices given in Eqs. (3.1.25) and (3.1.27), respectively. The incident complex wavevector can also be expressed in the interface coordinate system as

$$\tilde{\mathbf{k}}_i(\omega) \equiv \tilde{k}_{i_t} \hat{\mathbf{t}} + \beta_{i_v} \hat{\mathbf{v}} + \tilde{k}_{i_n} \hat{\mathbf{n}}, \quad (3.1.71)$$

where their components are defined by the matrices given in Eq. (3.1.29). In this case, $\alpha_{i_v} = 0$ and β_{i_v} is not a function of angular frequency ω .

The reflected and transmitted electromagnetic field vectors and complex wavevectors are expressed in a similar manner within the interface coordinate system as

$$\mathbf{E}_r(\omega) \equiv E_{r_t} \hat{\mathbf{t}} + E_{r_v} \hat{\mathbf{v}} + E_{r_n} \hat{\mathbf{n}}, \quad \mathbf{H}_r(\omega) \equiv H_{r_t} \hat{\mathbf{t}} + H_{r_v} \hat{\mathbf{v}} + H_{r_n} \hat{\mathbf{n}}, \quad (3.1.72)$$

$$\boldsymbol{\beta}_r(\omega) \equiv \beta_{r_t} \hat{\mathbf{t}} + \beta_{r_v} \hat{\mathbf{v}} + \beta_{r_n} \hat{\mathbf{n}}, \quad \boldsymbol{\alpha}_r(\omega) \equiv \alpha_{r_t} \hat{\mathbf{t}} + \alpha_{r_v} \hat{\mathbf{v}} + \alpha_{r_n} \hat{\mathbf{n}}, \quad (3.1.73)$$

$$\mathbf{E}_t(\omega) \equiv E_{t_t} \hat{\mathbf{t}} + E_{t_v} \hat{\mathbf{v}} + E_{t_n} \hat{\mathbf{n}}, \quad \mathbf{H}_t(\omega) \equiv H_{t_t} \hat{\mathbf{t}} + H_{t_v} \hat{\mathbf{v}} + H_{t_n} \hat{\mathbf{n}}, \quad (3.1.74)$$

$$\boldsymbol{\beta}_t(\omega) \equiv \beta_{t_t} \hat{\mathbf{t}} + \beta_{t_v} \hat{\mathbf{v}} + \beta_{t_n} \hat{\mathbf{n}}, \quad \boldsymbol{\alpha}_t(\omega) \equiv \alpha_{t_t} \hat{\mathbf{t}} + \alpha_{t_v} \hat{\mathbf{v}} + \alpha_{t_n} \hat{\mathbf{n}}, \quad (3.1.75)$$

although their respective components are not yet defined. The complex components of the reflected complex wavevector are expressed in matrix form while in the interface coordinate system as

$$\tilde{\mathbf{k}}_r(\omega) = \begin{bmatrix} \tilde{k}_{r_x}(\omega) \\ \tilde{k}_{r_y}(\omega) \\ \tilde{k}_{r_n}(\omega) \end{bmatrix} = \begin{bmatrix} \beta_{r_x}(\omega) + i\alpha_{r_x}(\omega) \\ \beta_{r_y}(\omega) + i\alpha_{r_y}(\omega) \\ \beta_{r_n}(\omega) + i\alpha_{r_n}(\omega) \end{bmatrix}, \quad (3.1.76)$$

while the complex components of the transmitted complex wavevector are expressed in matrix form while in the interface coordinate system as

$$\tilde{\mathbf{k}}_t(\omega) = \begin{bmatrix} \tilde{k}_{t_x}(\omega) \\ \tilde{k}_{t_y}(\omega) \\ \tilde{k}_{t_n}(\omega) \end{bmatrix} = \begin{bmatrix} \beta_{t_x}(\omega) + i\alpha_{t_x}(\omega) \\ \beta_{t_y}(\omega) + i\alpha_{t_y}(\omega) \\ \beta_{t_n}(\omega) + i\alpha_{t_n}(\omega) \end{bmatrix}. \quad (3.1.77)$$

Substitution of Eqs. (3.1.69) – (3.1.75) into the the boundary conditions given in Eqs. (3.1.68a–d) then yields the set of vector relations

$$\hat{\mathbf{n}} \times \left[\mathbf{E}_i(\omega)e^{i\tilde{\mathbf{k}}_i(\omega) \cdot \mathbf{r}_p} - \mathbf{E}_i(\omega)e^{i\tilde{\mathbf{k}}_i(\omega) \cdot \mathbf{r}_p} - \mathbf{E}_r(\omega)e^{i\tilde{\mathbf{k}}_r(\omega) \cdot \mathbf{r}_p} \right] = \mathbf{0}, \quad (3.1.78a)$$

$$\hat{\mathbf{n}} \times \left[\mathbf{H}_i(\omega)e^{i\tilde{\mathbf{k}}_i(\omega) \cdot \mathbf{r}_p} - \mathbf{H}_i(\omega)e^{i\tilde{\mathbf{k}}_i(\omega) \cdot \mathbf{r}_p} - \mathbf{H}_r(\omega)e^{i\tilde{\mathbf{k}}_r(\omega) \cdot \mathbf{r}_p} \right] = \mathbf{0}, \quad (3.1.78b)$$

$$\hat{\mathbf{n}} \cdot \left[\tilde{n}_2^2(\omega)\mathbf{E}_i(\omega)e^{i\tilde{\mathbf{k}}_i(\omega) \cdot \mathbf{r}_p} - \tilde{n}_1^2(\omega)\mathbf{E}_i(\omega)e^{i\tilde{\mathbf{k}}_i(\omega) \cdot \mathbf{r}_p} - \tilde{n}_1^2(\omega)\mathbf{E}_r(\omega)e^{i\tilde{\mathbf{k}}_r(\omega) \cdot \mathbf{r}_p} \right] = 0, \quad (3.1.78c)$$

$$\hat{\mathbf{n}} \cdot \left[\mathbf{H}_i(\omega)e^{i\tilde{\mathbf{k}}_i(\omega) \cdot \mathbf{r}_p} - \mathbf{H}_i(\omega)e^{i\tilde{\mathbf{k}}_i(\omega) \cdot \mathbf{r}_p} - \mathbf{H}_r(\omega)e^{i\tilde{\mathbf{k}}_r(\omega) \cdot \mathbf{r}_p} \right] = 0, \quad (3.1.78d)$$

where the complex refractive indices $\tilde{n}_1(\omega)$ and $\tilde{n}_2(\omega)$ are given by Eqs. (3.1.1) and (3.1.2), respectively. Here \mathbf{r}_p denotes the *transverse position vector* in the interface coordinate system, which is given by

$$\mathbf{r}_p \equiv x\hat{\mathbf{t}} + y\hat{\mathbf{v}}, \quad (3.1.79)$$

which then lies anywhere along the planar interface .

Since Eqs. (3.1.78a–d) must be satisfied for any value of \mathbf{r}_p , the following condition must then be satisfied:

$$\tilde{\mathbf{k}}_i \cdot \mathbf{r}_p = \tilde{\mathbf{k}}_r \cdot \mathbf{r}_p = \tilde{\mathbf{k}}_t \cdot \mathbf{r}_p. \quad (3.1.80)$$

The vector \mathbf{r}_p is the cross product $\mathbf{r}_p = \hat{\mathbf{n}} \times \mathbf{r}$, where \mathbf{r} denotes the position vector that may be expressed in the interface coordinate system as

$$\mathbf{r} \equiv x\hat{\mathbf{t}} + y\hat{\mathbf{v}} + z\hat{\mathbf{n}} . \quad (3.1.81)$$

Together with the cyclic property $\mathbf{a} \cdot \mathbf{b} \times \mathbf{c} = \mathbf{c} \cdot \mathbf{a} \times \mathbf{b}$ of the scalar triple product, Eq. (3.1.80) may be rewritten as

$$\tilde{\mathbf{k}}_i \times \hat{\mathbf{n}} \cdot \mathbf{r} = \tilde{\mathbf{k}}_t \times \hat{\mathbf{n}} \cdot \mathbf{r} = \tilde{\mathbf{k}}_r \times \hat{\mathbf{n}} \cdot \mathbf{r} .$$

Separation of the equation into its real and imaginary parts then yields

$$\begin{aligned} [\boldsymbol{\beta}_i(\omega) \times \hat{\mathbf{n}}] \cdot \mathbf{r} &= [\boldsymbol{\beta}_r(\omega) \times \hat{\mathbf{n}}] \cdot \mathbf{r} = [\boldsymbol{\beta}_t(\omega) \times \hat{\mathbf{n}}] \cdot \mathbf{r} , \\ [\boldsymbol{\alpha}_i(\omega) \times \hat{\mathbf{n}}] \cdot \mathbf{r} &= [\boldsymbol{\alpha}_r(\omega) \times \hat{\mathbf{n}}] \cdot \mathbf{r} = [\boldsymbol{\alpha}_t(\omega) \times \hat{\mathbf{n}}] \cdot \mathbf{r} , \end{aligned}$$

where $\mathbf{r} \in \{\mathbb{R}^3\}$. Since the position vector \mathbf{r} appearing here is completely arbitrary, it then follows that

$$\boldsymbol{\beta}_i(\omega) \times \hat{\mathbf{n}} = \boldsymbol{\beta}_r(\omega) \times \hat{\mathbf{n}} = \boldsymbol{\beta}_t(\omega) \times \hat{\mathbf{n}} , \quad (3.1.82)$$

$$\boldsymbol{\alpha}_i(\omega) \times \hat{\mathbf{n}} = \boldsymbol{\alpha}_r(\omega) \times \hat{\mathbf{n}} = \boldsymbol{\alpha}_t(\omega) \times \hat{\mathbf{n}} . \quad (3.1.83)$$

Therefore, the continuity of the tangential components of $\boldsymbol{\beta}(\omega)$ across the interface is independent of the continuity of the tangential components of $\boldsymbol{\alpha}(\omega)$. This independence means that the ensuing development must treat the continuity of the tangential components of the propagation and attenuation vectors as two separate problems.

The relationship appearing in Eq. (3.1.82) forces all three propagation vectors $\boldsymbol{\beta}_i, \boldsymbol{\beta}_r, \boldsymbol{\beta}_t$ to lie in the plane formed by the incident propagation vector $\boldsymbol{\beta}_i$ and the unit normal vector $\hat{\mathbf{n}}$ to the interface. This plane defines the so-called *$\boldsymbol{\beta}$ -plane of incidence*. The incident propagation vector $\boldsymbol{\beta}_i$ is defined in terms of its magnitude, elevation angle and azimuthal angle in Eq. (3.1.32). The incident propagation vector and *$\boldsymbol{\beta}$ -plane of incidence* are rotated out of the xz reference plane by the angle ϕ_i^β , as illustrated in Figure 3.1.8.

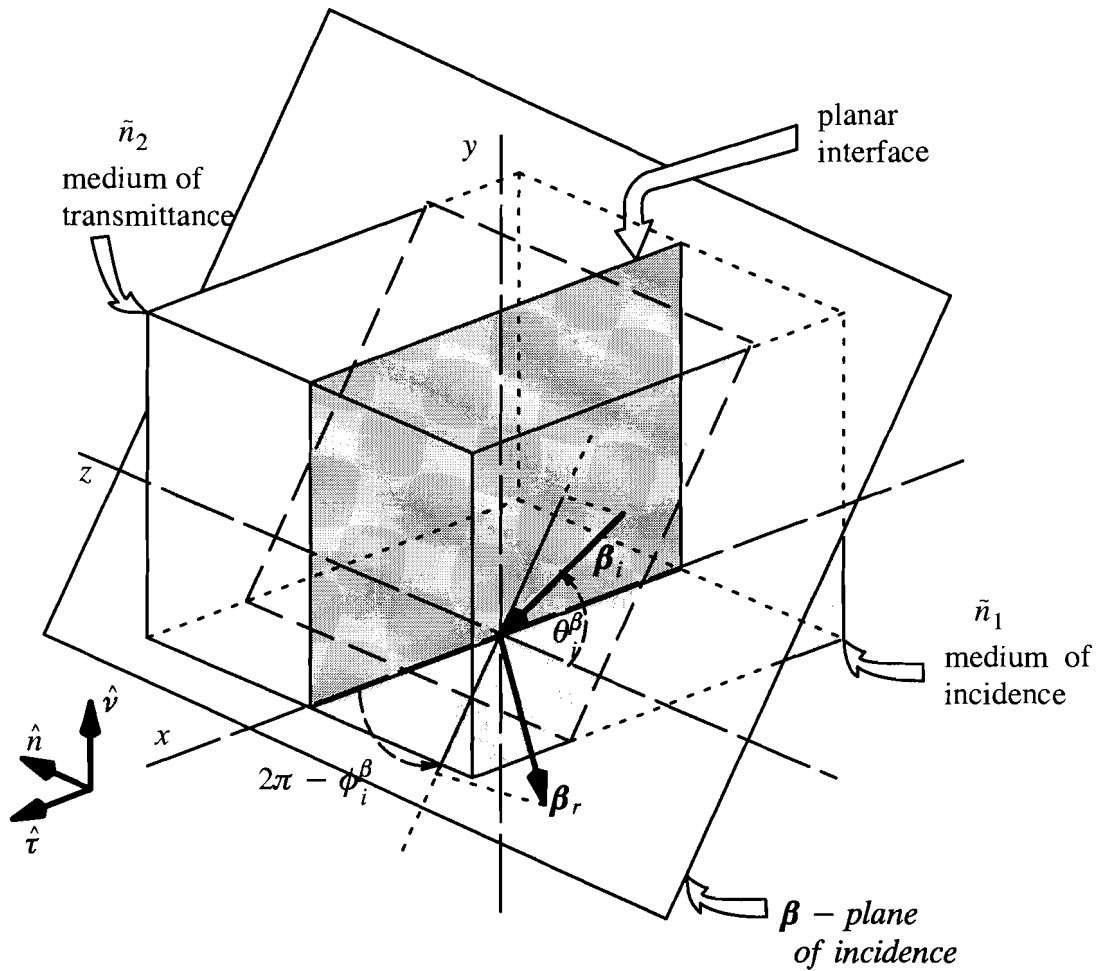


Figure 3.1.8 Diagram of the β -plane of incidence, which contains the incident, reflected, and transmitted propagation vectors and also the interface normal vector. The transmitted propagation vector is not shown in order to reduce clutter.

In a similar manner, the relationship appearing in Eq. (3.1.83) forces all three attenuation vectors \mathbf{a}_i , \mathbf{a}_r , \mathbf{a}_t to lie in the plane formed by the incident attenuation vector \mathbf{a}_i and the unit normal vector $\hat{\mathbf{n}}$ to the interface. This plane defines the so-called α -plane of incidence. The incident attenuation vector \mathbf{a}_i is defined in spherical coordinates in Eq. (3.1.42). Since the α -plane of incidence has no azimuthal component, it is coplanar with the xz reference plane, as illustrated in Figure 3.1.9. For the lossy case, the β -plane of incidence and the α -plane of incidence are not coplanar in general. However, in the limit of a lossless medium of incidence, there is no α -plane of incidence.

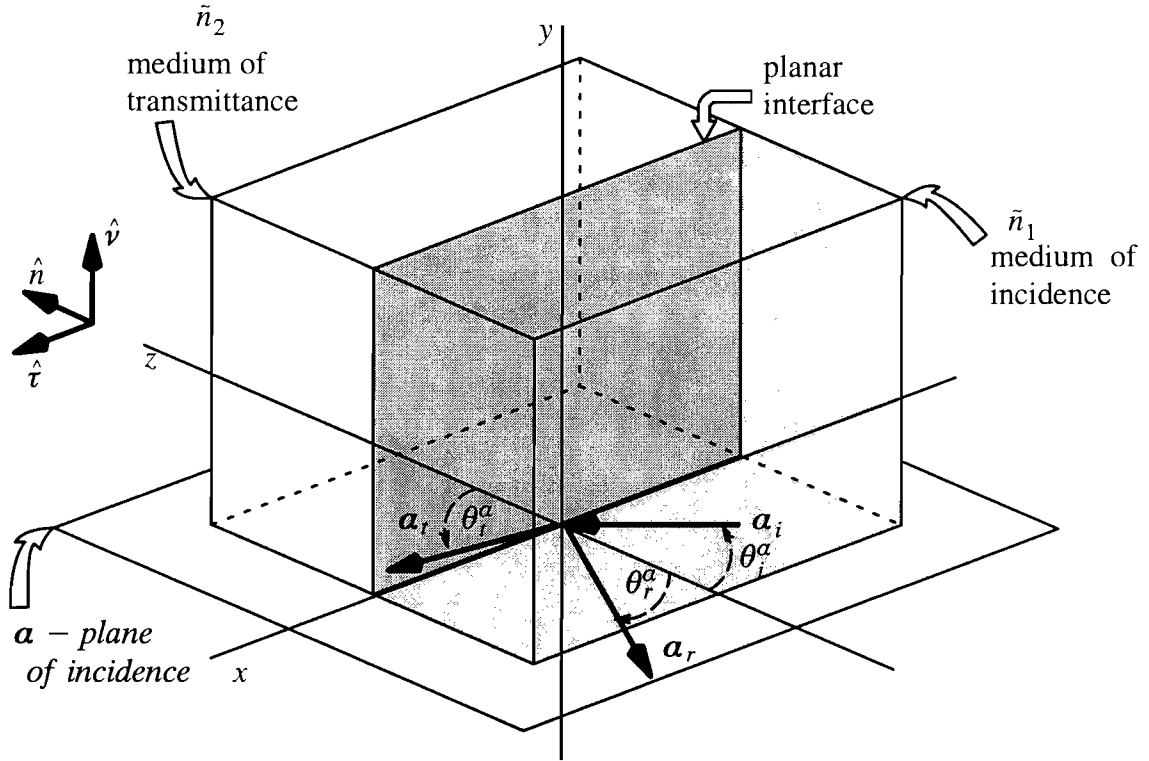


Figure 3.1.9 Diagram of the α -plane of incidence, which contains the incident, reflected, and transmitted attenuation vectors and also the interface normal vector.

The unknown reflected and transmitted complex wavevector's tangential components may be determined in terms of the known incident complex wavevector's tangential components. Using the definitions given in Eqs. (3.1.70), (3.1.73) and (3.1.75), the propagation vectors appearing in Eq. (3.1.82) may be expressed in component form as

$$\boldsymbol{\beta}_i(\omega) \times \hat{\mathbf{n}} = \beta_{i\nu} \hat{\boldsymbol{\tau}} - \beta_{i\tau}(\omega) \hat{\boldsymbol{\nu}},$$

$$\boldsymbol{\beta}_r(\omega) \times \hat{\mathbf{n}} = \beta_{r\nu}(\omega) \hat{\boldsymbol{\tau}} - \beta_{r\tau}(\omega) \hat{\boldsymbol{\nu}},$$

$$\boldsymbol{\beta}_t(\omega) \times \hat{\mathbf{n}} = \beta_{t\nu}(\omega) \hat{\boldsymbol{\tau}} - \beta_{t\tau}(\omega) \hat{\boldsymbol{\nu}},$$

while the attenuation vectors appearing in Eq. (3.1.83) may be expressed in component form as

$$\boldsymbol{\alpha}_i(\omega) \times \hat{\mathbf{n}} = -\alpha_{i\tau}(\omega) \hat{\boldsymbol{\nu}},$$

$$\boldsymbol{\alpha}_r(\omega) \times \hat{\mathbf{n}} = \alpha_{r\nu}(\omega) \hat{\boldsymbol{\tau}} - \alpha_{r\tau}(\omega) \hat{\boldsymbol{\nu}},$$

$$\alpha_i(\omega) \times \hat{\mathbf{n}} = \alpha_{t_r}(\omega) \hat{\mathbf{r}} - \alpha_{t_t}(\omega) \hat{\mathbf{v}} .$$

Since the different tangential components are mutually orthogonal, it then follows that

$$\beta_{i_r}(\omega) = \beta_{r_r}(\omega) = \beta_{t_r}(\omega) , \quad (3.1.84a)$$

$$\beta_{i_v} = \beta_{r_v} = \beta_{t_v} . \quad (3.1.84b)$$

Based on the result given in Eq. (3.1.25), the $\hat{\mathbf{v}}$ component β_{i_v} is not a function of the angular frequency ω . Similarly, the tangential components of the attenuation vector are

$$\alpha_{i_r}(\omega) = \alpha_{r_r}(\omega) = \alpha_{t_r}(\omega) , \quad (3.1.85a)$$

$$\alpha_{i_v} = \alpha_{r_v} = \alpha_{t_v} = 0 , \quad (3.1.85b)$$

where the second relation follows from the fact that $\alpha_{i_v} = 0$ [cf. Eq. (3.1.27)].

The unknown reflected complex wavevector's normal components may now be determined in terms of the known incident complex wavevector's normal components. The incident and reflected complex wavevectors share a common complex wavenumber $\tilde{k}_1(\omega)$ that is given in Eq. (3.1.6). The results given in Eqs. (3.1.5) and (3.1.53) then yield

$$\tilde{\mathbf{k}}_r(\omega) \cdot \tilde{\mathbf{k}}_r(\omega) = \tilde{n}_1(\omega) k_0^2 = \tilde{\mathbf{k}}_i(\omega) \cdot \tilde{\mathbf{k}}_i(\omega) .$$

Each side of this expression is expanded into component form using the relations appearing in Eqs. (3.1.70) and (3.1.73). Application of the tangential relations given in Eqs. (3.1.84) and (3.1.85) then permits the indicated cancelations

$$(\beta_{r_n} + i\alpha_{r_n})^2 + (\beta_{r_t} + i\alpha_{r_t})^2 + (\beta_{r_v})^2 = (\beta_{r_n} + i\alpha_{r_n})^2 + (\beta_{i_t} + i\alpha_{i_t})^2 + (\beta_{i_v})^2 ,$$

resulting in the expression

$$(\beta_{r_n} + i\alpha_{r_n})^2 = (\beta_{i_n} + i\alpha_{i_n})^2 . \quad (3.1.86)$$

The reflected wave travels in the opposite normal direction to the interface, which implies that the appropriate branch of the square root appearing in Eq. (3.1.86) is

$$\beta_{r_n} + i\alpha_{r_n} = -(\beta_{i_n} + i\alpha_{i_n}) .$$

Upon equating the real and imaginary parts, there results

$$\beta_{r_n} = -\beta_{i_n} , \quad (3.1.87a)$$

$$\alpha_{r_n} = -\alpha_{i_n} . \quad (3.1.87b)$$

Finally, consider determining the unknown transmitted complex wavevector's normal components in terms of the known incident wavevector's tangential components. The relation given in Eq. (3.1.54), viz.

$$\tilde{\mathbf{k}}_t(\omega) \cdot \tilde{\mathbf{k}}_t(\omega) \equiv \tilde{k}_2^2(\omega) ,$$

may be expanded into component form using definition given in Eq. (3.1.75), yielding

$$(\beta_{t_\tau} + i\alpha_{t_\tau})^2 + (\beta_{t_\nu} + i\alpha_{t_\nu})^2 + (\beta_{t_n} + i\alpha_{t_n})^2 = \tilde{k}_2^2(\omega) .$$

Substitution of the tangential relations appearing in Eqs. (3.1.84) and (3.1.85) into the left hand side of the above expression yields

$$(\beta_{i_\tau} + i\alpha_{i_\tau})^2 + \beta_{i_\nu}^2 + (\beta_{t_n} + i\alpha_{t_n})^2 = \tilde{k}_2^2(\omega) .$$

The unknown complex transmitted normal component may then be expressed in terms of the known complex incident tangential components as

$$\tilde{k}_{t_n}(\omega) = \beta_{t_n} + i\alpha_{t_n} = + \sqrt{\tilde{k}_2^2(\omega) - (\beta_{i_\tau} + i\alpha_{i_\tau})^2 - \beta_{i_\nu}^2} . \quad (3.1.88)$$

From a physical point of view, a transmitted wave must deliver power into the medium of transmittance. Quantitatively, this means that the inequality $\Re\{\tilde{k}_{t_n}(\omega)\} \geq 0$ must be satisfied in order that the portion of the time-averaged *Poynting* vector given in Eq. (2.5.44) that is directed by the transmitted propagation vector $\boldsymbol{\beta}_t(\omega)$ points into the medium of transmittance. Otherwise, if $\Re\{\tilde{k}_{t_n}(\omega)\} < 0$, power would then be directed towards the interface from the medium of transmittance. As a consequence, the appropriate branch-cut lies along the negative real axis of the domain of the square root. Notice that this is different from the

branch–cut chosen for the longitudinal wavenumber $\gamma_i(\omega)$ which was based on entirely different physical criteria.

Now that the reflected and transmitted complex wavevectors are completely specified, it is useful to express these vectors in terms of their magnitudes, elevation angle and azimuthal angle so that the corresponding angular relationships may be developed. To that end, let the reflected propagation vector $\boldsymbol{\beta}_r(\omega)$ be expressed in spherical components as

$$\boldsymbol{\beta}_r(\omega) \equiv \beta_r \left[\cos \phi_r^\beta \sin \theta_r^\beta \hat{\boldsymbol{\tau}} + \sin \phi_r^\beta \sin \theta_r^\beta \hat{\boldsymbol{\nu}} - \cos \theta_r^\beta \hat{\boldsymbol{n}} \right], \quad (3.1.89)$$

where the negative sign appears because θ_r^β is measured relative to $-\hat{\boldsymbol{n}}$. The magnitude is then given by

$$\beta_r \equiv \sqrt{\beta_{r_\tau}^2 + \beta_{r_\nu}^2 + \beta_{r_n}^2}. \quad (3.1.90)$$

The elevation angle is then given by

$$\pi - \theta_r^\beta \equiv \cos^{-1} \left\{ \frac{\beta_{r_n}}{\beta_r} \right\}, \quad (3.1.91)$$

where only the principle branch of the inverse cosine function is required, and the azimuthal angle is given by

$$\phi_r^\beta \equiv \text{Tan}^{-1} \left\{ \frac{\beta_{r_\nu}}{\beta_{r_\tau}} \right\}, \quad (3.1.92)$$

where the multi–branched inverse tangent function is sensitive to the signs of both factors appearing in its argument. The reflected attenuation vector $\boldsymbol{\alpha}_r(\omega)$ is expressed in angular component form as

$$\boldsymbol{\alpha}_r(\omega) \equiv \alpha_r \left[\sin \theta_r^\alpha \hat{\boldsymbol{\tau}} - \cos \theta_r^\alpha \hat{\boldsymbol{n}} \right], \quad (3.1.93)$$

where the negative sign appears because θ_r^α is measured relative to $-\hat{\boldsymbol{n}}$. The magnitude is given by

$$\alpha_r \equiv \sqrt{\alpha_{r_\tau}^2 + \alpha_{r_n}^2}, \quad (3.1.94)$$

and the elevation angle is given by

$$\theta_r^\alpha \equiv -\tan^{-1}\left\{\frac{\alpha_{r_\tau}}{\alpha_{r_n}}\right\}, \quad (3.1.95)$$

where only the principle branch of the inverse tangent function is required.

Similarly, let the transmitted propagation vector $\boldsymbol{\beta}_t(\omega)$ be expressed in spherical coordinate components as

$$\boldsymbol{\beta}_t(\omega) \equiv \beta_t \left[\cos \phi_t^\beta \sin \theta_t^\beta \hat{\boldsymbol{\tau}} + \sin \phi_t^\beta \sin \theta_t^\beta \hat{\boldsymbol{\nu}} + \cos \theta_t^\beta \hat{\boldsymbol{n}} \right]. \quad (3.1.96)$$

The magnitude is given by

$$\beta_t \equiv \sqrt{\beta_{t_\tau}^2 + \beta_{t_\nu}^2 + \beta_{t_n}^2}, \quad (3.1.97)$$

the elevation angle is given by

$$\theta_t^\beta \equiv \cos^{-1}\left\{\frac{\beta_{t_n}}{\beta_t}\right\}, \quad (3.1.98)$$

where only the principle branch of the inverse cosine function is required, and the azimuthal angle is given by

$$\phi_t^\beta \equiv \text{Tan}^{-1}\left\{\frac{\beta_{t_\nu}}{\beta_{t_\tau}}\right\}, \quad (3.1.99)$$

where the multi-branched inverse tangent function is sensitive to the signs of both factors appearing in its argument. The transmitted attenuation vector $\boldsymbol{\alpha}_t(\omega)$ is expressed in angular component form as

$$\boldsymbol{\alpha}_t(\omega) \equiv \alpha_t \left[\sin \theta_t^\alpha \hat{\boldsymbol{\tau}} + \cos \theta_t^\alpha \hat{\boldsymbol{n}} \right]. \quad (3.1.100)$$

The magnitude is given by

$$\alpha_t \equiv \sqrt{\alpha_{t_\tau}^2 + \alpha_{t_n}^2}, \quad (3.1.101)$$

and the elevation angle is given by

$$\theta_t^\alpha \equiv \tan^{-1}\left\{\frac{\alpha_{t_\tau}}{\alpha_{t_n}}\right\}, \quad (3.1.102)$$

where only the principle branch of the inverse tangent function is required.

The tangential and normal component relations given in Eqs. (3.1.84a,b), (3.1.85a,b) and (3.1.87a,b) for the propagation and attenuation vectors imply that the magnitudes of the incident and reflected wavevectors are equal, so that

$$\beta_r \equiv + \sqrt{\beta_{r_t}^2 + \beta_{r_v}^2 + \beta_{r_n}^2} = + \sqrt{\beta_{i_t}^2 + \beta_{i_v}^2 + \beta_{i_n}^2} = \beta_i , \quad (3.1.103a)$$

$$\alpha_r \equiv + \sqrt{\alpha_{r_t}^2 + \alpha_{r_n}^2} = + \sqrt{\alpha_{i_t}^2 + \alpha_{i_n}^2} = \alpha_i . \quad (3.1.103b)$$

Substitution of Eqs. (3.1.87a) and (3.1.103a) into Eq. (3.1.91) for θ_r^β yields

$$\pi - \theta_r^\beta \equiv \cos^{-1} \left\{ \frac{\beta_{r_n}}{\beta_r} \right\} = \cos^{-1} \left\{ - \frac{\beta_{i_n}}{\beta_i} \right\} ,$$

and substitution of the normal component of the relation given in Eq. (3.1.32) yields

$$\pi - \theta_r^\beta = \cos^{-1} \left\{ - \frac{\beta_i \cos(\theta_i^\beta)}{\beta_i} \right\} = \pi - \theta_i^\beta ,$$

which then states that

$$\theta_r^\beta = \theta_i^\beta . \quad (3.1.104)$$

The appropriate substitution of the tangential component relations given in Eqs. (3.1.84a,b) for the propagation vector into Eq. (3.1.92) yields

$$\phi_r^\beta \equiv \text{Tan}^{-1} \left\{ \frac{\beta_{r_v}}{\beta_{r_t}} \right\} = \text{Tan}^{-1} \left\{ \frac{\beta_{i_v}}{\beta_{i_t}} \right\} .$$

The right-hand side of this equation defines the incident azimuthal angle ϕ_i^β [cf. Eq. (3.1.36)] so that

$$\phi_r^\beta = \phi_i^\beta , \quad (3.1.105)$$

which is no surprise since all of the propagation vectors must lie in the **β -plane of incidence**. Substitution of the tangential and normal component relations for the attenuation vector given in Eqs. (3.1.85a) and (3.1.87b) into the definition of the angle θ_r^α given in Eq. (3.1.95) then yields

$$\theta_r^\alpha \equiv -\tan^{-1}\left\{\frac{\alpha_{r_t}}{\alpha_{r_n}}\right\} = \tan^{-1}\left\{\frac{\alpha_{i_t}}{\alpha_{i_n}}\right\}.$$

The right-hand side of this equation defines the incident elevation angle θ_i^α [cf. Eq. (3.1.46)] so that

$$\theta_r^\alpha = \theta_i^\alpha. \quad (3.1.106)$$

The tangential and normal relations for the attenuation vector given in Eqs. (3.1.84), (3.1.85) and (3.1.87), when substituted into the relations given in Eqs. (3.1.97) and (3.1.101) yield, respectively,

$$\begin{aligned} \beta_t &\equiv +\sqrt{\beta_{t_r}^2 + \beta_{t_v}^2 + \beta_{t_n}^2} = +\sqrt{\beta_{i_r}^2 + \beta_{i_v}^2 + \beta_{i_n}^2}, \\ \alpha_t &\equiv +\sqrt{\alpha_{t_r}^2 + \alpha_{t_n}^2} = +\sqrt{\alpha_{i_r}^2 + \alpha_{i_n}^2}. \end{aligned}$$

Substitution of the real and imaginary parts of Eq. (3.1.88) into the quantities β_{t_n} and α_{t_n} then gives

$$\beta_t = \sqrt{\beta_{i_r}^2 + \beta_{i_v}^2 + \left[\Re \left\{ \sqrt{k_2(\omega) - (\beta_{i_r}(\omega) + i\alpha_{i_r}(\omega))^2 - \beta_{i_v}^2} \right\} \right]^2}, \quad (3.1.107a)$$

$$\alpha_t = \sqrt{\alpha_{i_r}^2 + \alpha_{i_v}^2 + \left[\Im \left\{ \sqrt{k_2(\omega) - (\beta_{i_r}(\omega) + i\alpha_{i_r}(\omega))^2 - \beta_{i_v}^2} \right\} \right]^2}. \quad (3.1.107b)$$

Substitution of Eq. (3.1.107a) and the real part of Eq. (3.1.88) into the definition of the angle θ_t^β given in Eq. (3.1.98) yields,

$$\theta_t^\beta = \cos^{-1} \left\{ \frac{\Re \left\{ \sqrt{k_2(\omega) - (\beta_{i_r}(\omega) + i\alpha_{i_r}(\omega))^2 - \beta_{i_v}^2} \right\}}{\sqrt{\beta_{i_r}^2 + \beta_{i_v}^2 + \left[\Re \left\{ \sqrt{k_2(\omega) - (\beta_{i_r}(\omega) + i\alpha_{i_r}(\omega))^2 - \beta_{i_v}^2} \right\} \right]^2}} \right\}. \quad (3.1.108)$$

Substitution of the tangential component relations for the propagation vector given in Eqs. (3.1.84a,b) into the definition of the angle ϕ_t^β given in Eq. (3.1.99) yields

$$\phi_t^\beta \equiv \text{Tan}^{-1} \left\{ \frac{\beta_{t_v}}{\beta_{t_r}} \right\} = \text{Tan}^{-1} \left\{ \frac{\beta_{i_v}}{\beta_{i_r}} \right\} .$$

The right-hand side of this equation defines the incident azimuthal angle ϕ_i^β [cf. Eq. (3.1.36)] so that

$$\phi_t^\beta = \phi_i^\beta , \quad (3.1.109)$$

which states that the transmitted propagation vector with azimuthal angle ϕ_t^β also lies in the **β -plane of incidence**. Substitution of Eq. (3.1.85a) and the imaginary part of Eq. (3.1.88) into the definition of the angle θ_t^α given in Eq. (3.1.102) yields,

$$\theta_t^\alpha = \tan^{-1} \left\{ \frac{\alpha_{i_r}(\omega)}{\Im \left\{ \sqrt{k_2^2(\omega) - (\beta_{i_r}(\omega) + i\alpha_{i_r}(\omega))^2 - \beta_{i_v}^2} \right\}} \right\} . \quad (3.1.110)$$

The complete set of equations that form the *generalized laws of reflection* are summarized in the following three sets of equations which specify the reflected wavevector components in terms of the incident wavevector components in both the rectangular and spherical coordinate components:

(i) *Tangential component relations:*

$$\beta_{r_r}(\omega) = \beta_{i_r}(\omega) , \quad \beta_{r_v} = \beta_{i_v} , \quad \alpha_{r_r}(\omega) = \alpha_{i_r}(\omega) , \quad \alpha_{r_v} = \alpha_{i_v} = 0 . \quad (3.1.111a)$$

(ii) *Normal component relations:*

$$\beta_{r_n}(\omega) = -\beta_{i_n}(\omega) , \quad \alpha_{r_n}(\omega) = -\alpha_{i_n}(\omega) . \quad (3.1.111b)$$

(iii) *Spherical component relations:*

$$\beta_r = \beta_i , \quad \theta_r^\beta = \theta_i^\beta , \quad \phi_r^\beta = \phi_i^\beta , \quad \alpha_r = \alpha_i , \quad \theta_r^\alpha = \theta_i^\alpha . \quad (3.1.111c)$$

The complete set of equations that form the *generalized laws of refraction* are then summarized in the following three sets of equations which specify the transmitted wavevector components in terms of the incident wavevector components in both the rectangular and spherical coordinate components:

(iv) *Tangential component relations:*

$$\begin{aligned}\beta_{t_r}(\omega) &= \beta_{i_r}(\omega) , & \alpha_{t_r}(\omega) &= \alpha_{i_r}(\omega) , \\ \beta_{t_v} &= \beta_{i_v} , & \alpha_{t_v} &= \alpha_{i_v} = 0 .\end{aligned}\quad (3.1.112a)$$

(v) *Normal component relations:*

$$\bar{k}_{t_n}(\omega) = \beta_{t_n}(\omega) + i\alpha_{t_n}(\omega) = + \sqrt{k_2^2(\omega) - (\beta_{i_r}(\omega) + i\alpha_{i_r}(\omega))^2 - \beta_{i_v}^2} . \quad (3.1.112b)$$

(vi) *Spherical component relations:*

$$\begin{aligned}\beta_t &= \sqrt{\beta_{i_r}^2 + \beta_{i_v}^2 + \left[\Re \left\{ \sqrt{k_2^2(\omega) - (\beta_{i_r}(\omega) + i\alpha_{i_r}(\omega))^2 - \beta_{i_v}^2} \right\} \right]^2} , \\ \theta_t^\beta &= \cos^{-1} \left\{ \frac{\Re \left\{ \sqrt{k_2^2(\omega) - (\beta_{i_r}(\omega) + i\alpha_{i_r}(\omega))^2 - \beta_{i_v}^2} \right\}}{\beta_t} \right\} , & \phi_t^\beta &= \phi_i^\beta , \\ \alpha_t &= \sqrt{\alpha_{i_r}^2 + \left[\Im \left\{ \sqrt{k_2^2(\omega) - (\beta_{i_r}(\omega) + i\alpha_{i_r}(\omega))^2 - \beta_{i_v}^2} \right\} \right]^2} , & & (3.1.112c) \\ \theta_t^\alpha &= \tan^{-1} \left\{ \frac{\alpha_{i_r}(\omega)}{\Im \left\{ \sqrt{k_2^2(\omega) - (\beta_{i_r}(\omega) + i\alpha_{i_r}(\omega))^2 - \beta_{i_v}^2} \right\}} \right\} .\end{aligned}$$

3.1.3 The Generalized *Fresnel* Equations

The generalized *Fresnel* equations relate the tangential reflected and transmitted electric field vectors in terms of the tangential incident electric field vector within the interface coor-

dinate system. These relations are obtained from the tangential boundary conditions given in Eqs. (3.1.78a,b). Prior to this, however, a relationship between the tangential magnetic field vectors and the tangential electric field vectors needs to be obtained.

Either the incident, reflected or transmitted complex wavevector of an inhomogeneous plane wave in the interface coordinate system may be written as

$$\tilde{\mathbf{k}}(\omega) = \boldsymbol{\beta}(\omega) + i\boldsymbol{\alpha}(\omega) = \tilde{k}_\tau(\omega)\hat{\boldsymbol{\tau}} + \beta_\nu\hat{\boldsymbol{\nu}} + \tilde{k}_n(\omega)\hat{\boldsymbol{n}} ,$$

where

$$\tilde{k}_\tau(\omega) \equiv \beta_\tau(\omega) + i\alpha_\tau(\omega) , \quad \tilde{k}_n(\omega) \equiv \beta_n(\omega) + i\alpha_n(\omega) ,$$

and where β_ν is independent of the angular frequency ω and $\alpha_\nu = 0$, as explained at the beginning of §3.1. Expansion of the transversality condition given in Eq. (2.5.25) into component form yields

$$0 = \tilde{\mathbf{k}}(\omega) \cdot \mathbf{E}(\omega) = \tilde{k}_\tau(\omega)E_\tau(\omega) + \beta_\nu E_\nu(\omega) + \tilde{k}_n(\omega)E_n(\omega) ,$$

which may then be solved for E_n in terms of E_τ and E_ν as

$$E_n(\omega) = -\frac{\tilde{k}_\tau(\omega)E_\tau(\omega) + \beta_\nu E_\nu(\omega)}{\tilde{k}_n(\omega)} . \quad (3.1.113)$$

Upon expansion of the transversality condition given in Eq. (2.5.24) into component form yields

$$\begin{aligned} \eta_0 k_0 \mathbf{H}(\omega) &= \tilde{\mathbf{k}}(\omega) \times \mathbf{E}(\omega) \\ &= \left[\tilde{k}_\tau(\omega)\hat{\boldsymbol{\tau}} + \beta_\nu\hat{\boldsymbol{\nu}} + \tilde{k}_n(\omega)\hat{\boldsymbol{n}} \right] \times \left[E_\tau(\omega)\hat{\boldsymbol{\tau}} + E_\nu(\omega)\hat{\boldsymbol{\nu}} + E_n(\omega)\hat{\boldsymbol{n}} \right] \\ &= \left[\beta_\nu E_n - \tilde{k}_n(\omega)E_\nu \right] \hat{\boldsymbol{\tau}} + \left[-\tilde{k}_\tau(\omega)E_n + \tilde{k}_n(\omega)E_\tau \right] \hat{\boldsymbol{\nu}} + \left[\tilde{k}_\tau(\omega)E_\nu - \beta_\nu E_\tau \right] \hat{\boldsymbol{n}} \end{aligned}$$

which contains the normal component E_n . Substitution of Eq. (3.1.113) for E_n and rearranging terms then yields in matrix form,

$$\eta_0 k_0 \begin{bmatrix} H_\tau(\omega) \\ H_\nu(\omega) \\ H_n(\omega) \end{bmatrix} = \begin{bmatrix} \frac{\beta_\nu \tilde{k}_\tau(\omega)}{\tilde{k}_n(\omega)} & \frac{\beta_\nu^2}{\tilde{k}_n(\omega)} + \tilde{k}_n(\omega) \\ \frac{\tilde{k}_\tau^2(\omega)}{\tilde{k}_n(\omega)} + \tilde{k}_n(\omega) & \frac{\beta_\nu \tilde{k}_\tau(\omega)}{\tilde{k}_n(\omega)} \\ -\beta_\nu & \tilde{k}_\tau(\omega) \end{bmatrix} \begin{bmatrix} E_\tau(\omega) \\ E_\nu(\omega) \end{bmatrix}. \quad (3.1.114)$$

The 1,2 matrix entry may be simplified as

$$\frac{\beta_\nu^2}{\tilde{k}_n(\omega)} + \tilde{k}_n(\omega) = \frac{\beta_\nu^2 + \tilde{k}_n^2(\omega)}{\tilde{k}_n(\omega)} = \frac{\tilde{k}^2(\omega) - \tilde{k}_\tau^2(\omega)}{\tilde{k}_n(\omega)},$$

while the 2,1 matrix entry may be simplified as

$$\frac{\tilde{k}_\tau^2(\omega)}{\tilde{k}_n(\omega)} + \tilde{k}_n(\omega) = \frac{\tilde{k}_\tau^2(\omega) + \tilde{k}_n^2(\omega)}{\tilde{k}_n(\omega)} = \frac{\tilde{k}^2(\omega) - \beta_\nu^2}{\tilde{k}_n(\omega)}, \quad (3.1.115)$$

where the identity $\tilde{\mathbf{k}}(\omega) \cdot \tilde{\mathbf{k}}(\omega) \equiv \tilde{k}^2(\omega)$ was applied.

Application of the above two simplifications to Eq. (3.1.114) and the utilization of a sub-matrix containing only the tangential field vectors yields the relation

$$\mathbf{H}_{tan}(\omega) \equiv \tilde{\mathbf{Y}}(\omega) \mathbf{E}_{tan}(\omega) \quad (3.1.116)$$

where

$$\mathbf{H}_{tan}(\omega) \equiv \begin{bmatrix} H_\tau(\omega) \\ H_\nu(\omega) \end{bmatrix}, \quad \mathbf{E}_{tan}(\omega) \equiv \begin{bmatrix} E_\tau(\omega) \\ E_\nu(\omega) \end{bmatrix}.$$

Here,

$$\tilde{\mathbf{Y}}(\omega) \equiv \frac{1}{\eta_0 k_0} \frac{1}{\tilde{k}_n(\omega)} \begin{bmatrix} -\beta_\nu \tilde{k}_\tau(\omega) & \tilde{k}_\tau^2(\omega) - \tilde{k}^2(\omega) \\ \tilde{k}^2(\omega) - \beta_\nu^2 & \beta_\nu \tilde{k}_\tau(\omega) \end{bmatrix}, \quad (3.1.117)$$

is the *complex admittance matrix*[77]. The complex admittance matrix is anisotropic in that both the H_τ and H_ν tangential components of the magnetic field strength are dependent upon both tangential components E_τ and E_ν of the electric field strength. This anisotropy is due to the diagonal matrix elements which are both linear in β_ν .

With Eqs. (3.1.116) and (3.1.117) as a model, the specific tangential relations for each of the incident, reflected and transmitted field vectors are given by

$$\mathbf{H}_{i_{tan}}(\omega) \equiv \vec{\mathbf{Y}}_i(\omega) \mathbf{E}_{i_{tan}}(\omega) , \quad (3.1.118)$$

$$\mathbf{H}_{r_{tan}}(\omega) \equiv \vec{\mathbf{Y}}_r(\omega) \mathbf{E}_{r_{tan}}(\omega) , \quad (3.1.119)$$

and

$$\mathbf{H}_{t_{tan}}(\omega) \equiv \vec{\mathbf{Y}}_t(\omega) \mathbf{E}_{t_{tan}}(\omega) . \quad (3.1.120)$$

The incident complex admittance matrix is given by

$$\vec{\mathbf{Y}}_i(\omega) \equiv \frac{1}{\eta_0 k_0} \frac{1}{\tilde{k}_{i_n}(\omega)} \begin{bmatrix} -\beta_{i_v} \tilde{k}_{i_r}(\omega) & \tilde{k}_{i_r}^2(\omega) - \tilde{k}_1^2(\omega) \\ \tilde{k}_1^2(\omega) - \beta_{i_v}^2 & \beta_{i_v} \tilde{k}_{i_r}(\omega) \end{bmatrix} , \quad (3.1.121)$$

the reflected complex admittance matrix is given by

$$\vec{\mathbf{Y}}_r(\omega) \equiv \frac{1}{\eta_0 k_0} \frac{1}{\tilde{k}_{r_n}(\omega)} \begin{bmatrix} -\beta_{r_v} \tilde{k}_{r_r}(\omega) & \tilde{k}_{r_r}^2(\omega) - \tilde{k}_1^2(\omega) \\ \tilde{k}_1^2(\omega) - \beta_{r_v}^2 & \beta_{r_v} \tilde{k}_{r_r}(\omega) \end{bmatrix} , \quad (3.1.122)$$

and the transmitted complex admittance matrix is given by

$$\vec{\mathbf{Y}}_t(\omega) \equiv \frac{1}{\eta_0 k_0} \frac{1}{\tilde{k}_{t_n}(\omega)} \begin{bmatrix} -\beta_{t_v} \tilde{k}_{t_r}(\omega) & \tilde{k}_{t_r}^2(\omega) - \tilde{k}_2^2(\omega) \\ \tilde{k}_2^2(\omega) - \beta_{t_v}^2 & \beta_{t_v} \tilde{k}_{t_r}(\omega) \end{bmatrix} . \quad (3.1.123)$$

The tangential components of the generalized law of reflection given in Eq. (3.1.111a) are

$$\begin{aligned} \beta_{r_t}(\omega) &= \beta_{i_t}(\omega) , & \alpha_{r_t}(\omega) &= \alpha_{i_t}(\omega) , \\ \beta_{r_v} &= \beta_{i_v} , & \alpha_{r_v} &= \alpha_{i_v} = 0 . \end{aligned}$$

In addition, the normal component relationships of the generalized law of reflection given in Eq. (3.1.111b) are

$$\beta_{r_n}(\omega) = -\beta_{i_n}(\omega) , \quad \alpha_{r_n}(\omega) = -\alpha_{i_n}(\omega) .$$

These facts indicate that the incident and reflected complex admittance matrices are equal

but of opposite sign, viz.

$$\vec{\mathbf{Y}}_r(\omega) = -\vec{\mathbf{Y}}_i(\omega) . \quad (3.1.124)$$

The tangential components of the generalized law of reflection given in Eq. (3.1.111a) yield

$$\begin{aligned} \beta_{t_r}(\omega) &= \beta_{i_r}(\omega) , & \alpha_{t_r}(\omega) &= \alpha_{i_r}(\omega) , \\ \beta_{t_v} &= \beta_{i_v} , & \alpha_{r_v} &= \alpha_{i_v} = 0 . \end{aligned}$$

With these results, Eq. (3.1.123) becomes

$$\vec{\mathbf{Y}}_i(\omega) \equiv \frac{1}{\eta_0 k_0} \frac{1}{\tilde{k}_{t_n}(\omega)} \begin{bmatrix} -\beta_{i_v} \tilde{k}_{i_r}(\omega) & \tilde{k}_{i_r}^2(\omega) - \tilde{k}_2^2(\omega) \\ \tilde{k}_2^2(\omega) - \beta_{i_v}^2 & \beta_{i_v} \tilde{k}_{i_r}(\omega) \end{bmatrix} . \quad (3.1.125)$$

Since it was determined in §3.1.2 that the complex phase terms appearing in the boundary value conditions given in Eqs. (3.1.78a,b) are equal, these terms may be eliminated from those relations with the result

$$\begin{aligned} \hat{n} \times [\mathbf{E}_t(\omega) - \mathbf{E}_i(\omega) - \mathbf{E}_r(\omega)] &= \mathbf{0} , \\ \hat{n} \times [\mathbf{H}_t(\omega) - \mathbf{H}_i(\omega) - \mathbf{H}_r(\omega)] &= \mathbf{0} . \end{aligned}$$

Substitution of the electromagnetic field vectors in component form, from Eqs. (3.1.69), (3.1.72) and (3.1.74), into the above relations then yields

$$\begin{aligned} -E_{i_r}(\omega) \hat{v} + E_{i_v}(\omega) \hat{t} - E_{r_r}(\omega) \hat{v} + E_{r_v}(\omega) \hat{t} &= -E_{t_r}(\omega) \hat{v} + E_{t_v}(\omega) \hat{t} , \\ -H_{i_r}(\omega) \hat{v} + H_{i_v}(\omega) \hat{t} - H_{r_r}(\omega) \hat{v} + H_{r_v}(\omega) \hat{t} &= -H_{t_r}(\omega) \hat{v} + H_{t_v}(\omega) \hat{t} , \end{aligned}$$

which may be rearranged as

$$\begin{aligned} -[E_{i_r}(\omega) + E_{r_r}(\omega)] \hat{v} + [E_{i_v}(\omega) + E_{r_v}(\omega)] \hat{t} &= -E_{t_r}(\omega) \hat{v} + E_{t_v}(\omega) \hat{t} , \\ -[H_{i_r}(\omega) + H_{r_r}(\omega)] \hat{v} + [H_{i_v}(\omega) + H_{r_v}(\omega)] \hat{t} &= -H_{t_r}(\omega) \hat{v} + H_{t_v}(\omega) \hat{t} . \end{aligned}$$

Due to the independence of the mutually orthogonal tangential vector components, the separate vector components appearing in this pair of equations must then be equal, resulting in the set of equations

$$E_{i_r}(\omega) + E_{r_r}(\omega) = E_{t_r}(\omega) ,$$

$$E_{i_v}(\omega) + E_{r_v}(\omega) = E_{t_v}(\omega) ,$$

$$H_{i_r}(\omega) + H_{r_r}(\omega) = H_{t_r}(\omega) ,$$

$$H_{i_v}(\omega) + H_{r_v}(\omega) = H_{t_v}(\omega) .$$

These tangential boundary conditions may be rewritten in matrix form as

$$\mathbf{E}_{t_{tan}}(\omega) = \begin{bmatrix} E_{t_r}(\omega) \\ E_{t_v}(\omega) \end{bmatrix} = \begin{bmatrix} E_{i_r}(\omega) + E_{r_r}(\omega) \\ E_{i_v}(\omega) + E_{r_v}(\omega) \end{bmatrix} = \mathbf{E}_{i_{tan}}(\omega) + \mathbf{E}_{r_{tan}}(\omega) , \quad (3.1.126a)$$

$$\mathbf{H}_{t_{tan}}(\omega) = \begin{bmatrix} H_{t_r}(\omega) \\ H_{t_v}(\omega) \end{bmatrix} = \begin{bmatrix} H_{i_r}(\omega) + H_{r_r}(\omega) \\ H_{i_v}(\omega) + H_{r_v}(\omega) \end{bmatrix} = \mathbf{H}_{i_{tan}}(\omega) + \mathbf{H}_{r_{tan}}(\omega) . \quad (3.1.126b)$$

Upon substitution of the relationships given in Eqs. (3.1.118), (3.1.119) and (3.1.120) into Eq. (3.1.126b) yields

$$\mathbf{H}_{t_{tan}}(\omega) = \vec{\mathbf{Y}}_t(\omega)\mathbf{E}_{t_{tan}}(\omega) = \vec{\mathbf{Y}}_i(\omega)\mathbf{E}_{i_{tan}}(\omega) + \vec{\mathbf{Y}}_r(\omega)\mathbf{E}_{r_{tan}}(\omega) . \quad (3.1.127)$$

With the substitution of Eq. (3.1.126a) into the transmitted electric field vector $\mathbf{E}_{t_{tan}}(\omega)$, this equation becomes

$$\vec{\mathbf{Y}}_t(\omega)\left[\mathbf{E}_{i_{tan}}(\omega) + \mathbf{E}_{r_{tan}}(\omega)\right] = \vec{\mathbf{Y}}_i(\omega)\mathbf{E}_{i_{tan}}(\omega) + \vec{\mathbf{Y}}_r(\omega)\mathbf{E}_{r_{tan}}(\omega) ,$$

which may be solved for the reflected tangential field vector as

$$\mathbf{E}_{r_{tan}}(\omega) = \left[-\vec{\mathbf{Y}}_r(\omega) + \vec{\mathbf{Y}}_t(\omega)\right]^{-1}\left[-\vec{\mathbf{Y}}_t(\omega) + \vec{\mathbf{Y}}_i(\omega)\right]\mathbf{E}_{i_{tan}}(\omega) .$$

Since $-\vec{\mathbf{Y}}_r(\omega) = \vec{\mathbf{Y}}_i(\omega)$, there results

$$\mathbf{E}_{r_{tan}}(\omega) = \vec{\mathbf{F}} \mathbf{E}_{i_{tan}}(\omega) , \quad (3.1.128)$$

where the *tangential reflection matrix* $\vec{\mathbf{F}}$ is defined as

$$\vec{\mathbf{F}} \equiv \left[\vec{\mathbf{Y}}_i(\omega) + \vec{\mathbf{Y}}_t(\omega)\right]^{-1}\left[\vec{\mathbf{Y}}_i(\omega) - \vec{\mathbf{Y}}_t(\omega)\right] , \quad (3.1.129)$$

whose elements represent the generalized *Fresnel* equations for the reflection coefficients. Substitution of the complex admittance matrices given in Eqs. (3.1.121) and (3.1.125) into

the tangential reflection matrix, yields

$$\vec{r} = \begin{bmatrix} r_{\tau_r} & r_{\tau_v} \\ r_{\nu_r} & r_{\nu_v} \end{bmatrix}, \quad (3.1.130)$$

where

$$\begin{aligned} r_{\tau_r} \equiv & \frac{\beta_{i_v}^2}{\Delta} \left\{ \left[2\beta_{i_v}^2 - 2\tilde{k}_1^2(\omega) \right] \frac{\tilde{k}_{t_n}(\omega)}{\tilde{k}_{i_n}(\omega)} - \tilde{k}_{t_n}(\omega) + \tilde{k}_2(\omega) \right\} \\ & - \frac{\beta_{i_v}^2}{\Delta} \left\{ \left[2\beta_{i_v}^2 - 2\tilde{k}_2^2(\omega) \right] \frac{\tilde{k}_{i_n}(\omega)}{\tilde{k}_{t_n}(\omega)} - \tilde{k}_{i_n}(\omega) + \tilde{k}_1(\omega) \right\} \\ & + \frac{1}{\Delta} \left\{ \tilde{k}_1^2(\omega)\tilde{k}_{t_n}(\omega) - \tilde{k}_2^2(\omega)\tilde{k}_{i_n}(\omega) \right\} \left\{ \tilde{k}_{i_n}(\omega) + \tilde{k}_{t_n}(\omega) \right\}, \quad (3.1.131a) \end{aligned}$$

$$\begin{aligned} r_{\nu_v} \equiv & \frac{\beta_{i_v}^2}{\Delta} \left\{ \left[2\beta_{i_v}^2 - 2\tilde{k}_1^2(\omega) \right] \frac{\tilde{k}_{t_n}(\omega)}{\tilde{k}_{i_n}(\omega)} + \tilde{k}_{t_n}(\omega) - \tilde{k}_2(\omega) \right\} \\ & - \frac{\beta_{i_v}^2}{\Delta} \left\{ \left[2\beta_{i_v}^2 - 2\tilde{k}_2^2(\omega) \right] \frac{\tilde{k}_{i_n}(\omega)}{\tilde{k}_{t_n}(\omega)} + \tilde{k}_{i_n}(\omega) - \tilde{k}_1(\omega) \right\} \\ & + \frac{1}{\Delta} \left\{ \tilde{k}_1^2(\omega)\tilde{k}_{t_n}(\omega) + \tilde{k}_2^2(\omega)\tilde{k}_{i_n}(\omega) \right\} \left\{ \tilde{k}_{i_n}(\omega) - \tilde{k}_{t_n}(\omega) \right\}, \quad (3.1.131b) \end{aligned}$$

$$r_{\tau_v} \equiv \frac{2}{\Delta} \left\{ \left[\beta_{i_v}\tilde{k}_{i_r}(\omega) \right] \left[\beta_{i_v}^2 - \tilde{k}_{i_n}^2(\omega) \right] - \left[\beta_{i_v}\tilde{k}_{t_r}(\omega) \right] \left[\beta_{i_v}^2 - \tilde{k}_{t_n}^2(\omega) \right] \right\}, \quad (3.1.131c)$$

$$r_{\nu_r} \equiv \frac{2}{\Delta} \left\{ \left[\beta_{i_v}\tilde{k}_{i_r}(\omega) \right] \left[\beta_{i_v}^2 - \tilde{k}_1^2(\omega) \right] - \left[\beta_{i_v}\tilde{k}_{t_r}(\omega) \right] \left[\beta_{i_v}^2 - \tilde{k}_2^2(\omega) \right] \right\}. \quad (3.1.131d)$$

The determinant Δ appearing here is given by

$$\begin{aligned}
\Delta \equiv & \beta_{i_v}^2 \left\{ \left[2\beta_{i_v}^2 - 2\tilde{k}_1^2(\omega) \right] \frac{\tilde{k}_{t_n}(\omega)}{\tilde{k}_{i_n}(\omega)} - \tilde{k}_{t_n}^2(\omega) - \tilde{k}_2^2(\omega) \right\} \\
& + \beta_{i_v}^2 \left\{ \left[2\beta_{i_v}^2 - 2\tilde{k}_2^2(\omega) \right] \frac{\tilde{k}_{i_n}(\omega)}{\tilde{k}_{t_n}(\omega)} - \tilde{k}_{i_n}^2(\omega) - \tilde{k}_1^2(\omega) \right\} \\
& + \left\{ \tilde{k}_1^2(\omega)\tilde{k}_{t_n}(\omega) + \tilde{k}_2^2(\omega)\tilde{k}_{i_n}(\omega) \right\} \left\{ \tilde{k}_{i_n}(\omega) + \tilde{k}_{t_n}(\omega) \right\} \\
& + \left\{ 2\beta_{i_v}^4 - 2\beta_{i_v}^2\tilde{k}_{i_t}^2(\omega) \right\} . \tag{3.1.132}
\end{aligned}$$

Upon rearranging Eq. (3.1.126a) for the reflected electric field vector and substituting the result into Eq. (3.1.127), there results

$$\vec{Y}_t(\omega)\mathbf{E}_{t_{tan}}(\omega) = \vec{Y}_i(\omega)\mathbf{E}_{i_{tan}}(\omega) + \vec{Y}_r(\omega)\left[\mathbf{E}_{t_{tan}}(\omega) - \mathbf{E}_{i_{tan}}(\omega)\right],$$

whose solution for the transmitted tangential field yields

$$\mathbf{E}_{t_{tan}}(\omega) = \left[\vec{Y}_t(\omega) - \vec{Y}_r(\omega) \right]^{-1} \left[\vec{Y}_i(\omega) - \vec{Y}_r(\omega) \right] \mathbf{E}_{i_{tan}}(\omega) .$$

Since $-\vec{Y}_r(\omega) = \vec{Y}_i(\omega)$, there results

$$\mathbf{E}_{t_{tan}}(\omega) = \vec{t} \mathbf{E}_{i_{tan}}(\omega) , \tag{3.1.133}$$

where the *tangential transmission matrix* \vec{t} is defined as

$$\vec{t} \equiv \left[\vec{Y}_i(\omega) + \vec{Y}_t(\omega) \right]^{-1} \left[2\vec{Y}_i(\omega) \right] , \tag{3.1.134}$$

whose elements represent the generalized *Fresnel* equations for the transmission coefficients. Substitution of the complex admittance matrices given in Eqs. (3.1.121) and (3.1.123) into the tangential transmission matrix, yields

$$\vec{t} = \begin{bmatrix} t_{\tau_\tau} & t_{\tau_\nu} \\ t_{\nu_\tau} & t_{\nu_\nu} \end{bmatrix} , \tag{3.1.135}$$

where

$$\begin{aligned}
t_{\tau_i} \equiv & \frac{2\beta_{i_v}^2}{\Delta} \left\{ \left[2\beta_{i_v}^2 - 2\tilde{k}_1(\omega) \right] \frac{\tilde{k}_{t_n}(\omega)}{\tilde{k}_{i_n}(\omega)} - \tilde{k}_{t_n}(\omega) \right\} \\
& - \frac{2\beta_{i_v}^2}{\Delta} \left\{ \tilde{k}_1(\omega) \right\} + \frac{2}{\Delta} \beta_{i_v}^4 - \frac{2}{\Delta} \beta_{i_v}^2 \tilde{k}_{i_t}(\omega) \\
& + \frac{2}{\Delta} \left\{ \tilde{k}_1(\omega) \tilde{k}_{t_n}(\omega) \right\} \left\{ \tilde{k}_{i_n}(\omega) + \tilde{k}_{t_n}(\omega) \right\}, \tag{3.1.136a}
\end{aligned}$$

$$\begin{aligned}
t_{v_v} \equiv & \frac{2\beta_{i_v}^2}{\Delta} \left\{ \left[2\beta_{i_v}^2 - 2\tilde{k}_1(\omega) \right] \frac{\tilde{k}_{t_n}(\omega)}{\tilde{k}_{i_n}(\omega)} - \tilde{k}_2(\omega) \right\} \\
& - \frac{2\beta_{i_v}^2}{\Delta} \left\{ \tilde{k}_{i_n}(\omega) \right\} + \frac{2}{\Delta} \beta_{i_v}^4 - \frac{2}{\Delta} \beta_{i_v}^2 \tilde{k}_{i_t}(\omega) \\
& + \frac{2}{\Delta} \left\{ \tilde{k}_1(\omega) \tilde{k}_{t_n}(\omega) + \tilde{k}_2(\omega) \tilde{k}_{i_n}(\omega) \right\} \left\{ \tilde{k}_{i_n}(\omega) \right\}, \tag{3.1.136b}
\end{aligned}$$

$$t_{\tau_v} \equiv r_{\tau_v}, \tag{3.1.136c}$$

$$t_{v_\tau} \equiv r_{v_\tau}. \tag{3.1.136d}$$

Notice the fundamental relationship between the tangential reflection and transmission matrices

$$\vec{t} = \vec{I} + \vec{r}, \tag{3.1.137}$$

where $\vec{I} = [\delta_{ij}]$ is the unit matrix.

3.1.4 Special cases of the Generalized Laws of Reflection and Refraction and the Generalized *Fresnel* Equations

The generalized *Fresnel* equations developed in §3.1.3 exhibit an inherent anisotropy, which is due to the presence of the β_{i_v} and β_{t_v} terms in the complex admittance matrices. These terms couple one tangential component of the reflected or transmitted field vector in terms of both tangential components of the incident field vector. The existence of the components β_{i_v} and β_{t_v} is due to the fact that the α -plane of incidence is, in general, different from the β -plane of incidence. An important implication of this inherent anisotropy is that any

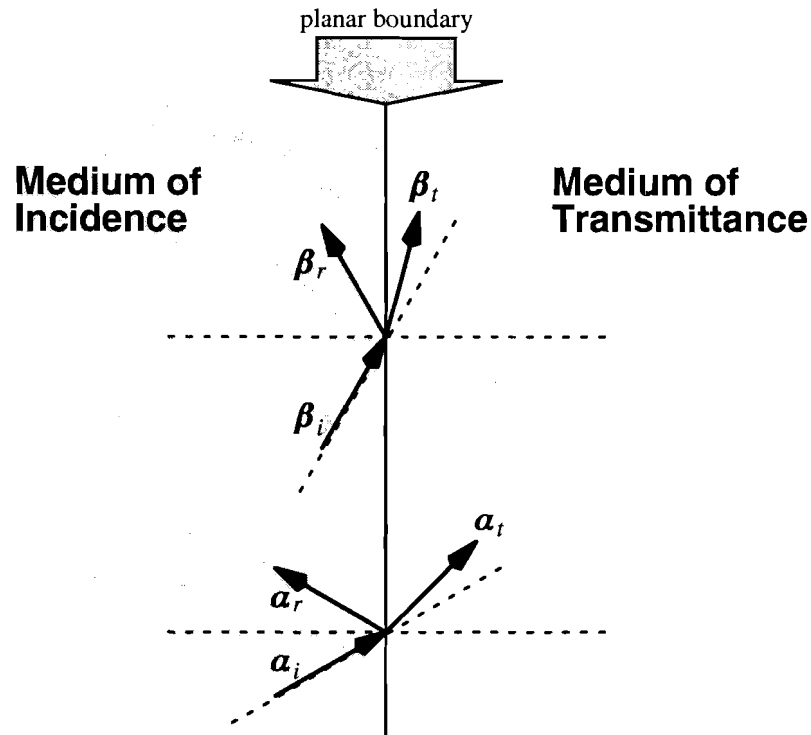


Figure 3.1.10 Geometry of the inhomogeneous plane wave reflection and refraction at a planar interface separating two lossy, dispersive dielectric half-spaces when the α -plane of incidence is coplanar with the β -plane of incidence.

logical separation of the electromagnetic fields into strictly TE or TM polarized fields (also denoted as s- or p-polarized fields, respectively) does not exist. However, if the α - and β -planes of incidence are coplanar then this anisotropy disappears. Two special cases are now examined to help explain this phenomenon.

Case I: The β -Plane of Incidence is Coplanar with the α -Plane of Incidence: Linearly Polarized TE and TM Fields

Under certain circumstances, the polarization state of the electromagnetic field will be known. If one of the field components is linearly polarized in the direction perpendicular to the xz reference plane then, by the results of §2.6.2, the other field component is elliptically polarized and the xz reference plane contains both the elliptically polarized field and the complex wavevector. If the electric field is perpendicular to the xz reference plane then the field is called TE or Transverse Electric and is sometimes referred to as s-polarized (where 's' stands for *senkrecht*, which means perpendicular in German). If the magnetic field is per-

pendicular to the xz reference plane then the field is called TM or Transverse Magnetic and is sometimes referred to as p-polarized (where 'p' stands for parallel). As a consequence, the transverse wavenumber vanishes ($\beta_{i_v} = 0$) and, from Eq. (3.1.36),

$$\phi_i^\beta = 0, \pi , \quad (3.1.138)$$

the choice depending on the sign of β_{i_r} . The β -plane of incidence is assumed to be coplanar with the α -plane of incidence. When this occurs, the generalized laws of reflection and refraction in spherical components, given in Eqs. (3.1.111c) and (3.1.112c), show that

$$\phi_i^\beta = \phi_r^\beta = \phi_t^\beta = 0, \pi . \quad (3.1.139)$$

As a result, all of the propagation and attenuation vectors lie in the same plane, as illustrated in Figure 3.1.10. The remaining generalized laws of refraction and reflection, given in Eqs. (3.1.111) and (3.1.112), are correspondingly altered.

The complete set of equations that form the *generalized laws of reflection* at a planar interface separating two lossy dielectrics when the β -plane of incidence and the α -plane of incidence are coplanar are summarized in the following three sets of equations that are expressed in terms of the incident wavevector components in both the rectangular and spherical coordinate components:

(i) *Tangential component relations* when the β -plane of incidence and the α -plane of incidence are coplanar:

$$\beta_{r_r}(\omega) = \beta_{i_r}(\omega) , \quad \beta_{r_v} = \beta_{i_v} = 0 , \quad \alpha_{r_r}(\omega) = \alpha_{i_r}(\omega) , \quad \alpha_{r_v} = \alpha_{i_v} = 0 . \quad (3.1.140a)$$

(ii) *Normal component relations* when the β -plane of incidence and the α -plane of incidence are coplanar:

$$\beta_{r_n}(\omega) = -\beta_{i_n}(\omega) , \quad \alpha_{r_n}(\omega) = -\alpha_{i_n}(\omega) . \quad (3.1.140b)$$

(iii) *Spherical component relations* when the β -plane of incidence and the α -plane of incidence are coplanar:

$$\beta_r = \beta_i , \quad \theta_r^\beta = \theta_i^\beta , \quad \phi_r^\beta = \phi_i^\beta = 0, \pi , \quad \alpha_r = \alpha_i , \quad \theta_r^\alpha = \theta_i^\alpha . \quad (3.1.140c)$$

The complete set of equations that form the *generalized laws of refraction* at a planar interface separating two lossy dielectrics when the $\boldsymbol{\beta}$ -plane of incidence and the $\boldsymbol{\alpha}$ -plane of incidence are coplanar are summarized in the following three sets of equations that are expressed in terms of the incident wavevector components in both the rectangular and spherical coordinate components:

(iv) *Tangential component relations* when the $\boldsymbol{\beta}$ -plane of incidence and the $\boldsymbol{\alpha}$ -plane of incidence are coplanar:

$$\beta_{t_r}(\omega) = \beta_{i_r}(\omega) , \beta_{t_v} = \beta_{i_v} = 0 , \alpha_{t_r}(\omega) = \alpha_{i_r}(\omega) , \alpha_{t_v} = \alpha_{i_v} = 0 . \quad (3.1.141a)$$

(v) *Normal component relations* when the $\boldsymbol{\beta}$ -plane of incidence and the $\boldsymbol{\alpha}$ -plane of incidence are coplanar:

$$\beta_{t_n}(\omega) + i\alpha_{t_n}(\omega) = + \sqrt{k_2^2(\omega) - (\beta_{i_r}(\omega) + i\alpha_{i_r}(\omega))^2} . \quad (3.1.141b)$$

(vi) *Spherical component relations* when the $\boldsymbol{\beta}$ -plane of incidence and the $\boldsymbol{\alpha}$ -plane of incidence are coplanar:

$$\begin{aligned} \beta_t &= \sqrt{\beta_{i_r}^2 + \left[\Re \left\{ \sqrt{k_2^2(\omega) - (\beta_{i_r}(\omega) + i\alpha_{i_r}(\omega))^2} \right\} \right]^2} , \\ \theta_t^\beta &= \cos^{-1} \left\{ \frac{\Re \left\{ \sqrt{k_2^2(\omega) - (\beta_{i_r}(\omega) + i\alpha_{i_r}(\omega))^2} \right\}}{\beta_t} \right\} , \quad \phi_t^\beta = 0, \pi , \\ \alpha_t &= \sqrt{\alpha_{i_r}^2 + \left[\Im \left\{ \sqrt{k_2^2(\omega) - (\beta_{i_r}(\omega) + i\alpha_{i_r}(\omega))^2} \right\} \right]^2} , \\ \theta_t^\alpha &= \tan^{-1} \left\{ \frac{\alpha_{i_r}(\omega)}{\Im \left\{ \sqrt{k_2^2(\omega) - (\beta_{i_r}(\omega) + i\alpha_{i_r}(\omega))^2} \right\}} \right\} . \end{aligned} \quad (3.1.141c)$$

In this special case, the form of the generalized *Fresnel* equations for the reflection and transmission coefficients remains unaltered from that given in Eqs. (3.1.129) and (3.1.134). However, the complex admittance matrices are reduced to isotropic forms using Eq. (3.1.115) and noting that $\beta_\nu = 0$ for this special case, viz.

$$\vec{Y}_i(\omega) \equiv \frac{1}{\eta_0 k_0} \frac{1}{\tilde{k}_{i_n}(\omega)} \begin{bmatrix} 0 & -\tilde{k}_{i_n}^2(\omega) \\ \tilde{k}_1(\omega) & 0 \end{bmatrix}, \quad (3.1.142)$$

and

$$\vec{Y}_t(\omega) \equiv \frac{1}{\eta_0 k_0} \frac{1}{\tilde{k}_{t_n}(\omega)} \begin{bmatrix} 0 & -\tilde{k}_{t_n}^2(\omega) \\ \tilde{k}_2(\omega) & 0 \end{bmatrix}. \quad (3.1.143)$$

Substitution of the above isotropic incident and transmitted complex admittance matrices into the generalized *Fresnel* equations produces isotropic versions of the tangential reflection and transmission matrices in that they are both diagonal. The diagonal terms can be identified as the reflection and transmission coefficients for TE or TM polarized fields. The tangential reflection matrix becomes

$$\vec{r} \equiv \begin{bmatrix} r_\tau & 0 \\ 0 & r_\nu \end{bmatrix} = \begin{bmatrix} \frac{\tilde{n}_1^2(\omega)\tilde{k}_{t_n}(\omega) - \tilde{n}_2^2(\omega)\tilde{k}_{i_n}(\omega)}{\tilde{n}_1^2(\omega)\tilde{k}_{t_n}(\omega) + \tilde{n}_2^2(\omega)\tilde{k}_{i_n}(\omega)} & 0 \\ 0 & \frac{\tilde{k}_{i_n}(\omega) - \tilde{k}_{t_n}(\omega)}{\tilde{k}_{i_n}(\omega) + \tilde{k}_{t_n}(\omega)} \end{bmatrix}, \quad (3.1.144)$$

where the r_τ component is the reflection coefficient for TM polarized fields and the r_ν component is the reflection coefficient for TE polarized fields. The tangential transmission matrix becomes

$$\vec{t} \equiv \begin{bmatrix} t_\tau & 0 \\ 0 & t_\nu \end{bmatrix} = 2 \begin{bmatrix} \frac{\tilde{n}_1^2(\omega)\tilde{k}_{t_n}(\omega)}{\tilde{n}_1^2(\omega)\tilde{k}_{t_n}(\omega) + \tilde{n}_2^2(\omega)\tilde{k}_{i_n}(\omega)} & 0 \\ 0 & \frac{\tilde{k}_{i_n}(\omega)}{\tilde{k}_{i_n}(\omega) + \tilde{k}_{t_n}(\omega)} \end{bmatrix}, \quad (3.1.145)$$

where the t_τ component is the transmission coefficient for TM polarized fields and the t_ν component is the transmission coefficient for TE polarized fields. The relationship between \vec{r} and \vec{t} becomes [cf. Eq. (3.1.137)]

$$\vec{t} = \begin{bmatrix} t_\tau & 0 \\ 0 & t_\nu \end{bmatrix} = \begin{bmatrix} 1 + r_\tau & 0 \\ 0 & 1 + r_\nu \end{bmatrix} = \vec{I} + \vec{r} . \quad (3.1.146)$$

Case II: The Refractive Index of the Medium of Incidence is Lossless

Let the refractive index of the medium of incidence be real-valued so that $\tilde{n}_1 = n_1$, where $n_1 \in \mathbb{R}$. Consequently, the incident and reflected complex wavevectors are also real-valued, where

$$\tilde{\mathbf{k}}_i(\omega) = \boldsymbol{\beta}_i(\omega) \quad (3.1.147)$$

and

$$\tilde{\mathbf{k}}_r(\omega) = \boldsymbol{\beta}_r(\omega) . \quad (3.1.148)$$

The generalized laws of refraction and reflection appearing in Eqs. (3.1.111) and (3.1.112) are then correspondingly altered.

The complete set of equations that form the *generalized laws of reflection* when the medium of incidence is lossless are summarized in the following three sets of equations that are expressed in terms of the incident wavevector components in both the rectangular and spherical coordinate components:

(i) *Tangential component relations* when the medium of incidence is lossless:

$$\beta_{r_\tau}(\omega) = \beta_{i_\tau}(\omega) , \quad \beta_{r_\nu} = \beta_{i_\nu} , \quad \alpha_{r_\tau} = \alpha_{i_\tau} = 0 , \quad \alpha_{r_\nu} = \alpha_{i_\nu} = 0 . \quad (3.1.149a)$$

(ii) *Normal component relations* when the medium of incidence is lossless:

$$\beta_{r_n}(\omega) = -\beta_{i_n}(\omega) , \quad \alpha_{r_n} = -\alpha_{i_n} = 0 . \quad (3.1.149b)$$

(iii) *Spherical component relations* when the medium of incidence is lossless:

$$\beta_r = \beta_i , \quad \theta_r^\beta = \theta_i^\beta , \quad \phi_r^\beta = \phi_i^\beta , \quad \alpha_r = \alpha_i = 0 , \quad \theta_r = \theta_i . \quad (3.1.149c)$$

The complete set of equations that form the *generalized laws of refraction* when the medium of incidence is lossless are summarized in the following three sets of equations that are expressed in terms of the incident wavevector components in both the rectangular and spherical coordinate components:

(iv) *Tangential component relations* when the medium of incidence is lossless:

$$\beta_{t_r}(\omega) = \beta_{i_r}(\omega) , \quad \beta_{t_v} = \beta_{i_v} , \quad \alpha_{t_r} = \alpha_{i_r} = 0 , \quad \alpha_{t_v} = \alpha_{i_v} = 0 . \quad (3.1.150a)$$

(v) *Normal component relations* when the medium of incidence is lossless:

$$\beta_{t_n}(\omega) + i\alpha_{t_n}(\omega) = + \sqrt{k_2^2(\omega) - \beta_{i_r}^2(\omega) - \beta_{i_v}^2} . \quad (3.1.150b)$$

(vi) *Spherical component relations* when the medium of incidence is lossless:

$$\begin{aligned} \beta_t &= \sqrt{\beta_{i_r}^2 + \left[\Re \left\{ \sqrt{k_2^2(\omega) - \beta_{i_r}^2(\omega) - \beta_{i_v}^2} \right\} \right]^2} , \\ \theta_t^\beta &= \cos^{-1} \left\{ \frac{\Re \left\{ \sqrt{k_2^2(\omega) - \beta_{i_r}^2(\omega) - \beta_{i_v}^2} \right\}}{\beta_t} \right\} , \quad \phi_t^\beta = \phi_i^\beta , \\ \alpha_t &= \sqrt{\alpha_{i_r}^2 + \left[\Im \left\{ \sqrt{k_2^2(\omega) - \beta_{i_r}^2(\omega) - \beta_{i_v}^2} \right\} \right]^2} , \\ \theta_t^\alpha &= \tan^{-1} \left\{ \frac{\alpha_{i_r}(\omega)}{\Im \left\{ \sqrt{k_2^2(\omega) - \beta_{i_r}^2(\omega) - \beta_{i_v}^2} \right\}} \right\} . \end{aligned} \quad (3.1.150c)$$

In this case, the form of the generalized *Fresnel* equations for the reflection and transmission coefficients remains unaltered from that given in Eqs. (3.1.129) and (3.1.134). The components of the incident complex wavevector are affected and reduce to

$$\tilde{k}_{i_r}(\omega) \equiv \beta_{i_r}(\omega) , \quad \tilde{k}_{i_n}(\omega) \equiv \beta_{i_n}(\omega) ,$$

and the tangential component of the transmitted complex wavevector reduces to

$$\tilde{k}_t(\omega) \equiv \beta_{t_r}(\omega) .$$

The complex admittance matrices are affected by the simplified case and are reduced to

$$\vec{Y}_i(\omega) \equiv \frac{1}{\eta_0 k_0} \frac{1}{\beta_{i_n}(\omega)} \begin{bmatrix} -\beta_i \beta_{i_r}(\omega) & \beta_{i_r}^2(\omega) - n_1^2 k_0^2 \\ n_1^2 k_0^2 - \beta_{i_v}^2 & \beta_i \beta_{i_r}(\omega) \end{bmatrix}, \quad (3.1.151)$$

$$\vec{Y}_t(\omega) \equiv \frac{1}{\eta_0 k_0} \frac{1}{\tilde{k}_{t_n}(\omega)} \begin{bmatrix} -\beta_t \beta_{t_r}(\omega) & \beta_{t_r}^2(\omega) - \tilde{n}_2^2(\omega) k_0^2 \\ \tilde{k}_2^2(\omega) & \beta_t \beta_{t_r}(\omega) \end{bmatrix}. \quad (3.1.152)$$

The admittance matrices still exhibit anisotropy because the incident propagation vector is not limited to the xz reference plane.

3.2 The Reflected and Refracted Inhomogeneous Plane Wave Fields Expressed Within Their Respective Local Coordinate Systems

In this section, the incident inhomogeneous plane wave, given in terms of the local incident coordinate system, is related to the reflected and transmitted fields within their respective local coordinate systems. A common reference point between all three local coordinate systems must be found, which lies within the interface, because it is here that the relationships between the incident inhomogeneous plane wave and the reflected and transmitted fields as governed by the generalized laws of reflection and refraction and the generalized *Fresnel* equations are defined. The interface origin provides a convenient common reference point because all three local longitudinal axes intersect at that point.

This problem assumes that the incident local coordinate system is fixed, i.e. the characteristic angle Θ_i is given and that the real-valued transverse wavenumbers k_u and k_v are allowed to span their whole domain while the real-valued frequency ω is another independent variable. Initially, while within the incident local coordinate system, propagating the incident inhomogeneous plane wave field along the \hat{w} -axis a distance w_0 from the local origin places the field at the interface origin. The incident field is then transformed into the inter-

face coordinate system using the transformation matrix defined in Eq. (3.1.23). The reflected and refracted inhomogeneous plane wave fields may then be expressed in terms of the given incident inhomogeneous plane wave field within the interface coordinate system using the generalized laws of reflection and refraction, given in Eqs. (3.1.111a–c) and (3.1.112a–c) and the generalized *Fresnel* equations given in Eqs. (3.1.130) and (3.1.135). The reflected and refracted inhomogeneous plane wave fields are then expressed within their respective local coordinate systems using the transformation matrices defined in Eqs. (3.1.56) and (3.1.57). Finally, while within their respective local coordinate systems, propagating the reflected and refracted fields along the \hat{w}' -axis and \hat{w}'' -axis a distance w'_0 and w''_0 , places the fields at their respective local origins. Before this final result is derived a few preliminary definitions are required.

There exists a certain degree of freedom in choosing the characteristic angle of the reflected local coordinate system Θ_r . The angle Θ_r could, in principle, be any angle. However, defining $\Theta_r = \Theta_i$ intuitively makes sense based on the spherical component relations of the generalized laws of reflection given in Eq. (3.1.111c). The associated angles of the reflected propagation and attenuation vectors of any reflected inhomogeneous plane wave field are equal to that of the corresponding angles of the incident propagation and attenuation vectors. In particular, the angular relationship for the attenuation vector yields $\theta_r^\alpha = \theta_i^\alpha$. Since the incident local coordinate system was defined to have the \hat{w} -axis aligned with the incident attenuation vector, aligning the reflected \hat{w}' -axis along the reflected attenuation vector achieves a consistent relationship. Therefore, $\Theta_r = \Theta_i$ will be assumed throughout all subsequent analysis.

As a result of the generalized laws of reflection given in Eqs. (3.1.111a–c), the complex wavevector of the reflected field relates to the complex wavevector of the incident field within the interface coordinate system as [cf. Eq. (3.1.76)]

$$\tilde{\mathbf{k}}_r(\omega) = \begin{bmatrix} \tilde{k}_{r_x}(\omega) \\ \beta_{r_y} \\ \tilde{k}_{r_z}(\omega) \end{bmatrix} = \begin{bmatrix} 1 & 0 & 0 \\ 0 & 1 & 0 \\ 0 & 0 & -1 \end{bmatrix} \begin{bmatrix} \tilde{k}_{i_x}(\omega) \\ \beta_{i_y} \\ \tilde{k}_{i_z}(\omega) \end{bmatrix},$$

where the $\hat{\nu}$ component is pure real and not a function of frequency. The reflected complex wavevector transforms into the reflected local coordinate system through multiplication of the inverse transformation matrix $\tilde{\mathbf{R}}_{ot_r}^T$ as

$$\tilde{\mathbf{k}}_r(\omega) = \begin{bmatrix} \tilde{k}_{r_u}(\omega) \\ \beta_{r_v} \\ \tilde{k}_{r_w}(\omega) \end{bmatrix} = \tilde{\mathbf{R}}_{ot_r}^T \cdot \begin{bmatrix} 1 & 0 & 0 \\ 0 & 1 & 0 \\ 0 & 0 & -1 \end{bmatrix} \begin{bmatrix} \tilde{k}_{i_x}(\omega) \\ \beta_{i_y} \\ \tilde{k}_{i_z}(\omega) \end{bmatrix}.$$

Substitution of Eqs. (3.1.25) and (3.1.27) into this equation defines the reflected complex wavevector in terms of the given wavenumbers k_u and k_v ,

$$\tilde{\mathbf{k}}_r(\omega) = \tilde{\mathbf{R}}_{ot_r}^T \begin{bmatrix} 1 & 0 & 0 \\ 0 & 1 & 0 \\ 0 & 0 & -1 \end{bmatrix} \tilde{\mathbf{R}}_{ot_i} \begin{bmatrix} k_u \\ k_v \\ \gamma_i(\omega) \end{bmatrix},$$

where the complex wavenumber $\gamma_i(\omega)$ is a function of k_u and k_v as defined in Eq. (3.1.8a). The matrix multiplication is then achieved using Eqs. (3.1.23) and (3.1.58) and the fact that $\Theta_r = \Theta_i$ which results in an expression for the reflected complex wavevector within the reflected local coordinate system in terms of the given wavenumbers k_u and k_v , viz.

$$\tilde{\mathbf{k}}_r(\omega) = \begin{bmatrix} \tilde{k}_{r_u}(\omega) \\ \beta_{r_v} \\ \tilde{k}_{r_w}(\omega) \end{bmatrix} = \begin{bmatrix} -k_u \\ k_v \\ \gamma_i(\omega) \end{bmatrix}. \quad (3.2.1)$$

There also exists a certain degree of freedom in choosing the characteristic angle of the transmitted local coordinate system Θ_t . The angle Θ_t could, also be any angle. However, let the angle of the transmitted local coordinate system Θ_t be the angle $\Theta_t = \theta_t^a|_{k_u=k_v=0}$, i.e. the refracted angle of the attenuation vector for an incident homogeneous plane wave.

As a result of the generalized law of refraction given in Eqs. (3.1.112a–c), the refracted field's complex wavevector relates to the incident field's complex wavevector within the interface coordinate system as [cf. Eq. (3.1.77)]

$$\tilde{\mathbf{k}}_t(\omega) = \begin{bmatrix} \tilde{k}_{t_r}(\omega) \\ \beta_{t_v} \\ \tilde{k}_{t_n}(\omega) \end{bmatrix} = \begin{bmatrix} \tilde{k}_{i_r}(\omega) \\ \beta_{i_v} \\ \left[\tilde{k}_2(\omega) - \tilde{k}_{i_r}(\omega) - \beta_{i_v}^2 \right]^{1/2} \end{bmatrix},$$

notice that the \hat{v} component is pure real and not a function of frequency. The transmitted complex wavevector transforms into the transmitted local coordinate system through multiplication of the inverse transformation matrix $\tilde{\mathbf{R}}_{ot_t}^T$ as

$$\tilde{\mathbf{k}}_t(\omega) = \begin{bmatrix} \tilde{k}_{t_{u''}}(\omega) \\ \beta_{t_{v''}} \\ \tilde{k}_{t_{w''}}(\omega) \end{bmatrix} = \tilde{\mathbf{R}}_{ot_t}^T \begin{bmatrix} \tilde{k}_{i_r}(\omega) \\ \beta_{i_v} \\ \left[\tilde{k}_2(\omega) - \tilde{k}_{i_r}(\omega) - \beta_{i_v}^2 \right]^{1/2} \end{bmatrix}.$$

Use of the defining Eqs. (3.1.25) and (3.1.27) puts the transmitted complex wavevector in terms of the given wavenumbers k_u and k_v

$$\tilde{\mathbf{k}}_t(\omega) = \begin{bmatrix} \tilde{k}_{t_{u''}}(\omega) \\ \beta_{t_{v''}} \\ \tilde{k}_{t_{w''}}(\omega) \end{bmatrix} = \tilde{\mathbf{R}}_{ot_t}^T \begin{bmatrix} k_u \cos \Theta_i + \gamma_i(\omega) \sin \Theta_i \\ k_v \\ \left[\tilde{k}_2(\omega) - (k_u \cos \Theta_i + \gamma_i(\omega) \sin \Theta_i)^2 - k_v^2 \right]^{1/2} \end{bmatrix},$$

where the complex wavenumber $\gamma_i(\omega)$ is a function of k_u and k_v as defined in Eq. (3.1.8a).

Substituting the definition of $\tilde{\mathbf{R}}_{ot_t}^T$ given in Eq. (3.1.58) results in an expression for the transmitted complex wavevector within the transmitted local coordinate system in terms of the given wavenumbers k_u and k_v , viz.

$$\tilde{\mathbf{k}}_t(\omega) = \begin{bmatrix} \tilde{k}_{t_u}(\omega) \\ \beta_{t_v} \\ \tilde{k}_{t_w}(\omega) \end{bmatrix} \quad (3.2.2)$$

$$= \begin{bmatrix} \cos \Theta_t & 0 & -\sin \Theta_t \\ 0 & 1 & 0 \\ \sin \Theta_t & 0 & \cos \Theta_t \end{bmatrix} \begin{bmatrix} k_u \cos \Theta_i + \gamma_i(\omega) \sin \Theta_i \\ k_v \\ \left[k_2^2(\omega) - (k_u \cos \Theta_i + \gamma_i(\omega) \sin \Theta_i)^2 - k_v^2 \right]^{1/2} \end{bmatrix} .$$

The normal component of the reflected electric field vector can be expressed in matrix form in terms of the two tangential components within the interface coordinate system as a result of the transversality condition given in Eq. (2.5.25) [cf. Eq. (3.1.113)], viz.

$$\mathbf{E}_{r_n}(\omega) = -\frac{1}{\tilde{k}_{r_n}(\omega)} \begin{bmatrix} \tilde{k}_{r_t}(\omega) & \beta_{r_v} \end{bmatrix} \begin{bmatrix} E_{r_t}(\omega) \\ E_{r_v}(\omega) \end{bmatrix} .$$

The generalized laws of reflection given in Eqs. (3.1.111a–c) determine that

$$\mathbf{E}_{r_n}(\omega) = \frac{1}{\tilde{k}_{i_n}(\omega)} \begin{bmatrix} \tilde{k}_{i_t}(\omega) & \beta_{i_v} \end{bmatrix} \mathbf{E}_{r_{tan}}(\omega) ,$$

where $\mathbf{E}_{r_{tan}}(\omega) \equiv \begin{bmatrix} E_{r_t}(\omega) \\ E_{r_v}(\omega) \end{bmatrix}$. The generalized *Fresnel* equations relate $\mathbf{E}_{r_{tan}}(\omega)$ to $\mathbf{E}_{i_{tan}}(\omega)$

in Eq. (3.1.128) via the tangential reflection matrix $\vec{\mathbf{r}}$ given in Eq. (3.1.130) so that

$$\mathbf{E}_{r_n}(\omega) = \frac{1}{\tilde{k}_{i_n}(\omega)} \begin{bmatrix} \tilde{k}_{i_t}(\omega) & \beta_{i_v} \end{bmatrix} \vec{\mathbf{r}} \mathbf{E}_{i_{tan}}(\omega) . \quad (3.2.3)$$

By combining this result with that of Eq. (3.1.128), the reflected electric field vector relates to the incident electric field vector within the interface coordinate system by

$$\mathbf{E}_r(\omega) = \vec{\mathbf{R}}' \mathbf{E}_i(\omega) , \quad (3.2.4)$$

where the *intermediate reflection matrix* $\vec{\mathbf{R}}'$ is defined as

$$\vec{\mathbf{R}}' \equiv \begin{bmatrix} r_{\tau\tau} & r_{\tau\nu} & 0 \\ r_{\nu\tau} & r_{\nu\nu} & 0 \\ \frac{\tilde{k}_{i\tau}(\omega)r_{\tau\tau} + \beta_{i\nu}r_{\nu\tau}}{\tilde{k}_{i_n}(\omega)} & \frac{\tilde{k}_{i\tau}(\omega)r_{\tau\nu} + \beta_{i\nu}r_{\nu\nu}}{\tilde{k}_{i_n}(\omega)} & 0 \end{bmatrix}, \quad (3.2.5)$$

and $r_{\tau\tau}$, $r_{\tau\nu}$, $r_{\nu\tau}$ and $r_{\nu\nu}$ are the elements of the tangential reflection matrix $\vec{\mathbf{r}}$. All of the elements of $\vec{\mathbf{R}}'$ are defined in terms of the transverse wavenumbers k_u and k_v from Eqs. (3.1.25), (3.1.27) and (3.1.112b). Due to the dependence of the normal incident electric field component on the tangential components, only the tangential components effect Eq. (3.2.4).

The reflected field is defined within the reflected local coordinate system as [cf Eq. (3.1.49a)]

$$\mathbf{E}_r(\mathbf{r}_r, \omega) = \mathbf{E}_r(\omega) e^{+i\tilde{\mathbf{k}}_r(\omega) \cdot \mathbf{r}_r},$$

where the reflected complex wavevector $\tilde{\mathbf{k}}_r(\omega)$ is given in Eq. (3.2.1). Reverse propagating the reflected electric field from the local origin towards the interface along the $\hat{\mathbf{w}}'$ -axis for a distance $-w'_0$ yields an expression for the reflected electric field vector at the interface origin within the reflected local coordinate system, viz.

$$\mathbf{E}_r(\omega) e^{-iy_i(\omega)w'_0}. \quad (3.2.6)$$

An alternate expression for the reflected electric field vector at the interface within the reflected local coordinate system can be written in terms of the incident electric field vector. The incident electric field is defined within the incident local coordinate system as [cf Eq. (3.1.4a)]

$$\mathbf{E}_i(\mathbf{r}_i, \omega) = \mathbf{E}_i(\omega) e^{+i\tilde{\mathbf{k}}_i(\omega) \cdot \mathbf{r}_i}.$$

Propagating the incident electric field along the $\hat{\mathbf{w}}$ -axis for a distance w_0 gives the incident electric field vector at the interface origin

$$\mathbf{E}_i(\omega) e^{iy_i(\omega)w_0}.$$

Multiplying this incident electric field vector by the transformation matrix $\vec{\vec{R}}_{ot_i}$ defines the incident field vector at the interface origin within the interface coordinate system, viz.

$$\vec{\vec{R}}_{ot_i} \mathbf{E}_i(\omega) e^{i\gamma_i(\omega)w_0} . \quad (3.2.7)$$

Multiplying the field vector by the intermediate reflection matrix $\vec{\vec{R}}'$ defines the reflected electric field vector at the interface origin within the interface coordinate system, viz.

$$\vec{\vec{R}}' \vec{\vec{R}}_{ot_i} \mathbf{E}_i(\omega) e^{i\gamma_i(\omega)w_0} .$$

Multiplying the reflected electric field vector by the inverse transformation matrix $\vec{\vec{R}}_{ot_r}^T$ defines the reflected electric field vector at the interface origin within the reflected local coordinate system, viz.

$$\vec{\vec{R}} \mathbf{E}_i(\omega) e^{i\gamma_i(\omega)w_0} , \quad (3.2.8)$$

where the *reflection matrix* $\vec{\vec{R}}$ is defined as

$$\vec{\vec{R}} \equiv \vec{\vec{R}}_{ot_r}^T \vec{\vec{R}}' \vec{\vec{R}}_{ot_i} . \quad (3.2.9)$$

Equating the two different expressions for the reflected electric field vector at the interface within the transmitted local coordinate system given in Eqs. (3.2.6) and (3.2.8) and solving for the quantity $\mathbf{E}_r(\omega)$ results in

$$\mathbf{E}_r(\omega) = \vec{\vec{R}} \mathbf{E}_i(\omega) e^{i\gamma_i(\omega)(w_0+w'_0)} . \quad (3.2.10)$$

Consequently, the reflected electric and magnetic fields can be defined in terms of the known incident electric field vector and the transverse wavenumbers k_u and k_v within the reflected local coordinate system. Substituting Eq. (3.2.10) into Eq. (3.1.49a) yields

$$\mathbf{E}_r(\mathbf{r}_r, \omega) = \vec{\vec{R}} \mathbf{E}_i(\omega) e^{i\gamma_i(\omega)(w_0+w'_0)} e^{+i\vec{k}_r(\omega) \cdot \mathbf{r}_r} , \quad (3.2.11a)$$

and substituting Eq. (3.2.11a) into the transversality condition given in Eq. (2.5.24) yields

$$\mathbf{H}_r(\mathbf{r}_r, \omega) = \frac{\|c\|}{\mu\omega} \vec{k}_r(\omega) \times \vec{\vec{R}} \mathbf{E}_i(\omega) e^{i\gamma_i(\omega)(w_0+w'_0)} e^{+i\vec{k}_r(\omega) \cdot \mathbf{r}_r} , \quad (3.2.11b)$$

where the reflection matrix $\vec{\vec{R}}$ is defined in Eq. (3.2.9), the reflected complex wavevector

$\tilde{\mathbf{k}}_r(\omega)$ is defined in Eq. (3.2.1) and the position vector \mathbf{r}_r is defined in the reflected local coordinate system.

The normal component of the transmitted electric field vector can be expressed in matrix form in terms of the two tangential components within the interface coordinate system as a result of the transversality condition given in Eq. (2.5.25) [cf. Eq. (3.1.113)]

$$E_{t_n}(\omega) = -\frac{1}{\tilde{k}_{t_n}(\omega)} \begin{bmatrix} \tilde{k}_{t_\tau}(\omega) & \beta_{t_\nu} \end{bmatrix} \begin{bmatrix} E_{t_\tau}(\omega) \\ E_{t_\nu}(\omega) \end{bmatrix}.$$

The generalized laws of refraction given in Eqs. (3.1.112a–c) determine that

$$E_{t_n}(\omega) = -\frac{1}{\tilde{k}_{t_n}(\omega)} \begin{bmatrix} \tilde{k}_{i_\tau}(\omega) & \beta_{i_\nu} \end{bmatrix} \mathbf{E}_{t_{tan}}(\omega),$$

where $\mathbf{E}_{t_{tan}}(\omega) \equiv \begin{bmatrix} E_{t_\tau}(\omega) \\ E_{t_\nu}(\omega) \end{bmatrix}$. The generalized *Fresnel* equations relate $\mathbf{E}_{t_{tan}}(\omega)$ to $\mathbf{E}_{i_{tan}}(\omega)$

in Eq. (3.1.133) via the tangential transmission matrix $\vec{\mathbf{t}}$ given in Eq. (3.1.135) so that

$$E_{t_n}(\omega) = \frac{1}{\tilde{k}_{t_n}(\omega)} \begin{bmatrix} \tilde{k}_{i_\tau}(\omega) & \beta_{i_\nu} \end{bmatrix} \vec{\mathbf{t}} \mathbf{E}_{i_{tan}}(\omega). \quad (3.2.12)$$

By combining this result with that of Eq. (3.1.133), the transmitted electric field vector relates to the incident electric field vector within the interface coordinate system by

$$\mathbf{E}_r(\omega) = \vec{\mathbf{T}}' \mathbf{E}_i(\omega), \quad (3.2.13)$$

where the *intermediate transmission matrix* $\vec{\mathbf{T}}'$ is defined as

$$\vec{\mathbf{T}}' \equiv \begin{bmatrix} t_{\tau_\tau} & t_{\tau_\nu} & 0 \\ t_{\nu_\tau} & t_{\nu_\nu} & 0 \\ \frac{\tilde{k}_{i_\tau}(\omega)t_{\tau_\tau} + \beta_{i_\nu}t_{\nu_\tau}}{\tilde{k}_{t_n}(\omega)} & \frac{\tilde{k}_{i_\tau}(\omega)t_{\tau_\nu} + \beta_{i_\nu}t_{\nu_\nu}}{\tilde{k}_{t_n}(\omega)} & 0 \end{bmatrix}, \quad (3.2.14)$$

and t_{τ_τ} , t_{τ_ν} , t_{ν_τ} and t_{ν_ν} are the elements of the tangential reflection matrix $\vec{\mathbf{t}}$. All of the elements of $\vec{\mathbf{T}}'$ are defined in terms of the transverse wavenumbers k_u and k_ν from Eqs. (3.1.25),

(3.1.27) and (3.1.112b). Due to the dependence of the normal incident electric field component on the tangential components, only the tangential components effect Eq. (3.2.13).

The transmitted field is defined within the transmitted local coordinate system as [cf. Eq. (3.1.50a)]

$$\mathbf{E}_t(\mathbf{r}_t, \omega) = \mathbf{E}_t(\omega) e^{+i\tilde{\mathbf{k}}_t(\omega) \cdot \mathbf{r}_t} ,$$

where the transmitted complex wavevector $\tilde{\mathbf{k}}_t(\omega)$ is given in Eq. (3.2.2). Reverse propagating the transmitted electric field from the local origin towards the interface along the $\hat{\mathbf{w}}''$ -axis for a distance $-w_0''$ yields an expression for the reflected electric field vector at the interface origin within the reflected local coordinate system, viz.

$$\mathbf{E}_t(\omega) e^{-i\tilde{\mathbf{k}}_t''(\omega) w_0''} . \quad (3.2.15)$$

An alternate expression for the transmitted electric field vector at the interface within the transmitted local coordinate system can be written in terms of the incident electric field vector. The incident electric field vector at the interface origin within the interface coordinate system is given in Eq. (3.2.7). Multiplying this incident electric field vector by the intermediate transmission matrix $\vec{\mathbf{T}}'$ defines the transmitted electric field vector at the interface origin within the interface coordinate system, viz.

$$\vec{\mathbf{T}}' \vec{\mathbf{R}}_{ot_i} \mathbf{E}_i(\omega) e^{i\gamma_i(\omega) w_0} .$$

Multiplying the transmitted electric field vector by the inverse transformation matrix $\vec{\mathbf{R}}_{ot_t}^T$ defines the transmitted electric field vector at the interface origin within the transmitted local coordinate system, viz.

$$\vec{\mathbf{T}} \mathbf{E}_i(\omega) e^{i\gamma_i(\omega) w_0} , \quad (3.2.16)$$

where the *transmission matrix* $\vec{\mathbf{T}}$ is defined as

$$\vec{\mathbf{T}} \equiv \vec{\mathbf{R}}_{ot_t}^T \vec{\mathbf{T}}' \vec{\mathbf{R}}_{ot_i} . \quad (3.2.17)$$

Equating the two different expressions for the transmitted electric field vector at the interface within the transmitted local coordinate system given in Eqs. (3.2.15) and (3.2.16) and solving for the quantity $E_t(\omega)$ results in

$$E_t(\omega) = \vec{T} E_i(\omega) e^{i\gamma_t(\omega)w_0} e^{i\vec{k}_t(\omega)w_0} . \quad (3.2.18)$$

Consequently, the transmitted electric and magnetic fields can be defined in terms of the known incident electric field vector and the transverse wavenumbers k_u and k_v within the transmitted local coordinate system. Substitution of Eq. (3.2.18) into Eq. (3.1.50a) yields

$$E_t(\mathbf{r}_t, \omega) = \vec{T} E_i(\omega) e^{i\gamma_t(\omega)w_0} e^{i\vec{k}_t(\omega)w_0} e^{i\vec{k}_t(\omega) \cdot \mathbf{r}_t} . \quad (3.2.19a)$$

Substitution of Eq. (3.2.19a) into the transversality condition given in Eq. (2.5.24) yields

$$H_t(\mathbf{r}_t, \omega) = \frac{\|c\|}{\mu\omega} \vec{k}_t(\omega) \times \vec{T} E_i(\omega) e^{i\gamma_t(\omega)w_0} e^{i\vec{k}_t(\omega)w_0} e^{i\vec{k}_t(\omega) \cdot \mathbf{r}_t} , \quad (3.2.19b)$$

where the transmission matrix \vec{T} is defined in Eq. (3.2.14), the transmitted complex wave-vector $\vec{k}_t(\omega)$ is defined in Eq. (3.2.2) and the position vector \mathbf{r}_t is defined in the transmitted local coordinate system.

3.3 Pulsed Electromagnetic Inhomogeneous Plane Waves Incident Upon a Planar Interface Separating Two Lossy, Dispersive Dielectric Half-Spaces

The results presented here are concise integral expressions that describe pulsed electromagnetic inhomogeneous plane waves incident upon a planar interface separating two lossy, dispersive dielectric half-spaces. These results are the sum of all the previous work and are quite significant. They are achieved by simply applying the inverse *Fourier–Laplace* transform to the final results of §3.2.

The inverse *Fourier–Laplace* transform, as defined in Eq. (2.1.1b), of Eqs. (3.2.11a,b) yields the reflected fields as

$$\mathfrak{E}_r(\mathbf{r}_r, t) = \frac{1}{2\pi} \int_{C_\omega} \vec{R} E_i(\omega) e^{i\gamma_r(\omega)(w_0 + w_0)} e^{-i\omega t} e^{i\vec{k}_r(\omega) \cdot \mathbf{r}_r} d\omega, \quad (3.3.1a)$$

and

$$\mathfrak{H}_r(\mathbf{r}_r, t) = \frac{\|c\|}{\mu\omega} \frac{1}{2\pi} \int_{C_\omega} \tilde{\mathbf{k}}_r(\omega) \times \vec{\mathbf{R}} E_i(\omega) e^{i\gamma_i(\omega)(w_0+w'_0)} e^{-i\omega t} e^{i\tilde{\mathbf{k}}_r(\omega) \cdot \mathbf{r}_r} d\omega, \quad (3.3.1b)$$

where $\vec{\mathbf{R}}$ is defined in Eq. (3.2.9) and \mathbf{r}_r is the position vector defined in the reflected local coordinate system.

The inverse *Fourier–Laplace* transform of Eqs. (3.2.19a,b) yields the transmitted fields as

$$\mathfrak{S}_t(\mathbf{r}_t, t) = \frac{1}{2\pi} \int_{C_\omega} \vec{\mathbf{T}} E_i(\omega) e^{i\gamma_i(\omega)w_0} e^{i\tilde{\mathbf{k}}_t(\omega)w'_0} e^{-i\omega t} e^{i\tilde{\mathbf{k}}_t(\omega) \cdot \mathbf{r}_t} d\omega, \quad (3.3.2a)$$

and

$$\mathfrak{H}_t(\mathbf{r}_t, t) = \frac{\|c\|}{\mu\omega} \frac{1}{2\pi} \int_{C_\omega} \tilde{\mathbf{k}}_t(\omega) \times \vec{\mathbf{T}} E_i(\omega) e^{i\gamma_i(\omega)w_0} e^{i\tilde{\mathbf{k}}_t(\omega)w'_0} e^{-i\omega t} e^{i\tilde{\mathbf{k}}_t(\omega) \cdot \mathbf{r}_t} d\omega, \quad (3.3.2b)$$

where $\vec{\mathbf{T}}$ is defined in Eq. (3.2.17) and \mathbf{r}_t is the position vector defined in the transmitted local coordinate system.

If the temporal conditions of the incident field $\mathfrak{S}_i(\mathbf{r}_i, t)$ permit the use of a *Fourier* transform, then the contour of integration C_ω in Eqs. (3.3.1a,b) and (3.3.2a,b), denotes the straight line path along the real axis in the complex ω –plane. However, if the temporal conditions of the incident field $\mathfrak{S}_i(\mathbf{r}_i, t)$ require the use of a *Laplace* transform then the contour C_ω is the *Bromwich contour* which is the straight line path given by $\omega = \omega' + ia$, with a being a real constant that resides within the region of convergence and where $\omega' \equiv \text{Re}(\omega)$ ranges from negative to positive infinity.

CHAPTER IV

Reflection of Linearly Polarized TM Plane Waves Incident Upon a Planar Interface Separating Two Lossy, Dispersive Dielectrics

The results from §3.1.4 are now applied to TM polarized homogeneous and inhomogeneous plane waves incident upon a planar interface separating two lossy, dispersive dielectrics. A double resonance Lorentz model describes the two dielectric media.

4.1 Double Resonance Lorentz Models of the Two Lossy, Dispersive Dielectric Media

The double resonance Lorentz model equation that describes two different media types is given by [cf. Eq. (2.3.10)]

$$\tilde{n}_j(\omega) = \sqrt{\frac{\tilde{\varepsilon}(\omega)}{\varepsilon_0}} = \sqrt{\varepsilon_{j_\infty} - \sum_{l=0,2} \frac{b_{j_l}^2}{\omega^2 - \omega_{j_l}^2 + 2i\delta_{j_l}\omega}} \quad (4.1.1)$$

where the index j denotes the media type ($j = 1$ for the medium of incidence and $j = 2$ for the medium of transmittance). For each of the numerical examples considered here, Eq. (4.1.1) is used to characterize the complex refractive index of each medium separated by the planar interface. Two different types of relations between the two materials are considered here.

The first type has equal-valued double resonance Lorentz parameters for the both the medium of incidence (medium 1) and medium of transmittance (medium 2), with the exception of the ε_{j_∞} parameter. By choice, $\varepsilon_{1_\infty} > \varepsilon_{2_\infty}$, so that the real parts of the complex refractive indices make an optically dense to rare transition when going from the medium of incidence to the medium of transmittance at any given angular frequency. In effect, the real and imaginary parts of the complex refractive index of the medium of incidence are vertically displaced, although not uniformly, relative to the those of the medium of transmittance. This means that $\Re\{\tilde{n}_1(\omega)\} > \Re\{\tilde{n}_2(\omega)\}$ and $\Im\{\tilde{n}_1(\omega)\} < \Im\{\tilde{n}_2(\omega)\}$ for all ω . The benefit of this choice of double resonance Lorentz parameters is that the more complicated effects of overlapping real and imaginary parts within the anomalous dispersion regions are eliminated and are reserved exclusively for the other interface type considered here. The double resonance Lorentz model parameters chosen for this interface type are based on those presented in

Table 2.3.1 and are tabulated here in Table 4.1.1. The frequency dispersion for these two similar media are illustrated in Figure 4.1.1.

The second type has dissimilar Lorentz parameters for the both the medium of incidence and the medium of transmittance. Again, by choice, $\varepsilon_{1_\infty} > \varepsilon_{2_\infty}$, so that the real parts of the complex refractive indices make an optically dense to rare transition in those spectral regions that are removed from any medium resonances, i.e. in the regions of normal dispersion. However, within and about the regions of anomalous dispersion, the real parts of the complex refractive indices are inverted to make an optically rare to dense transition. The double resonance Lorentz model parameters chosen for this interface type resemble those presented in Table 2.3.1 and are tabulated in Table 4.1.2. The frequency dispersion for these two dissimilar media are illustrated in Figure 4.1.2.

4.2 The Transmitted Complex Wavevector

The behavior of the angle θ_t^α , the normal component $\tilde{k}_{t_n}(\omega)$ and its square $\tilde{k}_{t_n}^2(\omega)$ of the transmitted complex wavevector in the complex plane reveals many unique features that provide insight into the dynamics of both the generalized law of refraction and the generalized *Fresnel* equations. For simplicity, the normal component $\tilde{k}_{t_n}(\omega)$ of the transmitted complex wavevector will be referred to as the *transmitted normal complex wavenumber*.

The behavior of the square of the transmitted normal complex wavenumber in the complex plane is considered first. The quantity $\tilde{k}_{t_n}^2(\omega)$ within the interface coordinate system is given by the generalized law of refraction given in Eq. (3.1.112b) as

$$\tilde{k}_{t_n}^2(\omega) = \tilde{k}_2^2(\omega) - \left(\beta_{i_r}(\omega) + i\alpha_{i_r}(\omega) \right)^2 - \beta_{i_v}^2. \quad (4.2.1)$$

Two critical values of $\tilde{k}_{t_n}^2(\omega)$ occur: one when $\Re \left\{ \tilde{k}_{t_n}^2(\omega) \right\} = 0$ and the other when

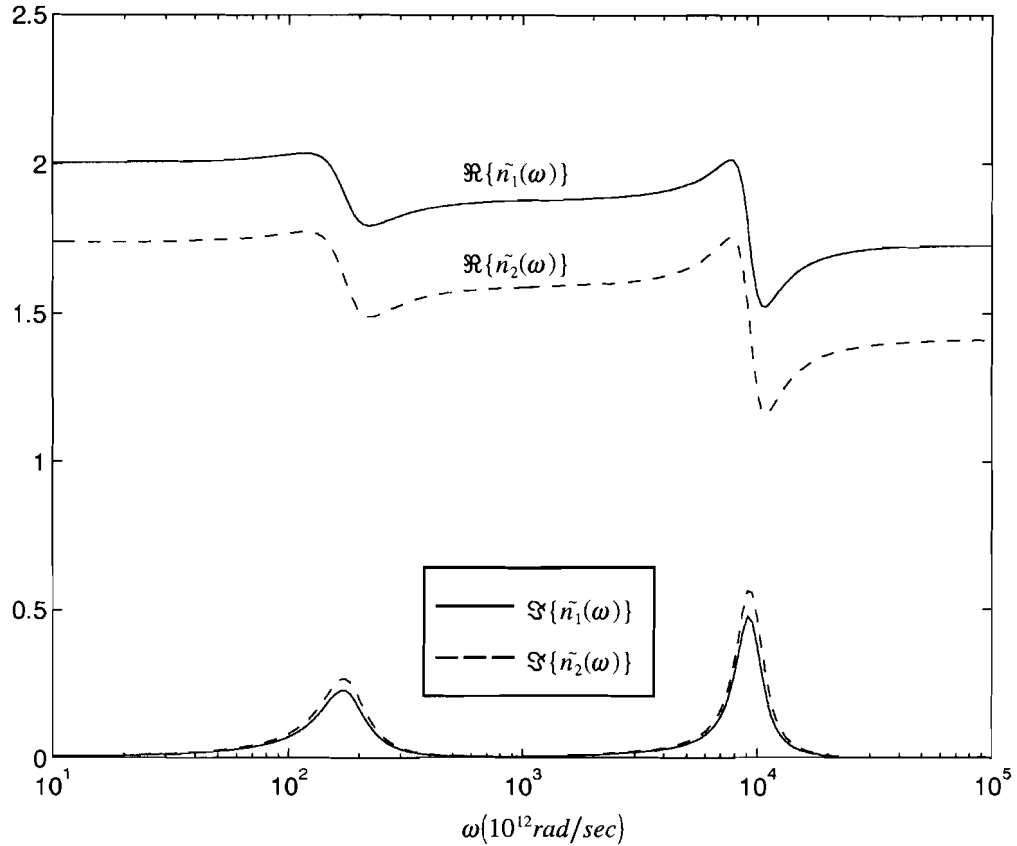


Figure 4.1.1 The complex refractive index for both the medium of incidence (solid lines) and the medium of transmittance (dashed lines) using the double resonance Lorentz model with parameters taken from Table 4.1.1.

| Medium Type | Double Resonance Lorentz Model Parameters | | | | |
|------------------------------------|---|----------------------|--|-----------------------------------|--|
| | $\epsilon_{j\infty}$ | Resonance Number l | ω_{j_l} ($10^{14}rad/sec$) | b_{j_l} ($10^{14}rad/sec$) | δ_{j_l} ($10^{13}rad/sec$) |
| medium of incidence $j = 1$ | 2.9938 | 0 | 1.7412 | 1.2155 | 4.9555 |
| | | 2 | 91.448 | 67.198 | 143.41 |
| medium of transmittance $j = 2$ | 1.9938 | 0 | 1.7412 | 1.2155 | 4.9555 |
| | | 2 | 91.448 | 67.198 | 143.41 |

Table 4.1.1 Double resonance Lorentz model parameters of the two media separated by an interface where the only difference lies in the choice of the parameter $\epsilon_{j\infty}$.

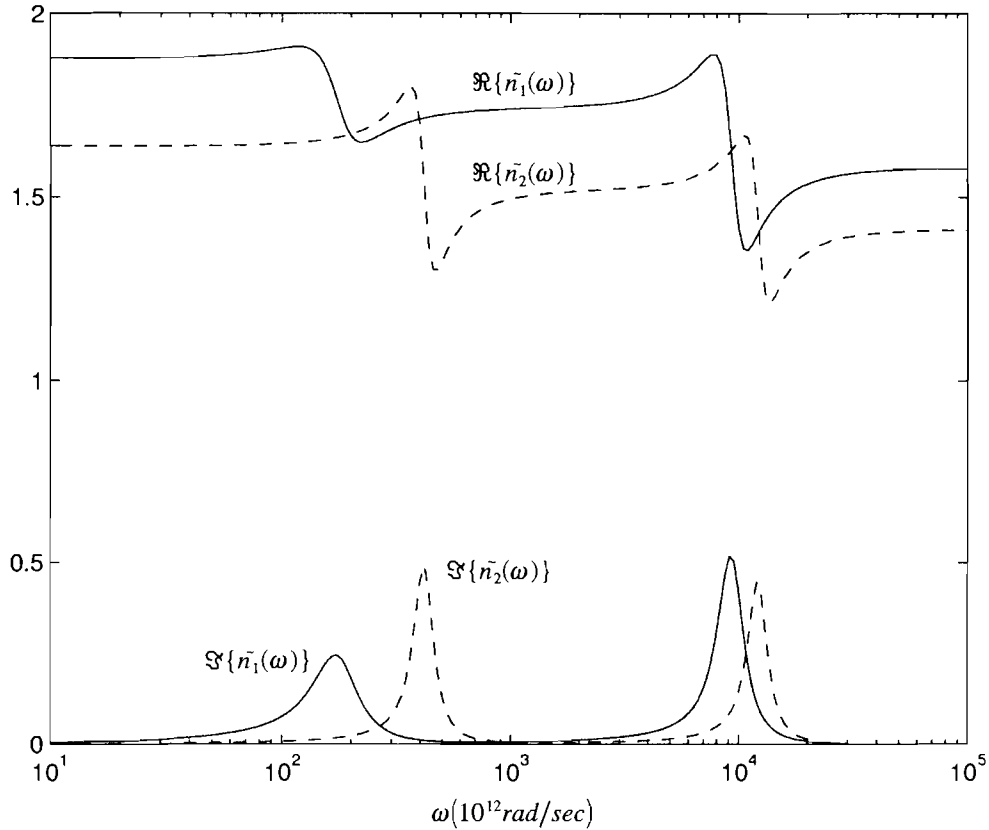


Figure 4.1.2 The complex refractive index for both the medium of incidence (solid lines) and the medium of transmittance (dashed lines) using the double resonance Lorentz model with parameters taken from Table 4.1.2.

| Medium Type | Double Resonance Lorentz Model Parameters | | | | |
|------------------------------------|---|----------------------|--|-----------------------------------|--|
| | $\epsilon_{j\infty}$ | Resonance Number l | ω_{j_l} ($10^{14}rad/sec$) | b_{j_l} ($10^{14}rad/sec$) | δ_{j_l} ($10^{13}rad/sec$) |
| medium of incidence $j = 1$ | 2.4938 | 0 | 1.7412 | 1.2155 | 4.9555 |
| | | 2 | 91.448 | 67.198 | 143.41 |
| medium of transmittance $j = 2$ | 1.9938 | 0 | 4.1000 | 2.5155 | 4.9555 |
| | | 2 | 120.00 | 67.198 | 143.41 |

Table 4.1.2 Double resonance Lorentz model parameters of the two media separated by an interface where the behavior of the real part of the complex refractive index switches from the normal optically dense to rare transition to optically rare to dense transition within the anomalous dispersion regions.

$\Im\left\{\tilde{k}_{t_n}^{-2}(\omega)\right\} = 0$. These two critical values influence the behavior of both the generalized law of refraction and the generalized *Fresnel* equations.

The transmitted normal complex wavenumber $\tilde{k}_{t_n}(\omega)$ in the complex plane is then considered. A branch cut in the complex plane of $\tilde{k}_{t_n}^{-2}(\omega)$ is chosen as the negative real axis [cf. §3.1.2]. The quantity $\tilde{k}_{t_n}(\omega)$ is primarily propagative when $\Re\left\{\tilde{k}_{t_n}^{-2}(\omega)\right\} > 0$ and becomes primarily attenuative when $\Re\left\{\tilde{k}_{t_n}^{-2}(\omega)\right\} < 0$. Also, when $\Im\left\{\tilde{k}_{t_n}^{-2}(\omega)\right\} < 0$ the field exponentially grows in the direction normal to the interface in the medium of transmittance and is referred to as a leaky surface wave under certain conditions.

4.2.1 The Asymptotic Behavior of the Normal Component and the Angle of the Transmitted Complex Wavevector

Let the asymptotic behavior of $\tilde{k}_{t_n}(\omega)$, $\tilde{k}_{t_n}^{-2}(\omega)$ and θ_t^a be examined for a case when $|k_u|$ approaches infinity while $k_v = 0$. The asymptotic values given in this section are used to determine the asymptotes which provide valuable insight into the general functional behavior of the normal component of the transmitted complex wavevector. Bearing in mind that when $\Theta_i > 0$, the transverse wavenumber k_u reaches a positive limit $k_{u_{max}}$. The values $k_u > k_{u_{max}}$ are ignored for a practical problem since no time averaged power is incident upon the interface for this situation [cf. §3.1]. However, the asymptotes still provide valuable information so that k_u is allowed to go to positive infinity in order to obtain these asymptotes.

The incident field is assumed to be an inhomogeneous plane wave whose transverse wavenumber k_u varies over the domain $-\infty < k_u < \infty$ while $k_v = 0$ and the angle of the incident local coordinate system Θ_i is fixed. The longitudinal component $\gamma_i(\omega)$ of the complex wavevector within the incident local coordinate system is given by [cf. Eq. (3.1.8a)]

$$\gamma_i(\omega) = \left(\tilde{k}_1^2(\omega) - k_u^2 \right)^{1/2}. \quad (4.2.2)$$

Under the transformations defined in Eqs. (3.1.25) and (3.1.27), the incident components of the complex wavevector may be expressed in the interface coordinate system in matrix form as

$$\boldsymbol{\beta}_i(\omega) = \begin{bmatrix} \beta_{i_r}(\omega) \\ \beta_{i_v} \\ \beta_{i_n}(\omega) \end{bmatrix} = \begin{bmatrix} k_u \cos \Theta_i + \Re\{\gamma_i(\omega)\} \sin \Theta_i \\ 0 \\ -k_u \sin \Theta_i + \Re\{\gamma_i(\omega)\} \cos \Theta_i \end{bmatrix}, \quad (4.2.3a)$$

and

$$\boldsymbol{\alpha}_i(\omega) = \begin{bmatrix} \alpha_{i_r}(\omega) \\ \alpha_{i_v} \\ \alpha_{i_n}(\omega) \end{bmatrix} = \begin{bmatrix} \Im\{\gamma_i(\omega)\} \sin \Theta_i \\ 0 \\ \Im\{\gamma_i(\omega)\} \cos \Theta_i \end{bmatrix}. \quad (4.2.3b)$$

The in-plane tangential component $\beta_{i_r}(\omega)$ of the incident propagation vector has the simple asymptotic approximation given by [cf. Eq. (3.1.14)]

$$\beta_{i_r}(\omega) \sim k_u \cos \Theta_i, \quad k_u \rightarrow \pm \infty, k_v = 0. \quad (4.2.4)$$

Similarly, the in-plane tangential component $\alpha_{i_r}(\omega)$ of the incident attenuation vector has the simple asymptotic approximation given by

$$\alpha_{i_r}(\omega) \sim |k_u| \sin \Theta_i, \quad k_u \rightarrow \pm \infty, k_v = 0. \quad (4.2.5)$$

The square of the normal transmitted complex wavenumber given in Eq. (4.2.1) then has the asymptotic approximation

$$\begin{aligned} \tilde{k}_{i_n}^2(\omega) &= \tilde{k}_2^2(\omega) - \left(\beta_{i_r}(\omega) + i\alpha_{i_r}(\omega) \right)^2 \\ &\sim - \left(k_u \cos \Theta_i + i|k_u| \sin \Theta_i \right)^2 \\ &= -k_u^2 \cos^2 \Theta_i + |k_u|^2 \sin^2 \Theta_i - i2k_u|k_u| \sin \Theta_i \cos \Theta_i \\ &= \left(|k_u| \sin \Theta_i - ik_u \cos \Theta_i \right)^2, \quad k_u \rightarrow \pm \infty, k_v = 0, \end{aligned} \quad (4.2.6)$$

where the fact $k_u^2 = |k_u|^2$ was used to obtain the final expression. The real part of this asymptotic approximation yields

$$\Re\left\{\tilde{k}_{t_n}^2(\omega)\right\} \sim k_u^2[-\cos^2\Theta_i + \sin^2\Theta_i] \quad , \quad k_u \rightarrow \pm \infty, k_v = 0 \quad , \quad (4.2.7)$$

using the fact $k_u^2 = |k_u|^2$. This equation equals zero for an angle $\Theta_{\text{tilt}}^{k_u}$ which has an exact value of $\frac{\pi}{4}$. Based on the range of Θ_i , the quantity $\Re\left\{\tilde{k}_{t_n}^2(\omega)\right\}$ satisfies the inequalities

$$\begin{aligned} \Re\left\{\tilde{k}_{t_n}^2(\omega)\right\} &< 0 \quad ; \quad \Theta_i < \Theta_{\text{tilt}}^{k_u} \\ \Re\left\{\tilde{k}_{t_n}^2(\omega)\right\} &= 0 \quad ; \quad \Theta_i = \Theta_{\text{tilt}}^{k_u} \quad , \quad k_u \rightarrow \pm \infty, k_v = 0 \quad . \\ \Re\left\{\tilde{k}_{t_n}^2(\omega)\right\} &> 0 \quad ; \quad \Theta_i > \Theta_{\text{tilt}}^{k_u} \end{aligned} \quad (4.2.8)$$

Taking the square root of Eq. (4.2.6) using the chosen branch cut yields an asymptotic approximation of the transmitted complex wavenumber which is given by

$$\tilde{k}_{t_n}(\omega) \sim \begin{cases} |k_u| \sin\Theta_i - ik_u \cos\Theta_i & ; \quad \Theta_i > 0 \\ i|k_u| & ; \quad \Theta_i = 0 \end{cases} \quad , \quad k_u \rightarrow \pm \infty, k_v = 0 \quad , \quad (4.2.9)$$

where the special case for $\Theta_i = 0$ is necessary because the domain of the square root is along the branch cut in this situation. The imaginary part of of this expression yields the asymptotic approximation

$$\Im\left\{\tilde{k}_{t_n}(\omega)\right\} \sim \begin{cases} -k_u \cos\Theta_i & ; \quad \Theta_i > 0 \\ |k_u| & ; \quad \Theta_i = 0 \end{cases} \quad , \quad k_u \rightarrow \pm \infty, k_v = 0 \quad . \quad (4.2.10)$$

The elevation angle θ_t^α of the transmitted attenuation vector, as given in Eq. (3.1.112c), is given by

$$\theta_t^\alpha = \tan^{-1}\left\{\frac{\alpha_{i_r}(\omega)}{\Im\left\{\tilde{k}_{t_n}(\omega)\right\}}\right\} .$$

Substitution of the asymptotic approximations given in Eqs. (4.2.5) and (4.2.10) into the this expression yields the asymptotic approximation of the angle θ_t^α of the transmitted attenuation vector, viz.

$$\theta_t^\alpha \sim \tan^{-1} \left\{ -\frac{|k_u| \sin \Theta_i}{k_u \cos \Theta_i} \right\} = \begin{cases} \pi - \Theta_i & ; k_u \rightarrow +\infty \\ \Theta_i & ; k_u \rightarrow -\infty \end{cases}, k_v = 0. \quad (4.2.11)$$

4.2.2 The Transmitted Normal Complex Wavenumber, Critical Angles and the Critical Transverse Wavenumbers

There are two basic ways to present the dynamics of $\tilde{k}_{t_n}^{-2}(\omega)$ and $\bar{k}_{t_n}(\omega)$ within the complex plane. First, the incident wave is assumed to be a homogeneous plane wave whose angle of incidence Θ_i varies over the range given in Eq. (3.1.21). Second, the incident wave is assumed to be an inhomogeneous plane wave with a fixed angle of incidence Θ_i . The transverse wavenumber k_u varies over the domain $-\infty < k_u < k_{u_{max}}$ while the other transverse wavenumber is fixed at $k_v = 0$ so that the incident field can be either TE or TM.

In the first case, the incident field is assumed to be a homogeneous plane wave so that both of the transverse wavenumbers are zero, i.e. $k_u = k_v = 0$. This means that the longitudinal component $\gamma_i(\omega)$ of the complex wavevector within the incident local coordinate system is given by [cf. Eq. (3.1.8a)]

$$\gamma_i(\omega) = \tilde{k}_1(\omega). \quad (4.2.12)$$

With the use of the transformations defined in Eqs. (3.1.25) and (3.1.27), the incident complex wavevector components are given in the interface coordinate system in matrix form as

$$\boldsymbol{\beta}_i(\omega) = \begin{bmatrix} \beta_{i_r}(\omega) \\ \beta_{i_v} \\ \beta_{i_n}(\omega) \end{bmatrix} = \begin{bmatrix} \Re\{\tilde{k}_1(\omega)\} \sin \Theta_i \\ 0 \\ \Re\{\tilde{k}_1(\omega)\} \cos \Theta_i \end{bmatrix}, \quad (4.2.13a)$$

and

$$\alpha_i(\omega) = \begin{bmatrix} \alpha_{i_t}(\omega) \\ \alpha_{i_n}(\omega) \end{bmatrix} = \begin{bmatrix} \Re\{\tilde{k}_1(\omega)\} \sin \Theta_i \\ 0 \\ \Re\{\tilde{k}_1(\omega)\} \cos \Theta_i \end{bmatrix}. \quad (4.2.13b)$$

Substitution of the tangential components of the matrices given in Eqs. (4.2.13a,b) into Eq. (4.2.1) then yields

$$\tilde{k}_{i_n}^2(\omega) = \tilde{k}_2^2(\omega) - \tilde{k}_1^2(\omega) \sin^2 \Theta_i, \quad (4.2.14)$$

for any incident homogeneous plane wave. Let the complex wavenumbers be defined as [cf. Eq. (2.5.5)]

$$\tilde{k}_1(\omega) \equiv \beta_1(\omega) + i\alpha_1(\omega), \quad (4.2.15)$$

and

$$\tilde{k}_2(\omega) \equiv \beta_2(\omega) + i\alpha_2(\omega), \quad (4.2.16)$$

so that Eq. (4.2.14) becomes

$$\begin{aligned} \tilde{k}_{i_n}^2(\omega) = & \left[(\beta_2^2(\omega) - \alpha_2^2(\omega)) - (\beta_1^2(\omega) - \alpha_1^2(\omega)) \sin^2 \Theta_i \right] \\ & + 2i[\beta_2(\omega)\alpha_2(\omega) - \beta_1(\omega)\alpha_1(\omega) \sin^2 \Theta_i]. \end{aligned} \quad (4.2.17)$$

It is assumed here that the conditions $\beta_1^2(\omega) - \alpha_1^2(\omega) > 0$ and $\beta_2^2(\omega) - \alpha_2^2(\omega) > 0$ are satisfied. If not, then the glass would be highly attenuative and useless from an engineering standpoint. The real part of Eq. (4.2.17) is then positive when $\Theta_i = 0$. For $\Theta_i > 0$, the quantity $\Re\{\tilde{k}_{i_n}^2(\omega)\}$ will equal zero for some *critical angle* $\Theta_i = \Theta_C$ if the dielectric media are such that the condition

$$\beta_1^2(\omega) - \alpha_1^2(\omega) > \beta_2^2(\omega) - \alpha_2^2(\omega), \quad (4.2.18)$$

is satisfied. The critical angle Θ_C is the lossy analog of the critical angle that causes total internal reflection for supercritical angles of incidence $\Theta_i > \Theta_C$ for lossless media. If the condition given in Eq. (4.2.18) is satisfied, then the critical angle is given by

$$\Theta_C = \sin^{-1} \left\{ \sqrt{\frac{\beta_2^2(\omega) - \alpha_2^2(\omega)}{\beta_1^2(\omega) - \alpha_1^2(\omega)}} \right\}. \quad (4.2.19)$$

The quantity $\Re \left\{ \tilde{k}_{t_n}(\omega) \right\}$ then satisfies the inequalities

$$\begin{aligned} \Re \left\{ \tilde{k}_{t_n}(\omega) \right\} &< 0 \quad ; \quad \Theta_i > \Theta_C \\ \Re \left\{ \tilde{k}_{t_n}(\omega) \right\} &= 0 \quad ; \quad \Theta_i = \Theta_C . \\ \Re \left\{ \tilde{k}_{t_n}(\omega) \right\} &> 0 \quad ; \quad \Theta_i < \Theta_C \end{aligned} \quad (4.2.20)$$

Application of the results of Eq. (3.1.18) to these inequalities yields the inequalities

$$\begin{aligned} \Re \left\{ \tilde{k}_{t_n}(\omega) \right\} &< \left| \Im \left\{ \tilde{k}_{t_n}(\omega) \right\} \right| \quad ; \quad \Theta_i > \Theta_C \\ \Re \left\{ \tilde{k}_{t_n}(\omega) \right\} &= \left| \Im \left\{ \tilde{k}_{t_n}(\omega) \right\} \right| \quad ; \quad \Theta_i = \Theta_C , \\ \Re \left\{ \tilde{k}_{t_n}(\omega) \right\} &> \left| \Im \left\{ \tilde{k}_{t_n}(\omega) \right\} \right| \quad ; \quad \Theta_i < \Theta_C \end{aligned} \quad (4.2.21)$$

which imply that if $\Theta_i < \Theta_C$ then the term $\tilde{k}_{t_n}(\omega)$ is primarily a *propagative* factor. Conversely, if $\Theta_i > \Theta_C$ then the term $\tilde{k}_{t_n}(\omega)$ is primarily an *attenuative* factor.

From Eq. (2.5.7), the inequality $\beta_2(\omega)\alpha_2(\omega) > 0$ is always satisfied for $\omega > 0$ so that the imaginary part of Eq. (4.2.17) is positive when $\Theta_i = 0$. For $\Theta_i > 0$, the quantity $\Im \left\{ \tilde{k}_{t_n}(\omega) \right\}$ will equal zero for some critical angle $\Theta_i = \Theta_{LS}$ if the dielectric media are such that the condition

$$\beta_1(\omega)\alpha_1(\omega) > \beta_2(\omega)\alpha_2(\omega) , \quad (4.2.22)$$

is satisfied. The angle Θ_{LS} is called the *leaky surface wave critical angle*. If the condition given in Eq. (4.2.22) is satisfied, then the leaky surface wave critical angle is given by

$$\Theta_{LS} = \sin^{-1} \left\{ \sqrt{\frac{\beta_2(\omega)\alpha_2(\omega)}{\beta_1(\omega)\alpha_1(\omega)}} \right\}. \quad (4.2.23)$$

The quantity $\Im \left\{ k_{t_n}^{(-2)}(\omega) \right\}$ then satisfies the inequalities

$$\begin{aligned} \Im \left\{ k_{t_n}^{(-2)}(\omega) \right\} &< 0 \quad ; \quad \Theta_i > \Theta_{LS} \\ \Im \left\{ k_{t_n}^{(-2)}(\omega) \right\} &= 0 \quad ; \quad \Theta_i = \Theta_{LS} . \\ \Im \left\{ k_{t_n}^{(-2)}(\omega) \right\} &> 0 \quad ; \quad \Theta_i < \Theta_{LS} \end{aligned} \quad (4.2.24)$$

According to the chosen branch-cut, these inequalities yield the inequalities

$$\begin{aligned} \Im \left\{ \tilde{k}_{t_n}(\omega) \right\} &< 0 \quad ; \quad \Theta_i > \Theta_{LS} \\ \Im \left\{ \tilde{k}_{t_n}(\omega) \right\} &= 0 \quad ; \quad \Theta_i = \Theta_{LS} \text{ and } \Theta_C > \Theta_{LS} . \\ \Im \left\{ \tilde{k}_{t_n}(\omega) \right\} &> 0 \quad ; \quad \Theta_i < \Theta_{LS} \end{aligned} \quad (4.2.25)$$

The top condition given in Eq. (4.2.25) implies that the amplitude exponentially increases with distance normal to the interface. Transmitted waves of this type do not violate the required condition that $\boldsymbol{\beta}_t(\omega) \cdot \boldsymbol{\alpha}_t(\omega) \geq 0$ [cf. Eq.(2.5.15)] so that the transmitted waves attenuate in the direction of phase front propagation $\boldsymbol{\beta}_t(\omega)$ for $\omega > 0$ and $-\boldsymbol{\beta}_t(\omega)$ for $\omega < 0$. For spectral regions where $\alpha_1(\omega)$ is small and the condition given in Eq. (4.2.22) is still satisfied, then the angle $\Theta_{LS} \lesssim \frac{\pi}{2}$ and the incident homogeneous plane wave is considered a *leaky surface wave*¹⁸ when $\Theta_i > \Theta_{LS}$ because Θ_i is then at near grazing incidence to the interface.

If the conditions given in Eqs. (4.2.18) and (4.2.22) are both satisfied in addition to the condition

18. See Caviglia and Morro [69] §1.3 p. 10.

| ω ($10^{14}rad/sec$) | $\beta_1(\omega)$ ($10^5 rad/m$) | $\alpha_1(\omega)$ ($10^4 rad/m$) | $\beta_2(\omega)$ ($10^5 rad/m$) | $\alpha_2(\omega)$ ($10^4 rad/m$) |
|----------------------------------|---------------------------------------|--|---------------------------------------|--|
| 1.7379 | 10.986 | 13.168 | 9.3665 | 15.445 |
| 3.0201 | 18.410 | 2.8021 | 15.410 | 3.3475 |
| 9.3326 | 58.418 | 1.6208 | 49.433 | 1.9154 |

Table 4.2.1 The values of the propagation factor and the attenuation factor for various frequencies. This example utilizes the double resonance Lorentz model parameters taken from Table 4.1.1.

| ω ($10^{14}rad/sec$) | $\beta_1(\omega)$ ($10^5 rad/m$) | $\alpha_1(\omega)$ ($10^4 rad/m$) | $\beta_2(\omega)$ ($10^5 rad/m$) | $\alpha_2(\omega)$ ($10^4 rad/m$) |
|----------------------------------|---------------------------------------|--|---------------------------------------|--|
| 1.7379 | 10.206 | 14.175 | 9.6302 | 1.0037 |
| 3.0201 | 16.976 | 3.0387 | 17.532 | 8.1068 |
| 3.4675 | 19.668 | 2.0826 | 20.725 | 20.284 |
| 4.0740 | 23.280 | 1.4815 | 22.011 | 65.667 |
| 9.3326 | 54.112 | 1.7498 | 46.390 | 1.8324 |
| 10.000 | 58.011 | 1.9648 | 49.862 | 1.7033 |
| 91.225 | 508.04 | 1572.3 | 493.18 | 253.31 |

Table 4.2.2 The values of the propagation factor and the attenuation factor for various frequencies. This example utilizes the double resonance Lorentz model parameters taken from Table 4.1.2.

$$\frac{\beta_2^2(\omega) - \alpha_2^2(\omega)}{\beta_1^2(\omega) - \alpha_1^2(\omega)} > \frac{\beta_2(\omega)\alpha_2(\omega)}{\beta_1(\omega)\alpha_1(\omega)}, \quad (4.2.26)$$

then $\Theta_C > \Theta_{LS}$. All three of these conditions are satisfied for the real and imaginary parts of the complex wavenumbers of the medium of incidence and the medium of transmittance given in Table 4.2.2 for $\omega = 173.79THz$. The results are tabulated in Table 4.2.4. The

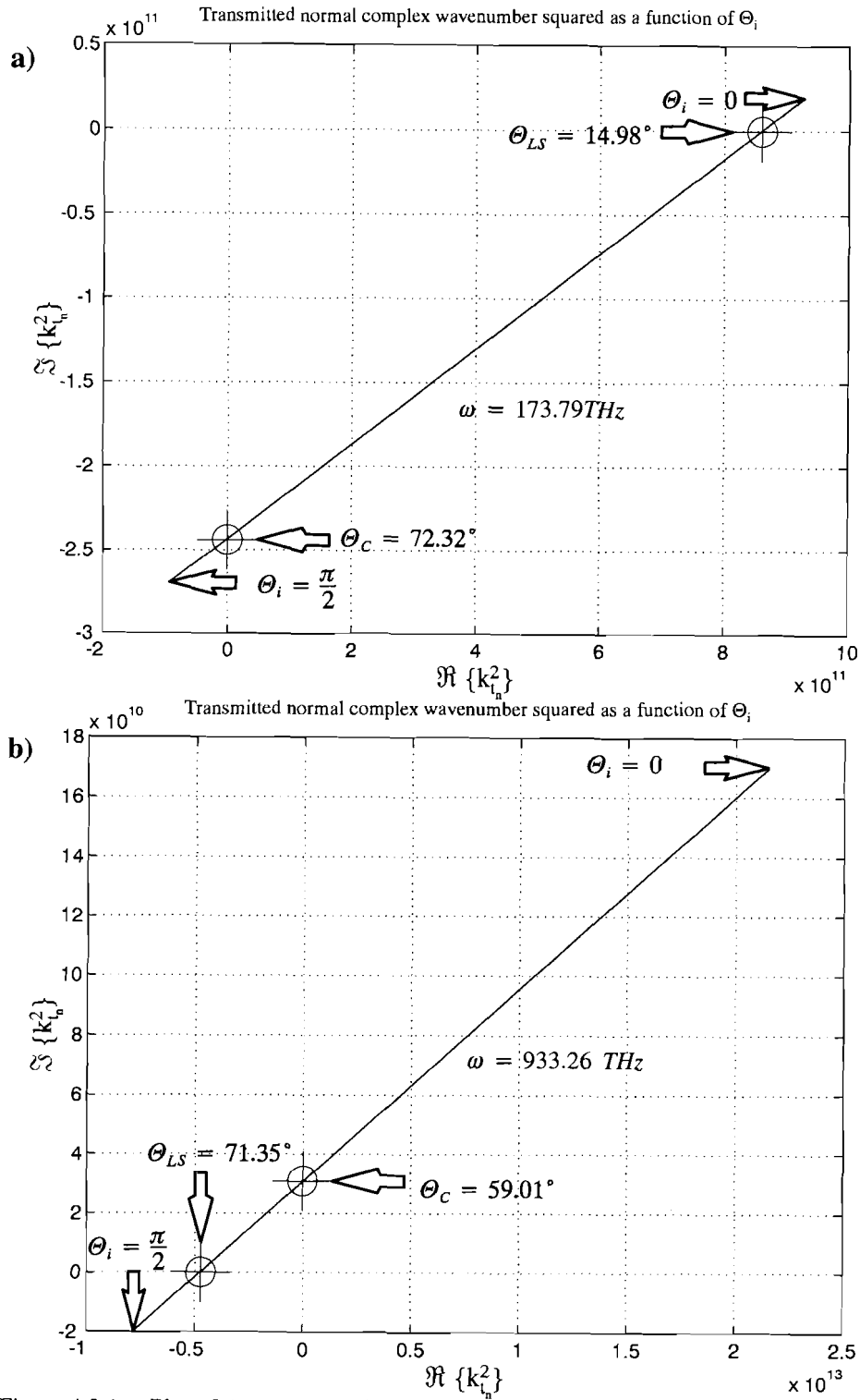


Figure 4.2.1 Plot of the transmitted normal complex wavenumber squared as a function of the angle of the incident local coordinate system for the fixed frequencies a) 174 THz and b) 933 THz for a homogeneous plane wave incident upon the interface separating two lossy, dispersive media.

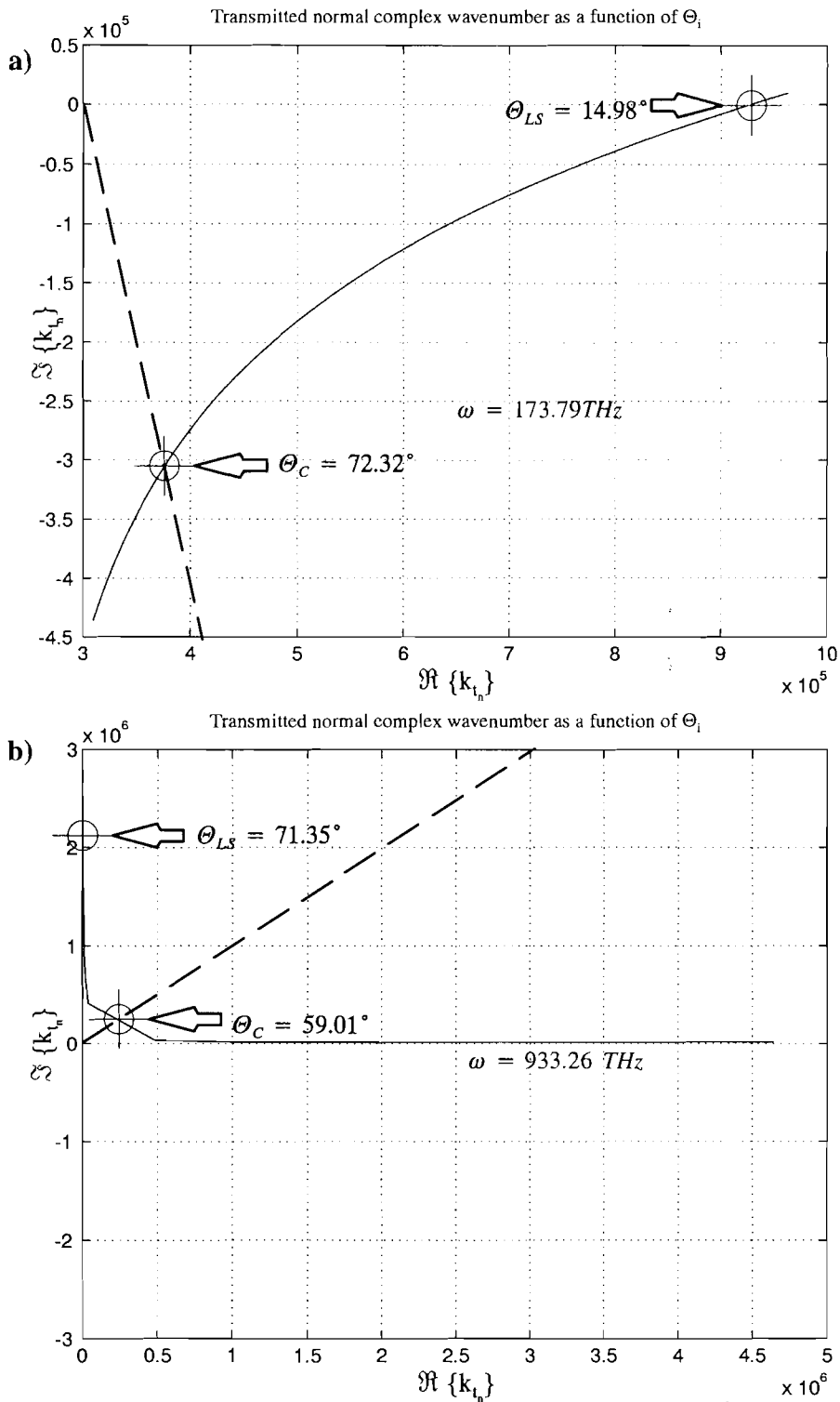


Figure 4.2.2 Plot of the transmitted normal complex wavenumber as a function of the angle of the incident local coordinate system for the fixed frequencies a) 174 THz and b) 933 THz for a homogeneous plane wave incident upon the interface separating two lossy, dispersive media.

functions $\tilde{k}_{t_n}^2(\omega)$ and $\tilde{k}_{t_n}(\omega)$ for this situation are plotted in the complex plane in Figure 4.2.1 a) and Figure 4.2.2 a). Notice that, in this situation, $\tilde{k}_{t_n}(\omega)$ is pure real when $\Theta_i = \Theta_{LS}$ as seen in Figure 4.2.2 a).

In contrast, if the conditions given in Eqs. (4.2.18) and (4.2.22) are both satisfied in addition to the condition

$$\frac{\beta_2^2(\omega) - \alpha_2^2(\omega)}{\beta_1^2(\omega) - \alpha_1^2(\omega)} < \frac{\beta_2(\omega)\alpha_2(\omega)}{\beta_1(\omega)\alpha_1(\omega)}, \quad (4.2.27)$$

then $\Theta_C < \Theta_{LS}$. All three of these conditions are satisfied for the real and imaginary parts of the complex wavenumbers of the medium of incidence and the medium of transmittance given in Table 4.2.2 for $\omega = 933.26THz$ and $\omega = 1000.0THz$. The results are tabulated in Table 4.2.4. The functions $\tilde{k}_{t_n}^2(\omega)$ and $\tilde{k}_{t_n}(\omega)$ for $\omega = 933.26THz$ are plotted in the complex plane in Figure 4.2.1 b) and Figure 4.2.2 b). When this situation prevails, the branch cut is crossed so that there will be a discontinuity in the function $\tilde{k}_{t_n}(\omega)$ with respect to the variable Θ_i when $\Theta_i = \Theta_{LS}$. Notice that, in this situation, $\tilde{k}_{t_n}(\omega)$ is pure imaginary at the point of discontinuity $\Theta_i = \Theta_{LS}$. According to the inequalities given in Eq. (4.2.25), imaginary part of $\tilde{k}_{t_n}(\omega)$ is in the positive imaginary half plane immediately before the discontinuity and then continues in the negative half plane after the discontinuity. This effect is not discernable in Figure 4.2.1 b) because $\tilde{k}_{t_n}(\omega)$ lies very close to the imaginary axis in this case.

If the condition given in Eq. (4.2.18) is satisfied but not the condition given in Eq. (4.2.22) then the critical angle Θ_C occurs but not the leaky wave critical angle Θ_{LS} . This situation is satisfied for the real and imaginary parts of the complex wavenumbers of the medium of incidence and the medium of transmittance given in Table 4.2.2 for $\omega = 407.40THz$. The results are tabulated in Table 4.2.4. In contrast, if the condition given

| ω (10^{14}rad/sec) | Θ_C (degrees) | Θ_{LS} (degrees) | $\Theta_{\min(\Re\{r_r\})}$ (degrees) |
|---|-------------------------|----------------------------|--|
| 1.7379 | 57.8918 | none | 58.4703 |
| 3.0201 | 56.8203 | 90.0000 | 57.2489 |
| 9.3326 | 57.7992 | 90.0000 | 57.9635 |

Table 4.2.3 The critical angles for an interface for various frequencies. This example utilizes the double resonance Lorentz model parameters taken from Table 4.1.1.

| ω (10^{14}rad/sec) | Θ_C (degrees) | Θ_{LS} (degrees) | $\Theta_{\min(\Re\{r_r\})}$ (degrees) |
|---|--|----------------------------|--|
| 1.7379 | 72.3191 | 14.9800 | 48.7435 |
| 3.0201 | optically rare \rightarrow dense n/a | none | 0 |
| 3.4675 | optically rare \rightarrow dense n/a | none | 0 |
| 4.0740 | 64.4802 | none | 0 |
| 9.3326 | 59.0144 | 71.3538 | 59.1446 |
| 10.000 | 59.2633 | 59.6772 | 59.2780 |
| 91.225 | none | 23.2947 | 15.5527 |

Table 4.2.4 The critical angles for an interface for various frequencies. This example utilizes the double resonance Lorentz model parameters taken from Table 4.1.2.

in Eq. (4.2.22) is satisfied but not the condition given in Eq. (4.2.18) then the leaky wave critical angle Θ_{LS} occurs but not the critical angle Θ_C . This situation can occur even if the real parts of the complex refractive indices of the two dielectric media separated by the interface represent an optically dense to rare transition. An example of this behavior is tabulated in Table 4.2.4 for $\omega = 9122.5\text{THz}$ for the real and imaginary parts of the complex wave-numbers of the medium of incidence and the medium of transmittance given in Table 4.2.2.

The values of Θ_C and Θ_{LS} for various frequencies are tabulated in Table 4.2.3 and Table 4.2.4. The term ‘*none*’ indicates the failure to meet to either of the inequalities given in Eq. (4.2.18) or Eq. (4.2.22). However, when Eq. (4.2.18) is not satisfied due to an optically rare to dense transition, then this instance is indicated in these tables by the term ‘*optically rare \rightarrow dense*’.

In the second case, the incident field is assumed to be an inhomogeneous plane wave with a fixed angle of incidence Θ_i whose transverse wavenumber k_u varies over the domain $-\infty < k_u < k_{u_{max}}$ while $k_v = 0$. Substitution of Eqs. (4.2.3a,b) into Eq. (4.2.1) yields

$$\tilde{k}_{t_n}^2(\omega) = \tilde{k}_2^2(\omega) - \left(k_u \cos \Theta_i + \Re\{\gamma_i(\omega)\} \sin \Theta_i + i\Im\{\gamma_i(\omega)\} \sin \Theta_i \right)^2, \quad (4.2.28)$$

for an incident inhomogeneous plane wave. The quantity $\tilde{k}_2^2(\omega)$ is given in Eq. (4.2.16), so that Eq. (4.2.28) becomes

$$\begin{aligned} \tilde{k}_{t_n}^2(\omega) = & \left\{ \left(\beta_2^2(\omega) - \alpha_2^2(\omega) \right) \right. \\ & - \left[k_u^2 \cos^2 \Theta_i + \left(\Re\{\gamma_i(\omega)\}^2 - \Im\{\gamma_i(\omega)\}^2 \right) \sin^2 \Theta_i + 2k_u \Re\{\gamma_i(\omega)\} \cos \Theta_i \sin \Theta_i \right] \left. \right\} \\ & + 2i \left[\beta_2(\omega) \alpha_2(\omega) - \left(k_u \cos \Theta_i + \Re\{\gamma_i(\omega)\} \sin \Theta_i \right) \Im\{\gamma_i(\omega)\} \sin \Theta_i \right]. \quad (4.2.29) \end{aligned}$$

If the condition given in Eq. (4.2.18) is satisfied then a real-valued *critical transverse wavenumber* $k_u = k_{u_c}$ can exist such that $\Re\left\{ \tilde{k}_{t_n}^2(\omega) \right\} = 0$. The sign of k_{u_c} is dependent on the value of Θ_i relative to Θ_C . This can be understood by noting that when the transverse wavenumber $k_u = 0$ then the incident plane wave becomes homogeneous and the results from Eq. (4.2.20) apply. Consequently, if $\Theta_i < \Theta_C$, then $\Re\left\{ \tilde{k}_{t_n}^2(\omega) \Big|_{k_u=0} \right\} > 0$ which

means that $k_{u_c} > 0$. Similarly, if $\Theta_i > \Theta_C$, then $\Re \left\{ k_{t_n}^{(-2)}(\omega) \Big|_{k_u=0} \right\} < 0$ which means that $k_{u_c} < 0$.

The factor k_u^2 in real part of Eq. (4.2.29) suggests that another real-valued *secondary critical transverse wavenumber* $k_u = k_{u_{c2}}$ can exist such that $\Re \left\{ k_{t_n}^{(-2)}(\omega) \right\} = 0$. The sign of $k_{u_{c2}}$ is dependent on the value of Θ_i relative to $\Theta_{ilt}^{k_u}$. This can be understood by inspecting the asymptotic behavior of the quantity $\Re \left\{ k_{t_n}^{(-2)}(\omega) \right\}$ given in Eq. (4.2.8), as it relates to the value of Θ_i relative to $\Theta_{ilt}^{k_u}$. If $\Theta_i > \Theta_{ilt}^{k_u}$ then $\Re \left\{ k_{t_n}^{(-2)}(\omega) \right\} > 0$ as $k_u \rightarrow \pm \infty$ so that if both k_{u_c} and $k_{u_{c2}}$ exist then it must be that $\Re \left\{ k_{t_n}^{(-2)}(\omega) \right\} < 0$ over the range in between k_{u_c} and $k_{u_{c2}}$. If $\Theta_i < \Theta_C$ then the signs of k_{u_c} and $k_{u_{c2}}$ must be the same because the quantity $\Re \left\{ k_{t_n}^{(-2)}(\omega) \Big|_{k_u=0} \right\} > 0$ lies in the same half space as the asymptotic limit. The quantity $k_{u_c} > 0$ for this case, which means that $k_{u_{c2}} > 0$ where it is defined that $k_{u_{c2}} > k_{u_c}$. If $\Theta_i > \Theta_C$ then the signs of k_{u_c} and $k_{u_{c2}}$ must be opposite because the quantity $\Re \left\{ k_{t_n}^{(-2)}(\omega) \Big|_{k_u=0} \right\} < 0$ lies in the opposite half space as the asymptotic limit. The quantity $k_{u_c} < 0$ for this case, which means that $k_{u_{c2}} > 0$. Therefore, if $\Theta_i > \Theta_{ilt}^{k_u}$ then $k_{u_{c2}} > 0$ and the quantity $\Re \left\{ k_{t_n}^{(-2)}(\omega) \right\}$ satisfies the inequalities

$$\begin{aligned}
\Re \left\{ k_{t_n}^{(-2)}(\omega) \right\} &< 0 \quad ; \quad k_{u_c} < k_u < k_{u_{c2}} \\
\Re \left\{ k_{t_n}^{(-2)}(\omega) \right\} &= 0 \quad ; \quad k_u = k_{u_c} \quad \text{or} \quad k_u = k_{u_{c2}} \quad . \\
\Re \left\{ k_{t_n}^{(-2)}(\omega) \right\} &> 0 \quad ; \quad k_u < k_{u_c} \quad \text{or} \quad k_u > k_{u_{c2}}
\end{aligned} \tag{4.2.30a}$$

Conversely, if $\Theta_i < \Theta_{\text{tilt}}^{k_u}$ then $\Re \left\{ k_{t_n}^{(-2)}(\omega) \right\} < 0$ as $k_u \rightarrow \pm \infty$ so that if both k_{u_c} and $k_{u_{c2}}$ exist then it must be that $\Re \left\{ k_{t_n}^{(-2)}(\omega) \right\} > 0$ over the range in between k_{u_c} and $k_{u_{c2}}$. Using similar logic leads to the conclusion that if $\Theta_i < \Theta_{\text{tilt}}^{k_u}$ then $k_{u_{c2}} < 0$ (where it is defined that $k_{u_{c2}} < k_{u_c} < 0$ when $\Theta_i > \Theta_C$) and the quantity $\Re \left\{ k_{t_n}^{(-2)}(\omega) \right\}$ then satisfies the inequalities

$$\begin{aligned}
\Re \left\{ k_{t_n}^{(-2)}(\omega) \right\} &< 0 \quad ; \quad k_{u_c} < k_u < k_{u_{\max}} \quad \text{or} \quad k_u < k_{u_{c2}} \\
\Re \left\{ k_{t_n}^{(-2)}(\omega) \right\} &= 0 \quad ; \quad k_u = k_{u_c} \quad \text{or} \quad k_u = k_{u_{c2}} \quad . \\
\Re \left\{ k_{t_n}^{(-2)}(\omega) \right\} &> 0 \quad ; \quad k_{u_{c2}} < k_u < k_{u_c}
\end{aligned} \tag{4.2.30b}$$

Application of the results of Eq. (3.1.18) to the inequalities given in Eqs. (4.2.30a,b) yields the following two sets of inequalities

$$\begin{aligned}
\Re \left\{ \tilde{k}_{t_n}(\omega) \right\} &< \left| \Im \left\{ \tilde{k}_{t_n}(\omega) \right\} \right| \quad ; \quad k_{u_c} < k_u < k_{u_{c2}} \\
\Re \left\{ \tilde{k}_{t_n}(\omega) \right\} &= \left| \Im \left\{ \tilde{k}_{t_n}(\omega) \right\} \right| \quad ; \quad k_u = k_{u_c} \quad \text{or} \quad k_u = k_{u_{c2}} \quad , \\
\Re \left\{ \tilde{k}_{t_n}(\omega) \right\} &> \left| \Im \left\{ \tilde{k}_{t_n}(\omega) \right\} \right| \quad ; \quad k_u < k_{u_c} \quad \text{or} \quad k_u > k_{u_{c2}}
\end{aligned} \tag{4.2.31a}$$

when $\Theta_i > \Theta_{\text{tilt}}^{k_u}$ and

| ω (10^{14}rad/sec) | $k_{u_{max}}$ (10^5 rad/m) | k_{u_c} (10^5 rad/m) | $k_{u_{c2}}$ (10^5 rad/m) | $k_{u_{LS}}$ (10^5 rad/m) | $k_{u_{Cy}}$ (10^5 rad/m) |
|--|---|---------------------------------------|--|--|--|
| 1.7379 | 10.815 | 6.6454 | -11.193 | 10.815 | ± 10.906 |
| 3.0201 | 17.315 | 11.030 | -17.950 | 17.315 | ± 18.408 |

Table 4.2.5 The critical values of the transverse wavenumber. The angle of the incident local coordinate system $\Theta_i = 20^\circ$. This example utilizes the double resonance Lorentz model with parameters taken from Table 4.1.1.

| ω (10^{14}rad/sec) | $k_{u_{max}}$ (10^5 rad/m) | k_{u_c} (10^5 rad/m) | $k_{u_{c2}}$ (10^5 rad/m) | $k_{u_{LS}}$ (10^5 rad/m) | $k_{u_{Cy}}$ (10^5 rad/m) |
|--|---|---------------------------------------|--|--|--|
| 1.7379 | 7.0963 | 1.4855 | $> k_{u_{max}}$ | 7.0963 | ± 10.906 |
| 9.3326 | 37.551 | 7.9274 | $> k_{u_{max}}$ | 37.551 | ± 58.418 |

Table 4.2.6 The critical values of the transverse wavenumber. The angle of the incident local coordinate system $\Theta_i = 50^\circ$. This example utilizes the double resonance Lorentz model with parameters taken from Table 4.1.1.

$$\begin{aligned}
\Re\{\tilde{k}_{t_n}(\omega)\} &< \left| \Im\{\tilde{k}_{t_n}(\omega)\} \right| && ; k_u > k_{u_c} \text{ or } k_u < k_{u_{c2}} \\
\Re\{\tilde{k}_{t_n}(\omega)\} &= \left| \Im\{\tilde{k}_{t_n}(\omega)\} \right| && ; k_u = k_{u_c} \text{ or } k_u = k_{u_{c2}} \\
\Re\{\tilde{k}_{t_n}(\omega)\} &> \left| \Im\{\tilde{k}_{t_n}(\omega)\} \right| && ; k_{u_{c2}} < k_u < k_{u_c}
\end{aligned} \quad . (4.2.31b)$$

when $\Theta_i < \Theta_{\text{tilt}}^{k_u}$. When the bottom conditions of Eqs. (4.2.31a,b) are met then the term $\tilde{k}_{t_n}(\omega)$ is primarily a *propagative* factor and when the top conditions of Eqs. (4.2.31a,b) are met then the term $\tilde{k}_{t_n}(\omega)$ is primarily an *attenuative* factor. All of the above inequalities have assumed that both k_{u_c} and $k_{u_{c2}}$ exist and that $k_{u_c} < k_{u_{max}}$ and $k_{u_{c2}} < k_{u_{max}}$. The ranges will need to be adjusted if either critical transverse wavenumber is greater than $k_{u_{max}}$.

If the condition given in Eq. (4.2.22) is satisfied then a real-valued *leaky surface wave critical transverse wavenumber* $k_u = k_{u_{LS}}$ can exist such that $\Im\{\tilde{k}_{t_n}^{-2}(\omega)\} = 0$. The sign

| ω (10^{14} rad/sec) | $k_{u_{max}}$ (10^5 rad/m) | k_{u_c} (10^5 rad/m) | $k_{u_{c2}}$ (10^5 rad/m) | $k_{u_{LS}}$ (10^5 rad/m) | $k_{u_{cy}}$ (10^5 rad/m) |
|----------------------------------|----------------------------------|---|---|---------------------------------|---------------------------------|
| 1.7379 | 6.6032 | 3.7668 | $> k_{u_{max}}$ | -7.4869 | ± 10.107 |
| 3.4675 | 12.643 | optically n/a rare \rightarrow dense | optically n/a rare \rightarrow dense | $> k_{u_{max}}$ | ± 19.666 |
| 4.0740 | 14.965 | 5.8209 | $> k_{u_{max}}$ | $> k_{u_{max}}$ | ± 23.280 |
| 9.3326 | 34.783 | 8.4784 | $> k_{u_{max}}$ | 28.893 | ± 54.112 |

Table 4.2.7 The critical values of the transverse wavenumber. The angle of the incident local coordinate system $\Theta_i = 50^\circ$. This example utilizes the double resonance Lorentz model with parameters taken from Table 4.1.2.

of $k_{u_{LS}}$ is dependent on the value of Θ_i relative to Θ_{LS} . Notice that when the transverse wavenumber $k_u = 0$ then the incident plane wave becomes homogeneous and the results from

Eq. (4.2.24) apply. Consequently, if $\Theta_i < \Theta_{LS}$ then $\Im \left\{ \tilde{k}_{t_n}^2(\omega) \Big|_{k_u=0} \right\} > 0$ which means

that $k_{u_{LS}} > 0$. Similarly, if $\Theta_i > \Theta_{LS}$ then $\Im \left\{ \tilde{k}_{t_n}^2(\omega) \Big|_{k_u=0} \right\} < 0$ which means that

$k_{u_{LS}} < 0$. The quantity $\tilde{k}_{t_n}^2(\omega)$ then satisfies the inequalities

$$\begin{aligned}
\Im \left\{ \tilde{k}_{t_n}^2(\omega) \right\} &< 0 \quad ; \quad k_u > k_{u_{LS}} \\
\Im \left\{ \tilde{k}_{t_n}^2(\omega) \right\} &= 0 \quad ; \quad k_u = k_{u_{LS}} \quad . \\
\Im \left\{ \tilde{k}_{t_n}^2(\omega) \right\} &> 0 \quad ; \quad k_u < k_{u_{LS}}
\end{aligned} \tag{4.2.32}$$

According to the chosen branch cut, these inequalities yield the following inequalities

$$\begin{aligned}
\Im\{\tilde{k}_{t_n}(\omega)\} &< 0 \quad ; \quad k_u > k_{u_{LS}} \\
\Im\{\tilde{k}_{t_n}(\omega)\} &= 0 \quad ; \quad k_u = k_{u_{LS}} \text{ and } k_{u_c} > k_{u_{LS}} \quad . \\
\Im\{\tilde{k}_{t_n}(\omega)\} &> 0 \quad ; \quad k_u < k_{u_{LS}}
\end{aligned} \tag{4.2.33}$$

When $k_{u_c} > k_{u_{LS}}$, the quantity $\tilde{k}_{t_n}(\omega)$ is pure real when $k_u = k_{u_{LS}}$. When $k_{u_c} < k_{u_{LS}}$, the quantity $\tilde{k}_{t_n}(\omega)$ is pure imaginary when $k_u = k_{u_{LS}}$ which means that the branch cut is crossed so that there will be a discontinuity in the function $\tilde{k}_{t_n}(\omega)$ with respect to the variable k_u . According to the inequalities given in Eq. (4.2.33), the imaginary part of $\tilde{k}_{t_n}(\omega)$ is in the positive imaginary half plane immediately before the discontinuity and then continues in the negative half plane after the discontinuity.

It is impossible to obtain exact expressions for the critical values k_{u_c} , $k_{u_{c2}}$ and $k_{u_{LS}}$ since the longitudinal component $\gamma_i(\omega)$ of the complex wavevector is a function of k_u . Numerical results are tabulated in Table 4.2.6, Table 4.2.5 and Table 4.2.7. The expression ‘ $> k_{u_{max}}$ ’ indicates that the evaluated values of k_{u_c} , $k_{u_{c2}}$ and $k_{u_{LS}}$ are greater than the maximum allowed value $k_{u_{max}}$. When Eq. (4.2.18) is not satisfied due to an optically rare to dense transition, then this instance is indicated in these tables by the term ‘*optically rare \rightarrow dense*’, e.g. in Table 4.2.7 for $\omega = 346.75\text{THz}$. The critical transverse wavenumber $k_{u_{c1}}$ for the longitudinal component of the complex wavevector given in these tables is the evaluation of Eq. (3.1.16) for the situation where $k_v = 0$.

4.3 Results of the Generalized *Fresnel* Reflection Coefficient for Incident Linearly Polarized TM Plane Waves

The classical evaluation of the generalized *Fresnel* reflection coefficient utilizes homogeneous plane waves. The angle of incidence of the homogeneous plane waves is varied from normal incidence to grazing incidence. The reflection coefficient is then plotted against the angle of incidence. Certain critical angles that relate to total internal reflection

and *Brewster's* angle are encountered when both of the media on opposite sides of the interface are lossless. When loss is included, the critical angle that relates to near total internal reflection is the analog to the lossless case. The character of the reflection coefficient is similar to that of the lossless case for spectral regions removed from any resonance. In contrast, when evaluating the generalized *Fresnel* reflection coefficient for an inhomogeneous plane wave, the angle of incidence Θ_i is fixed and the transverse wavenumber k_u varies over the domain $-\infty < k_u < k_{u_{max}}$ while the other transverse wavenumber is fixed at $k_v = 0$. This section only treats TM polarized plane waves. In this situation, certain critical transverse wavenumbers are encountered which are analogous to the critical angles for the homogenous case.

4.3.1 Results of the Generalized *Fresnel* Reflection Coefficient for an Incident Linearly Polarized TM Homogeneous Plane Wave Where Both Media are Lossless

The incident field is assumed to be a TM polarized homogeneous plane wave where the refractive indices of the medium of incidence and the medium of transmittance are assumed to be pure real so that $\tilde{n}_1 = n_1$ and $\tilde{n}_2 = n_2$ where $n_1, n_2 \in \mathbb{R}$. Consequently, the incident complex wavevector is pure real, viz.

$$\tilde{\mathbf{k}}_i(\omega) = \boldsymbol{\beta}_i(\omega) . \quad (4.3.1)$$

The isotropic generalized *Fresnel* reflection coefficient for TM fields is given as the r_τ component of the matrix given in Eq. (3.1.144) and is changed into

$$r_\tau = \frac{n_1^2(\omega)\tilde{k}_{t_n}(\omega) - n_2^2(\omega)\beta_{i_n}(\omega)}{n_1^2(\omega)\tilde{k}_{t_n}(\omega) + n_2^2(\omega)\beta_{i_n}(\omega)} , \quad (4.3.2)$$

where $\beta_{i_n}(\omega)$ is the normal component of Eq. (4.3.1). The quantity $\tilde{k}_{t_n}(\omega)$ is given by [cf. Eq. (4.2.1)]

$$\tilde{k}_{t_n}(\omega) = + \sqrt{k_2^2(\omega) - \beta_{i_r}^2(\omega)} , \quad (4.3.3)$$

where $\tilde{k}_2(\omega) \equiv n_2(\omega)k_0$ is real-valued and $\beta_{i_t}(\omega)$ is the in-plane tangential component of Eq. (4.3.1) which is given by $\beta_{i_t}(\omega) = \tilde{k}_1(\omega) \sin \Theta_i$ where $\tilde{k}_1(\omega) \equiv n_1(\omega)k_0$.

Since $\tilde{k}_1(\omega)$ and $\tilde{k}_2(\omega)$ are real-valued the critical angle Θ_C is given by [cf. Eq. (4.2.19)]

$$\Theta_C = \sin^{-1} \left\{ \frac{\beta_2(\omega)}{\beta_1(\omega)} \right\}, \quad (4.3.4)$$

when the inequality

$$\beta_1(\omega) > \beta_2(\omega), \quad (4.3.5)$$

is satisfied. If this inequality is satisfied and $\Theta_i > \Theta_C$ then Eq. (4.3.3) becomes pure imaginary so that

$$\tilde{k}_{i_n}(\omega) = i\alpha_{i_n}(\omega). \quad (4.3.6)$$

As a consequence, Eq. (4.3.2) can be written as

$$r_\tau = \frac{z}{z^*} = e^{i\phi} \quad ; \quad \Theta_i > \Theta_C, \quad (4.3.7)$$

where $z = n_1^2(\omega)\alpha_{i_n}(\omega) + in_2^2(\omega)\beta_{i_n}(\omega)$. The reflection coefficient then has a magnitude of unity. This situation is called *total internal reflection* and occurs for supercritical angles of incidence $\Theta_i > \Theta_C$.

As an example, Figure 4.3.1 a) and b) depict the real part and the magnitude of the reflection coefficient, respectively, plotted against the angle of incidence Θ_i . The values of the dielectric permittivity are chosen as $\frac{\epsilon_1}{\epsilon_0} = 2.9938$ and $\frac{\epsilon_2}{\epsilon_0} = 1.9938$ to match those in Table 4.1.1. If $\Theta_i = 0$, then $|r_\tau| > 0$ as seen in Figure 4.3.1 a). As Θ_i increases, the quantity $\Re\{r_\tau\}$ decreases until $\Re\{r_\tau\} = 0$ at the angle $\Theta_i = \Theta_B$ where Θ_B is known as *Brewster's angle*. In this example $\Theta_B = 39.2170^\circ$. As Θ_i continues to increase, the quantity $\Re\{r_\tau\}$ continues to decrease until $\Re\{r_\tau\}$ reaches a minimum value of -1 at $\Theta_i = \Theta_C$. In

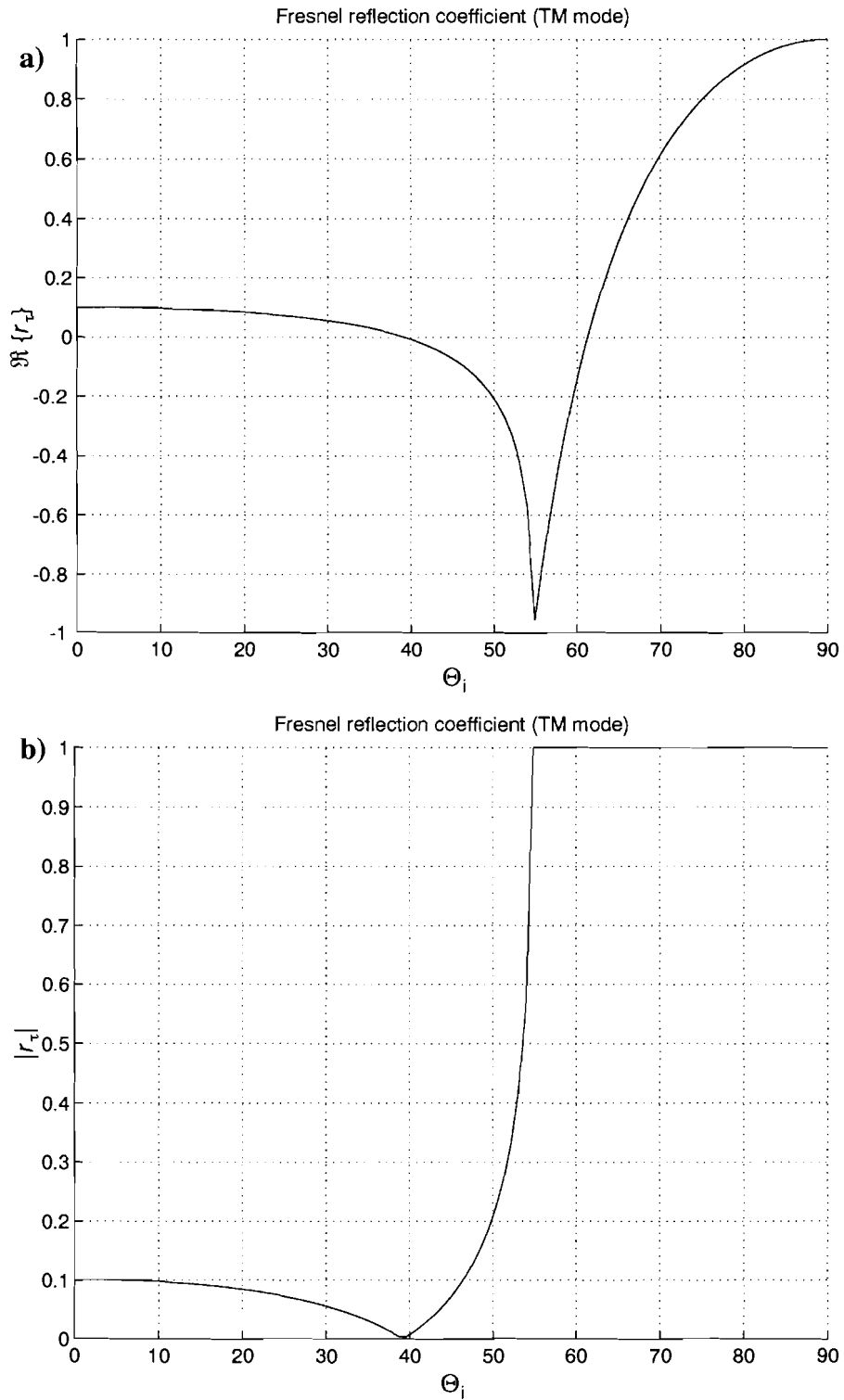


Figure 4.3.1 Plots of the a) real part and b) magnitude of the isotropic generalized *Fresnel* reflection coefficient for the TM mode as a function of the angle of the incident local coordinate system. Homogeneous plane waves are incident upon the interface separating two lossy, dispersive media. This example represents lossless media where the values of the dielectric permittivity are taken from Table 4.1.1.

this example $\Theta_C = 54.6937^\circ$. In between Θ_C and the grazing angle $\frac{\pi}{2}$, total internal reflection occurs as illustrated in Figure 4.3.1 b).

4.3.2 Results of the Generalized *Fresnel* Reflection Coefficient for an Incident Linearly Polarized TM Homogeneous Plane Wave

The incident field is assumed to be a TM polarized homogeneous plane wave where the refractive indices of the medium of incidence and the medium of transmittance are assumed to be lossy. The generalized *Fresnel* reflection coefficient for TM fields is given as [cf. Eq. (3.1.144)]

$$r_\tau = \frac{\tilde{n}_1^2(\omega)\tilde{k}_{t_n}(\omega) - \tilde{n}_2^2(\omega)\tilde{k}_{i_n}(\omega)}{\tilde{n}_1^2(\omega)\tilde{k}_{t_n}(\omega) + \tilde{n}_2^2(\omega)\tilde{k}_{i_n}(\omega)}, \quad (4.3.8)$$

where $\tilde{k}_{i_n}(\omega)$ is given by [cf. Eqs. (4.2.13a,b)]

$$\tilde{k}_{i_n}(\omega) = \tilde{k}_2(\omega) \cos \Theta_i \quad (4.3.9)$$

and $\tilde{k}_{t_n}(\omega)$ is given by [cf. Eq. (4.2.14)]

$$\tilde{k}_{t_n}(\omega) = \left[\tilde{k}_2^2(\omega) - \left(\tilde{k}_1(\omega) \sin \Theta_i \right)^2 \right]^{1/2}, \quad (4.3.10)$$

where $\tilde{k}_1(\omega)$ and $\tilde{k}_2(\omega)$ are given by Eqs. (3.1.6) and (3.1.54), respectively.

Examples of both the real part and the magnitude of the generalized *Fresnel* reflection coefficient are illustrated in Figure 4.3.2 and Figure 4.3.3, respectively. The results are plotted against the angular frequency ω and the angle of incidence Θ_i . These examples utilize the double resonance Lorentz model with parameters taken from Table 4.1.1. In regions removed from any resonance, the character of the generalized *Fresnel* reflection coefficient closely resembles that of the lossless case, as illustrated in Figure 4.3.1. The quantity $\Re\{r_\tau\}$ reaches a minimum near the critical angle Θ_C , as given in Eq. (4.2.19), in spectral regions removed from any resonances. The angle at which $\Re\{r_\tau\}$ reaches a minimum is called

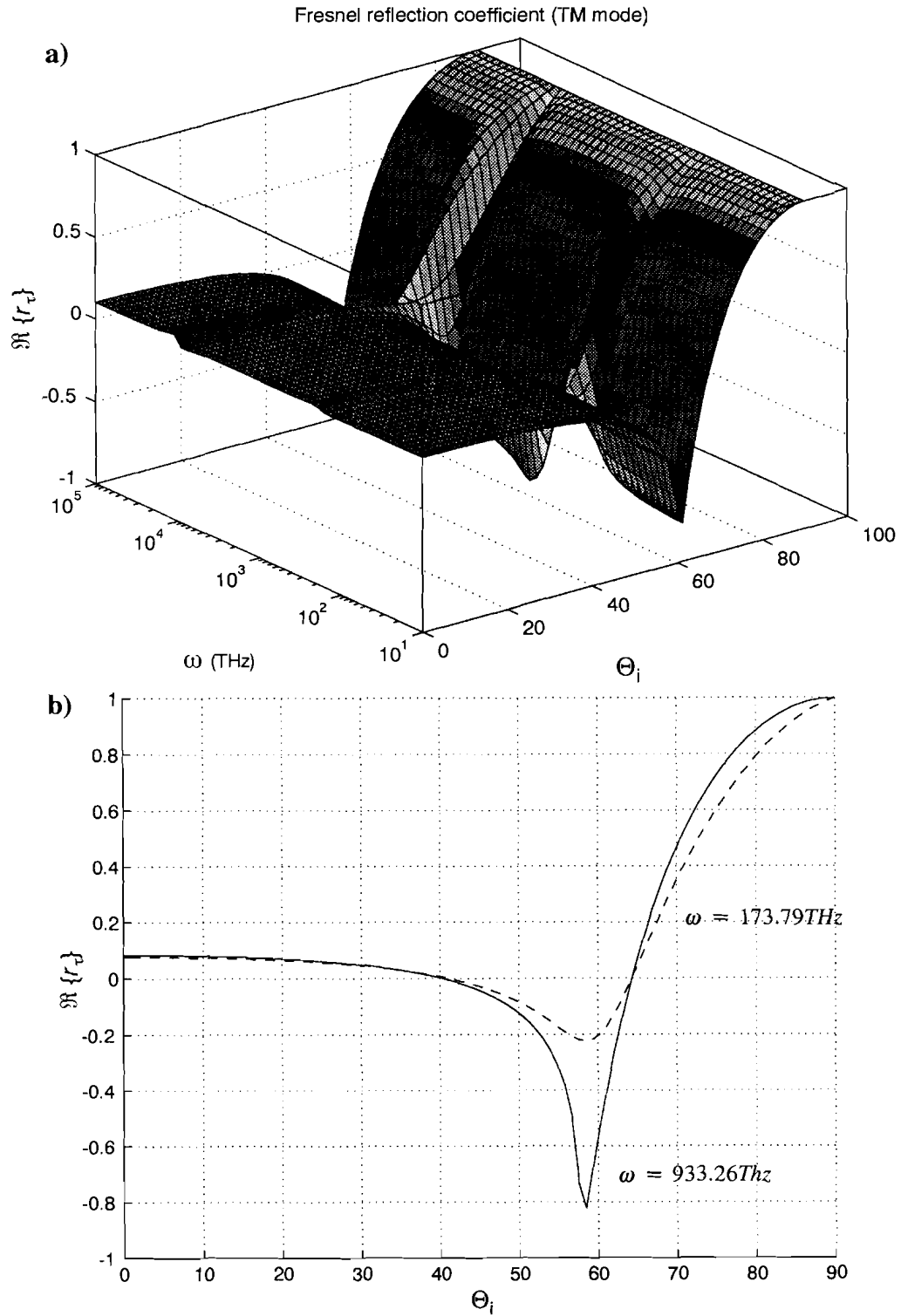


Figure 4.3.2 a) Three and b) two dimensional plots of the real part of the isotropic generalized *Fresnel* reflection coefficient for the TM mode as a function of the angle of the incident local coordinate system and frequency ω as indicated. Homogeneous plane waves are incident upon the interface separating two lossy, dispersive media. This example utilizes the double resonance Lorentz model with parameters taken from Table 4.1.1.

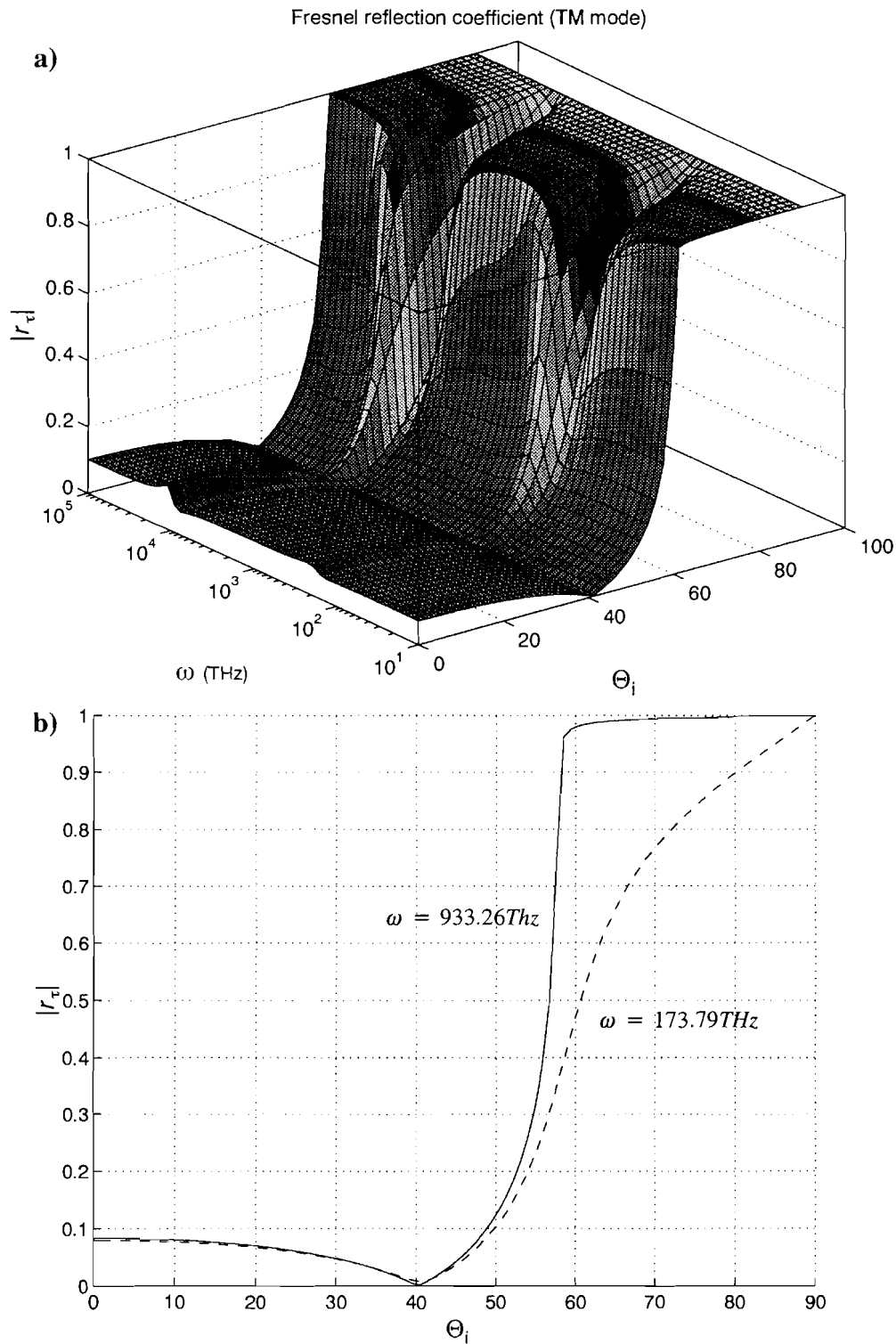


Figure 4.3.3 a) Three and b) two dimensional plots of magnitude of the isotropic generalized *Fresnel* reflection coefficient for the TM mode as a function of the angle of the incident local coordinate system and frequency ω as indicated. Homogeneous plane waves are incident upon the interface separating two lossy, dispersive media. This example utilizes the double resonance Lorentz model with parameters taken from Table 4.1.1.

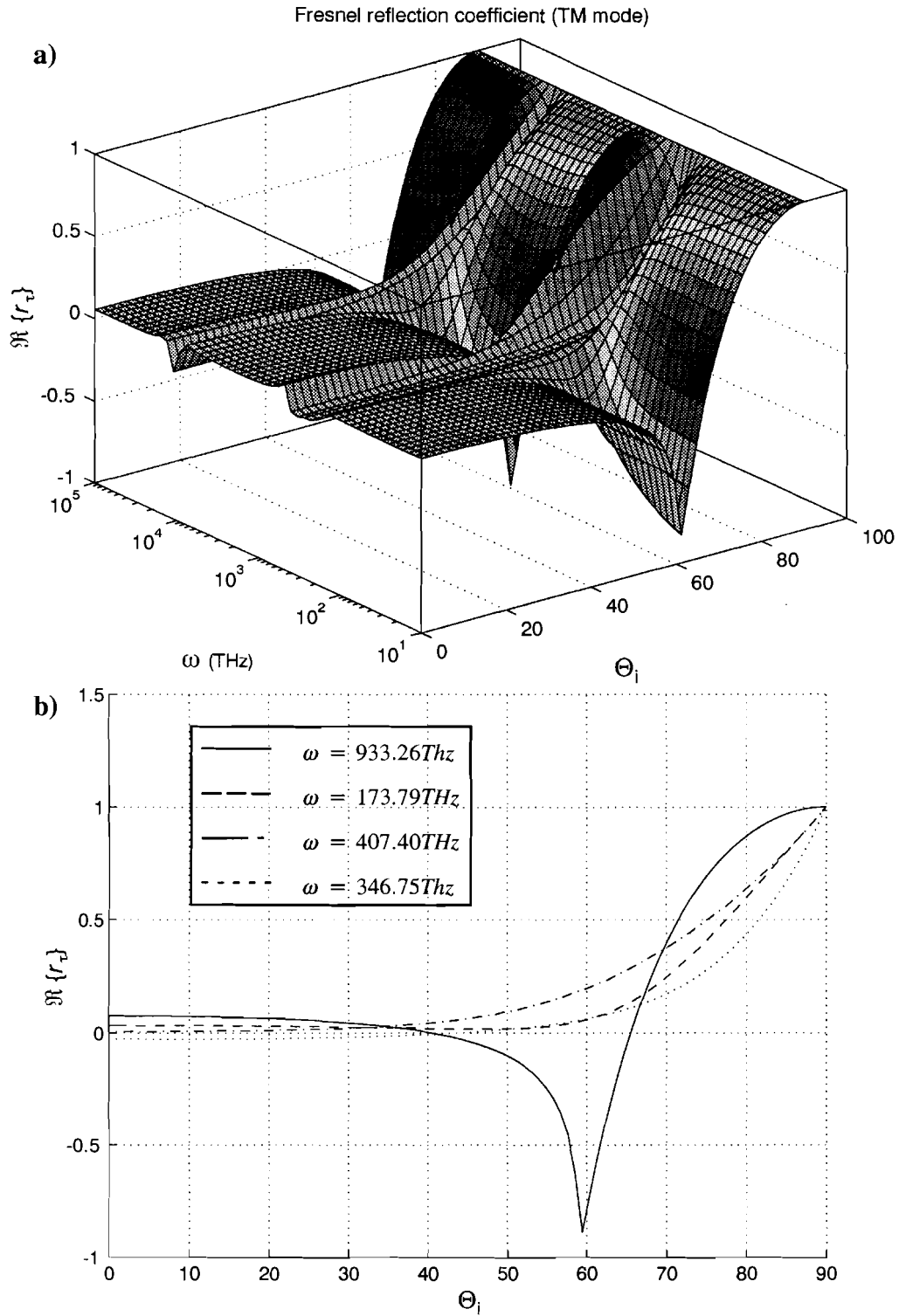


Figure 4.3.4 a) Three and b) two dimensional plots of the real part of the isotropic generalized *Fresnel* reflection coefficient for the TM mode as a function of the angle of the incident local coordinate system and frequency ω as indicated. Homogeneous plane waves are incident upon the interface separating two lossy, dispersive media. This example utilizes the double resonance Lorentz model with parameters taken from Table 4.1.2.

$\Theta_{\min(\Re\{r_\tau\})}$. In between Θ_C and the grazing angle $\frac{\pi}{2}$, total internal reflection does not occur even for regions removed from the resonance as illustrated in Figure 4.3.3 b) where $|r_\tau|$ plateaus at a value less than 1 for $\omega = 933.26\text{THz}$. For this reason, when $\Theta_i > \Theta_C$, the condition of *near total internal reflection* prevails for spectral regions removed from any resonance for lossy, dispersive dielectric media.

Another example of the real part of the generalized *Fresnel* reflection coefficient is illustrated in Figure 4.3.4. The result is plotted against the frequency ω and the incident local coordinate system's angle of incidence Θ_i . This example utilizes the double resonance Lorentz model with parameters taken from Table 4.1.2. The main difference in this example is that the character of the reflection coefficient changes due to the two media switching from the normal optically dense to rare transition to an optically rare to dense transition in the anomalous dispersion spectral regions, as illustrated by Figure 4.3.4 b) for $\omega = 346.75\text{THz}$.

4.3.3 Results of the Generalized *Fresnel* Reflection Coefficient for an Incident Linearly Polarized TM Inhomogeneous Plane Wave

The incident field is assumed to be an inhomogeneous plane wave with a fixed angle of incidence Θ_i whose transverse wavenumber k_u varies over the domain $-\infty < k_u < k_{u,\max}$ while $k_v = 0$. The complex refractive indices of the medium of incidence and the medium of transmittance are assumed to be lossy and are then given by Eqs. (3.1.1) and (3.1.2). The generalized *Fresnel* reflection coefficient for TM fields is given as [cf. Eq. (3.1.144)]

$$r_\tau = \frac{\tilde{n}_1^2(\omega)\tilde{k}_{t_n}(\omega) - \tilde{n}_2^2(\omega)\tilde{k}_i(\omega)}{\tilde{n}_1^2(\omega)\tilde{k}_{t_n}(\omega) + \tilde{n}_2^2(\omega)\tilde{k}_i(\omega)}, \quad (4.3.11)$$

where $\tilde{k}_i(\omega)$ is given by [cf. Eqs. (4.2.3a,b)]

$$\tilde{k}_i(\omega) = -k_u \sin \Theta_i + \gamma_i(\omega) \cos \Theta_i \quad (4.3.12)$$

and $\tilde{k}_{t_n}(\omega)$ is given by

$$\tilde{k}_{t_n}(\omega) = \left[\tilde{k}_2^2(\omega) - (k_u \cos \Theta_i + \gamma_i(\omega) \sin \Theta_i)^2 \right]^{1/2}, \quad (4.3.13)$$

where $\tilde{k}_2(\omega)$ is given by Eq. (3.1.54) and $\gamma_i(\omega)$ is given by Eq. (4.2.2).

Let the incident and transmitted normal complex wavenumbers be defined as

$$\tilde{k}_{i_n}(\omega) \equiv \beta_{i_n}(\omega) + i\alpha_{i_n}(\omega), \quad (4.3.14)$$

and

$$\tilde{k}_{t_n}(\omega) \equiv \beta_{t_n}(\omega) + i\alpha_{t_n}(\omega), \quad (4.3.15)$$

where $\beta_{i_n}(\omega)$, $\alpha_{i_n}(\omega)$, $\beta_{t_n}(\omega)$ and $\alpha_{t_n}(\omega)$ are the real and imaginary parts of $\tilde{k}_{i_n}(\omega)$ and $\tilde{k}_{t_n}(\omega)$, respectively. Let the squares of the complex refractive indices be defined as [cf. Eq. (2.2.14)]

$$\tilde{n}_1^2(\omega) \equiv \frac{\mu}{\mu_0 \epsilon_0} \left[\epsilon_{1_r}(\omega) + i\epsilon_{1_i}(\omega) \right], \quad (4.3.16)$$

and

$$\tilde{n}_2^2(\omega) \equiv \frac{\mu}{\mu_0 \epsilon_0} \left[\epsilon_{2_r}(\omega) + i\epsilon_{2_i}(\omega) \right], \quad (4.3.17)$$

where $\epsilon_{1_r}(\omega)$, $\epsilon_{1_i}(\omega)$, $\epsilon_{2_r}(\omega)$ and $\epsilon_{2_i}(\omega)$ are the real and imaginary parts of $\tilde{\epsilon}_1(\omega)$ and $\tilde{\epsilon}_2(\omega)$, respectively. Substitution of Eqs. (4.3.14 – 4.3.17) into Eq. (4.3.11) yields

$$r_\tau = \frac{\epsilon_{1_r} \beta_{t_n} - \epsilon_{1_i} \alpha_{t_n} - \epsilon_{2_r} \beta_{i_n} + \epsilon_{2_i} \alpha_{i_n} - i \left[\epsilon_{2_i} \beta_{i_n} + \epsilon_{2_r} \alpha_{i_n} - \epsilon_{1_i} \beta_{t_n} - \epsilon_{1_r} \alpha_{t_n} \right]}{\epsilon_{1_r} \beta_{t_n} - \epsilon_{1_i} \alpha_{t_n} + \epsilon_{2_r} \beta_{i_n} - \epsilon_{2_i} \alpha_{i_n} + i \left[\epsilon_{2_i} \beta_{i_n} + \epsilon_{2_r} \alpha_{i_n} + \epsilon_{1_i} \beta_{t_n} + \epsilon_{1_r} \alpha_{t_n} \right]}. \quad (4.3.18)$$

A simplifying assumption can be made for both media in the spectral regions removed from a resonance, viz.

$$\epsilon_{1_r}(\omega) \gg \epsilon_{1_i}(\omega), \quad \epsilon_{2_r}(\omega) \gg \epsilon_{2_i}(\omega). \quad (4.3.19)$$

This approximation reduces Eq. (4.3.18) to

$$r_\tau \cong \frac{\varepsilon_{1r}\beta_{t_n} - \varepsilon_{2r}\beta_{i_n} - i[\varepsilon_{2r}\alpha_{i_n} - \varepsilon_{1r}\alpha_{t_n}]}{\varepsilon_{1r}\beta_{t_n} + \varepsilon_{2r}\beta_{i_n} + i[\varepsilon_{2r}\alpha_{i_n} + \varepsilon_{1r}\alpha_{t_n}]} . \quad (4.3.20)$$

First, consider that if both of the quantities $\tilde{k}_{i_n}(\omega)$ and $\tilde{k}_{t_n}(\omega)$ are highly propagative then $\beta_{i_n}(\omega) \gg \alpha_{i_n}(\omega)$ and $\beta_{t_n}(\omega) \gg \alpha_{t_n}(\omega)$ so that Eq. (4.3.20) reduces to

$$r_\tau \cong \frac{\varepsilon_{1r}\beta_{t_n} - \varepsilon_{2r}\beta_{i_n}}{\varepsilon_{1r}\beta_{t_n} + \varepsilon_{2r}\beta_{i_n}} . \quad (4.3.21a)$$

This situation can occur when the value of k_u is such that the bottom inequalities given in Eq. (3.1.19) and either Eq. (4.2.31a) or Eq. (4.2.31b) are satisfied. Second, consider that if the quantity $\tilde{k}_{i_n}(\omega)$ is highly propagative and the quantity $\tilde{k}_{t_n}(\omega)$ is highly attenuative then $\beta_{i_n}(\omega) \gg \alpha_{i_n}(\omega)$ and $\beta_{t_n}(\omega) \ll \alpha_{t_n}(\omega)$ so that Eq. (4.3.20) reduces to

$$r_\tau \cong \frac{\varepsilon_{1r}\alpha_{t_n} + i\varepsilon_{2r}\beta_{i_n}}{\varepsilon_{1r}\alpha_{t_n} - i\varepsilon_{2r}\beta_{i_n}} = \frac{z}{z^*} = e^{i\phi} . \quad (4.3.21b)$$

This situation can occur when the value of k_u is such that the bottom inequality given in Eq. (3.1.19) and the top inequality in either Eq. (4.2.31a) or Eq. (4.2.31b) are satisfied. This situation represents the condition of *near total internal reflection*. Third, consider that if the quantity $\tilde{k}_{i_n}(\omega)$ is highly attenuative and the quantity $\tilde{k}_{t_n}(\omega)$ is highly propagative then $\beta_{i_n}(\omega) \ll \alpha_{i_n}(\omega)$ and $\beta_{t_n}(\omega) \gg \alpha_{t_n}(\omega)$ so that Eq. (4.3.20) reduces to

$$r_\tau \cong \frac{\varepsilon_{1r}\beta_{t_n} - i\varepsilon_{2r}\alpha_{i_n}}{\varepsilon_{1r}\beta_{t_n} + i\varepsilon_{2r}\alpha_{i_n}} = \frac{z^*}{z} = e^{i\phi} . \quad (4.3.21c)$$

This situation can occur when the value of k_u is such that the top inequality given in Eq. (3.1.19) and the bottom inequalities in either Eq. (4.2.31a) or Eq. (4.2.31b) are satisfied. This situation also represents the condition of *near total internal reflection*. Finally, if both of the quantities $\tilde{k}_{i_n}(\omega)$ and $\tilde{k}_{t_n}(\omega)$ are highly attenuative then $\beta_{i_n}(\omega) \ll \alpha_{i_n}(\omega)$ and $\beta_{t_n}(\omega) \ll \alpha_{t_n}(\omega)$ so that Eq. (4.3.20) reduces to

$$r_\tau \cong -\frac{\left[\varepsilon_{2r}\alpha_{i_n} - \varepsilon_{1r}\alpha_{t_n}\right]}{\left[\varepsilon_{2r}\alpha_{i_n} + \varepsilon_{1r}\alpha_{t_n}\right]}. \quad (4.3.21d)$$

This situation can occur when the value of k_u is such that the top inequalities given in Eq. (3.1.19) and either Eq. (4.2.31a) or Eq. (4.2.31b) are satisfied.

If the angle of incidence $\Theta_i = 0$ then $\tilde{k}_{i_n}(\omega) = \tilde{k}_{t_n}(\omega) = i|k_u|$ [cf. Eqs. (4.2.3a,b) and (4.2.9)] in the limit $k_u \rightarrow \pm \infty$. The quantities $\tilde{k}_{i_n}(\omega)$ and $\tilde{k}_{t_n}(\omega)$ are both highly attenuative. The approximation given in Eq. (4.3.21d) applies to this situation and reduces to

$$r_\tau \cong \frac{\left[\varepsilon_{1r} - \varepsilon_{2r}\right]}{\left[\varepsilon_{1r} + \varepsilon_{2r}\right]}. \quad (4.3.22)$$

If the angle of incidence $\Theta_i = \frac{\pi}{4}$ then $\tilde{k}_{i_n}(\omega) = -k_u + i|k_u|$ [cf. Eqs. (4.2.3a,b)] and $\tilde{k}_{t_n}(\omega) = |k_u| - ik_u$ [cf. Eq. (4.2.9)] in the limit $k_u \rightarrow -\infty$. The approximation given in Eq. (4.3.20) applies to this situation and also reduces to the expression given in Eq. (4.3.22).

Examples of both the real part and the magnitude of the generalized *Fresnel* reflection coefficient are illustrated in Figure 4.3.5 and Figure 4.3.6, respectively. The results are plotted against the angular frequency ω and the real-valued wavenumber k_u where the angle of incidence is fixed at $\Theta_i = 50^\circ$. The angle $\Theta_i = 50^\circ$ is chosen since it is less than the critical angle Θ_c for incident homogeneous plane waves [cf. Table 4.2.4]. This example utilizes the double resonance Lorentz model with parameters taken from Table 4.1.1. Due to the complexity of the generalized *Fresnel* reflection coefficient, only the spectral region around the first resonance is plotted. The data generated for $k_u > k_{u_{max}}$ is removed from the plots, seen in the 3D plots as the missing regions and in the 2D plots as the clipped data.

A real-valued *Brewster's critical transverse wavenumber* $k_u = k_{u_B}$ can exist such that $\Re\{r_\tau\} = 0$ as observed in Figure 4.3.5 b). The value k_{u_B} corresponds to the angle $\theta_i^\beta = \theta_{i_B}^\beta$

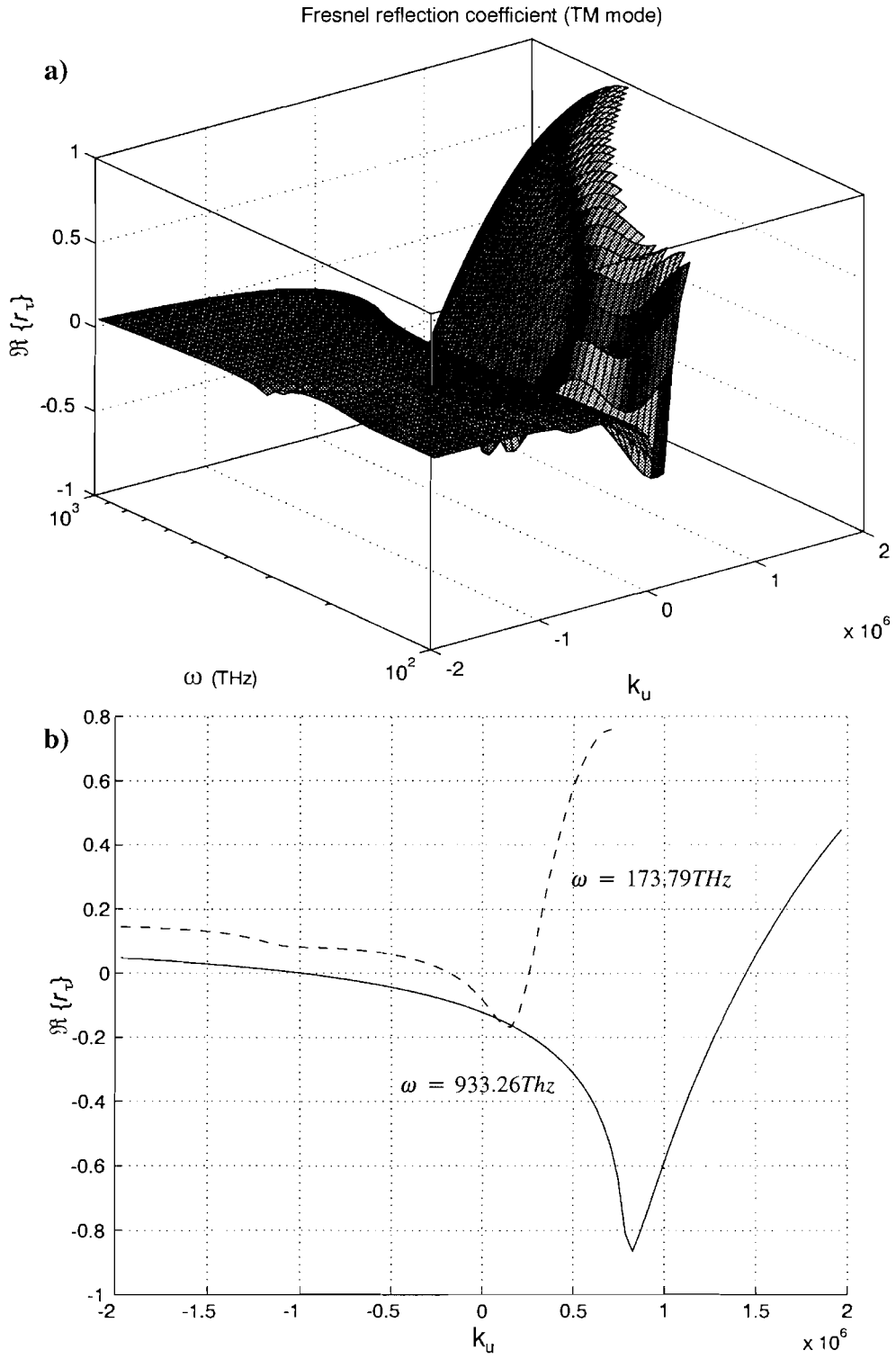


Figure 4.3.5 a) Three and b) two dimensional plots of the real part of the isotropic generalized *Fresnel* reflection coefficient for the TM mode as a function of k_u and frequency ω as indicated. Inhomogeneous plane waves are incident upon the interface separating two lossy, dispersive media. The angle of the incident local coordinate system is fixed at $\Theta_i = 50^\circ$. This example utilizes the double resonance Lorentz model with parameters taken from Table 4.1.1.

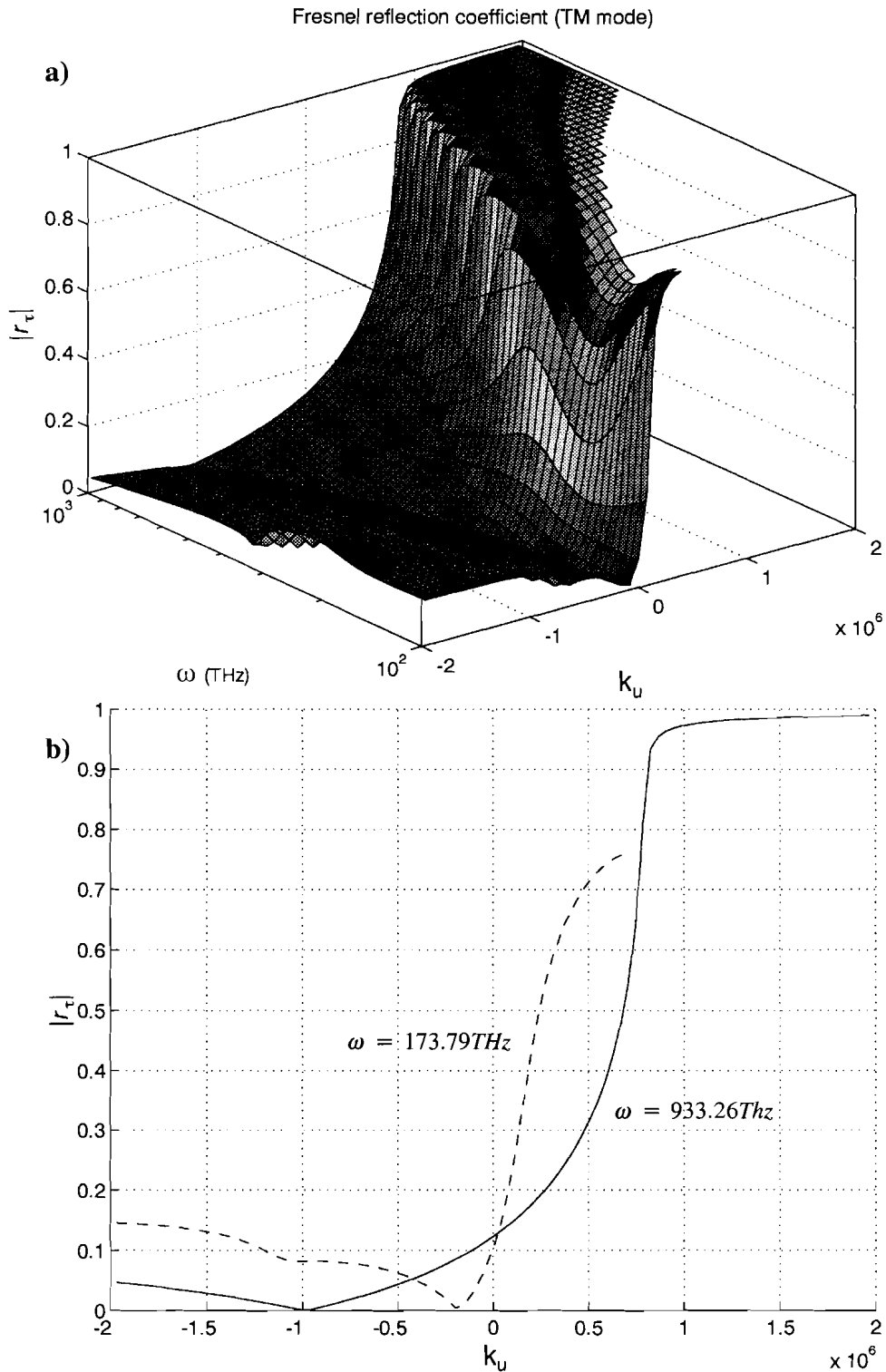


Figure 4.3.6 a) Three and b) two dimensional plots of magnitude of the isotropic generalized *Fresnel* reflection coefficient for the TM mode as a function of k_u and frequency ω as indicated. Inhomogeneous plane waves are incident upon the interface separating two lossy, dispersive media. The angle of the incident local coordinate system is fixed at $\Theta_i = 50^\circ$. This example utilizes the double resonance Lorentz model with parameters taken from Table 4.1.1.

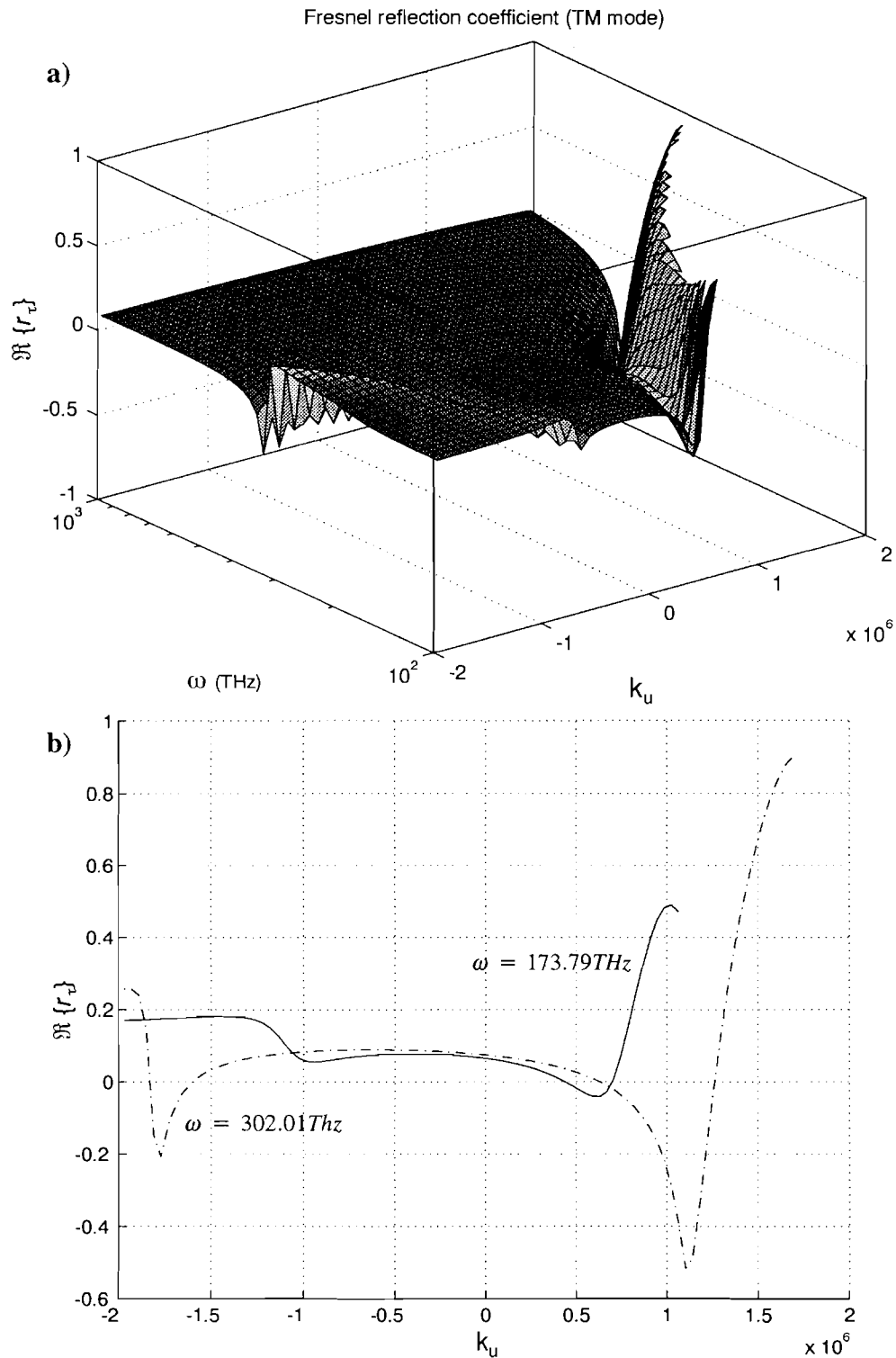


Figure 4.3.7 a) Three and b) two dimensional plots of the real part of the isotropic generalized *Fresnel* reflection coefficient for the TM mode as a function of k_u and frequency ω as indicated. Inhomogeneous plane waves are incident upon the interface separating two lossy, dispersive media. The angle of the incident local coordinate system is fixed at $\Theta_i = 20^\circ$. This example utilizes the double resonance Lorentz model with parameters taken from Table 4.1.1.

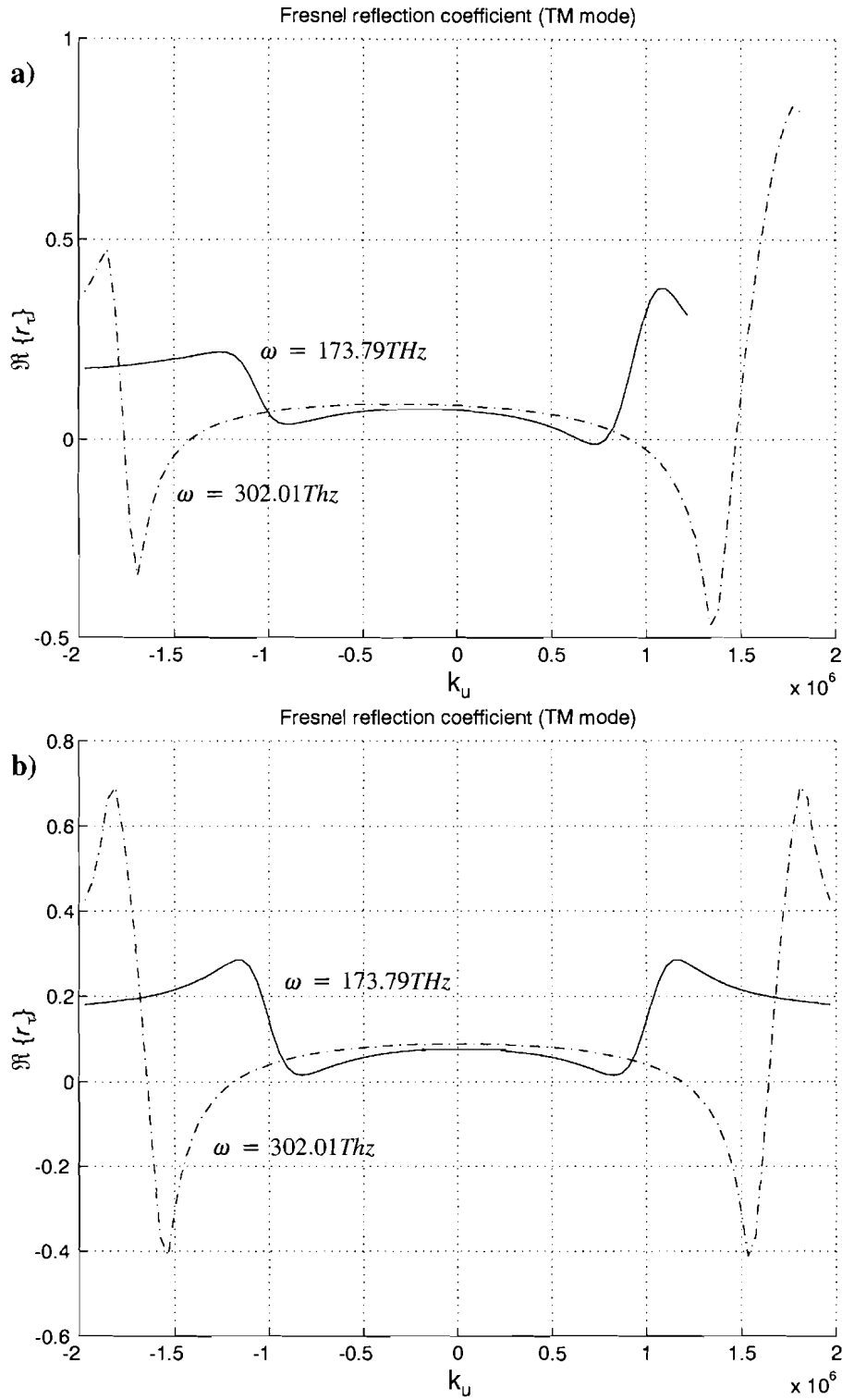


Figure 4.3.8 Plots of the real part of the isotropic generalized *Fresnel* reflection coefficient for the TM mode as a function of k_u and frequency ω as indicated for the angle of the incident local coordinate system fixed at a) $\Theta_i = 10^\circ$ and b) $\Theta_i = 0^\circ$. Inhomogeneous plane waves are incident upon the interface separating two lossy, dispersive media. This example utilizes the double resonance Lorentz model with parameters taken from Table 4.1.1.

| ω (10^{14} rad/sec) | $\theta_{i_c}^\beta$ (degrees) | $\theta_{i_{LS}}^\beta$ (degrees) |
|----------------------------------|-----------------------------------|--------------------------------------|
| 1.7379 | 57.0494 | 90.0000 |
| 3.0201 | 56.8071 | 90.0000 |

Table 4.3.1 The angles of the incident propagation vector that correspond to the critical values of the transverse wavenumber. The angle of the incident local coordinate system $\Theta_i = 20^\circ$. This example utilizes the double resonance Lorentz model with parameters taken from Table 4.1.1.

of the incident propagation vector that is nearly equal to *Brewster's* angle Θ_B . Notice that the quantity k_{u_B} fans out as a function of the angular frequency ω . Some values of $\theta_{i_B}^\beta$ are tabulated in Table 4.3.1, Table 4.3.2 and Table 4.3.3.

In Figure 4.3.5 b), a significant dip is observed in the plot of the quantity $\Re\{r_\tau\}$ for $k_u > 0$ where the minimum is reached near the critical transverse wavenumber $k_u = k_{u_c}$ as defined in §4.2.2. The value k_{u_c} corresponds to the angle $\theta_i^\beta = \theta_{i_c}^\beta$ of the incident propagation vector that is nearly equal to the critical angle Θ_c . If $k_{u_c} < k_u < k_{u_{cy}}$ then the approximation given in Eq. (4.3.21b) is valid in the spectral regions removed from any resonance. In this situation, near total internal reflection occurs as illustrated in Figure 4.3.6 b) for $\omega = 933.26\text{THz}$. Notice that the quantity k_{u_c} fans out as a function of the angular frequency ω . Some values of $\theta_{i_c}^\beta$ are tabulated in Table 4.3.1, Table 4.3.2 and Table 4.3.3.

Attention is now drawn to the secondary dip or ripple that is observed in Figure 4.3.5 a) and b) for $k_u < 0$. The secondary dip is caused by the *critical transverse wavenumber for the longitudinal complex wavenumber* $k_{u_{cy}}$, as defined by Eq. (3.1.16). If $k_u < -k_{u_{cy}}$ then the approximation given in Eq. (4.3.22) is valid since $\Theta_i \geq \Theta_{\text{tilt}}^{k_u}$.

For some values of Θ_i the effect of this secondary dip is strong enough to cause a *secondary Brewster's critical transverse wavenumber* $k_{u_{B2}}$ as observed in Figure 4.3.7 b) for

| ω (10^{14} rad/sec) | $\theta_{i_c}^\beta$ (degrees) | $\theta_{i_{LS}}^\beta$ (degrees) |
|----------------------------------|-----------------------------------|--------------------------------------|
| 1.7379 | 57.7703 | 90.0000 |
| 3.0201 | 56.8186 | 90.0000 |
| 9.3326 | 57.9920 | 90.0000 |

Table 4.3.2 The angles of the incident propagation vector that correspond to the critical values of the transverse wavenumber. The angle of the incident local coordinate system $\Theta_i = 50^\circ$. This example utilizes the double resonance Lorentz model with parameters taken from Table 4.1.1.

| ω (10^{14} rad/sec) | $\theta_{i_c}^\beta$ (degrees) | $\theta_{i_{LS}}^\beta$ (degrees) |
|----------------------------------|--|--------------------------------------|
| 1.7379 | 71.6258 | 3.4380 |
| 3.4675 | <i>optically rare \rightarrow dense</i> n/a | <i>none</i> |
| 4.0740 | 64.4794 | <i>none</i> |
| 9.3326 | 59.0143 | 82.2724 |

Table 4.3.3 The angles of the incident propagation vector that correspond to the critical values of the transverse wavenumber. The angle of the incident local coordinate system $\Theta_i = 50^\circ$. This example utilizes the double resonance Lorentz model with parameters taken from Table 4.1.2.

$\omega = 302.01\text{THz}$. As Θ_i decreases towards normal incidence, the secondary dip becomes symmetric with the primary dip and a strong near total internal reflection can occur as described by the approximation given in either Eq. (4.3.21b) or Eq. (4.3.21c) depending on the value of k_{u_c} or $k_{u_{c2}}$ relative to $|k_{u_{cy}}|$. These effects are illustrated through the series of plots in Figure 4.3.7 b) and Figure 4.3.8 a) and b). Notice that the effect of near total internal reflection is not maintained over a large span of k_u because, eventually, both of the quantities $\tilde{k}_{i_n}(\omega)$ and $\tilde{k}_{t_n}(\omega)$ represent strong attenuative factors. The reflection coefficient is then described by Eq. (4.3.21d) and near total internal reflection is lost. When $\Theta_i = 0$, the primary near total internal reflection happens when $k_u > k_{u_c}$ and the secondary near total internal

| ω (10^{14} rad/sec) | $k_{u_{max}}$ (10^5 rad/m) | k_{u_c} (10^5 rad/m) | $k_{u_{c2}}$ (10^5 rad/m) | $k_{u_{LS}}$ (10^5 rad/m) | $k_{u_{cy}}$ (10^5 rad/m) |
|----------------------------------|----------------------------------|------------------------------|---------------------------------|---------------------------------|---------------------------------|
| 20.0 | 10.815 | 6.6454 | -11.193 | 10.815 | ± 10.906 |
| 10.0 | 12.528 | 8.0459 | -12.528 | 12.528 | ± 10.906 |
| 0.0 | ∞ | 9.2383 | -9.2383 | ∞ | ± 10.906 |

Table 4.3.4 The critical values of the transverse wavenumber for the frequency 173.79THz. The angle of the incident local coordinate system varies as indicated. This example utilizes the double resonance Lorentz model with parameters taken from Table 4.1.1.

| Θ_i (degrees) | $k_{u_{max}}$ (10^5 rad/m) | k_{u_c} (10^5 rad/m) | $k_{u_{c2}}$ (10^5 rad/m) | $k_{u_{LS}}$ (10^5 rad/m) | $k_{u_{cy}}$ (10^5 rad/m) |
|-------------------------|----------------------------------|------------------------------|---------------------------------|---------------------------------|---------------------------------|
| 20.0 | 17.315 | 11.030 | -17.950 | 17.315 | ± 18.408 |
| 10.0 | 18.197 | 13.422 | -16.926 | 18.197 | ± 18.408 |
| 0.0 | ∞ | 15.407 | -15.407 | ∞ | ± 18.408 |

Table 4.3.5 The critical values of the transverse wavenumber for the frequency 302.01THz. The angle of the incident local coordinate system varies as indicated. This example utilizes the double resonance Lorentz model with parameters taken from Table 4.1.1.

reflection happens when $k_u < k_{u_{c2}}$. The primary near total internal reflection is lost when $k_u > +k_{u_{cy}}$ and the secondary near total internal reflection is lost when $k_u < -k_{u_{cy}}$. This situation is then described by the approximation given in Eq. (4.3.22). Substitution of the double resonance Lorentz model parameters from Table 4.1.1 into Eq. (4.3.22) yields $r_\tau \cong 0.20005$. Some values of the critical transverse wavenumbers for various angles of the incident local coordinate system are tabulated in Table 4.3.4 and Table 4.3.5.

CHAPTER V

Reflection and Transmission of a Pulsed Electromagnetic Beam Field at a Planar Interface Separating Two Lossy Dielectrics

An analysis of pulsed electromagnetic beam field reflection and refraction at a planar interface is examined within a framework of the angular spectrum representation. The results of inhomogeneous plane wave reflection and refraction from Chapter 3, may be applied to each of these inhomogeneous plane waves. Then the inverse spatio-temporal *Fourier-Laplace* transforms are applied to yield the integral equations that represent pulsed electromagnetic beam field reflection and refraction from a planar interface separating two lossy, dispersive dielectrics.

5.1 Angular Spectrum Representation of Pulsed Electromagnetic Beam Fields When the Field is Known at a Planar Boundary Surface

In this section, the angular spectrum representation of pulsed electromagnetic beam fields is developed. The spatio-temporal frequency domain form of *Maxwell's* equations is solved as a set of homogeneous vector *Helmholtz* equations in terms of some known source that generates the electromagnetic fields. Once the solution is derived, it is returned to the space-time domain via the inverse spatio-temporal *Fourier-Laplace* transform. The solution is then referred to as the angular spectrum representation which effectively decomposes the electromagnetic pulsed beam field into a sum of inhomogeneous plane waves, each with its own characteristic complex wavevector. Since each one of the inhomogeneous plane waves of the decomposition is itself a solution to the homogeneous vector *Helmholtz* equations, they can be treated individually in the solution of complex problems and then appropriately superimposed to yield the more general pulsed beam field solution.

In many cases the details that describe the current sources that generate the electromagnetic fields are not explicitly known with exception of the sources which are contained within a region of space, e.g. $|w| \leq W$ in the (u, v, w) rectangular coordinate system. The radiated electromagnetic field is often known on a specified planar boundary surface located beyond the source region, e.g. on the plane $w = \mathcal{W}_0 \cong W$. In this situation, one has a planar boundary value problem for *Maxwell's* equations that is valid in the source-free half space $w > \mathcal{W}_0$ as depicted in Figure 5.1.1. The prescribed planar boundary values act as a pseu-

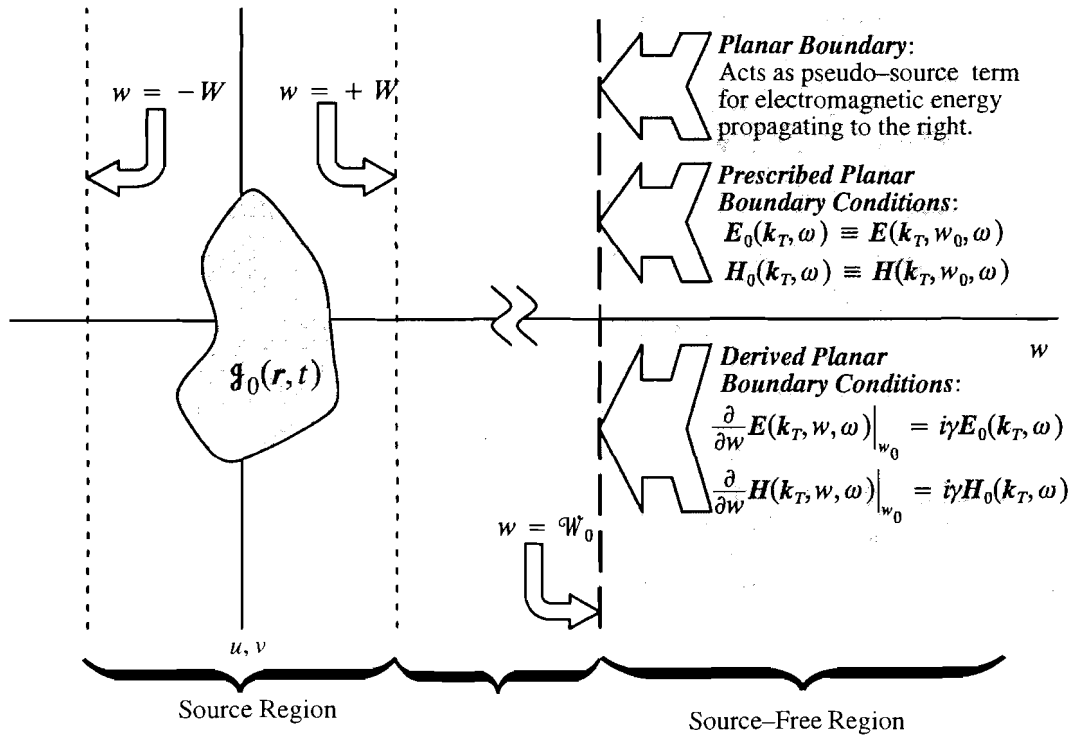


Figure 5.1.1 Schematic diagram of an unknown isolated current source imbedded within the dielectric region $w < |W|$. The current source is solely responsible for the electromagnetic energy propagating in the region $w > |W|$. The electromagnetic field is known on the planar boundary $w = W_0$ which then serves as a pseudo-source term for the *Maxwell's* equations in the source-free half space $w > W_0$.

do-source term which effectively drives the electromagnetic fields. The spatio-temporal frequency domain form of the source free form of *Maxwell's* equations developed in §2.2.5 then applies in the the half space $w \geq W_0$.

For the situation depicted in Figure 5.1.1, let the *position vector* and the *transverse position vector*

$$\mathbf{r} \equiv u\hat{u} + v\hat{v} + w\hat{w}, \quad (5.1.1)$$

$$\mathbf{r}_T \equiv u\hat{u} + v\hat{v}, \quad (5.1.2)$$

be defined in an arbitrarily oriented rectangular coordinate system (u, v, w) with corresponding unit vectors $(\hat{u}, \hat{v}, \hat{w})$. The *complex wavevector* and the *transverse wavevector* are similarly defined with respect to the same coordinate system, respectively, as

$$\mathbf{k} \equiv k_u \hat{\mathbf{u}} + k_v \hat{\mathbf{v}} + k_w \hat{\mathbf{w}}, \quad (5.1.3)$$

$$\mathbf{k}_T \equiv k_u \hat{\mathbf{u}} + k_v \hat{\mathbf{v}}, \quad (5.1.4)$$

where the transverse wavenumbers k_u and k_v are real-valued.

Let the *prescribed boundary conditions* of the pulsed electromagnetic beam field be given in the space-time domain as

$$\mathfrak{E}_0(\mathbf{r}_T, t) = \mathfrak{E}(\mathbf{r}, t)|_{w=\mathcal{W}_0}, \quad (5.1.5a)$$

$$\mathfrak{H}_0(\mathbf{r}_T, t) = \mathfrak{H}(\mathbf{r}, t)|_{w=\mathcal{W}_0}. \quad (5.1.5b)$$

The forward temporal *Fourier-Laplace* and two-dimensional spatial *Fourier* transforms, as defined in Eqs. (2.1.1a) and (2.1.22a) respectively, of these equations yield the prescribed boundary conditions in the mixed space and spatio-temporal frequency domain as

$$\mathbf{E}_0(\mathbf{k}_T, \omega) \equiv \mathbf{E}(\mathbf{k}_T, \mathcal{W}_0, \omega) = \int_{-\infty}^{\infty} \int_{-\infty}^{\infty} \int \mathfrak{E}_0(\mathbf{r}_T, t) e^{+i\omega t - i\mathbf{k}_T \cdot \mathbf{r}_T} du dv dt, \quad (5.1.6a)$$

and

$$\mathbf{H}_0(\mathbf{k}_T, \omega) \equiv \mathbf{H}(\mathbf{k}_T, \mathcal{W}_0, \omega) = \int_{-\infty}^{\infty} \int_{-\infty}^{\infty} \int \mathfrak{H}_0(\mathbf{r}_T, t) e^{+i\omega t - i\mathbf{k}_T \cdot \mathbf{r}_T} du dv dt, \quad (5.1.6b)$$

which will be referred to as the *pseudo-source terms* or *spectral amplitudes*.

The cross product of the complex wavevector $i\mathbf{k}$ with *Faraday's Law* given in Eq. (2.2.37a) yields

$$i\mathbf{k} \times i\mathbf{k} \times \mathbf{E}(\mathbf{k}, \omega) = \left\| \frac{1}{c} \right\| i\omega \mu i\mathbf{k} \times \mathbf{H}(\mathbf{k}, \omega) + i\mathbf{k} \times \hat{\mathbf{w}} \times \mathbf{E}_0(\mathbf{k}_T, \omega) e^{-ik_w \mathcal{W}_0}. \quad (5.1.7)$$

Application of the vector identity $\mathbf{a} \times \mathbf{b} \times \mathbf{c} = (\mathbf{a} \cdot \mathbf{c})\mathbf{b} - (\mathbf{a} \cdot \mathbf{b})\mathbf{c}$ to the left hand side of this equation yields

$$\begin{aligned} i\mathbf{k} \times i\mathbf{k} \times \mathbf{E}(\mathbf{k}, \omega) &= (i\mathbf{k} \cdot \mathbf{E}(\mathbf{k}, \omega))i\mathbf{k} + k^2 \mathbf{E}(\mathbf{k}, \omega) \\ &= ik E_{w_0}(\mathbf{k}_T, \omega) e^{-ik_w \mathcal{W}_0} + k^2 \mathbf{E}(\mathbf{k}, \omega), \end{aligned} \quad (5.1.8)$$

where *Gauss' Law* given in Eq. (2.2.37c) was applied. Here the complex wavenumber k is

defined as

$$k^2 \equiv \mathbf{k} \cdot \mathbf{k} . \quad (5.1.9)$$

A rearrangement of *Ampère's Law* given in Eq. (2.2.37b) results in

$$i\mathbf{k} \times \mathbf{H}(\mathbf{k}, \omega) = -\left\| \frac{1}{c} \right\| i\omega \tilde{\epsilon}(\omega) \mathbf{E}(\mathbf{k}, \omega) + \hat{\mathbf{w}} \times \mathbf{H}_0(\mathbf{k}_T, \omega) e^{-ik_w \mathcal{W}_0} , \quad (5.1.10)$$

where evaluation of *Faraday's Law* given in Eq. (2.2.24a) at the planar boundary yields

$$\mathbf{H}_0(\mathbf{k}_T, \omega) = \left[\frac{\|c\|}{i\omega\mu} \left[i\mathbf{k}_T, \frac{\partial}{\partial w} \hat{\mathbf{w}} \right] \times \mathbf{E}(\mathbf{k}_T, w, \omega) \right] \Big|_{w=\mathcal{W}_0} . \quad (5.1.11)$$

Substitution of Eq. (5.1.11) into *Ampère's Law* given in Eq. (5.1.10) then yields the expression

$$\begin{aligned} & i\mathbf{k} \times \mathbf{H}(\mathbf{k}, \omega) \\ &= -\left\| \frac{1}{c} \right\| i\omega \tilde{\epsilon}(\omega) \mathbf{E}(\mathbf{k}, \omega) + \hat{\mathbf{w}} \times \left[\frac{\|c\|}{i\omega\mu} \left[i\mathbf{k}_T, \frac{\partial}{\partial w} \hat{\mathbf{w}} \right] \times \mathbf{E}(\mathbf{k}_T, w, \omega) \right] \Big|_{w=\mathcal{W}_0} e^{-ik_w \mathcal{W}_0} . \end{aligned} \quad (5.1.12)$$

Substitution of Eqs. (5.1.12) and (5.1.8) into Eq. (5.1.7) then yields the expression

$$\begin{aligned} \mathbf{E}(\mathbf{k}, \omega) = & \\ & \frac{\hat{\mathbf{w}} \times \left[\left[i\mathbf{k}_T, \frac{\partial}{\partial w} \hat{\mathbf{w}} \right] \times \mathbf{E}(\mathbf{k}_T, w, \omega) \right] \Big|_{w=\mathcal{W}_0} + i\mathbf{k} \times \hat{\mathbf{w}} \times \mathbf{E}_0(\mathbf{k}_T, \omega) - ikE_{w_0}(\mathbf{k}_T, \omega)}{k^2 - \tilde{k}^2(\omega)} e^{-ik_w \mathcal{W}_0} , \end{aligned} \quad (5.1.13a)$$

where $E_{w_0}(\mathbf{k}_T, \omega)$ is the $\hat{\mathbf{w}}$ component of the prescribed boundary condition given in Eq. (5.1.6a). While an analogous derivation for the magnetic field vector gives

$$\begin{aligned} \mathbf{H}(\mathbf{k}, \omega) = & \\ & \frac{\hat{\mathbf{w}} \times \left[\left[i\mathbf{k}_T, \frac{\partial}{\partial w} \hat{\mathbf{w}} \right] \times \mathbf{H}(\mathbf{k}_T, w, \omega) \right] \Big|_{w=\mathcal{W}_0} + i\mathbf{k} \times \hat{\mathbf{w}} \times \mathbf{H}_0(\mathbf{k}_T, \omega) - ikH_{w_0}(\mathbf{k}_T, \omega)}{k^2 - \tilde{k}^2(\omega)} e^{-ik_w \mathcal{W}_0} , \end{aligned} \quad (5.1.13b)$$

where $H_{w_0}(\mathbf{k}_T, \omega)$ is the $\hat{\mathbf{w}}$ component of the prescribed boundary condition given in Eq. (5.1.6b). Here

$$\tilde{k}(\omega) \equiv \tilde{n}(\omega)k_0 \quad (5.1.14)$$

is the *complex wavenumber* of the electromagnetic disturbance with angular frequency ω

that is propagating in the medium with *complex refractive index*

$$\tilde{n}(\omega) \equiv \sqrt{\frac{\mu\tilde{\epsilon}(\omega)}{\mu_0\epsilon_0}} , \quad (5.1.15)$$

where $k_0 \equiv \frac{\omega}{c}$ is the vacuum wavenumber and $c \equiv \frac{\|c\|}{\sqrt{\mu_0\epsilon_0}}$ is the vacuum speed of light.

The numerators appearing in Eqs. (5.1.13a,b) may be greatly reduced by using the vector identity $\mathbf{a} \times \mathbf{b} \times \mathbf{c} = (\mathbf{a} \cdot \mathbf{c})\mathbf{b} - (\mathbf{a} \cdot \mathbf{b})\mathbf{c}$. The first term appearing in the numerator of Eq. (5.1.13a) may be expressed as

$$\begin{aligned} \hat{w} \times \left[\left[i\mathbf{k}_T, \frac{\partial}{\partial w} \hat{w} \right] \times \mathbf{E}(\mathbf{k}_T, w, \omega) \right] \Big|_{w=w_0} \\ = \left[i\mathbf{k}_T, \frac{\partial}{\partial w} \hat{w} \right] E_w(\mathbf{k}_T, z, \omega) \Big|_{w=w_0} - \frac{\partial}{\partial w} \mathbf{E}(\mathbf{k}_T, w, \omega) \Big|_{w=w_0} \end{aligned} \quad (5.1.16)$$

while the second term may be expressed as

$$i\mathbf{k} \times \hat{w} \times \mathbf{E}_0(\mathbf{k}_T, \omega) = [i\mathbf{k} \cdot \mathbf{E}_0(\mathbf{k}_T, \omega)]\hat{w} - ik_w \mathbf{E}_0(\mathbf{k}_T, \omega) . \quad (5.1.17)$$

Notice that the second terms appearing on the right hand sides of the above two equations will be the only terms remaining after they are combined with the third term appearing in the numerator of Eq. (5.1.13a). This fact is best illustrated by expanding these terms in component form as

$$\begin{aligned} \left[i\mathbf{k}_T, \frac{\partial}{\partial w} \hat{w} \right] E_w(\mathbf{k}_T, w, \omega) \Big|_{w=w_0} \\ = ik_u E_{w_0}(\mathbf{k}_T, \omega) \hat{u} + ik_v E_{w_0}(\mathbf{k}_T, \omega) \hat{v} + \frac{\partial}{\partial w} E_w(\mathbf{k}_T, w, \omega) \Big|_{w=w_0} \hat{w} , \end{aligned}$$

$$[i\mathbf{k} \cdot \mathbf{E}_0(\mathbf{k}_T, \omega)]\hat{w} = ik_u E_{u_0}(\mathbf{k}_T, \omega) \hat{u} + ik_v E_{v_0}(\mathbf{k}_T, \omega) \hat{v} + ik_w E_{w_0}(\mathbf{k}_T, \omega) \hat{w} ,$$

$$-ik \mathbf{E}_{w_0}(\mathbf{k}_T, \omega) = -ik_u E_{w_0}(\mathbf{k}_T, \omega) \hat{u} - ik_v E_{w_0}(\mathbf{k}_T, \omega) \hat{v} - ik_w E_{w_0}(\mathbf{k}_T, \omega) \hat{w} ,$$

which, when summed, yield

$$\begin{aligned}
& \left[ik_T \frac{\partial}{\partial w} \hat{w} \right] E_w(\mathbf{k}_T, w, \omega) \Big|_{w=\mathcal{W}_0} + \left[i\mathbf{k} \cdot \mathbf{E}_0(\mathbf{k}_T, \omega) \right] \hat{w} - ik E_{w_0}(\mathbf{k}_T, \omega) \\
& = ik_u E_{u_0}(\mathbf{k}_T, \omega) \hat{u} + ik_v E_{v_0}(\mathbf{k}_T, \omega) \hat{v} + \frac{\partial}{\partial w} E_w(\mathbf{k}_T, w, \omega) \Big|_{w=\mathcal{W}_0} \hat{w} \\
& = \left[ik_T \frac{\partial}{\partial w} \hat{w} \right] \cdot \mathbf{E}(\mathbf{k}_T, w, \omega) \Big|_{w=\mathcal{W}_0} .
\end{aligned}$$

This identically vanishes by virtue of the mixed space and spatio-temporal frequency domain version of *Gauss' Law* given in Eq. (2.2.24c) evaluated at the pseudo-source planar boundary, viz.

$$\left[ik_T \frac{\partial}{\partial w} \hat{w} \right] \cdot \mathbf{D}(\mathbf{k}_T, w, \omega) \Big|_{w=\mathcal{W}_0} = 0 . \quad (5.1.18)$$

This simplification reduces Eq. (5.1.13a) to

$$\mathbf{E}(\mathbf{k}, \omega) = - \frac{\frac{\partial}{\partial w} \mathbf{E}(\mathbf{k}_T, w, \omega) \Big|_{w=\mathcal{W}_0} + ik_w \mathbf{E}_0(\mathbf{k}_T, \omega)}{k^2 - \tilde{k}^2(\omega)} e^{-ik_w \mathcal{W}_0} . \quad (5.1.19)$$

An analogous simplification for the magnetic field vector given in Eq. (5.1.13b) yields

$$\mathbf{H}(\mathbf{k}, \omega) = - \frac{\frac{\partial}{\partial w} \mathbf{H}(\mathbf{k}_T, w, \omega) \Big|_{w=\mathcal{W}_0} + ik_w \mathbf{H}_0(\mathbf{k}_T, \omega)}{k^2 - \tilde{k}^2(\omega)} e^{-ik_w \mathcal{W}_0} . \quad (5.1.20)$$

The solution of the homogeneous vector *Helmholtz* equation for the electric field intensity vector in terms of the pseudo-source term $\mathbf{E}_0(\mathbf{k}_T, \omega)$ is now derived. The inverse one-sided spatial *Laplace* transform with respect to the w dimension as defined in Eq. (2.1.26b) operates on the electric fields vector $\mathbf{E}(\mathbf{k}, \omega)$ given in Eq. (5.1.19) to yield

$$\mathbf{E}(\mathbf{k}_T, w, \omega) \equiv \mathcal{L}^{-1}[\mathbf{E}(\mathbf{k}, \omega)] = \frac{1}{2\pi} \int_C \mathbf{E}(\mathbf{k}, \omega) e^{+ik_w w} dk_w . \quad (5.1.21)$$

The contour of integration C appearing in this equation denotes the *Bromwich contour* which is the straight line path from $k_w = -\infty + ia$ to $k_w = \infty + ia$, with a being a real constant that lies within the region of convergence. Due to the $e^{-ik_w \mathcal{W}_0}$ term in Eq. (5.1.19), the inverse

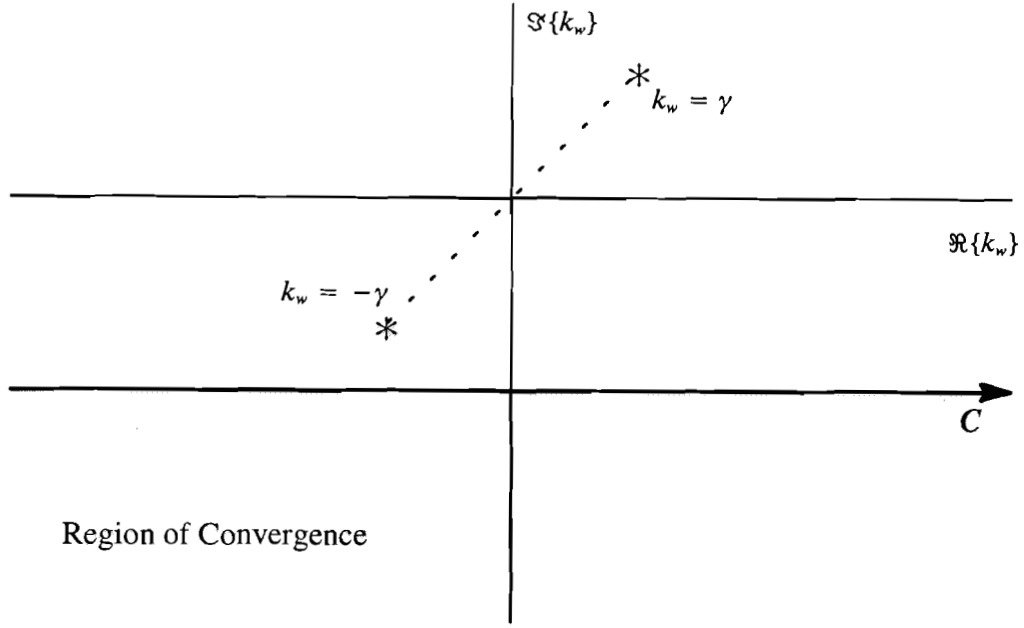


Figure 5.1.2 The contour of integration in the complex k_w -plane. The shaded region indicates the Region of Convergence.

one-sided spatial *Laplace* transform can be rewritten as

$$\mathbf{E}(\mathbf{k}_T, w, \omega) \equiv \mathcal{L}^{-1}\{\mathbf{E}(\mathbf{k}, \omega)\} = \frac{1}{2\pi} \int_C \mathbf{E}'(\mathbf{k}, \omega) e^{+ik_w(w - w_0)} dk_w, \quad (5.1.22a)$$

where

$$\mathbf{E}'(\mathbf{k}, \omega) \equiv - \frac{\frac{\partial}{\partial w} \mathbf{E}(\mathbf{k}_T, w, \omega) \Big|_{w=w_0} + ik_w \mathbf{E}_0(\mathbf{k}_T, \omega)}{k^2 - \tilde{k}^2(\omega)}. \quad (5.1.22b)$$

The numerator of Eq. (5.1.22b) is a polynomial of degree one with respect to the integration variable k_w , and is therefore an entire function or regular in the entire complex plane. The denominator of Eq. (5.1.22b) is a polynomial of degree two with respect to the integration variable k_w and is also an entire function. These two facts mean that any singularities of the integrand must be due to any zeros of the denominator which are located where

$$k^2 - \tilde{k}^2(\omega) = 0.$$

Hence Eq. (5.1.19) has two simple poles located whenever k_w satisfies

$$k_w = \pm \left(\tilde{k}^2(\omega) - k_T^2 \right)^{1/2}. \quad (5.1.23)$$

This is a multivalued function where the domain of the square root is defined on a *Riemann surface* that consists of two sheets joined together at the branch cut¹⁹ and where $k_T^2 \equiv k_u^2 + k_v^2$. The location of these simple poles determines the region of convergence since, by definition, a one-sided *Laplace* transform must be regular in the entire region below the abscissa of absolute convergence. Therefore the pole with the smallest imaginary part determines the abscissa of absolute convergence. Let the *longitudinal complex wave-number* γ be defined as the principle branch of the expression

$$\gamma \equiv \left(\tilde{k}^2(\omega) - k_T^2 \right)^{1/2},$$

where branch cut in the domain of the square root is defined on the positive real axis. Let the first *Riemann sheet* be defined as

$$\tilde{k}^2(\omega) - k_T^2 = \Gamma e^{i\theta} \quad ; \quad 0 \leq \theta < 2\pi, \quad (5.1.24)$$

where Γ is a positive real-valued quantity, and when substituted into the previous expression yields

$$\gamma \equiv \sqrt{\Gamma} e^{i\frac{\theta}{2}} \quad ; \quad 0 \leq \frac{\theta}{2} < \pi. \quad (5.1.25)$$

The valid angular range in Eq. (5.1.25) causes $\Im\{\gamma\} \geq 0$, which restricts the pole located at $k_w = \gamma$ to the upper half of the complex k_w -plane, and similarly restricts the pole located at $k_w = -\gamma$ to the lower half. Therefore, the upper abscissa of absolute convergence is $\gamma_b = -\Re\{\gamma\}$ and the region of convergence is $-\infty < \Re\{k_w\} < \gamma_b$. Figure 5.1.2 depicts the complex plane of integration and the simple pole locations for the present case where the shaded region indicates the region of convergence. As long as the *Bromwich contour* C re-

19. See LePage [62] §6-2 pp. 170-174.

mains within this region, the integral Eq. (5.1.22a) is convergent and uniquely determines $E(\mathbf{k}_T, \omega, \omega)$ [62].

Since Eq. (5.1.22b) is a rational function with respect to the integration variable k_w for which the degree of the numerator is less than the degree of the denominator, then

$$\lim_{|k_w| \rightarrow \infty} \{E(\mathbf{k}, \omega)\} = 0 \quad \forall \arg\{k_w\} , \quad (5.1.26)$$

uniformly with respect to $\arg\{k_w\}$ where $\arg\{\}$ denotes the argument or phase of the complex quantity appearing in the braces $\{\}$ ²⁰. *Jordan's lemma* then applies by virtue of condition given in Eq. (5.1.26) which means that the integration of Eq. (5.1.21) vanishes along the semicircle C_+ of radius $R \rightarrow \infty$ in the upper half plane if $\omega > \mathcal{W}_0$, and vanishes along the semicircle C_- of radius $R \rightarrow \infty$ in the lower half plane if $\omega < \mathcal{W}_0$. This fact allows the integration along the original *Bromwich contour* C to be equated with integration around either closed path $C + C_{\pm}$ as the semicircle's radius $R \rightarrow \infty$ (where either C_+ or C_- is used depending on the sign of the quantity $\omega - \mathcal{W}_0$). Each closed path $C + C_{\pm}$ facilitates the evaluation of the inverse one-sided transform Eq. (5.1.21) by virtue of the *Cauchy's Residue Theorem*[71]²¹. Both paths are illustrated in Figure 5.1.3.

The inverse *Laplace* transform Eq. (5.1.22a), for the positive half-space $\omega > \mathcal{W}_0$, is due to the two pole contributions at $k_w = \gamma$ and $k_w = -\gamma$ which are encircled by the closed path $C + C_+$. Since

$$k^2 - \tilde{k}^2(\omega) = (k_w - \gamma)(k_w + \gamma) , \quad (5.1.27)$$

application of *Cauchy's Residue Theorem* then yields

20. See LePage [62] §10–20 pp. 324–326, *Theorem* 10–11.

21. See LePage [62] §10–19.

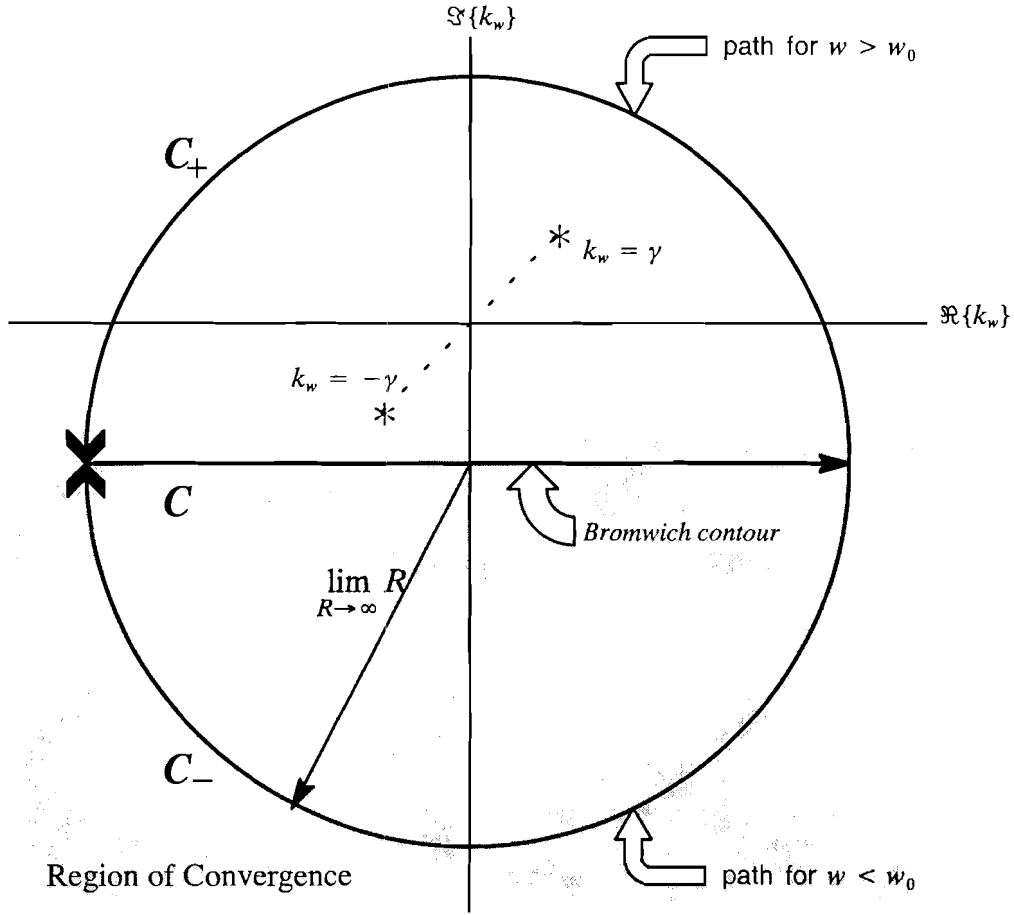


Figure 5.1.3 Construction of the closed path of integration in the complex k_w -plane.

$$E(\mathbf{k}_T, w, \omega) = -i \left\{ \frac{\left. \frac{\partial}{\partial z} E(\mathbf{k}_T, w, \omega) \right|_{w=\mathcal{W}_0} + i\gamma E_0(\mathbf{k}_T, \omega)}{2\gamma} e^{i\gamma(w-\mathcal{W}_0)} - \frac{\left. \frac{\partial}{\partial z} E(\mathbf{k}_T, w, \omega) \right|_{w=\mathcal{W}_0} - i\gamma E_0(\mathbf{k}_T, \omega)}{2\gamma} e^{-i\gamma(w-\mathcal{W}_0)} \right\}, \quad (5.1.28)$$

for $w > \mathcal{W}_0$. The inverse *Laplace* transform of Eq. (5.1.22a) for the negative half-space $w < \mathcal{W}_0$, vanishes because the closed path $C + C_-$ does not encircle any poles. Application of *Cauchy's Residue Theorem* then yields

$$E(\mathbf{k}_T, w, \omega) = 0 \quad (5.1.29)$$

for $w < \mathcal{W}_0$.

Within the positive half-space to the right of the pseudo-source boundary $w > \mathcal{W}_0$ each inhomogeneous plane wave must decay in the positive \hat{w} direction so that the solution remains bounded in that half-space. Inhomogeneous plane waves are guaranteed to decay in the positive \hat{w} direction for the exponential factor $e^{i\gamma(w-\mathcal{W}_0)}$ based on the angular range given in Eq. (5.1.25). However, Eq. (5.1.28) also contains the unbounded $e^{-i\gamma(w-\mathcal{W}_0)}$ exponential factor. Therefore, to eliminate the unbounded exponential factor, the following auxiliary boundary conditions must be applied:

$$\left. \frac{\partial}{\partial w} \mathbf{E}(\mathbf{k}_T, w, \omega) \right|_{w=\mathcal{W}_0} = i\gamma \mathbf{E}_0(\mathbf{k}_T, \omega) , \quad (5.1.30a)$$

$$\left. \frac{\partial}{\partial w} \mathbf{H}(\mathbf{k}_T, w, \omega) \right|_{w=\mathcal{W}_0} = i\gamma \mathbf{H}_0(\mathbf{k}_T, \omega) . \quad (5.1.30b)$$

These conditions are equivalent to defining a secondary boundary condition for the field at the pseudo-source boundary. Substitution of the auxiliary boundary condition given in Eq. (5.1.30a) into Eq. (5.1.28) then yields[59]

$$\mathbf{E}(\mathbf{k}_T, w, \omega) = \mathbf{E}_0(\mathbf{k}_T, \omega) e^{i\gamma(w-\mathcal{W}_0)} , \quad \text{for } w > \mathcal{W}_0 , \quad (5.1.31)$$

and similarly for the magnetic field vector one obtains[59]

$$\mathbf{H}(\mathbf{k}_T, w, \omega) = \mathbf{H}_0(\mathbf{k}_T, \omega) e^{i\gamma(w-\mathcal{W}_0)} , \quad \text{for } w > \mathcal{W}_0 . \quad (5.1.32)$$

The space-time domain form of the electric and magnetic field intensity vectors is obtained by applying the inverse two dimensional spatial *Laplace* and temporal *Fourier-Laplace* transforms, as defined by Eqs. (2.1.22b) and (2.1.1b) respectively, which are rewritten here as

$$\mathfrak{E}(\mathbf{r}, t) = \frac{1}{(2\pi)^3} \int_{C_\omega} d\omega e^{-i\omega t} \int_{-\infty}^{\infty} \int_{-\infty}^{\infty} \mathbf{E}(\mathbf{k}_T, w, \omega) e^{i\mathbf{k}_T \cdot \mathbf{r}_T} dk_u dk_v , \quad (5.1.33a)$$

$$\mathfrak{H}(\mathbf{r}, t) = \frac{1}{(2\pi)^3} \int_{C_\omega} d\omega e^{-i\omega t} \int_{-\infty}^{\infty} \int_{-\infty}^{\infty} \mathbf{H}(\mathbf{k}_T, w, \omega) e^{i\mathbf{k}_T \cdot \mathbf{r}_T} dk_u dk_v , \quad (5.1.33b)$$

The *angular spectrum representation* of the pulsed electromagnetic beam field is then obtained by substituting Eqs. (5.1.31) and (5.1.32) into the above expressions, with the result

$$\mathfrak{E}(\mathbf{r}, t) = \frac{1}{(2\pi)^3} \int_{C_\omega} d\omega e^{-i\omega t} \int_{-\infty}^{\infty} \int_{-\infty}^{\infty} \mathbf{E}_0(\mathbf{k}_T, \omega) e^{i\gamma(\omega - \mathcal{W}_0)} e^{i\mathbf{k}_T \cdot \mathbf{r}_T} dk_u dk_v, \quad (5.1.34a)$$

$$\mathfrak{H}(\mathbf{r}, t) = \frac{1}{(2\pi)^3} \int_{C_\omega} d\omega e^{-i\omega t} \int_{-\infty}^{\infty} \int_{-\infty}^{\infty} \mathbf{H}_0(\mathbf{k}_T, \omega) e^{i\gamma(\omega - \mathcal{W}_0)} e^{i\mathbf{k}_T \cdot \mathbf{r}_T} dk_u dk_v, \quad (5.1.34b)$$

for $\omega > \mathcal{W}_0 \geq W$ [59]. The integrands of Eqs. (5.1.34a,b) are inhomogeneous plane waves with *spectral amplitudes* $\mathbf{E}_0(\mathbf{k}_T, \omega)$ and $\mathbf{H}_0(\mathbf{k}_T, \omega)$ respectively, with forward *complex wavevector* [cf. §2.5]

$$\tilde{\mathbf{k}}(\omega) \equiv k_u \hat{u} + k_v \hat{v} + \gamma(\omega) \hat{w}, \quad (5.1.35)$$

where $\tilde{\mathbf{k}}$ is constrained the relation

$$\tilde{\mathbf{k}} \cdot \tilde{\mathbf{k}} = \tilde{k}^2(\omega) = \tilde{n}^2(\omega) k_0^2, \quad (5.1.36)$$

where $\tilde{k}(\omega)$ is the complex wavenumber as previously defined in Eq. (5.1.14). As a result of Eq. (5.1.36), the longitudinal complex wavenumber $\gamma(\omega)$ given in Eq. (5.1.25) is a function of the real-valued transverse wavenumbers k_u and k_v and of the angular frequency ω .

If the electromagnetic fields were specified on a planar boundary on the opposite side of the true current source $-\mathcal{W}_0 \leq -W$, then all of the former analysis would result in angular spectrum representations identical to Eqs. (5.1.34a,b) valid in the negative half-space region $\omega < -\mathcal{W}_0 \leq -W$ when the following is substituted for $\tilde{\mathbf{k}}$

$$\tilde{\mathbf{k}}^-(\omega) \equiv k_u \hat{u} + k_v \hat{v} - \gamma(\omega) \hat{w}. \quad (5.1.37)$$

Let the complex wave vector be defined in terms of two real vector quantities [cf. § 2.5] as

$$\tilde{\mathbf{k}}(\omega) \equiv \boldsymbol{\beta}(\omega) + i\boldsymbol{\alpha}(\omega) .$$

Here the *propagation vector* $\boldsymbol{\beta}(\omega) \equiv \Re\{\tilde{\mathbf{k}}(\omega)\}$ specifies the direction of propagation of the planar phase front while the *attenuation vector* $\boldsymbol{\alpha}(\omega) \equiv \Im\{\tilde{\mathbf{k}}(\omega)\}$ specifies the direction of propagation of the planar amplitude front. The propagation vector $\boldsymbol{\beta}(\omega)$ is normal to the surfaces of constant phase such that

$$\boldsymbol{\beta}(\omega) \cdot \mathbf{r} = \text{constant} ,$$

while the attenuation vector $\boldsymbol{\alpha}(\omega)$ is normal to the surfaces of constant amplitude such that

$$\boldsymbol{\alpha}(\omega) \cdot \mathbf{r} = \text{constant} .$$

The propagation vector may be written as

$$\boldsymbol{\beta}(\omega) \equiv k_u \hat{u} + k_v \hat{v} + \Re\{\gamma(\omega)\} \hat{w} \quad (5.1.38)$$

and the attenuation vector may be written as

$$\boldsymbol{\alpha}(\omega) \equiv \Im\{\gamma(\omega)\} \hat{w} \quad (5.1.39)$$

which are both illustrated in Figure 2.5.2. Thus, the inhomogeneous plane waves that comprise the angular spectrum representation of the radiation field only decay in the \hat{w} direction. This is merely a consequence of the imposed dependency of the k_w integration and has no real physical interpretation[59]. Further, the direction cosine representation developed in §2.5.2 is seen to directly apply to the angular spectrum representation of the electromagnetic field.

Assuming for the moment that the frequency ω is real-valued, the complex range of the longitudinal wavenumber $\gamma(\omega)$ given in Eq. (5.1.25) divides into two regions depending on the sign of the frequency [cf. Eq. (2.5.20)] as

$$\gamma = \sqrt{\Gamma} e^{i\frac{\theta}{2}} \quad ; \quad \begin{cases} 0 \leq \frac{\theta}{2} < \frac{\pi}{2} & , \forall \omega' > 0 \\ \frac{\pi}{2} \leq \frac{\theta}{2} < \pi & , \forall \omega' < 0 \end{cases} \quad (5.1.40)$$

which are both illustrated in Figure 5.1.4. As shown in §2.5, the surfaces of constant phase

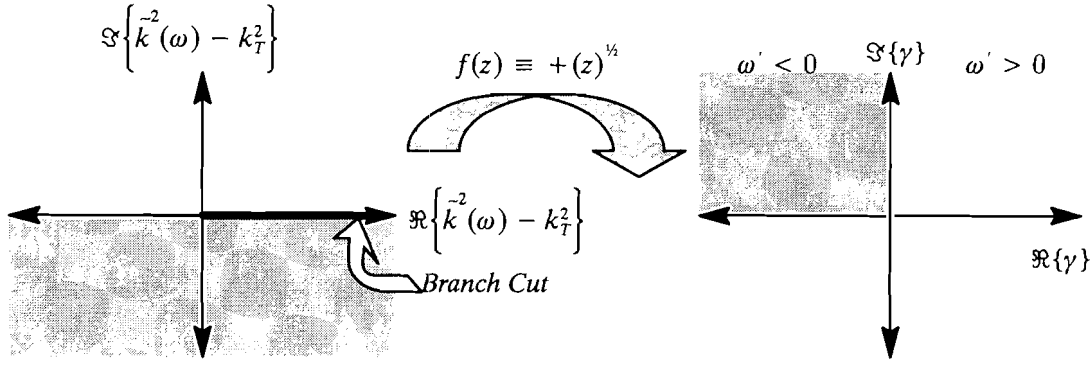


Figure 5.1.4 The first sheet of the *Riemann surface* and the range of the longitudinal wavenumber γ given that the imaginary part of the frequency $a = 0$. The sheet divides into two distinct regions depending on the sign of the real-valued angular frequency ω' as indicated by the differently shaded areas.

propagate along the positive \hat{w} -axis as a consequence of Eq. (5.1.40), regardless of the sign of the frequency ω .

This result is based on the assumption that the angular frequency ω is real-valued. If this condition cannot be met because of a positive abscissa of absolute convergence for a particular radiation problem, one can always split the ω -integration given in Eqs. (5.1.34a,b) into two parts. Let the angular frequency $\omega = \omega' + ia$ where $\omega' = \Re\{\omega\}$ and $a = \Im\{\omega\}$. The ω -integration can be broken into the two parts $a \leq \omega' < \infty$ and $-\infty < \omega' \leq -a$, then taken to the limit $a \rightarrow 0$ after completion of the integration[59]. In either event, the inequality given in Eq. (5.1.40) is assumed to be satisfied while evaluating the k_w -integration of Eq. (5.1.22) so that $\tilde{\mathbf{k}}$ can be appropriately labeled as the forward propagation vector.

5.2 Reflection and Refraction of a Pulsed Electromagnetic Beam Field at a Planar Interface Separating Two Lossy Dielectrics

The results presented here are concise integral expressions that describe pulsed electromagnetic beam fields incident upon a planar interface separating two lossy, dispersive dielectric half-spaces. They are achieved by simply applying the inverse *Fourier-Laplace* and two-dimensional spatial *Fourier* transforms to the angular spectrum representations of re-

flected and refracted pulsed beam fields. Some of the material from §3.1 is repeated here for completeness because the design of this problem is similar.

The incident and transmission dielectric media are described by the frequency dependant complex refractive indexes

$$\tilde{n}_1(\omega) \equiv \sqrt{\frac{\mu\tilde{\epsilon}_1(\omega)}{\mu_0\epsilon_0}} , \quad (5.2.1)$$

and

$$\tilde{n}_2(\omega) \equiv \sqrt{\frac{\mu\tilde{\epsilon}_2(\omega)}{\mu_0\epsilon_0}} , \quad (5.2.2)$$

respectively. The interface coordinate system is the standard rectangular x, y, z coordinate system with corresponding unit vectors $(\hat{\tau}, \hat{\nu}, \hat{n})$ chosen to delineate the tangential and normal components of the field vectors with respect to the interface.. The xy plane (i.e. where $z = 0$) defines the separation between the two media and therefore represents the interface. The xz plane defines the *reference plane* containing the incident attenuation vector and the normal vector to the interface. With this choice, the in-plane tangential component is in the $\hat{\tau}$ direction, the out of plane tangential component is in the $\hat{\nu}$ direction, and the normal component is in the \hat{n} direction for any given field vector with respect to the interface coordinate system, as illustrated in Figure 5.2.1.

The orientation of the incident pulsed electromagnetic beam field is defined in the *incident local rectangular u, v, w coordinate system* with corresponding unit vectors $(\hat{u}, \hat{v}, \hat{w})$.

The *incident position vector* \mathbf{r}_i is given by

$$\mathbf{r}_i \equiv u\hat{u} + v\hat{v} + w\hat{w} . \quad (5.2.3)$$

The incident pulsed electromagnetic beam field vectors defined in the incident local coordinate system are given by the following angular spectrum representations [cf. Eqs. (5.1.34a,b)]

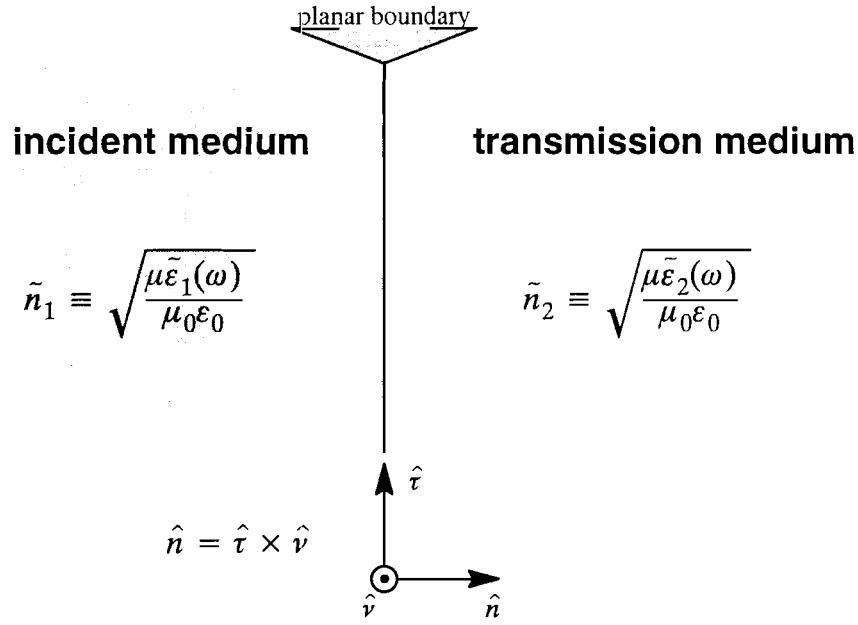


Figure 5.2.1 Planar interface separating two lossy, dispersive half spaces with complex refractive indexes n_1 for the incident medium and n_2 for the transmission medium.

$$\mathfrak{S}_i(\mathbf{r}, t) = \frac{1}{(2\pi)^3} \int_{\mathcal{C}_\omega} d\omega e^{-i\omega t} \int_{-\infty}^{\infty} \int_{-\infty}^{\infty} \mathbf{E}_i(\mathbf{k}_T, \omega) e^{i\bar{\mathbf{k}}_i(\omega) \cdot \mathbf{r}} dk_u dk_v, \quad (5.2.4a)$$

$$\mathfrak{H}_i(\mathbf{r}, t) = \frac{1}{(2\pi)^3} \int_{\mathcal{C}_\omega} d\omega e^{-i\omega t} \int_{-\infty}^{\infty} \int_{-\infty}^{\infty} \mathbf{H}_i(\mathbf{k}_T, \omega) e^{i\bar{\mathbf{k}}_i(\omega) \cdot \mathbf{r}} dk_u dk_v, \quad (5.2.4b)$$

where the *incident spectral amplitudes* are defined on the boundary plane $w = \mathcal{W}_0 = 0$ [cf. Eqs. (5.1.6a,b)] as

$$\mathbf{E}_i(\mathbf{k}_T, \omega) = \mathbf{E}_i(\mathbf{k}_T, w, \omega)|_{w=0} = \int_{-\infty}^{\infty} \int_{-\infty}^{\infty} \int_{-\infty}^{\infty} \mathfrak{S}_0(\mathbf{r}_T, t) e^{+i\omega t - i\mathbf{k}_T \cdot \mathbf{r}_T} dudvdt, \quad (5.2.5a)$$

$$\mathbf{H}_i(\mathbf{k}_T, \omega) = \mathbf{H}_i(\mathbf{k}_T, w, \omega)|_{w=0} = \int_{-\infty}^{\infty} \int_{-\infty}^{\infty} \int_{-\infty}^{\infty} \mathfrak{H}_0(\mathbf{r}_T, t) e^{+i\omega t - i\mathbf{k}_T \cdot \mathbf{r}_T} dudvdt, \quad (5.2.5b)$$

where $\mathfrak{S}_0(\mathbf{r}_T, t)$ and $\mathfrak{H}_0(\mathbf{r}_T, t)$ are the prescribed boundary values given in Eqs. (5.1.5a,b).

The *incident inhomogeneous plane wave spectra*

$$\mathbf{E}_i(\mathbf{k}_T, \omega) e^{i\tilde{\mathbf{k}}_i(\omega) \cdot \mathbf{r}} , \quad (5.2.6a)$$

$$\mathbf{H}_i(\mathbf{k}_T, \omega) e^{i\tilde{\mathbf{k}}_i(\omega) \cdot \mathbf{r}} , \quad (5.2.6b)$$

satisfy the homogeneous vector *Helmholtz* Eqs. (2.5.2a,b) and are defined only in the incident medium (i.e. for $z \leq 0$). The *incident complex wavevector* $\tilde{\mathbf{k}}_i(\omega)$ satisfies the relation [cf. Eq. (2.5.12)]

$$\tilde{\mathbf{k}}_i(\omega) \cdot \tilde{\mathbf{k}}_i(\omega) \equiv \tilde{k}_1^2(\omega) , \quad (5.2.7)$$

where

$$\tilde{k}_1(\omega) \equiv \tilde{n}_1(\omega) k_0 , \quad (5.2.8)$$

and $\tilde{n}_1(\omega)$ is given by Eq. (3.1.1). Here $k_0 \equiv \frac{\omega}{c}$ is the vacuum wavenumber. In general, the frequency $\omega \equiv \omega' + ia$ is complex, where ω' and a are both real-valued. As mentioned at the end of §5.1 it is assumed that $a = 0$ whenever possible otherwise the limit $a \rightarrow 0$ will be taken after completion of the integration.

The incident complex wavevector is defined within the incident local coordinate system [cf. Eq. (5.1.35)] as

$$\tilde{\mathbf{k}}_i(\omega) \equiv k_u \hat{\mathbf{u}} + k_v \hat{\mathbf{v}} + \gamma_i(\omega) \hat{\mathbf{w}} , \quad (5.2.9)$$

where the incident longitudinal complex wavenumber is defined as

$$\gamma_i(\omega) \equiv \left(\tilde{k}_1^2(\omega) - k_T^2 \right)^{1/2} , \quad (5.2.10)$$

where the branch cut of the domain of the square root is defined as the positive real axis and $k_T^2 \equiv k_u^2 + k_v^2$. Let the incident complex wavevector be defined in terms of two real vector quantities as $\tilde{\mathbf{k}}_i(\omega) \equiv \boldsymbol{\beta}_i(\omega) + i\boldsymbol{\alpha}_i(\omega)$. Here the *incident propagation vector* $\boldsymbol{\beta}_i(\omega) \equiv \Re\{\tilde{\mathbf{k}}_i(\omega)\}$ specifies the direction of propagation of the planar phase front while the *incident attenuation vector* $\boldsymbol{\alpha}_i(\omega) \equiv \Im\{\tilde{\mathbf{k}}_i(\omega)\}$ specifies the direction of propagation of the

planar amplitude front. The incident propagation vector equates to

$$\boldsymbol{\beta}_i(\omega) \equiv k_u \hat{u} + k_v \hat{v} + \Re\{\gamma_i(\omega)\} \hat{w} , \quad (5.2.11)$$

and the incident attenuation vector equates to

$$\boldsymbol{\alpha}_i(\omega) \equiv + \Im\{\gamma_i(\omega)\} \hat{w} . \quad (5.2.12)$$

The complex components of the incident complex wavevector are presented and defined in matrix form while in the incident local coordinate system as

$$\tilde{\mathbf{k}}_i(\omega) \equiv \begin{bmatrix} k_u \\ k_v \\ \gamma_i(\omega) \end{bmatrix} . \quad (5.2.13)$$

In this problem the incident local unit vector \hat{w} is directed towards the interface and is defined to make an angle Θ_i with respect to the interface normal \hat{n} . The origin of the incident local coordinate system is situated the distance w_0 away from the interface along the w -coordinate axis as illustrated in Figure 3.1.3. The angle Θ_i is confined to the quadrant

$$0 \leq \Theta_i < \frac{\pi}{2} . \quad (5.2.14)$$

The transverse unit vector \hat{v} is then chosen to coincide with the out of plane tangential unit vector \hat{v} of the interface coordinate system. The origin of the interface x, y, z coordinate system is defined as the point where the w -axis of the incident local coordinate system intersects the interface as depicted in Figure 5.2.2.

The resultant reflected and refracted fields are defined in their own local coordinate systems in an analogous manner to the incident field. The reflected field is defined in the *reflected local rectangular u', v', w' coordinate system* with corresponding unit vectors $(\hat{u}', \hat{v}', \hat{w}')$. The unit vector \hat{w}' is directed away from the interface and defined to make an angle $\pi - \Theta_r$ with respect to the interface normal \hat{n} . The origin of the reflected local coordinate system is situated the distance w'_0 away from the interface along the w' -coordinate axis and lies in the incident medium. The w' -axis intersects the interface at the interface's origin.

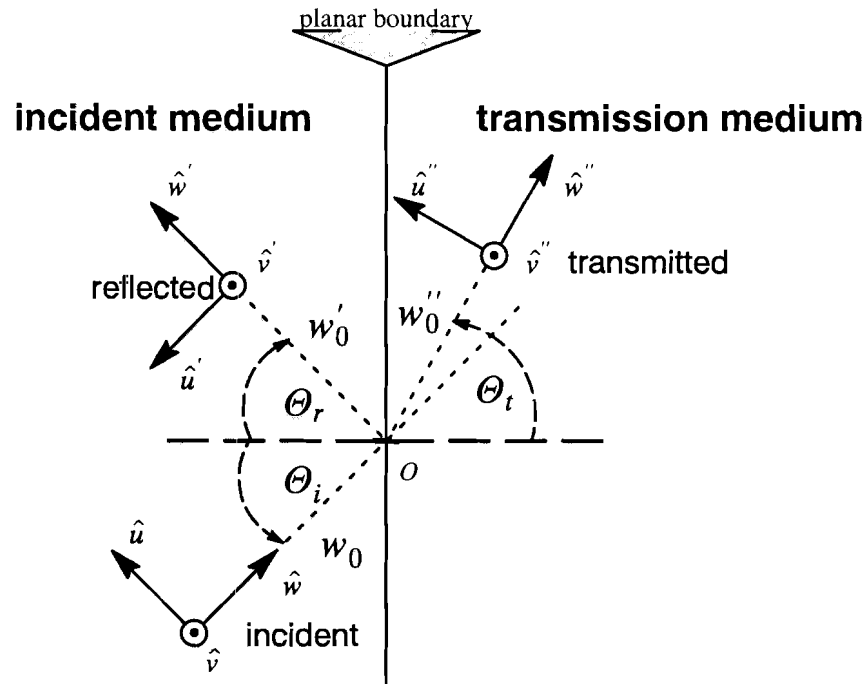


Figure 5.2.2 The incident, reflected and transmitted fields and complex wavevectors are defined on their respective incident, reflected and transmitted local coordinate systems. The w -axis, w' -axis and the w'' -axis are defined to make angles Θ_i , $\pi - \Theta_r$ and Θ_t , respectively with respect to the interface normal.

The refracted field is defined in the *transmitted local rectangular u'' , v'' , w'' coordinate system* with corresponding unit vectors $(\hat{u}'', \hat{v}'', \hat{w}'')$. The unit vector \hat{w}'' is directed away from the interface, and defined to make an angle Θ_t with respect to the interface normal \hat{n} . The origin of the transmitted local coordinate system is situated the distance w_0'' away from the interface along the w'' -coordinate axis and lies in the transmitted medium. The w'' -axis intersects the interface at the interface's origin. The out of plane local unit vectors \hat{v}' and \hat{v}'' are oriented parallel to the unit vector \hat{v} . This situation is depicted in Figure 5.2.2.

Following the development of §3.2, defining $\Theta_r = \Theta_i$ intuitively makes sense based on the spherical component relations of the generalized laws of reflection given in Eqs. (3.1.111c). Let the angle of the transmitted local coordinate system Θ_t be the angle

$\Theta_t = \theta_t^a|_{k_u=k_v=0}$, i.e. the refracted angle of the attenuation vector for an incident homogeneous plane wave.

The *reflected position vector* is given by

$$\mathbf{r}_r \equiv u' \hat{u}' + v' \hat{v}' + w' \hat{w}' . \quad (5.2.15)$$

As a result of the generalized law of reflection, the reflected complex wavevector within the reflected local coordinate system in terms of the given wavenumbers k_u and k_v is given by [cf. Eq. (3.2.1)]

$$\tilde{\mathbf{k}}_r(\omega) = \begin{bmatrix} \tilde{k}_{r_u}(\omega) \\ \beta_{r_v} \\ \tilde{k}_{r_w}(\omega) \end{bmatrix} = \begin{bmatrix} -k_u \\ k_v \\ \gamma_i(\omega) \end{bmatrix} . \quad (5.2.16)$$

The *transmitted position vector* is given by

$$\mathbf{r}_t \equiv u'' \hat{u}'' + v'' \hat{v}'' + w'' \hat{w}'' . \quad (5.2.17)$$

As a result of the generalized law of refraction, the transmitted complex wavevector within the transmitted local coordinate system in terms of the given wavenumbers k_u and k_v is given by [cf. Eq. (3.2.2)]

$$\tilde{\mathbf{k}}_t(\omega) = \begin{bmatrix} \tilde{k}_{t_u}(\omega) \\ \beta_{t_v} \\ \tilde{k}_{t_w}(\omega) \end{bmatrix} = \overset{\leftrightarrow}{\mathbf{R}}_{ot_t}^T \begin{bmatrix} k_u \cos \Theta_i + \gamma_i(\omega) \sin \Theta_i \\ k_v \\ \left[k_2^2(\omega) - (k_u \cos \Theta_i + \gamma_i(\omega) \sin \Theta_i)^2 - k_v^2 \right]^{1/2} \end{bmatrix} , \quad (5.2.18)$$

where the complex wavenumber $\gamma_i(\omega)$ is a function of k_u and k_v as defined in Eq. (5.2.10)

and the definition of $\overset{\leftrightarrow}{\mathbf{R}}_{ot_t}^T$ given in Eq. (3.1.58).

The *electric reflected spectral amplitude* within the reflected local coordinate system is given by [cf. Eq. (3.2.10)]

$$\vec{\mathbf{R}} \mathbf{E}_i(\mathbf{k}_T, \omega) e^{i\gamma_i(\omega)(w_0 + w_0')} . \quad (5.2.19a)$$

Substitution of this equation into the transversality condition given in Eq. (2.5.24) yields the

magnetic reflected spectral amplitude

$$\frac{\|c\|}{\mu\omega} \tilde{\mathbf{k}}_r(\omega) \times \vec{\mathbf{R}} \mathbf{E}_i(\mathbf{k}_T, \omega) e^{i\gamma_i(\omega)(w_0 + w'_0)} . \quad (5.2.19b)$$

The inverse temporal *Fourier-Laplace* and two-dimensional spatial *Fourier* transforms defined in Eqs. (2.1.1b) and (2.1.22b) respectively, of these spectral amplitudes yield the reflected fields as

$$\mathfrak{E}_r(\mathbf{r}_r, t) = \frac{1}{(2\pi)^3} \int_{-\infty}^{\infty} \int_{C_\omega} \vec{\mathbf{R}} \mathbf{E}_i(\mathbf{k}_T, \omega) e^{i\gamma_i(\omega)(w_0 + w'_0)} e^{i\tilde{\mathbf{k}}_r(\omega) \cdot \mathbf{r}_r - i\omega t} d\omega dk_x dk_y , \quad (5.2.20a)$$

and

$$\mathfrak{H}_r(\mathbf{r}_r, t) = \frac{\|c\|}{\mu\omega} \frac{1}{(2\pi)^3} \int_{-\infty}^{\infty} \int_{C_\omega} \tilde{\mathbf{k}}_r(\omega) \times \vec{\mathbf{R}} \mathbf{E}_i(\mathbf{k}_T, \omega) e^{i\gamma_i(\omega)(w_0 + w'_0)} e^{i\tilde{\mathbf{k}}_r(\omega) \cdot \mathbf{r}_r - i\omega t} d\omega dk_x dk_y , \quad (5.2.20b)$$

where $\vec{\mathbf{R}}$ is defined in Eq. (3.2.9), \mathbf{r}_r is the position vector defined in the reflected local coordinate system given in Eq. (5.2.15) and the reflected complex wavevector $\tilde{\mathbf{k}}_r(\omega)$ is given by Eq. (5.2.16). Eqs. (5.2.20a,b) represent the *reflected angular spectrum representations* in terms of the pseudo-source terms $\mathbf{E}_i(\mathbf{k}_T, \omega)$ and $\mathbf{H}_i(\mathbf{k}_T, \omega)$.

Similarly, following the development of §3.2, the *electric transmitted spectral amplitudes* within the transmitted local coordinate system [cf. Eq. (3.2.18)] is given by

$$\vec{\mathbf{T}} \mathbf{E}_i(\mathbf{k}_T, \omega) e^{i\gamma_i(\omega)w_0} e^{i\tilde{\mathbf{k}}_{t_w}(\omega)w'_0} . \quad (5.2.21a)$$

Substitution of Eq. (5.2.21a) into the transversality condition given in Eq. (2.5.24) yields the *magnetic transmitted spectral amplitude*

$$\frac{\|c\|}{\mu\omega} \tilde{\mathbf{k}}_r(\omega) \times \vec{\mathbf{T}} \mathbf{E}_i(\mathbf{k}_T, \omega) e^{i\gamma_i(\omega)w_0} e^{i\tilde{\mathbf{k}}_{t_w}(\omega)w'_0} . \quad (5.2.19b)$$

The inverse temporal *Fourier-Laplace* and two-dimensional spatial *Fourier* transforms of these spectral amplitudes yields the transmitted fields as

$$\mathfrak{S}_i(\mathbf{r}_t, t) = \frac{1}{(2\pi)^3} \int_{-\infty}^{\infty} \int_{C_\omega} \int \vec{\mathbf{T}} \mathbf{E}_i(\mathbf{k}_T, \omega) e^{i\gamma_i(\omega)w_0} e^{i\vec{\mathbf{k}}_r(\omega) \cdot \mathbf{r}_t} e^{-i\omega t} d\omega dk_x dk_y, \quad (5.2.22a)$$

and

$$\mathfrak{H}_i(\mathbf{r}_t, t) = \frac{\|c\|}{\mu\omega} \frac{1}{(2\pi)^3} \int_{-\infty}^{\infty} \int_{C_\omega} \int \vec{\mathbf{k}}_r(\omega) \times \vec{\mathbf{T}} \mathbf{E}_i(\mathbf{k}_T, \omega) e^{i\gamma_i(\omega)w_0} e^{i\vec{\mathbf{k}}_r(\omega) \cdot \mathbf{r}_t} e^{-i\omega t} d\omega dk_x dk_y, \quad (5.2.22b)$$

where $\vec{\mathbf{T}}$ is defined in Eq. (3.2.17), \mathbf{r}_t is the transmitted position vector defined in the transmitted local coordinate system given in Eq. (5.2.17) and the reflected complex wavevector $\vec{\mathbf{k}}_r(\omega)$ is given by Eq. (5.2.18). Eqs. (5.2.22a,b) are not the *transmitted angular spectrum representations* in their standard form since the angle of the transmitted attenuation vector θ_t^α given in Eq. (3.1.112c) varies as a function of the transverse wavenumbers k_u and k_v as discussed in §4.2.1.

If the temporal conditions of the incident field $\mathfrak{S}_i(\mathbf{r}_t, t)$ permit the use of a *Fourier* transform, then the contour of integration C_ω in Eqs. (5.2.20a,b) and (5.2.22a,b) denotes the straight line path along the real axis in the complex ω -plane. However, if the temporal conditions of the incident field $\mathfrak{S}_i(\mathbf{r}_t, t)$ require the use of a *Laplace* transform, then the contour C_ω is the *Bromwich contour* which is the straight line path given by $\omega = \omega' + ia$, with a being a real constant that resides within the region of convergence and where $\omega' \equiv \text{Re}(\omega)$ ranges from negative to positive infinity.

CHAPTER VI

Modal Analysis of Asymmetric Dielectric Slab Waveguides

Dielectric waveguides types are widely varied. They are generally distinguished from one another by the design of their cross-sections and by the types of media used to build them. Some common types are rectangular, circular, elliptical and slab. These four types are designed so that their cross-sections remain constant with respect to one direction, e.g. the propagation axis. In addition, the core region has a higher refractive index than the surrounding regions. The purpose of dielectric waveguides is to guide light down the propagation axis with high fidelity and as little loss or dispersion as possible.

The dielectric slab waveguide is the most fundamental of the waveguide structures. Consequently, developing the means to evaluate dielectric slab waveguides provides insight into other waveguide types. The dielectric slab waveguide has two planar interfaces which act as two independent reflecting surfaces. The results of Chapter 3 then apply to this problem. When the proper conditions are met, near total internal reflection is achieved and the guidance of light is made possible. This development can be applied to any type of linear dielectric medium. The most common dielectric medium for these waveguides is glass.

6.1 Electromagnetic Field Equations in “Two-Dimensional” Dielectric Regions

Consider the propagation of electromagnetic energy in a bounded dielectric region of space. A region is considered to be bounded if the refractive index is homogeneous over some finite range of at least one dimension. For the purposes of this chapter, the dielectric region is bounded in only the \hat{x} direction of a right handed (x, y, z) rectangular coordinate system and the refractive index remains constant along both the \hat{y} and the \hat{z} directions.

In particular, the core of the dielectric slab waveguide is a bounded dielectric region of space. The dielectric slab waveguide is comprised of three distinct regions: the substrate, core and cladding dielectrics [cf. Figure 6.1.1]. The substrate and cladding dielectric regions are two semi-infinite slabs which are parallel to each other and are separated by a finite distance. The core dielectric region fills the gap between the substrate and cladding.

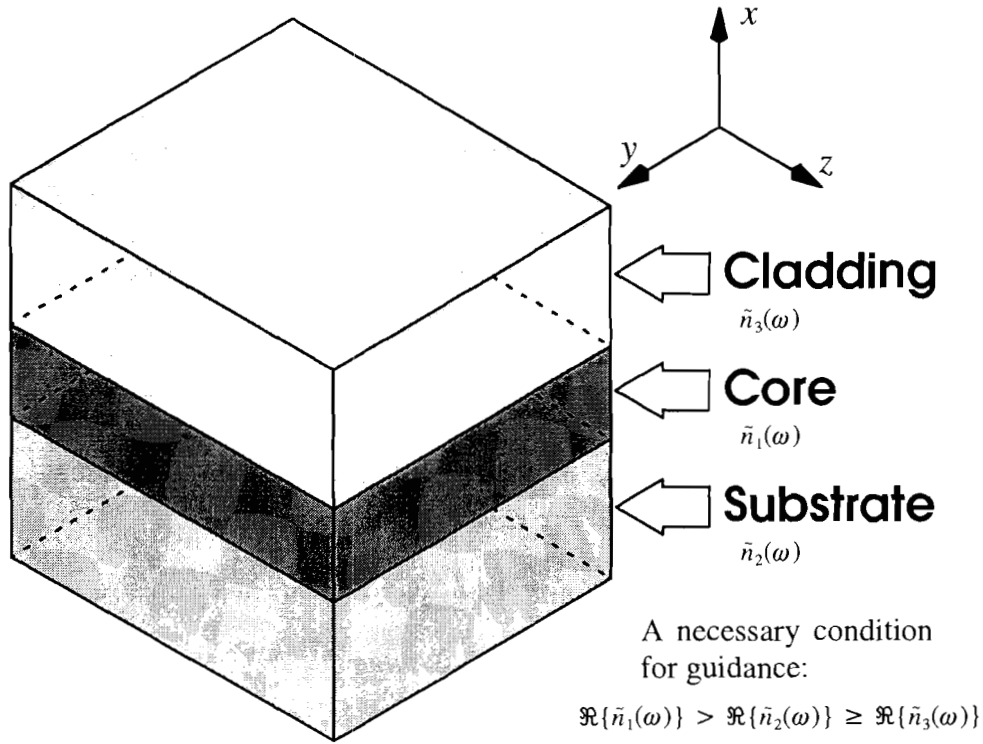


Figure 6.1.1 Diagram of a finite section of a dielectric slab waveguide, depicting three separate and distinct dielectric regions: the substrate, core and cladding dielectric materials. The substrate and cladding are both semi-infinite slabs that are abutted to the core region. The core region is infinite in two directions (in y and z) but of a finite thickness (in x). In general, all three regions are composed of different dielectric materials and as a consequence have different dielectric constants at a given frequency.

The source-free form of *Maxwell's* equations in the temporal frequency domain form given in Eqs. (2.2.12a-d) apply to this situation and are rewritten here as

$$\nabla \times \mathbf{E}(\mathbf{r}, \omega) = \left\| \frac{1}{c} \right\| i\omega \mathbf{B}(\mathbf{r}, \omega) , \quad (6.1.1a)$$

$$\nabla \times \mathbf{H}(\mathbf{r}, \omega) = -\left\| \frac{1}{c} \right\| i\omega \mathbf{D}(\mathbf{r}, \omega) , \quad (6.1.1b)$$

$$\nabla \cdot \mathbf{D}(\mathbf{r}, \omega) = 0 , \quad (6.1.1c)$$

$$\nabla \cdot \mathbf{B}(\mathbf{r}, \omega) = 0 . \quad (6.1.1d)$$

The constitutive relations given in Eqs. (2.2.13a,b) are rewritten here as

$$\mathbf{D}(\mathbf{r}, \omega) = \tilde{\epsilon}(\omega) \mathbf{E}(\mathbf{r}, \omega) , \quad (6.1.2a)$$

$$\mathbf{B}(\mathbf{r}, \omega) = \mu \mathbf{H}(\mathbf{r}, \omega) , \quad (6.1.2b)$$

where the complex valued dielectric permittivity response function is given as

$$\tilde{\epsilon}(\omega) = \int_0^{\infty} \hat{\epsilon}(t)e^{+i\omega t} dt . \quad (6.1.3)$$

The chosen axis orientations are such that the z -axis defines the propagation axis and the normals to the core/substrate and core/cladding interfaces are collinear with the x -axis. The variation along the y -axis is neglected so that the operator $\frac{\delta}{\delta y} = 0$ simplifies the problem to two dimensions.

Writing the *Gaussian* field equations given in Eqs. (6.1.1c,d) in component form and applying $\frac{\delta}{\delta y} = 0$ yields

$$\frac{\delta E_x(\mathbf{r}, \omega)}{\delta x} + \frac{\delta E_z(\mathbf{r}, \omega)}{\delta z} = 0 , \quad (6.1.4a)$$

$$\frac{\delta H_x(\mathbf{r}, \omega)}{\delta x} + \frac{\delta H_z(\mathbf{r}, \omega)}{\delta z} = 0 . \quad (6.1.4b)$$

Writing *Faraday's Law* given in Eq. (6.1.1a) in component form and applying $\frac{\delta}{\delta y} = 0$ yields

$$-\frac{\delta E_y(\mathbf{r}, \omega)}{\delta z} = \left\| \frac{1}{c} \right\| i\mu\omega H_x(\mathbf{r}, \omega) , \quad (6.1.5a)$$

$$\frac{\delta E_x(\mathbf{r}, \omega)}{\delta z} - \frac{\delta E_z(\mathbf{r}, \omega)}{\delta x} = \left\| \frac{1}{c} \right\| i\mu\omega H_y(\mathbf{r}, \omega) , \quad (6.1.5b)$$

$$\frac{\delta E_y(\mathbf{r}, \omega)}{\delta x} = \left\| \frac{1}{c} \right\| i\mu\omega H_z(\mathbf{r}, \omega) . \quad (6.1.5c)$$

Writing *Ampere's Law* given in Eq. (6.1.1b) in component form and applying $\frac{\delta}{\delta y} = 0$ yields

$$-\frac{\delta H_y(\mathbf{r}, \omega)}{\delta z} = -\left\| \frac{1}{c} \right\| i\tilde{\epsilon}(\omega)\omega E_x(\mathbf{r}, \omega) , \quad (6.1.6a)$$

$$\frac{\delta H_x(\mathbf{r}, \omega)}{\delta z} - \frac{\delta H_z(\mathbf{r}, \omega)}{\delta x} = -\left\|\frac{1}{c}\right\| i\tilde{\epsilon}(\omega)\omega E_y(\mathbf{r}, \omega) , \quad (6.1.6b)$$

$$\frac{\delta H_y(\mathbf{r}, \omega)}{\delta x} = -\left\|\frac{1}{c}\right\| i\tilde{\epsilon}(\omega)\omega E_z(\mathbf{r}, \omega) . \quad (6.1.6c)$$

By definition, TE fields do not have an electric field component in the \hat{z} direction. Therefore, Eqs. (6.1.4b), (6.1.5a,c) and (6.1.6b) relate to TE fields which are summarized as

$$\frac{\delta H_x(\mathbf{r}, \omega)}{\delta x} + \frac{\delta H_z(\mathbf{r}, \omega)}{\delta z} = 0 , \quad (6.1.7a)$$

$$-\frac{\delta E_y(\mathbf{r}, \omega)}{\delta z} = \left\|\frac{1}{c}\right\| i\mu\omega H_x(\mathbf{r}, \omega) , \quad (6.1.7b)$$

$$\frac{\delta E_y(\mathbf{r}, \omega)}{\delta x} = \left\|\frac{1}{c}\right\| i\mu\omega H_z(\mathbf{r}, \omega) , \quad (6.1.7c)$$

$$\frac{\delta H_x(\mathbf{r}, \omega)}{\delta z} - \frac{\delta H_z(\mathbf{r}, \omega)}{\delta x} = -\left\|\frac{1}{c}\right\| i\tilde{\epsilon}(\omega)\omega E_y(\mathbf{r}, \omega) . \quad (6.1.7d)$$

It should be noted that Eqs. (6.1.7a–d) are over-specified in that Eq. (6.1.7a) is an immediate consequence of Eqs. (6.1.7b) and (6.1.7c).

Traditionally, the wave equation is derived in terms of the field quantity, $E_y(\mathbf{r}, \omega)$. However, it could also be solved in terms of $H_z(\mathbf{r}, \omega)$, as is traditional for metallic waveguides. The wave equation is formed by substituting Eqs. (6.1.7b) and (6.1.7c) into Eq. (6.1.7d), which yields

$$\frac{\delta^2 E_y(\mathbf{r}, \omega)}{\delta x^2} + \frac{\delta^2 E_y(\mathbf{r}, \omega)}{\delta z^2} + \left\|\frac{1}{c^2}\right\| \mu\tilde{\epsilon}(\omega)\omega^2 E_y(\mathbf{r}, \omega) = 0 . \quad (6.1.8)$$

Solving Eqs. (6.1.7b,c) for $H_x(\mathbf{r}, \omega)$ and $H_z(\mathbf{r}, \omega)$ in terms of $E_y(\mathbf{r}, \omega)$ yields

$$H_x(\mathbf{r}, \omega) = \|c\| \frac{i}{\mu\omega} \frac{\delta E_y(\mathbf{r}, \omega)}{\delta z} , \quad (6.1.9a)$$

$$H_z(\mathbf{r}, \omega) = -\|c\| \frac{i}{\mu\omega} \frac{\delta E_y(\mathbf{r}, \omega)}{\delta x} . \quad (6.1.9b)$$

By definition, TM fields do not have a magnetic field component in the \hat{z} direction. Therefore, Eqs. (6.1.4a), (6.1.5b) and (6.1.6a,c) relate to TM fields which are summarized as

$$\frac{\delta E_x(\mathbf{r}, \omega)}{\delta x} + \frac{\delta E_z(\mathbf{r}, \omega)}{\delta z} = 0 , \quad (6.1.10a)$$

$$\frac{\delta E_x(\mathbf{r}, \omega)}{\delta z} - \frac{\delta E_z(\mathbf{r}, \omega)}{\delta x} = \left\| \frac{1}{c} \right\| i \mu \omega H_y(\mathbf{r}, \omega) , \quad (6.1.10b)$$

$$\frac{\delta H_y(\mathbf{r}, \omega)}{\delta z} = \left\| \frac{1}{c} \right\| i \tilde{\epsilon}(\omega) \omega E_x(\mathbf{r}, \omega) , \quad (6.1.10c)$$

$$\frac{\delta H_y(\mathbf{r}, \omega)}{\delta x} = - \left\| \frac{1}{c} \right\| i \tilde{\epsilon}(\omega) \omega E_z(\mathbf{r}, \omega) . \quad (6.1.10d)$$

It should be noted that Eqs. (6.1.10a–d) are over-specified in that Eq. (6.1.10a) is an immediate consequence of Eqs. (6.1.10c) and (6.1.10d).

Traditionally, the wave equation is derived in terms of the field quantity, $H_y(\mathbf{r}, \omega)$. The wave equation is formed by substituting Eqs. (6.1.10c) and (6.1.10d) into Eq. (6.1.10b) which yields

$$\frac{\delta^2 H_y(\mathbf{r}, \omega)}{\delta x^2} + \frac{\delta^2 H_y(\mathbf{r}, \omega)}{\delta z^2} + \left\| \frac{1}{c^2} \right\| \mu \tilde{\epsilon}(\omega) \omega^2 H_y(\mathbf{r}, \omega) = 0 . \quad (6.1.11)$$

Solving Eqs. (6.1.10c,d) for $E_x(\mathbf{r}, \omega)$ and $E_z(\mathbf{r}, \omega)$ in terms of $H_y(\mathbf{r}, \omega)$ yields

$$E_x(\mathbf{r}, \omega) = - \left\| c \right\| \frac{i}{\tilde{\epsilon}(\omega) \omega} \frac{\delta H_y(\mathbf{r}, \omega)}{\delta z} , \quad (6.1.12a)$$

$$E_z(\mathbf{r}, \omega) = \left\| c \right\| \frac{i}{\tilde{\epsilon}(\omega) \omega} \frac{\delta H_y(\mathbf{r}, \omega)}{\delta x} . \quad (6.1.12b)$$

6.2 Guided Modes of the Asymmetric Dielectric Slab Waveguide

The containment or guidance of electromagnetic energy in the optical portion of the electromagnetic spectrum is the ultimate goal of any type of dielectric waveguide. Guidance occurs when the condition of near total internal reflection is satisfied. Therefore, a necessary condition for guidance is that the real part of the complex refractive index of the core region

must be greater than that of the substrate and cladding dielectrics. In other words, the core must be optically more dense than the outer regions, i.e. $\Re\{\tilde{n}_1(\omega)\} > \Re\{\tilde{n}_2(\omega)\} \geq \Re\{\tilde{n}_3(\omega)\}$. However, this is not a sufficient condition since it does not guarantee that guidance can occur for lossy dielectrics. An example in §4.2.2 shows that the critical angle Θ_C does not occur even though the guidance condition is satisfied [cf. Table 4.2.2 and Table 4.2.4 for $\omega = 9122.5THz$]. If $\Re\{\tilde{n}_2(\omega)\} \neq \Re\{\tilde{n}_3(\omega)\}$ then the dielectric slab waveguide is labeled *asymmetric* and if $\Re\{\tilde{n}_2(\omega)\} = \Re\{\tilde{n}_3(\omega)\}$ then the dielectric slab waveguide is labeled *symmetric*.

If the guidance condition is satisfied then some of the electromagnetic energy can be contained (or guided) within the core region. Energy containment results from the fact that the majority of the energy will be reflected continually back into the core region by repeated reflection from the core/substrate and core/cladding interfaces. Typically the core region is where guidance takes place, even though a certain amount of electromagnetic energy is leaked into the substrate and cladding regions. This assumes that the dielectrics are lossy. If the dielectrics are lossless then all electromagnetic energy can be completely contained within the core and no energy propagates normal to the interface in the substrate or cladding regions.

6.2.1 Guided TE Modes in an Asymmetric Dielectric Slab Waveguide

Let the \hat{z} dependence of the modal fields be given as $e^{+i\tilde{k}_z(\omega)z}$ where $\tilde{k}_z(\omega)$ is the longitudinal component of the complex wavevector. The operator $\frac{\partial}{\partial z}$ then yields

$$\frac{\partial}{\partial z} = +i\tilde{k}_z(\omega) . \quad (6.2.1)$$

Application of this operator to the wave equation given in Eq. (6.1.8) yields

$$\frac{\partial^2 E_y(\mathbf{r}, \omega)}{\partial x^2} + \left\{ \tilde{k}^2(\omega) - \tilde{k}_z^2(\omega) \right\} E_y(\mathbf{r}, \omega) = 0 , \quad (6.2.2)$$

where

$$\tilde{k}^2(\omega) \equiv \tilde{n}^2(\omega)k_0^2 \quad (6.2.3)$$

where $\tilde{k}(\omega)$ is the *complex wavenumber* of the electromagnetic disturbance with angular frequency ω that is propagating in the medium with *complex refractive index*

$$\tilde{n}(\omega) \equiv \sqrt{\frac{\mu\tilde{\epsilon}(\omega)}{\mu_0\epsilon_0}} , \quad (6.2.4)$$

where $k_0 \equiv \frac{\omega}{c}$ is the vacuum wavenumber and $c \equiv \frac{\|c\|}{\sqrt{\mu_0\epsilon_0}}$ is the vacuum speed of light. The

general solution to the Eq. (6.2.2) is of the form

$$E_y(\mathbf{r}, \omega) = E_0 e^{\pm i\tilde{k}_x(\omega)x} . \quad (6.2.5)$$

Substitution of this solution into Eqs. (6.1.9a,b) yields

$$H_x(\mathbf{r}, \omega) = -\|c\| \frac{\tilde{k}_z(\omega)}{\mu\omega} E_y(\mathbf{r}, \omega) , \quad (6.2.6a)$$

$$H_z(\mathbf{r}, \omega) = \pm \|c\| \frac{\tilde{k}_x(\omega)}{\mu\omega} E_y(\mathbf{r}, \omega) , \quad (6.2.6b)$$

where

$$\tilde{k}_x^2(\omega) \equiv \tilde{k}^2(\omega) - \tilde{k}_z^2(\omega) , \quad (6.2.7)$$

since

$$\tilde{k}_y(\omega) \equiv 0 . \quad (6.2.8)$$

The solutions given in Eqs. (6.2.5) and (6.2.6a,b) may then be written for each region of the dielectric slab waveguide: the core, cladding and substrate. The nature of the fields outside of the core are assumed to be primarily attenuative, i.e. near total internal reflection is assumed to occur inside the core region. The transverse component of the complex wavevector in the \hat{x} direction is then redefined as $\tilde{\zeta}(\omega) \equiv i\tilde{k}_x(\omega)$ for the substrate or cladding regions. A two dimensional diagram of the dielectric slab waveguide is illustrated in Figure 6.2.1 which shows the origin of the x -axis in the center of the core region and the real parts of the complex wavevectors of the solutions within each dielectric region.

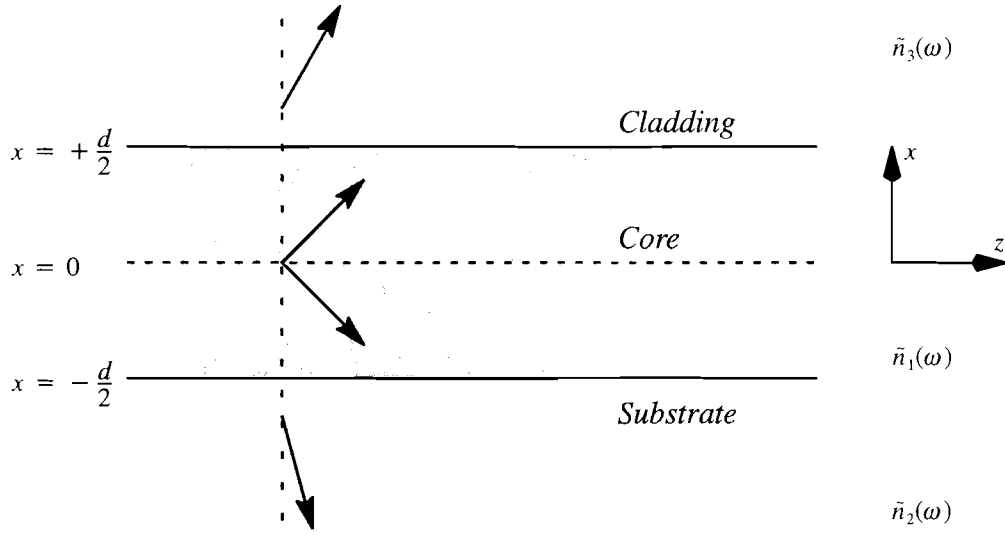


Figure 6.2.1 Two dimensional cross section of the dielectric slab waveguide, indicating the directions of the propagation vectors at a xy -plane in all three dielectric regions: the core, cladding and substrate.

The field components for the guided modes within the core region $|x| \leq \frac{d}{2}$ are given

by

$$E_y(\mathbf{r}, \omega) = A(\omega)e^{-i\tilde{k}_x(\omega)x} + B(\omega)e^{+i\tilde{k}_x(\omega)x} , \quad (6.2.9a)$$

$$H_x(\mathbf{r}, \omega) = -\|c\| \frac{\tilde{k}_z(\omega)}{\mu\omega} \left[A(\omega)e^{-i\tilde{k}_x(\omega)x} + B(\omega)e^{+i\tilde{k}_x(\omega)x} \right] , \quad (6.2.9b)$$

$$H_z(\mathbf{r}, \omega) = \|c\| \frac{\tilde{k}_x(\omega)}{\mu\omega} \left[A(\omega)e^{-i\tilde{k}_x(\omega)x} - B(\omega)e^{+i\tilde{k}_x(\omega)x} \right] , \quad (6.2.9c)$$

where

$$\tilde{k}_x(\omega) \equiv \sqrt{\tilde{n}_1^2(\omega)k_0^2 - \tilde{k}_z^2(\omega)} . \quad (6.2.9d)$$

The field components for the guided modes within the cladding region $x \geq \frac{d}{2}$ are given by

$$E_y(\mathbf{r}, \omega) = C(\omega)e^{-\tilde{\xi}_3(\omega)x} , \quad (6.2.10a)$$

$$H_x(\mathbf{r}, \omega) = -\|c\| \frac{\tilde{k}_z(\omega)}{\mu\omega} C(\omega)e^{-\tilde{\xi}_3(\omega)x} , \quad (6.2.10b)$$

$$H_z(\mathbf{r}, \omega) = -\|c\| i \frac{\tilde{\xi}_3(\omega)}{\mu\omega} C(\omega)e^{-\tilde{\xi}_3(\omega)x} , \quad (6.2.10c)$$

where [cf. Eq. (3.1.141b)]

$$\tilde{\xi}_3(\omega) \equiv \sqrt{\tilde{k}_z^2(\omega) - \tilde{n}_3^2(\omega)k_0^2} = i\tilde{k}_{3_x}(\omega) . \quad (6.2.10d)$$

The field components for the guided modes within the substrate region $x \leq \frac{d}{2}$ are given by

$$E_y(\mathbf{r}, \omega) = D(\omega)e^{+\tilde{\xi}_2(\omega)x} , \quad (6.2.11a)$$

$$H_x(\mathbf{r}, \omega) = -\|c\| \frac{\tilde{k}_z(\omega)}{\mu\omega} D(\omega)e^{+\tilde{\xi}_2(\omega)x} , \quad (6.2.11b)$$

$$H_z(\mathbf{r}, \omega) = \|c\|i \frac{\tilde{\xi}_2(\omega)}{\mu\omega} D(\omega)e^{+\tilde{\xi}_2(\omega)x} , \quad (6.2.11c)$$

where [cf. Eq. (3.1.141b)]

$$\tilde{\xi}_2(\omega) \equiv \sqrt{\tilde{k}_z^2(\omega) - \tilde{n}_2^2(\omega)k_0^2} = i\tilde{k}_{2_x}(\omega) . \quad (6.2.11d)$$

The E_y and H_z field components must satisfy the tangential boundary conditions [cf. Eqs. (3.1.68a,b)] at the core/cladding and core/substrate interfaces (i.e. at $x = \pm \frac{d}{2}$). Application of these boundary conditions yields

$$A(\omega)e^{-i\tilde{k}_x(\omega)\frac{d}{2}} + B(\omega)e^{+i\tilde{k}_x(\omega)\frac{d}{2}} = C(\omega)e^{-\tilde{\xi}_3(\omega)\frac{d}{2}} , \quad (6.2.12a)$$

$$A(\omega)e^{+i\tilde{k}_x(\omega)\frac{d}{2}} + B(\omega)e^{-i\tilde{k}_x(\omega)\frac{d}{2}} = D(\omega)e^{+\tilde{\xi}_2(\omega)\frac{d}{2}} , \quad (6.2.12b)$$

$$\tilde{k}_x(\omega)A(\omega)e^{-i\tilde{k}_x(\omega)\frac{d}{2}} - \tilde{k}_x(\omega)B(\omega)e^{+i\tilde{k}_x(\omega)\frac{d}{2}} = -i\tilde{\xi}_3(\omega)C(\omega)e^{-\tilde{\xi}_3(\omega)\frac{d}{2}} , \quad (6.2.12a)$$

$$\tilde{k}_x(\omega)A(\omega)e^{+i\tilde{k}_x(\omega)\frac{d}{2}} - \tilde{k}_x(\omega)B(\omega)e^{-i\tilde{k}_x(\omega)\frac{d}{2}} = i\tilde{\xi}_2(\omega)D(\omega)e^{+\tilde{\xi}_2(\omega)\frac{d}{2}} . \quad (6.2.12b)$$

For a given angular frequency ω , Eqs. (6.2.12a–d) form a homogeneous linear system of equations which may be rewritten in matrix form as

$$\begin{bmatrix} e^{-i\tilde{k}_x(\omega)\frac{d}{2}} & e^{+i\tilde{k}_x(\omega)\frac{d}{2}} & -e^{-\tilde{\xi}_3(\omega)\frac{d}{2}} & 0 \\ e^{+i\tilde{k}_x(\omega)\frac{d}{2}} & e^{-i\tilde{k}_x(\omega)\frac{d}{2}} & 0 & -e^{-\tilde{\xi}_2(\omega)\frac{d}{2}} \\ \tilde{k}_x(\omega)e^{-i\tilde{k}_x(\omega)\frac{d}{2}} & -\tilde{k}_x(\omega)e^{+i\tilde{k}_x(\omega)\frac{d}{2}} & i\tilde{\xi}_3(\omega)e^{-\tilde{\xi}_3(\omega)\frac{d}{2}} & 0 \\ \tilde{k}_x(\omega)e^{+i\tilde{k}_x(\omega)\frac{d}{2}} & -\tilde{k}_x(\omega)e^{-i\tilde{k}_x(\omega)\frac{d}{2}} & 0 & -i\tilde{\xi}_2(\omega)e^{-\tilde{\xi}_2(\omega)\frac{d}{2}} \end{bmatrix} \begin{bmatrix} A(\omega) \\ B(\omega) \\ C(\omega) \\ D(\omega) \end{bmatrix} = \mathbf{0} . \quad (6.2.13)$$

A homogeneous linear system of equations can be written as $\vec{A}\mathbf{x} = \mathbf{0}$, where \vec{A} is a $n \times n$ square matrix. A non-trivial solution exists if and only if $\text{rank}(\vec{A}) < n$ which implies that

$\det(\vec{\vec{A}}) = 0$, i.e. $\vec{\vec{A}}$ is singular. Therefore, a non-trivial solution to Eq. (6.2.13) exists when

$$\begin{vmatrix} e^{-i\bar{k}_x(\omega)\frac{d}{2}} & e+i\bar{k}_x(\omega)\frac{d}{2} & -e^{-\bar{\zeta}_3(\omega)\frac{d}{2}} & 0 \\ e+i\bar{k}_x(\omega)\frac{d}{2} & e-i\bar{k}_x(\omega)\frac{d}{2} & 0 & -e^{-\bar{\zeta}_2(\omega)\frac{d}{2}} \\ \tilde{k}_x(\omega)e^{-i\bar{k}_x(\omega)\frac{d}{2}} & -\tilde{k}_x(\omega)e+i\bar{k}_x(\omega)\frac{d}{2} & i\tilde{\zeta}_3(\omega)e^{-\bar{\zeta}_3(\omega)\frac{d}{2}} & 0 \\ \tilde{k}_x(\omega)e+i\bar{k}_x(\omega)\frac{d}{2} & -\tilde{k}_x(\omega)e-i\bar{k}_x(\omega)\frac{d}{2} & 0 & -i\tilde{\zeta}_2(\omega)e^{-\bar{\zeta}_2(\omega)\frac{d}{2}} \end{vmatrix} = 0 . \quad (6.2.14)$$

The solutions to this determinate equation yield what are called the modes of the system.

Taking advantage of the zeros in Eq. (6.2.14) yields

$$\begin{aligned} & -e^{-\bar{\zeta}_2(\omega)\frac{d}{2}} \begin{vmatrix} e^{-i\bar{k}_x(\omega)\frac{d}{2}} & e+i\bar{k}_x(\omega)\frac{d}{2} & -e^{-\bar{\zeta}_3(\omega)\frac{d}{2}} \\ \tilde{k}_x(\omega)e^{-i\bar{k}_x(\omega)\frac{d}{2}} & -\tilde{k}_x(\omega)e+i\bar{k}_x(\omega)\frac{d}{2} & i\tilde{\zeta}_3(\omega)e^{-\bar{\zeta}_3(\omega)\frac{d}{2}} \\ \tilde{k}_x(\omega)e+i\bar{k}_x(\omega)\frac{d}{2} & -\tilde{k}_x(\omega)e-i\bar{k}_x(\omega)\frac{d}{2} & 0 \end{vmatrix} \\ & -i\tilde{\zeta}_2(\omega)e^{-\bar{\zeta}_2(\omega)\frac{d}{2}} \begin{vmatrix} e^{-i\bar{k}_x(\omega)\frac{d}{2}} & e+i\bar{k}_x(\omega)\frac{d}{2} & -e^{-\bar{\zeta}_3(\omega)\frac{d}{2}} \\ e+i\bar{k}_x(\omega)\frac{d}{2} & e-i\bar{k}_x(\omega)\frac{d}{2} & 0 \\ \tilde{k}_x(\omega)e^{-i\bar{k}_x(\omega)\frac{d}{2}} & -\tilde{k}_x(\omega)e+i\bar{k}_x(\omega)\frac{d}{2} & i\tilde{\zeta}_3(\omega)e^{-\bar{\zeta}_3(\omega)\frac{d}{2}} \end{vmatrix} = 0 . \end{aligned}$$

Dividing out the common factors and taking advantage of the zeros in the 3×3 determinants yields

$$\begin{aligned} & -e^{-\bar{\zeta}_3(\omega)\frac{d}{2}} \left(\tilde{k}_x^2(\omega)e+i\bar{k}_x(\omega)d - \tilde{k}_x^2(\omega)e^{-i\bar{k}_x(\omega)d} \right) \\ & + i\tilde{\zeta}_3(\omega)e^{-\bar{\zeta}_3(\omega)\frac{d}{2}} \left(\tilde{k}_x(\omega)e+i\bar{k}_x(\omega)d + \tilde{k}_x(\omega)e^{-i\bar{k}_x(\omega)d} \right) \\ & + i\tilde{\zeta}_2(\omega)e^{-\bar{\zeta}_3(\omega)\frac{d}{2}} \left(\tilde{k}_x(\omega)e+i\bar{k}_x(\omega)d + \tilde{k}_x(\omega)e^{-i\bar{k}_x(\omega)d} \right) \\ & + \tilde{\zeta}_2(\omega)\tilde{\zeta}_3(\omega)e^{-\bar{\zeta}_3(\omega)\frac{d}{2}} \left(e+i\bar{k}_x(\omega)d - e^{-i\bar{k}_x(\omega)d} \right) = 0 . \end{aligned}$$

Dividing out the common factors and regrouping yields

$$\begin{aligned} & -\tilde{k}_x^2(\omega) \left(e+i\bar{k}_x(\omega)d - e^{-i\bar{k}_x(\omega)d} \right) + i\tilde{\zeta}_3(\omega)\tilde{k}_x(\omega) \left(e+i\bar{k}_x(\omega)d + e^{-i\bar{k}_x(\omega)d} \right) \\ & + i\tilde{\zeta}_2(\omega)\tilde{k}_x(\omega) \left(e+i\bar{k}_x(\omega)d + e^{-i\bar{k}_x(\omega)d} \right) \\ & + \tilde{\zeta}_2(\omega)\tilde{\zeta}_3(\omega) \left(e+i\bar{k}_x(\omega)d - e^{-i\bar{k}_x(\omega)d} \right) = 0 . \end{aligned}$$

Using *Euler's* formulae²² and regrouping yields,

$$\tilde{k}_x(\omega) \left[\tilde{\xi}_2(\omega) + \tilde{\xi}_3(\omega) \right] \cos(\tilde{k}_x(\omega)d) + \left[\tilde{\xi}_2(\omega)\tilde{\xi}_3(\omega) - \tilde{k}_x^2(\omega) \right] \sin(\tilde{k}_x(\omega)d) = 0 .$$

Using the definition for the tangent function results in the *dispersion relation*

$$\tan(\tilde{k}_x(\omega)d) = \frac{\tilde{k}_x(\omega) \left[\tilde{\xi}_2(\omega) + \tilde{\xi}_3(\omega) \right]}{\tilde{k}_x^2(\omega) - \tilde{\xi}_2(\omega)\tilde{\xi}_3(\omega)} = \frac{\frac{\tilde{\xi}_2(\omega)}{\tilde{k}_x(\omega)} + \frac{\tilde{\xi}_3(\omega)}{\tilde{k}_x(\omega)}}{1 - \frac{\tilde{\xi}_2(\omega)\tilde{\xi}_3(\omega)}{\tilde{k}_x(\omega)\tilde{k}_x(\omega)}} . \quad (6.2.15)$$

Solution of this dispersion relation yields the modes of the dielectric slab waveguide when the left-hand side equals the right-hand side. Substitution of the quantity [cf. Eq. (6.2.9d)]

$\tilde{k}_z^2(\omega) = \tilde{n}_1^2(\omega)k_0^2 - \tilde{k}_x^2(\omega)$ into Eqs. (6.2.10d) and (6.2.11d) yields

$$\tilde{\xi}_2^2(\omega) \equiv \left[\tilde{n}_1^2(\omega) - \tilde{n}_2^2(\omega) \right] k_0^2 - \tilde{k}_x^2(\omega) , \quad (6.2.16)$$

$$\tilde{\xi}_3^2(\omega) \equiv \left[\tilde{n}_1^2(\omega) - \tilde{n}_3^2(\omega) \right] k_0^2 - \tilde{k}_x^2(\omega) . \quad (6.2.17)$$

These equations are now are functions of $\tilde{k}_x(\omega)$. Let $\tilde{k}_x(\omega) \equiv \beta_x(\omega) + i\alpha_x(\omega)$ where $\beta_x(\omega) = \Re\{\tilde{k}_x(\omega)\}$ and $\alpha_x(\omega) = \Im\{\tilde{k}_x(\omega)\}$.

The condition of near total internal reflection can be lost in the *region of cutoff* of the complex plane of $\tilde{k}_x(\omega)$. In this region, at least one of the quantities $\tilde{\xi}_2(\omega)$ and $\tilde{\xi}_3(\omega)$ are primarily attenuative which occurs when $\Re\{\tilde{\xi}_2^2(\omega)\} < 0$ and/or $\Re\{\tilde{\xi}_3^2(\omega)\} < 0$, viz.

$$\beta_x^2(\omega) - \alpha_x^2(\omega) > \frac{\mu\omega^2}{\|c^2\|} \left[\epsilon_{1r}(\omega) - \epsilon_{2r}(\omega) \right] , \quad (6.2.18)$$

$$\beta_x^2(\omega) - \alpha_x^2(\omega) > \frac{\mu\omega^2}{\|c^2\|} \left[\epsilon_{1r}(\omega) - \epsilon_{3r}(\omega) \right] . \quad (6.2.19)$$

The branch cuts of $\tilde{\xi}_2^2(\omega)$ and $\tilde{\xi}_3^2(\omega)$ occur when Eqs. (6.2.16) and (6.2.17) are satisfied and

22. See Abramowitz and Stegun [73] p. 74.

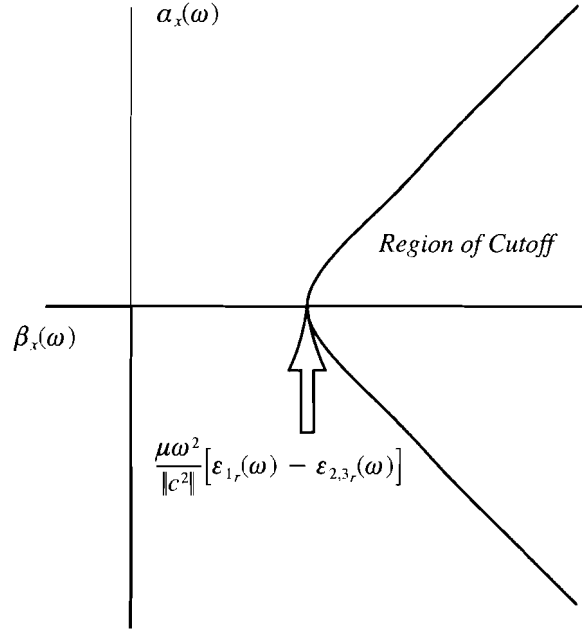


Figure 6.2.2 The region of cutoff is depicted as the shaded area.

$$\mathfrak{S}\left\{\tilde{\xi}_2(\omega)\right\} = 0 \text{ and } \mathfrak{S}\left\{\tilde{\xi}_3(\omega)\right\} = 0, \text{ viz.}$$

$$2\beta_x(\omega)\alpha_x(\omega) = \frac{\mu\omega^2}{\|c^2\|} \left[\epsilon_{1_i}(\omega) - \epsilon_{2_i}(\omega) \right], \quad (6.2.20)$$

$$2\beta_x(\omega)\alpha_x(\omega) = \frac{\mu\omega^2}{\|c^2\|} \left[\epsilon_{1_i}(\omega) - \epsilon_{3_i}(\omega) \right]. \quad (6.2.21)$$

The quantities $\epsilon_{1_r}(\omega)$, $\epsilon_{1_i}(\omega)$, $\epsilon_{2_r}(\omega)$, $\epsilon_{2_i}(\omega)$, $\epsilon_{3_r}(\omega)$ and $\epsilon_{3_i}(\omega)$ are the real and imaginary parts of $\tilde{\epsilon}_1(\omega)$, $\tilde{\epsilon}_2(\omega)$ and $\tilde{\epsilon}_3(\omega)$, respectively [cf. Eq. (2.2.14)]. An illustration of the region of cutoff is given in Figure 6.2.2. In the region of cutoff any solutions of Eq. (6.2.15) represent leaky modes which are highly attenuative along the propagation axis inside the core region.

6.2.2 Physical Connection for the Guided TE Modes in an Asymmetric Dielectric Slab Waveguide

The solution given in Eqs. (6.2.9a–c) represents the superposition of two inhomogeneous plane waves. A single inhomogeneous plane wave propagating within the core region after repeated reflections from the core/substrate and core/cladding interfaces is a physical

interpretation of this solution. The modal solutions must possess a self-repeating structure as a function of the propagation axis. Consequently, the single inhomogeneous plane wave effectively generates multiple reflection that must constructively interfere such that they are indistinguishable after every other reflection. If this physical interpretation is correct then the dispersion relationship given in Eq. (6.2.15) must be equivalent to that derived from the assumption of the constructive interference of two inhomogeneous plane waves propagating in the core region.

The dispersion relation given in Eq. (6.2.15) can be cast into a form that reinforces this notion. The sum of two arctangent functions of a complex variable is given by²³

$$\text{Tan}^{-1}(z_2) \pm \text{Tan}^{-1}(z_3) = \text{Tan}^{-1}\left[\frac{z_2 \pm z_3}{1 \mp z_2 z_3}\right], \quad (6.2.22)$$

where

$$\text{Tan}^{-1}(z) \equiv \tan^{-1}(z) + k\pi, \quad z^2 \neq -1, \quad (6.2.23)$$

and z , z_2 and z_3 are complex numbers and k is any integer. The arctangent of the dispersion relation given in Eq. (6.2.15) yields

$$\tilde{k}_x(\omega)d + k\pi = \text{Tan}^{-1}\left[\frac{\frac{\tilde{\xi}_2(\omega)}{\tilde{k}_x(\omega)} + \frac{\tilde{\xi}_3(\omega)}{\tilde{k}_x(\omega)}}{1 - \frac{\tilde{\xi}_2(\omega)\tilde{\xi}_3(\omega)}{\tilde{k}_x(\omega)\tilde{k}_x(\omega)}}\right]. \quad (6.2.24)$$

Application of Eq. (6.2.22) to this dispersion relation yields

$$\tilde{k}_x(\omega)d + k\pi = \text{Tan}^{-1}\left(\frac{\tilde{\xi}_2(\omega)}{\tilde{k}_x(\omega)}\right) + \text{Tan}^{-1}\left[\frac{\tilde{\xi}_3(\omega)}{\tilde{k}_x(\omega)}\right], \quad (6.2.25)$$

where the upper sign is used and $z_2 \equiv \frac{\tilde{\xi}_2(\omega)}{\tilde{k}_x(\omega)}$ and $z_3 \equiv \frac{\tilde{\xi}_3(\omega)}{\tilde{k}_x(\omega)}$.

23. See Abramowitz and Stegun [73] p. 80.

The inverse tangent function may be separated into real and imaginary parts as²⁴

$$\text{Tan}^{-1}(z) = k\pi + \frac{1}{2} \tan^{-1} \left[\frac{2x}{1 - x^2 - y^2} \right] + \frac{i}{4} \ln \left[\frac{x^2 + (y + 1)^2}{x^2 + (y - 1)^2} \right], \quad (6.2.26)$$

where z is a complex number and $x = \Re\{z\}$ and $y = \Im\{z\}$. Application of Eq. (6.2.26) to the dispersion relation given in Eq. (6.2.25) yields relationships for the real part

$$2\beta_x(\omega)d \pm 2k\pi = \tan^{-1} \left[\frac{2x_2}{1 - x_2^2 - y_2^2} \right] + \tan^{-1} \left[\frac{2x_3}{1 - x_3^2 - y_3^2} \right], \quad (6.2.27a)$$

and the imaginary part

$$2\alpha_x(\omega)d = \frac{1}{2} \ln \left[\frac{x_2^2 + (y_2 + 1)^2}{x_2^2 + (y_2 - 1)^2} \right] + \frac{1}{2} \ln \left[\frac{x_3^2 + (y_3 + 1)^2}{x_3^2 + (y_3 - 1)^2} \right], \quad (6.2.27b)$$

where $x_2 = \Re\{z_2\}$, $y_2 = \Im\{z_2\}$, $x_3 = \Re\{z_3\}$ and $y_3 = \Im\{z_3\}$.

The complex wavevector of an inhomogeneous plane wave may be defined in terms of two real vector quantities as $\tilde{\mathbf{k}}(\omega) \equiv \boldsymbol{\beta}(\omega) + i\boldsymbol{\alpha}(\omega)$. The *propagation vector* $\boldsymbol{\beta}(\omega) \equiv \Re\{\tilde{\mathbf{k}}(\omega)\}$ specifies the direction of propagation of the planar phase front while the *attenuation vector* $\boldsymbol{\alpha}(\omega) \equiv \Im\{\tilde{\mathbf{k}}(\omega)\}$ specifies the direction of propagation of the planar amplitude front. The uniqueness of these two types of fronts permits a restatement of the physical interpretation. Both the planar phase front and planar amplitude front must be indistinguishable from every other reflection. The schematic of the modal solution for either type of front (phase or amplitude) is illustrated in Figure 6.2.3 where the angle θ represents the angle of incidence for either θ_i^β for a phase front or θ_i^α for an amplitude front.

The planar phase front or the planar amplitude front of an inhomogeneous plane wave accumulates an exponential factor not only due to propagation in the core region but also because of the reflections from the core/cladding and core/substrate interfaces. The pro-

24. See Abramowitz and Stegun [73] p. 81.

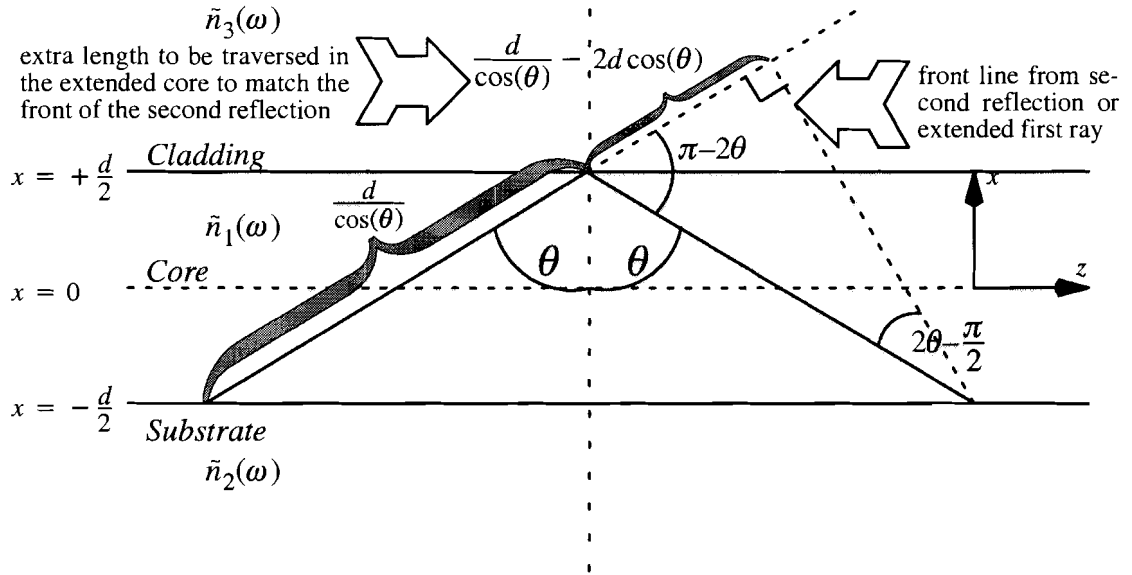


Figure 6.2.3 Two dimensional cross section of the dielectric slab waveguide, indicating the modal solution for either the planar phase front or the planar amplitude front.

posed physical interpretation equates this exponential accumulation to that of an imagined inhomogeneous plane wave propagating an extra distance in an imaginary extended core region. This extra distance traveled in the extended core region is computed as

$$-\frac{d}{\cos(\theta)} \cos(2\theta) = -\frac{d}{\cos(\theta)} [2 \cos^2(\theta) - 1] = \frac{d}{\cos(\theta)} - 2d \cos(\theta), \quad (6.2.28)$$

while the length traveled in the true core region is $\frac{d}{\cos(\theta)}$.

The exponential phase accumulation of the planar phase front after two consecutive reflections is given by

$$\frac{2d}{\cos(\theta_i^\beta)} \beta(\omega) - \Phi_3(\omega) - \Phi_2(\omega), \quad (6.2.29a)$$

where $\beta(\omega)$ is the magnitude of the propagation vector $\boldsymbol{\beta}(\omega)$. The quantities $\Phi_2(\omega)$ and $\Phi_3(\omega)$ represent the phase delay suffered by the reflection from the core/substrate and core/cladding interfaces, respectively. The exponential phase accumulation of the planar phase front traveling in the extended core region is given by

$$\left[\frac{2d}{\cos(\theta_i^\beta)} - 2d \cos(\theta_i^\beta) \right] \beta(\omega) \pm 2k\pi , \quad (6.2.29b)$$

where the term $2k\pi$ is included to be consistent with the cyclic nature of the planar phase front.

The exponential accumulation of the planar amplitude front after two consecutive reflections is given by

$$\frac{2d}{\cos(\theta_i^\alpha)} \alpha(\omega) + \Psi_3(\omega) + \Psi_2(\omega) , \quad (6.2.30a)$$

where $\alpha(\omega)$ is the magnitude of the propagation vector $\alpha(\omega)$. The quantities $\Psi_2(\omega)$ and $\Psi_3(\omega)$ represent the attenuation suffered by the reflection from the core/substrate and core/cladding interfaces, respectively. The exponential accumulation of the planar amplitude front traveling in the extended core region is given by

$$\left[\frac{2d}{\cos(\theta_i^\alpha)} - 2d \cos(\theta_i^\alpha) \right] \alpha(\omega) . \quad (6.2.30b)$$

For constructive interference, Eqs. (6.2.29a,b) are equivalent, viz.

$$2d\beta(\omega) \cos(\theta_i^\beta) \pm 2k\pi = \Phi_2(\omega) + \Phi_3(\omega) , \quad (6.2.31a)$$

and Eqs. (6.2.30a,b) are equivalent, viz.

$$2d\alpha(\omega) \cos(\theta_i^\alpha) = -[\Psi_2(\omega) + \Psi_3(\omega)] . \quad (6.2.31b)$$

The x -component of the propagation vector is $\beta_x(\omega) = \beta(\omega) \cos(\theta_i^\beta)$ so that Eq. (6.2.31a) becomes

$$2d\beta_x(\omega) \pm 2k\pi = \Phi_2(\omega) + \Phi_3(\omega) , \quad (6.2.32a)$$

and the x -component of the attenuation vector is $\alpha_x(\omega) = \alpha(\omega) \cos(\theta_i^\alpha)$ so that Eq. (6.2.31b) becomes

$$2d\alpha_x(\omega) = -[\Psi_2(\omega) + \Psi_3(\omega)] . \quad (6.2.32b)$$

The generalized *Fresnel* reflection coefficient for TE fields is given as the \tilde{r}_v component of the matrix given in Eq. (3.1.144),

$$r_v = \frac{\tilde{k}_x(\omega) + i\tilde{\xi}(\omega)}{\tilde{k}_x(\omega) - i\tilde{\xi}(\omega)} .$$

The reflection coefficient can be rewritten as

$$r_v = \frac{1 + i\frac{\tilde{\xi}(\omega)}{\tilde{k}_x(\omega)}}{1 - i\frac{\tilde{\xi}(\omega)}{\tilde{k}_x(\omega)}} = \frac{1 + iz}{1 - iz} = \frac{-(y-1) + ix}{(y+1) - ix} . \quad (6.2.33)$$

where $z = \frac{\tilde{\xi}(\omega)}{\tilde{k}_x(\omega)}$, $x = \Re\{z\}$ and $y = \Im\{z\}$. Conversion of Eq. (6.2.33) into a polar representation yields

$$r_v = \left[\frac{x^2 + (y+1)^2}{x^2 + (y-1)^2} \right]^{-\frac{1}{2}} e^{i\arg\left(\frac{x}{1-y}\right) - i\arg\left(\frac{-x}{1+y}\right)} .$$

where $\arg\{\} = \text{Tan}^{-1}\{\}$. Utilization of the trigonometric identity given in Eq. (6.2.22) yields

$$r_v = \left[\frac{x^2 + (y+1)^2}{x^2 + (y-1)^2} \right]^{-\frac{1}{2}} e^{i\arg\left\{ \frac{\frac{x}{1+y} + \frac{x}{1-y}}{1 + \left(\frac{x}{1+y}\right)\left(\frac{x}{1-y}\right)} \right\}} .$$

Further manipulation yields

$$r_v = \left[\frac{x^2 + (y+1)^2}{x^2 + (y-1)^2} \right]^{-\frac{1}{2}} e^{i\arg\left\{ \frac{2x}{1-x^2-y^2} \right\}} . \quad (6.2.34)$$

Substitution of the definitions $z_2 \equiv x_2 + iy_2 = \frac{\tilde{\xi}_2(\omega)}{\tilde{k}_x(\omega)}$ and $z_3 \equiv x_3 + iy_3 = \frac{\tilde{\xi}_3(\omega)}{\tilde{k}_x(\omega)}$

into Eq. (6.2.34) gives two reflection coefficients which represent reflection from the core/

substrate and core/cladding interfaces, respectively, viz.

$$r_{2v} = \left[\frac{x_2^2 + (y_2 + 1)^2}{x_2^2 + (y_2 - 1)^2} \right]^{-\frac{1}{2}} e^{i \arg \left\{ \frac{2x_2}{1-x_2^2-y_2^2} \right\}}, \quad (6.2.35a)$$

$$r_{3v} = \left[\frac{x_3^2 + (y_3 + 1)^2}{x_3^2 + (y_3 - 1)^2} \right]^{-\frac{1}{2}} e^{i \arg \left\{ \frac{2x_3}{1-x_3^2-y_3^2} \right\}}. \quad (6.2.35b)$$

The phase delays suffered by the reflection from the core/substrate and core/cladding interfaces, respectively, are given by the exponential factors in Eqs. (6.2.35a,b), viz.

$$\Phi_2(\omega) = \text{Tan}^{-1} \left(\frac{2x_2}{1-x_2^2-y_2^2} \right), \quad (6.2.36a)$$

$$\Phi_3(\omega) = \text{Tan}^{-1} \left(\frac{2x_3}{1-x_3^2-y_3^2} \right). \quad (6.2.36b)$$

The exponential attenuation suffered by the reflection from the core/substrate and core/cladding interfaces, respectively, are given by the natural logarithm of the magnitude of Eqs. (6.2.35a,b), viz.

$$\Psi_2(\omega) = -\frac{1}{2} \ln \left[\frac{x_2^2 + (y_2 + 1)^2}{x_2^2 + (y_2 - 1)^2} \right], \quad (6.2.36c)$$

$$\Psi_3(\omega) = -\frac{1}{2} \ln \left[\frac{x_3^2 + (y_3 + 1)^2}{x_3^2 + (y_3 - 1)^2} \right]. \quad (6.2.36d)$$

Substitution of Eqs. (6.2.36a–d) into the real and imaginary parts of the dispersion relation given in Eqs. (6.2.32a,b) yields identical results to those given in Eqs. (6.2.27a,b) thereby proving the supposition of the physical interpretation.

References

- [1]. J. D. Jackson, **Classical Electrodynamics**, 2nd edn. (Wiley, New York, 1975).
- [2]. E. D. Palik, ed., **Handbook of Optical Constants of Solids** (Academic Press, Orlando, 1985).
- [3]. K. E. Oughstun, "Pulse Propagation in a Linear, Causally Dispersive Medium," *IEEE Proc.* **79**, 1379 (1991).
- [4]. N. S. Kapany, **Fiber Optics, Principles and Applications** (Academic Press, New York, 1967).
- [5]. H. Kogelnik, "An Introduction to Integrated Optics," *IEEE Trans. MTT-23*, 1, 2–16 (1975).
- [6]. E. A. Lacey, **Fiber Optics** (Prentice–Hall, New Jersey, 1982).
- [7]. H. Nishihara, M. Haruna and T. Suhara, **Optical Integrated Circuits** (McGraw–Hill, New York, 1989).
- [8]. A. M. Glass, "Fiber Optics," *Physics Today* **46**, 10, 34 (1993).
- [9]. E. Tokunaga, A. Terasaki and T Kobayashi, "Femtosecond Phase Spectroscopy by use of frequency–domain interference," *J. Opt. Soc. Am. B* **5**, 753 (1995).
- [10]. D. Marcuse, **Theory of Dielectric Optical Waveguides** 2nd edn. (Quantum Electronics, Principles and Applications, Academic Press, New York, 1991).
- [11]. M. S. Sodha and A. K. Ghatak, **Inhomogeneous Optical Waveguides** (Optical Physics and Engineering, Plenum Press, New York, 1977).
- [12]. K. E. Oughstun, Ph.D. Thesis, The University of Rochester, (1978).
- [13]. K. E. Oughstun and G. C. Sherman, "Uniform asymptotic description of electromagnetic pulse propagation in a linear dispersive medium with absorption (the Lorentz medium)," *J. Opt. Soc. Am. A* **6**, 1394 (1988).
- [14]. K. E. Oughstun and G. C. Sherman, "Propagation of Electromagnetic Pulses in a Linear Dispersive Medium with Absorption (the Lorentz Medium)," *J. Opt. Soc. Am. B* **5**, 817 (1988).
- [15]. K. E. Oughstun and J. E. K. Laurens, "Asymptotic Description of Ultrashort Electromagnetic Pulse Propagation in a Linear, Causally Dispersive Medium," *Radio Science* **26**, 1, 245–258 (1991).
- [16]. G. C. Sherman and K. E. Oughstun, "Description of Pulse Dynamics in Lorentz Media in Terms of the Energy Velocity and Attenuation of Time–Harmonic Waves," *Phys. Rev. Lett.* **47**, 1451 (1981).
- [17]. K. E. Oughstun and G. C. Sherman, "Uniform asymptotic description of rectangular optical pulse propagation in a linear, causally dispersive medium," *Phys. Rev. A* **41**, 6090 (1990).
- [18]. S. Shen and K. E. Oughstun, "Dispersive pulse propagation in a double–resonance Lorentz medium," *J. Opt. Soc. Am. B* **6**, 948 (1989).
- [19]. K. E. Oughstun and S. Shen, "Velocity of energy transport for a time–harmonic field in a multiple–resonance Lorentz medium," *J. Opt. Soc. Am. B*, **5**, 2395 (1988).
- [20]. J. E. K. Laurens and K. E. Oughstun, "Asymptotic Description of Ultrawideband/Ultrashort Plane Wave Electromagnetic Pulse Propagation in Triply Distilled Liquid Water.

- Part I: A Causal, Analytic Model of the Frequency Dispersion of the Dielectric Permittivity,” *IEEE Trans. AP* (submitted).
- [21]. J. E. K. Laurens, “Plane Wave Pulse Propagation in a Linear, Causally Dispersive Polar Medium,” Ph.D. Thesis, University of Vermont (1993).
- [22]. K. E. Oughstun, J. E. K. Laurens and C. M. Balictsis, “Asymptotic Description of Electromagnetic Pulse Propagation in a Linear Dispersive Medium,” **Ultra-Wideband, Short-Pulse Electromagnetics**, eds. H. L. Bertoni, L. B. Felsen, and L. Carlin, 223–240 (Plenum Press, New York, 1993).
- [23]. Sir W. Hamilton, “Researches Respecting Vibration, Connected with the Theory of Light,” *Proceedings of the Royal Irish Academy* **1**, 267, 341 (1839).
- [24]. Lord Rayleigh, “On the Velocity of Light,” **Scientific Papers** **1**, 75, 537 (1881).
- [25]. Lord Rayleigh, “On Progressive Waves,” **Theory of Sound**, 2nd edn. (1894).
- [26]. P. Drude, **The Theory of Optics** (Dover Publications, New York, 1953).
- [27]. H. A. Lorentz, **Theory of Electrons**, 2nd edn. (Dover Publications, New York, 1952).
- [28]. L. Rosenfeld, **Theory of Electrons** (Dover Publications, New York, 1965).
- [29]. A. Sommerfeld, **Optics**, Volume IV, Lectures on Theoretical Physics, Chapter III, (Academic Press, New York, 1972).
- [30]. M. Born and E. Wolf, **Principles of Optics**, 6th edn. (Pergamon Press, New York, 1980).
- [31]. F. Wooten, **Optical Properties of Solids** (Academic Press, New York, 1971).
- [32]. A. Sommerfeld, “About the Propagation of Light in Dispersive Media,” *Ann. Physik* **4**, 44, 177 (1914).
- [33]. L. Brillouin, “About the Propagation of Light in Dispersive Media,” *Ann. Physik* **4**, 44, 203 (1914).
- [34]. L. Brillouin, **Wave Propagation and Group Velocity** (Academic Press, New York, 1960).
- [35]. H. Baerwald, “Über die Fortpflanzung von Signalen in disperdierenden Medien,” *Ann. Phys.*, **7**, 731 (1930).
- [36]. F. W. J. Olver, “Why Steepest Descents?,” *SIAM Rev.*, **24**, 2, 228 (1970).
- [37]. C. G. B. Garrett and D. McCumber, “Propagation of a Gaussian Light Pulse through an Anomalous Dispersion Medium,” *Phys. Rev. A* **1**, 305 (1970).
- [38]. D. Anderson, J. Askne and M. Lisak, “Wave packets in an absorptive and strongly dispersive medium,” *Phys Rev. A* **12**, 1546 (1975).
- [39]. D. Anderson and J. Askne, “Wave Packets in Strongly Dispersive Media,” *Proc. IEEE* **62**, 1518 (1974).
- [40]. C. M. Knop and G. I. Cohn, “Comments on Pulse Waveform Degradation Due to Dispersion in Waveguide,” *IEEE Trans. (correspondence)* **MTT-11**, 445 (1963).
- [41]. R. M. Lewis and J. B. Keller, “Asymptotic Methods for Partial Differential Equations: The Reduced Wave Equation and Maxwell’s Equations,” Courant Institute of Math. Science, New York University, NY, Rept. **EM-194**, (January 1964).
- [42]. L. B Felsen, “Transients in Dispersive Media, Part I: Theory,” *IEEE Trans. AP-17*, 2, 191 (1969).

- [43]. G. M. Whitman and L. B Felsen, "Transients in Dispersive Media, Part II: Excitation of Space Waves and Surface Waves in a Bounded Cold Magnetoplasma," *IEEE Trans. AP-17*, 2, 200 (1969).
- [44]. T. Hosono, "Numerical Inversion of Laplace Transform and Some Applications to Wave Optics," Proceedings of the International U.R.S.I. Symposium on Electromagnetic Waves (Munich, FRG, 1980).
- [45]. P. Wyns, D. Foty and K. E. Oughstun, "Numerical Analysis of the Precursor Fields in Linear Dispersive Pulse Propagation," *J. Opt. Soc. Am. A* **6**, 1421 (1989).
- [46]. P. Wyns, D. Foty and K. E. Oughstun, "Numerical Determination of the Signal Velocity in Dispersive Pulse Propagation," *J. Opt. Soc. Am. A* **6**, 1430 (1989).
- [47]. R. M. Joseph, S. C. Hagness and A. Taflove, "Direct time integration of Maxwell's equations in linear dispersive media with absorption for scattering and propagation of femtosecond electromagnetic pulses," *Opt. Lett.* **16**, 1412 (1991).
- [48]. P. K. Tien, "Light Waves in Thin Films and Integrated Optics," *Appl. Opt.* **10**, 2395 (1971).
- [49]. E. Snitzer, "Cylindrical Dielectric Waveguide Modes," *J. Opt. Soc. Am.* **51**, 491 (1961).
- [50]. W. Gen-Wang, "Steepest descent Approximation Theory for the study of Optical Waveguide," *Sci. in China* **34**, 885 (1991).
- [51]. M. A. B. Whitaker, "Improved treatment of Fresnel equations," *J. Phys A:Math. Gen.* **12**, 297 (1979).
- [52]. E. Gitterman and M. Gitterman, "Transient processes for incidence of a light signal on a vacuum-medium interface," *Phys. Rev.* **13**, 763 (1976).
- [53]. R. Olshanlsky and D. B. Keck, "Pulse broadening in graded-index optical fibers," *Appl. Opt.* **15**, 483 (1976).
- [54]. D. Anderson and M. Lisak, "Analytic Study of Pulse Broadening in Dispersive Optical Fibers", *Physical Rev. A* **35**, 1, 184 (1987).
- [55]. G. R. Boyer and X. F. Carlotti, "Pulse-spread minimization in single-mode fibers," *Phys. Rev.* **38**, 5140 (1988).
- [56]. J. Herrmann, "Propagation of ultrashort light pulses in fibers with saturable nonlinearity in the normal-dispersion region," *J. Opt. Soc. Am. B* **8**, 1507 (1991).
- [57]. W. Zhao and E. Bourkoff, "Femtosecond Pulse Propagation in Optical Fibers: Higher Order Effects," *IEEE J. Quan. Elec.* **24**, 365 (1988).
- [58]. D. H. Auston and M. C. Nuss, "Electrooptic Generation and Detection of Femtosecond Electrical Transients," *IEEE J. Quan. Elec.* **24**, 184 (1988).
- [59]. K. E. Oughstun and G. C. Sherman, **Electromagnetic Pulse Propagation in Causal Dielectrics** (Springer-Verlag, New York, 1994).
- [60]. R. N. Bracewell, **The Fourier Transform and Its Applications**, 2nd edn., rev. (McGraw-Hill, New York, 1986).
- [61]. H. B. Phillips, **Vector Analysis** (Wiley, New York, 1949).
- [62]. W. R. LePage, **Complex Variables and the Laplace Transform for Engineers** (Dover Publications, New York, 1980).

- [63]. A. v. Hippel, **Dielectrics and Waves** New edn. (Artech House, Boston, 1995).
- [64]. S. Mitachi and P. A. Tick, "Dispersion Characteristic of CLAP Glass Systems," SPIE: Propagation and Characteristics of Optical Glass **970**, 128 (1988).
- [65]. R. P. Feynman, R. B. Leighton and M. Sands, **The Feynman Lectures on Physics** (Addison–Wesley, Reading, MA, 1977).
- [66]. B. H. Bransden and C. J. Joachain, **Introduction to Quantum Mechanics** (Longman Scientific and Technical, Wiley, New York, 1989).
- [67]. W. H. Press, B. P. Flannery, S. A. Teukolsky and W. T. Vetterling, **Numerical Recipes in C** (Cambridge University Press, New York, 1988).
- [68]. J. A. Stratton, **Electromagnetic Theory** (McGraw–Hill, 1941).
- [69]. G. Caviglia and A. Morro, **Inhomogeneous Waves in Solids and Fluids** (World Scientific, New Jersey, 1992).
- [70]. R. Loudon, "The propagation of electromagnetic energy through an absorbing dielectric," J. Phys. **3**, 233 (1970).
- [71]. J. B. Conway, **Functions of One Complex Variable**, 2nd edn. (Springer–Verlag, New York, 1978).
- [72]. F. S. Cater, **Lectures on Real and Complex Vector Spaces** (Saunders, Philadelphia , 1966).
- [73]. eds. M. Abramowitz and I. E. Stegun, **Handbook of Mathematical Functions** (Nation Bureau of Standards, Appl. Math. Series – 55, Washington, D.C., 1972).
- [74]. N. Bleistein and R. A. Handelsman, **Asymptotic Expansions of Integrals** (Dover Publications, New York, 1986).
- [75]. I. D. Aggarwal and Grant Lu, **Fluoride Glass Fiber Optics** (Academic Press, New York, 1991).
- [76]. eds. S. Nudelman and S. S. Mitra, **Optical Properties of Solids** (Plenum Press, New York, 1969).
- [77]. R. F. Harrington, **Time Harmonic Electromagnetic Fields** (McGraw–Hill, New York, 1961).